DESIGN, SYNTHESIS, AND CHARACTERIZATION OF NOVEL LIGANDS CONTAINING SEVEN-MEMBERED RING FOR THE SENSITIZATION OF NEAR-INFRARED EMITTING LANTHANIDE CATIONS IN COMPLEXES AND NANOCRYSTALS

by

Jian Zhang

B.S., Lanzhou University, 1999

M.S., Lanzhou University, 2002

Submitted to the Graduate Faculty of

Arts and Sciences in partial fulfillment

of the requirements for the degree of

Doctor of Philosophy

University of Pittsburgh

2008

UNIVERSITY OF PITTSBURGH

SCHOOL OF ARTS AND SCIENCES

This dissertation was presented

by

Jian Zhang

It was defended on

March 25, 2008

and approved by

David H. Waldeck, PhD, Professor, Chemistry, University of Pittsburgh

Tara Y. Meyer, PhD, Associate Professor, Chemistry, University of Pittsburgh

Catalina Achim, PhD, Associate Professor, Chemistry, Carnegie Mellon Univesity

Dissertation Advisor: Stéphane Petoud, PhD, Assistant Professor, Chemistry, University of

Pittsburgh

Stéphane Petoud, PhD

DESIGN, SYNTHESIS, AND CHARACTERIZATION OF NOVEL LIGANDS CONTAINING SEVEN-MEMBERED RING FOR THE SENSITIZATION OF NEAR-INFRARED EMITTING LANTHANIDE CATIONS IN COMPLEXES AND NANOCRYSTALS

Jian Zhang, PhD

University of Pittsburgh, 2008

Near-infrared (NIR) emitting lanthanide cations have a great potential for practical applications such as fluoroimmunoassays, polymer-based optical signal amplifiers, active materials in lasers, and bioimaging. In the recent years, the quest for new lanthanide-based NIR compounds has been one of the most active research areas in lanthanide coordination chemistry and spectroscopy. The first part of this dissertation describes the discovery of tropolonate, a novel and efficient sensitizer for five different NIR emitting lanthanide cations (Yb^{3+}, Nd^{3+}, Er^{3+}, Tm^{3+}, and Ho^{3+}). The detailed structural and photophysical properties of the lanthanide complexes formed with tropolonate were investigated. On the basis of this initial work, four different approaches have been initiated with the goal to explore the possibilities to gain more control and to improve the luminescence properties of NIR emitting lanthanide compounds. 1) By the attachment of four tropolonate units to a common backbone to form octadentate ligand in order to increase the thermodynamic stability and increase the protection for Ln^{3+}. 2) By the substitution of the tropolonate ligand by six different functional groups to modify the electronic structure of tropolonate sensitizer to control the photophysical properties of the resulting complexes. 3) By the use of a ligand that incorporates azulene as a novel sensitizer, which is

structurally similar to tropolonate; 4) By capping tropolonate ligands on the surface of inorganic nanocrystals doped with NIR emitting Ln^{3+}. This approach allows the efficient sensitization of the NIR emitting lanthanides and eliminates the intrinsic non-radiative quenching from the ligand.

TABLE OF CONTENTS

LIST OF TABLES

LIST OF FIGURES

ACKNOWLEDGEMENT

The completion of my Ph.D could not been accomplished without the tremendous help of many people. I would like to thank my advisor, Professor Stéphane Petoud, for allowing me to join his group and advising me through my graduation. I have been deeply impressed by his knowledge and enthusiasm towards scientific research and education. I thank Prof. Petoud for his patience, mentorship, and help with my career after graduate school.

I would like to thank the members of my dissertation committee, Prof. David Waldeck for being a committee member and the mentor of my research proposal; Prof. Tara Meyer for her invaluable advices and help for my research and document preparation; Prof. Catalina Achim (CMU) for being a committee member and support for my seeking for academic employment.

Thank you to all the present and past members of the Petoud Group along with all my friends. This includes, but is not limited to Dr. Mark Ams, Dr. Paul Badger, Dr. Chunlong Chen, Dr. Jason Cross, Demetra Czegan, Grzegorz Filipczyk, Kristy Gogick, Jeff Hopson, Ling Li, Quansheng Liang, Matthew Lockett, Eric Miller, Adrienne Oxley, David Oxley, Chad Shade, Dr. Xiaoqiang Shen, Dr. Yu Tang, Hyounsoo Uh, Lin Wang, Dr. David Wang, Shuangyi Wan, Jie Zhang, and Dr. Hong Zhao.

I would like to thank the following individuals and shops for their help with different instruments and samples for my research: Dr. Kasi Somayajula (Mass Spectroscopy), Dr.

Damodaran Krishnan (NMR), Dr. Steve Geib (X-ray crystallography), Albert Stewart (XRD), Joseph Suhan (TEM), Electronics Shop (Chuck Fleishaker, Bob Muha, Dave Emala, and Jim McNerney), and Machine Shop (Tom Gasmire and Jeff Sicher).

Finally, I must thank my dear family. My mother (Bo), father (Jiquan), and brother (Yanyu) were always there to support me. I am forever grateful for their endless source of love.

1.0   INTRODUCTION

The noninvasive visualization of specific molecular targets, pathways and physiological effects *in vivo* is currently in great demand in life science. Many advances in fluorescent probes, fluorescent proteins, and imaging technologies allow for the analysis of the structures and functions of cells.[1] Near-infrared (NIR) fluorescence imaging is one of the most promising technologies for non-invasive high-resolution *in vivo* imaging.

In biomedical imaging, an excitation photon typically travels through tissues and biological liquids to reach the fluorescent agent. The photon emitted by the fluorophore travels back and is collected by the detector. Depending on their wavelengths, both excitation and emission photons could be absorbed and scattered by tissues and organs. Their signal can also be attenuated in the autofluorescence arising from the biological serum.[2] Near-infrared light from 640 nm to 1100 nm is advantageous for several reasons. Firstly, the tissue, skin, hemoglobin (the principal absorbers of visible light), water and lipids (the principal absorbers of infrared light) have a minimum of absorption in the NIR region (Figure 1.1).[3]

Secondly, NIR light has limited scattering (Figure. 1.2) in comparison to visible light, which is proportional to $1/\lambda^4$. Light scattering describes the deviation of a photon from the parallel axis of its path, and can occur when the tissue inhomogeneity is small (Rayleigh scattering), or roughly equal (Mie scattering) to wavelength.[2] Increased scattering leads to reduced resolution of the image.

Thirdly, when NIR light is used, the autofluorescence (the fluorescence of other substances than the fluorophore of interest, which increases the background signal) from the tissue can be eliminated because biological molecules seldomly have native fluorescence in the NIR region. As a consequence, the fluorescence background is reduced and the sensitivity of the measurement is increased (improved signal to noise ratios). Figure 1.3 shows the autofluorescence spectra of biological tissue at different excitation wavelengths.
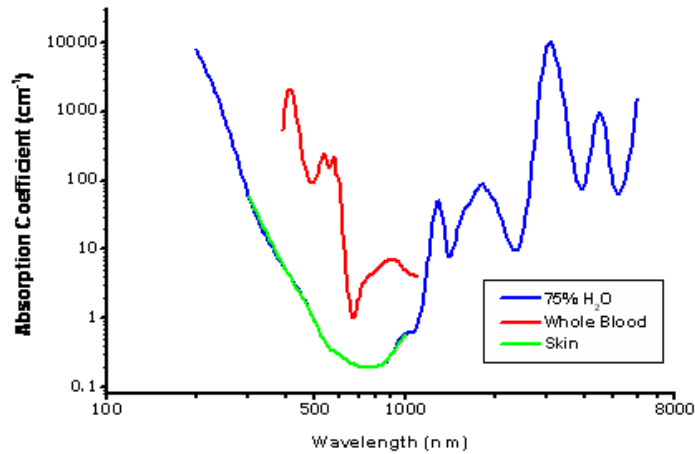
Figure 1.1: Absorption spectra of 75% H_2O, whole blood, and skin[3]
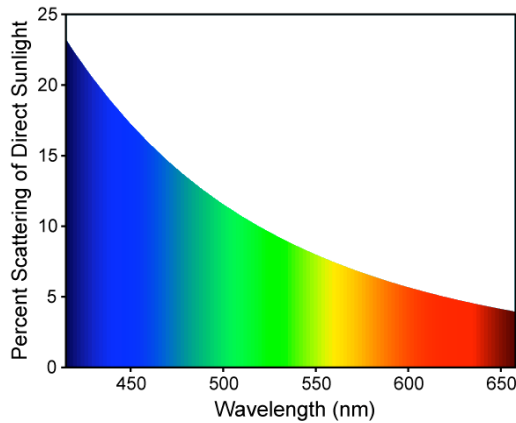
Figure 1.2: Diagram of percent scattering of direct sunlight vs. wavelength[2]

2
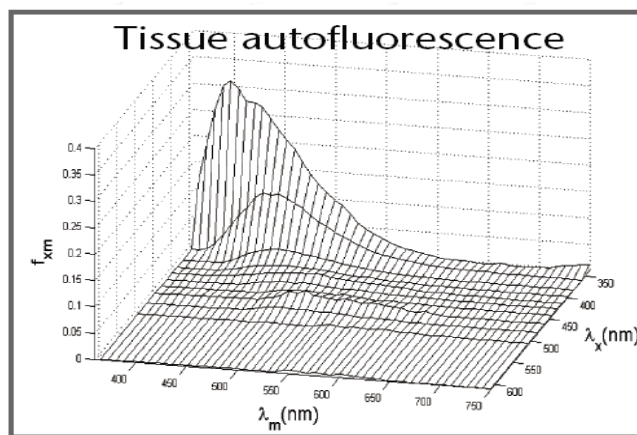
Figure 1.3: 3-D scanned spectra of autofluorescence of the tissue[1]

Currently, organic fluorophores, such as heptamethine cyanines are most commonly used as NIR fluorescence agents used in biological imaging. Indocyanines are one of the most widely used cyanines (Cy dyes).[2] They have typically 760-800 nm absorption bands and 790-830 nm emission bands.[2] The chemical structure of a recently developed heptamethine indocyanine (IRDye 780) is shown in Figure 1.4. Tetra-sulfonate groups in this compound increase the aqueous solubility and fluorescence quantum yield. Several fluorophores of this type and their bioconjugation chemistry have been reported.[4-6] Figure 1.5 is one example where the NIR dye was conjugated to folate, which is used to target cancer cell in mice[7].
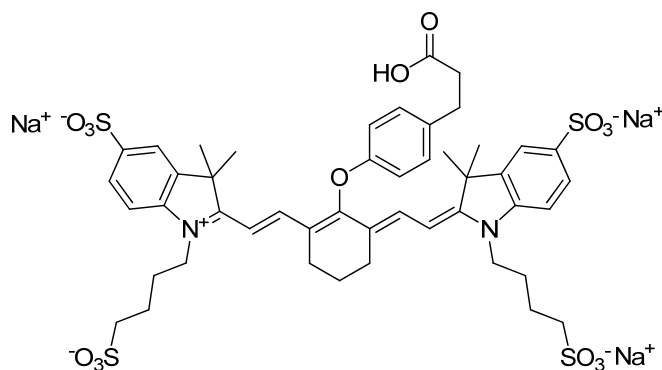
Figure 1.4: Molecular structure of IRDye78

3
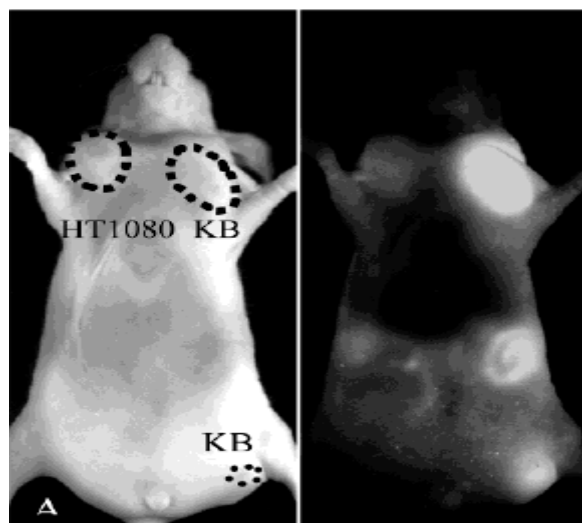
Figure 1.5: *In vivo* imaging of folate receptors conjugated to an indocyanine dye in mice.[7]

Although conventional organic fluorophores have good solubility (due to appropriate functionalization) and reasonable quantum yield (3% to 15% in aqueous solution[2]), they suffer from major limitations. The excitation and emission wavelength strongly depend on the experimental conditions. More importantly, organic fluorophores in general are highly susceptible to photobleaching,[8] which limits the number of photons per unit of time and surface (fluence rate) that can be applied to a sample, and hence the sensitivity of detection. For example, heptamethine indocyanines rapidly photobleach (in seconds) in serum when the fluence rate exceeds 50 mW/cm^2.[9] This prevents long and repeated exposure of the sample to light, which is a major limitation for biological imaging and fluorescence microscopy. This also explains that despite the significant advantages of their NIR emission, very few applications are taking advantage of organic NIR fluorophores.

Recently, novel work has been done with inorganic fluorescent semiconductor nanocrystals (quantum dots) for biological imaging, which have the potential to solve some problems of the conventional organic fluorophores.[10-12] Quantum dots (QD) are synthesized in

organic solvents. They are typically constituted from an inorganic core (CdSe or CdTe) and inorganic outer shell (such as ZnS). The emission wavelength can be tuned by controlling the size of the nanoparticles. To be used *in vivo*, they must be coated with an aqueous-compatible organic layer. They have good photophysical properties; in particular, a broadband absorption with large absorption coefficient that increases as the wavelength gets smaller. As a result, different quantum dots with different fluorescence emission wavelengths can be excited using the same wavelength. High quantum yield values (up to 50%-60% for quantum dots with organic coating in aqueous solution[2]) and good resistance to photobleaching make them excellent candidates for bioanalytical applications *in vivo* imaging.

However, quantum dots have several intrinsic limitations. First, they are large particles when compared to organic fluorophores or, in some cases, to cells themselves. A typical size for NIR emitting QDs is about 20 nm when the coating and biological reactive reagent (such as protein or antibody) is included. Their size limits their application in many areas of *in vivo* imaging, especially, for cellular imaging since their large size relative to the cell may prevent them from entering all regions of the cell. Secondly, several types of quantum dots are constituted of highly toxic elements such as Cadmium, Selenium, and Tellurium. The "oxidation effect"[13] on the quantum dots that can result in the liberation of toxic metallic cations (such as Cd^{2+}) into the cell has been reported recently.[13]

Considering the drawbacks of both organic fluorophores and quantum dots, new NIR fluorescent agents are in high demand. NIR luminescent lanthanide complexes have the potential to be a new member of NIR fluorescent agents for bioimaging.

1.1 LUMINESCENT LANTHANIDE CATIONS AND COMPLEXES

Lanthanides are the elements between Cerium (Ce: $Z = 58$) and Lutetium (Lu: $Z = 71$), which are located in the first row of f-block in the periodic table. The lanthanides most common oxidation state is 3+. The f orbitals are higher in energy than the outer $5s$ and $5p$ orbitals, but spatially shielded by them. This special electronic configuration gives the lanthanides very unique properties.[14-16] First, the transitions within the f-orbital manifold are parity forbidden, which leads to low molar absorption coefficients in the order of 10 $M^{-1}cm^{-1}$ or less and long lifetimes (from μs up to several ms) for the excited states and resulting luminescence. Secondly, the $4f$ orbitals are hardly affected by the surrounding environment and not involved in bonding, which makes the transitions (either absorption or emission) appear as sharp emission bands (line-like transitions) located at fixed wavelength and not affected by experimental conditions. Lutetium cation (Lu^{3+}), which has 9 completely filled $4f$ orbitals, is not luminescent. Gadolinium cation (Gd^{3+}) is also considered as non-luminescent because its excited states are located at high energy region. The other lanthanides have a large number of electronic levels and their luminescence ranges from the UV to the NIR region. An energy level diagram for Ln^{3+} is shown in Figure 1.6.

Due to the low molar absorption coefficient of Ln^{3+}, the direct excitation of their electronic states is not an efficient way to obtain intense luminescence emission. In 1942, Weissman discovered that sensitized emission from Ln^{3+} can be achieved by coordination of a suitable organic ligand followed by energy transfer from the ligand to the metal center.[17] To date few visible emitting lanthanide complexes have been used for practical applications such as luminescent markers in bioassay diagnostic imagery[18,19] and homogeneous time-resolved immunoassays[20,21].
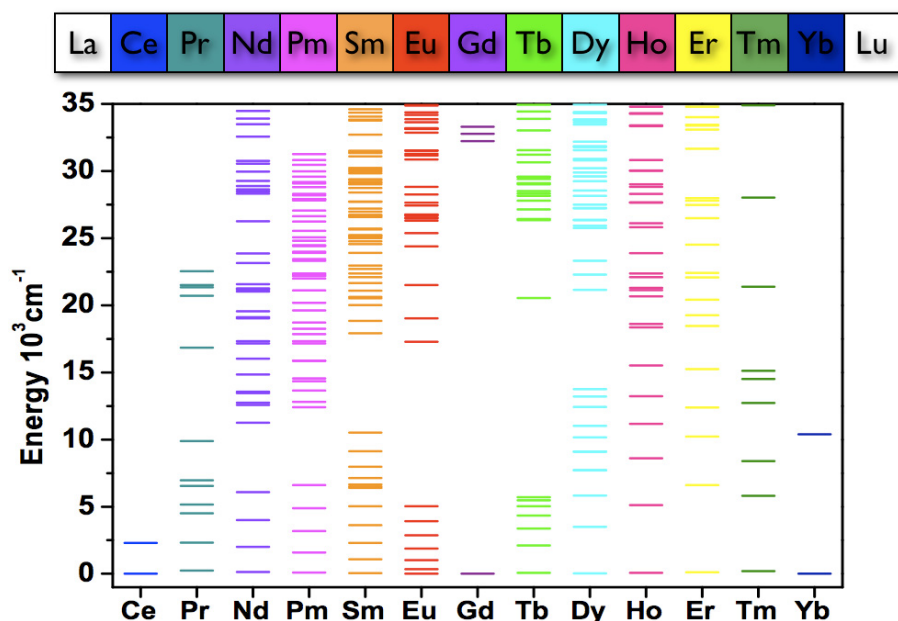
Figure 1.6: Diagram of electronic energy levels associated with the 4*f* orbitals of Ln[3+]

The development of NIR emitting lanthanide complexes has received much attention in recent years.[22-31] The luminescence of Yb^{3+}, Nd^{3+}, Ho^{3+}, and Tm^{3+} have emission bands ranging from 800 nm to 1100 nm, which is suitable for *in vivo* imaging. There are several additional advantages. Typically, these complexes display Ln^{3+}-centered long luminescence lifetime (μs to ms) in comparison to the organic fluorophores (ps to ns), allowing for their uses in time-resolved experiments.[14,32] The emission bands of Ln^{3+} are much narrower than the organic fluorophores and quantum dots, which makes them useful in multiplex applications because the emission of several Ln^{3+} can be quantified during the same experiment.[20] Unlike organic fluorophores, most lanthanide complexes do not photobleach.[33] Also, advances in two and three-photon laser technologies allow the excitation of molecules absorbing in an energy range from 400-500 nm, and even 315 nm by using NIR excitation light, which can penetrate deeply into tissues,[34-36] and also has reduced photo-toxicity to biological cells and tissues compared to UV light.

7

1.2   PHOTOPHYSICS OF LUMINESCENT LANTHANIDE COMPLEXES

A luminescent lanthanide complex consists of a lanthanide cation coordinated by a ligand(s). In most cases, the ligand contains a light-absorbing group in the form of an organic chromophore. Such group is generally referred to as the "antenna" chromophore.[37] The photon energy absorbed by this antenna can be transferred to the coordinated Ln^{3+}, and sensitize its luminescence. This process is referred as the "antenna effect" and is illustrated in Figure 1.7.[17]
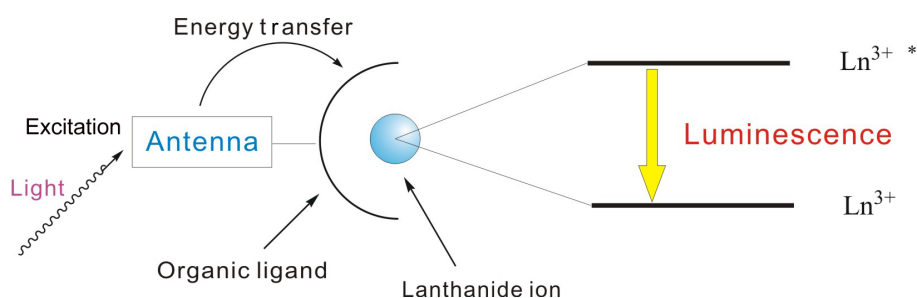
Figure 1.7: Schematic illustrating the antenna effect

Although there are some examples showing that the energy can transfer from the singlet states,[38,39] most of the luminescent lanthanide complexes have been hypothesized as following the mechanism of photosensitization from triplet states of the antenna ligand. This process is shown in Figure 1.8. Excitation of the antenna by a singlet-singlet transition is followed by intersystem crossing (ISC) which results in population of the antenna's triplet state. From the triplet excited antenna, the energy transfers (ET) to Ln^{3+}.[40,41] ISC competes with other processes that occur from the antenna's singlet state, particularly fluorescence. Also there are some other processes that deactivate the antenna triplet state, such as quenching by molecular oxygen which has a triplet ground state. So the overall quantum yield of the lanthanide luminescence (Q_{Ln}^{L}) that

is excited via the antenna chromophore, is dependent on the product of quantum yields of the individual three steps: intersystem crossing, (Q_{ISC}), energy transfer (Q_{ET}) and lanthanide luminescence (Q_{Ln}^{Ln}).

Antenna Effect
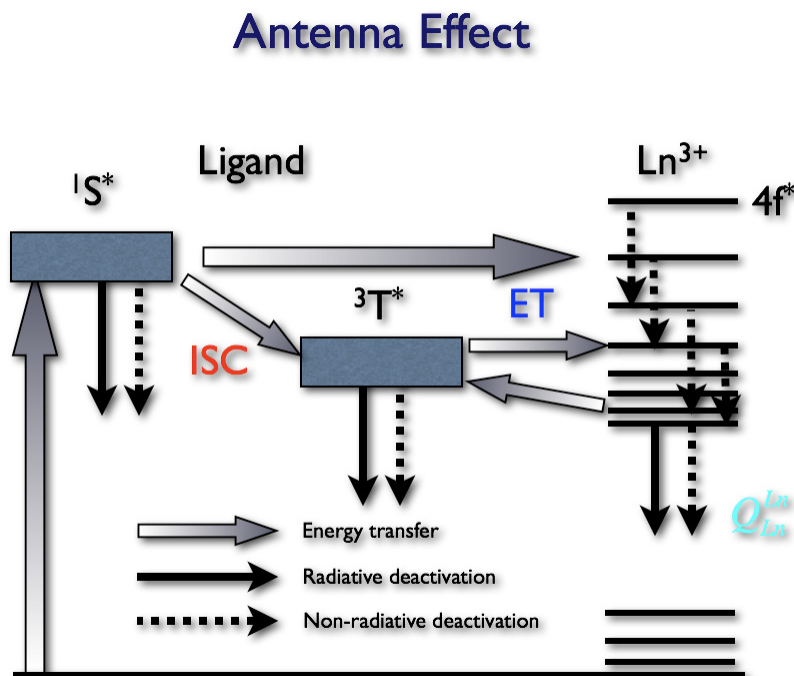
Figure 1.8: Jablonski diagram showing the sensitization of Ln^{3+} emission

Three main mechanisms have been proposed for the process of energy transfer from the ligand to the metal center. The Förster mechanism is a dipole-dipole interaction between the donor and acceptor.[42,43] The absorption spectrum of the energy acceptor and the emission spectrum of the energy donor must overlap for this type of energy transfer to occur. This mechanism takes place through space, the energy transfer efficiency is dependent on r^{-6}, where r is the distance between the donor and acceptor. The second mechanism is called a Dexter

mechanism, which is a concerted electron-exchange mechanism.[44] It requires simultaneous electron exchange between the energy donor and energy acceptor, and therefore direct contact and spin-orbit coupling are essential. Simultaneous exchange of electrons is required and the efficiency is proportional to e^{-r}, where r is the distance between the donor and acceptor.

In addition to these two mechanisms proposed for energy transferred from ligand's electronic states, in some specific cases, a sequential electron transfer mechanism has been used to explain the energy transfer in complexes in which the Ln^{3+} (Eu^{3+}, Sm^{3+}, and Yb^{3+}) can be reduced by the sensitizer (Figure 1.9).[45-47] This mechanism is favorable in cases where the electron transfer step is thermodynamically feasible, which depends upon the oxidation potential of the excited state of the donor and the reduction potential of Ln^{3+}.
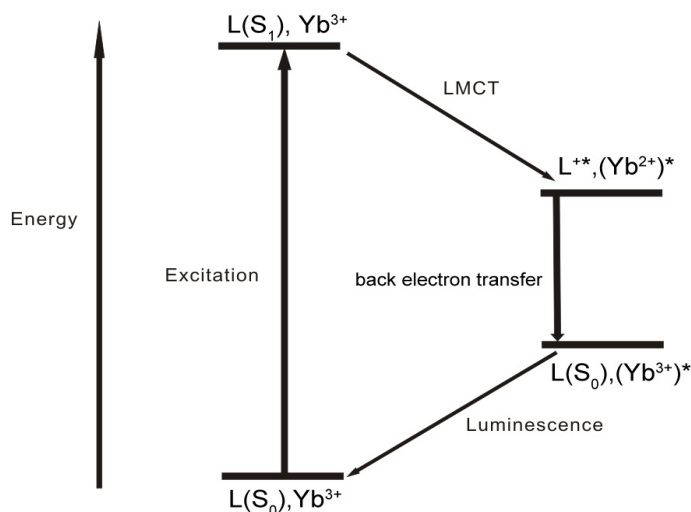
Figure 1.9: Representation of sequential mechanism of electron transfer

The small sized of the energy gap between the lowest excited state and the ground state is important for understanding nonradiative relaxation in lanthanide complexes.[48,49] The excited

states of Ln^{3+} can be rapidly deactivated by the overtones of high frequency vibrations through non-radiative processes involving O-H, N-H, and C-H vibration.[50] This type of quenching effect is much more pronounced for NIR emitting Ln^{3+}, because they have a smaller energy gap between the excited and ground states (Figure 1.10). For example, two quanta of OH vibration will quench the lowest excited state of Nd^{3+}.
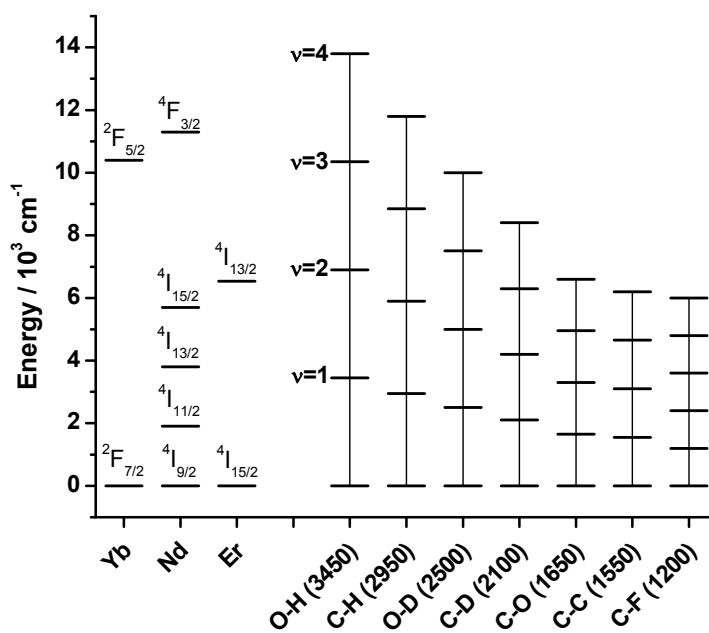
Figure 1.10: Radiative transition energies of Yb^{3+}, Nd^{3+}, Er^{3+}, and the vibrational energies of common bonds in organic systems

To summarize, in order to obtain highly luminescent lanthanide complexes, the following requirements have to be fulfilled.

- The ligand(s) has to bind Ln^{3+} tightly to form stable complexes. Oxygen donor ligands are preferred because of their hard base properties. The ligand(s) need to satisfy the requirement of Ln^{3+} for high coordination number in solution and to protect the Ln^{3+} from nonradiative

11

deactivations.[50] The coordination number of Ln^{3+} for complexes in solution is usually between 8 and 10.

- The ligand(s) must have appropriate energies of singlet and triplet states, so that they have a good energy match with the excited state energy level of Ln^{3+} to achieve efficient energy transfer. The difference in energy between these two levels can not be too small due to a risk of back transfer from the lanthanide to the ligand(s), reducing the overall luminescence intensity.[37,51]

- The ligand(s) should be easily modifiable, so that the photophysical, thermodynamic and solubility properties can be controlled and optimized for the targeted applications.

- Functionalities that allow conjugation to biomolecules, such as proteins, antibodies, and DNA are possible for use in specific biological applications.

Up to date, different chromophores have been reported for sensitizing NIR emitting Ln^{3+}. i) Organic dyes. Werts et al. used a fluorescein based on an amino-carboxylate derivative (**1**) as a sensitizer for Yb^{3+}. This complex was tested for NIR fluoroimmunoassay, and to the best of our knowledge, this is the only example of NIR emitting lanthanide complex tested in a practical assay.[52] Klink et al. synthesized ligand (**2**) based on *m*-terphenyl. Different organic dyes have been attached to this group as the sensitizers for the NIR emitting Ln^{3+}.[53] Boradiazaindacene dye (**3**) can sensitize several Ln^{3+} at a long excitation wavelength around 514 nm.[54]

ii) Transition metal complexes[25]. Pope et al. used DO3A type ligands, non-covalently bonded to an Os^{2+} complex (**4**), and studied the luminescence properties of these complexes.[55] Recently, Koullourou et al. reported the use of a similar compound incorporating Re^{2+} complex (**5**) as a prototype single molecule dual imaging agent.[56] Red emitting Ru^{2+} complex (**6**) has been used by Klink et al. to sensitize Yb^{3+} and Nd^{3+}.[57]

iii) Small metal chelators. For example, Hasegawa et al. studied the luminescent properties of Nd^{3+} complexes formed with deuterated and fluorinated β-diketone (**7**, **8**) as ligands.[58] These two ligands were designed to minimize the high energy vibrations of C-H. The analogs of β-diketone (**9**)[59] also have been used as ligands and sensitizers. Phenanthroline (**10**)[22], pyridine and its analogs (**11**)[60], and 8-hydroxyquinonline (**12**)[61] are among the most studied sensitizers as well. Other NIR emitting lanthanide complexes have also been studied by Bünzli, Ward, Wong, and Schanze.[60,62-65]

Selected examples of NIR luminescent lanthanide complexes are shown in Figure 1.11 and Table 1.1. Most of the luminescent lanthanide complexes reported so far have relatively low quantum yields in comparison to visible emitting organic fluorophores, which can be explained by the low efficiency of intramolecular ligand-to-Ln^{3+} energy transfer and/or by the insufficient protection of Ln^{3+} against nonradiative deactivation processes. Development of novel ligand systems and strategies to improve the quantum yields of the NIR emitting lanthanides complexes is being pursued for their use in NIR fluorescence imaging. Also, to date, most of the published work is focused on Nd^{3+} and Yb^{3+} complexes. Other NIR luminescent Ln^{3+} with different emission bands such as Ho^{3+} and Tm^{3+} also have potential for use as NIR reporters in solution. Such achievement would be beneficial for the development of multiplex assays where several analytes are quantified during the same experiment. The luminescence of Ln^{3+} allows such developments due to the availability of multiple emission bands from Ln^{3+} at fixed wavelengths and that do not overlap.

1

2

3

4

5

6
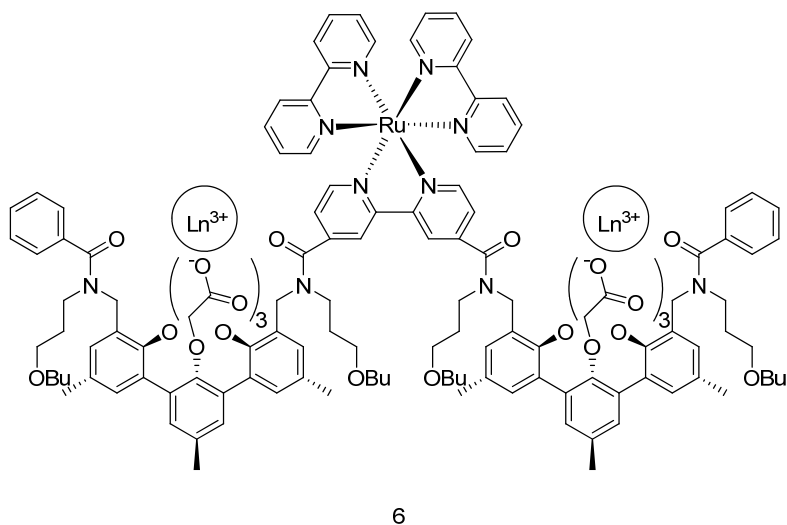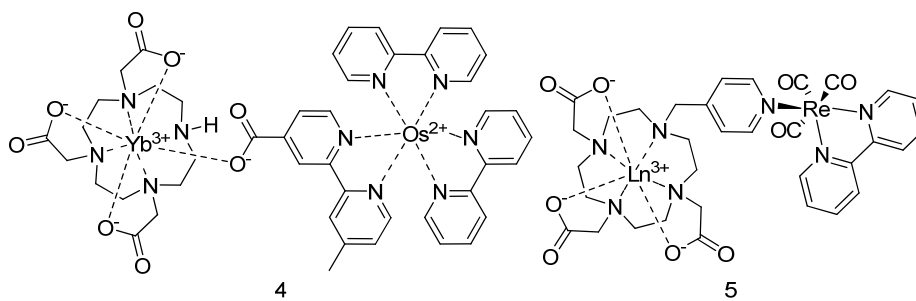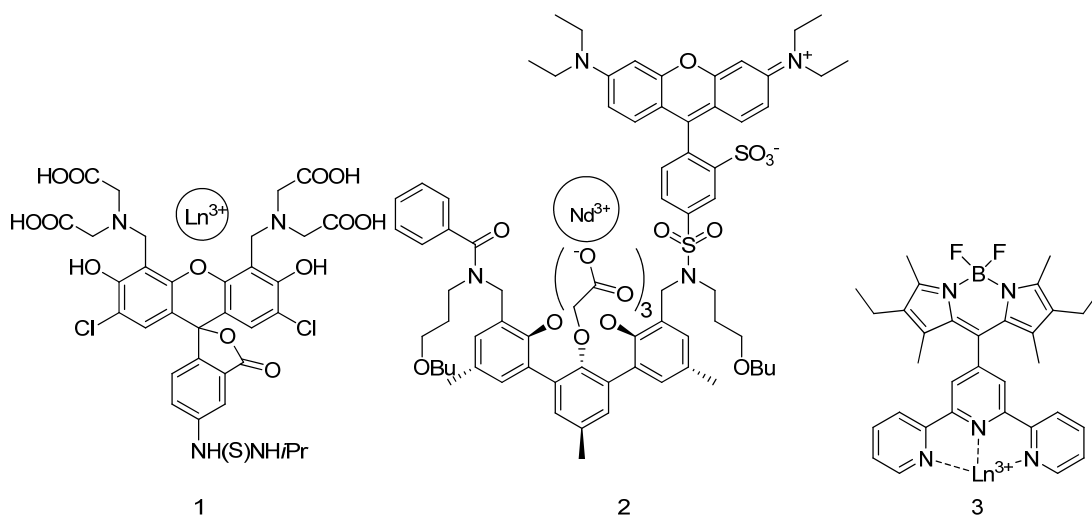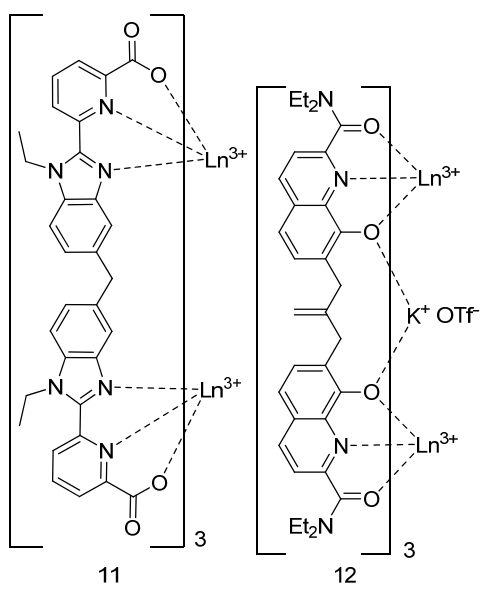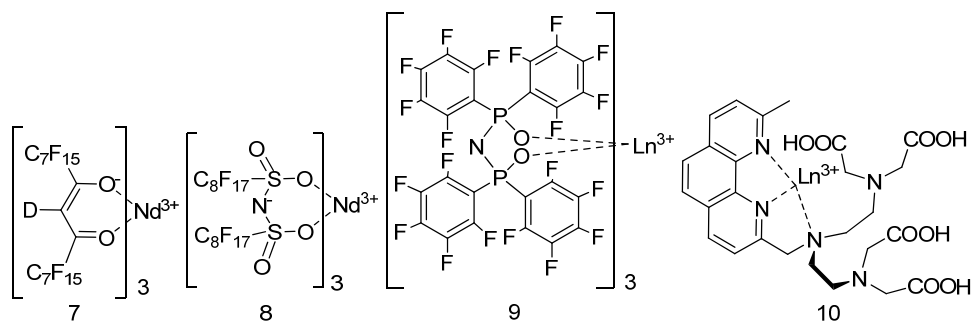
Figure 1.11: Selected NIR emitting lanthanide complexes

Table 1.1: Summary of photophysical data of selected NIR emitting lanthanide complexes

Ligand	Ln^{3+}	Solvent	λ_{max}/nm	ε_{max}/M^{-1}cm^{-1}	Φ_{tot}	τ_{obs}/µs	Ref
1	Yb^{3+}	Aqueous buffer	516	145,000	5.34×10^{-4}	1.8	[52]
2	Nd^{3+}	DMSO-d_6	455			2.1	[53]
	Yb^{3+}	DMSO-d_6	455			18.2	[53]
3	Nd^{3+}	CH_2Cl_2	514			0.27	[54]
	Yb^{3+}	CH_2Cl_2	514			9.7	[54]
4	Yb^{3+}	CH_3OH				1.38	[55]
		CH_3OD				8.192	[55]
5	Yb^{3+}	H_2O	337			1.20	[56]
		D_2O	337			5.34	[56]
6	Nd^{3+}	DMSO-d_6	570	88,000		2.21	[57]
7	Nd^{3+}	DMSO-d_6			0.033[a]	13[b]	[58]
8	Nd^{3+}	DMSO-d_6			0.032[a]		[58]
9	Er^{3+}	CD_2Cl_2	266		0.004	145, 28	[59]
10	Yb^{3+}	H_2O	279		0.0002	2.5	[22]
11	Yb^{3+}	D_2O	310		0.018	40	[60]
12	Yb^{3+}	Solid	355		0.0104	18.8	[61]

a. Direct excitation of Nd^{3+}
b. Quantum yield in CD_3COCD_3

1.3 OUTLINE

The work presented in this dissertation is mainly focused on different strategies to design, synthesize and characterize new antennae that allow for the improved photosensitization of NIR luminescent Ln^{3+} (Yb^{3+}, Nd^{3+}, and Er^{3+} and less commonly Ho^{3+} and Tm^{3+}). Chapter 2 discusses a novel ligand, tropolone, and its lanthanide complexes. The structural and luminescence properties of the complexes were investigated (*Angew. Chem., Int. Ed.* **2005**, 44, 2508; *Inorg. Chem.* **2007**, 46, 2643). In Chapter 3, synthesis, structure, and photophysical properties of various derivatives of tropolone and their NIR emitting lanthanide complexes are presented. As another strategy, two octadentate ligands, which incorporate four tropolone chelating units, were synthesized and the photophysical properties of the resulting complexes were investigated. The results are presented in Chapter 4. Chapter 5 introduces another novel ligand system based on a

derivative of the azulene chromophore. The photophysical properties of the corresponding complexes were studied and compared with tropolonate complexes (*Chem.-Eur. J.* **2008**, 14, 1264). Chapter 6 presents a novel strategy to improve the protection and sensitization of NIR emitting Ln^{3+} by capping tropolonate ligands on the surface Ln^{3+} doped $NaYF_4$ nanocrystals (*J. Am. Chem. Soc.,* **2007**, 129, 14834).

1.4   REFERENCES

(1)   Weissleder, R.; Ntziachristos, V. *Nat. Med.* **2003**, *9*, 123.

(2)   a) Frangioni, J. V. *Current Opin. Chem. Bio.* **2003**, *7*, 626; b) Waggoner, A. *Current Opin. Chem. Bio.* **2006**, *10*, 62.

(3)   Stolik, S.; Delgado, J. A.; Perez, A.; Anasagasti, L. *J. Photochem. Photobiol., B* **2000**, *57*, 90.

(4)   Lin, Y.; Weissleder, R.; Tung, C.-H. *Bioconjugate Chem.* **2002**, *13*, 605.

(5)   Flanagan, J. H., Jr.; Khan, S. H.; Menchen, S.; Soper, S. A.; Hammer, R. P. *Bioconjugate Chem.* **1997**, *8*, 751.

(6)   Zaheer, A.; Wheat, T. E.; Frangioni, J. V. *Mol. Imaging* **2002**, *1*, 354.

(7)   Moon, W. K.; Lin, Y. H.; O'Loughlin, T.; Tang, Y.; Kim, D. E.; Weissleder, R.; Tung, C. H. *Bioconjugate Chem.* **2003**, *14*, 539.

(8)   Yunus, W. M. M.; Sheng, C. K.; Yunus, W. M. Z. W. *J. Nonlinear Opt. Phys.* **2003**, *12*, 91.

(9)   Nakayama, A.; Bianco Antonio, C.; Zhang, C.-Y.; Lowell Bradford, B.; Frangioni John, V. *Mol. Imaging* **2003**, *2*, 37.

(10)   Green, M. *Angew. Chem., Int. Ed.* **2004**, *43*, 4129.

(11)   Giepmans, B. N. G.; Adams, S. R.; Ellisman, M. H.; Tsien, R. Y. *Science* **2006**, *312*, 217.

(12)   Fu, A.; Gu, W.; Larabell, C.; Alivisatos, A. P. *Curr. Opin. Neurobiol.* **2005**, *15*, 568.

(13)   Derfus, A. M.; Chan, W. C. W.; Bhatia, S. N. *Nano Lett.* **2004**, *4*, 11.

(14)   Bünzli, J.-C. G. In *Lanthanide Probes in Life, Chemical and Earth Sciences: Theory and Practice*; Bünzli, J.-C. G., Choppin, G. R., Editors, Eds.; Elsevier Science Publishers B. V.: Amsterdam, 1989, p 219.

(15)   Bünzli, J.-C. G. *Acc. Chem. Res.* **2006**, *39*, 53.

(16)   Bünzli, J.-C. G.; Piguet, C. *Chem. Soc. Rev.* **2005**, *34*, 1048.

(17)   Weissman, S. I. *J. Chem. Phys.* **1942**, *10*, 214.

(18)   Beeby, A.; Botchway, S. W.; Clarkson, I. M.; Faulkner, S.; Parker, A. W.; Parker, D.; Williams, J. A. G. *J. Photochem. Photobiol., B* **2000**, *57*, 83.

(19)   Faulkner, S.; Matthews, J. L. *Comp. Coord. Chem. II* **2004**, *9*, 913.

(20)   Mathis, G. *J. Biomol. Screen* **1999**, *4*, 309.

(21)   Hemmila, I.; Mukkala, V. M. *Crit. Rev. Cl. Lab. Sci.* **2001**, *38*, 441.

(22)   Quici, S.; Cavazzini, M.; Marzanni, G.; Accorsi, G.; Armaroli, N.; Ventura, B.; Barigelletti, F. *Inorg. Chem.* **2005**, *44*, 529.

(23)   Comby, S.; Imbert, D.; Vandevyver, C.; Bünzli, J.-C. G. *Chem.-Eur. J.* **2007**, *13*, 936.

(24)   Xu, H.-B.; Zhang, L.-Y.; Xie, Z.-L.; Ma, E.; Chen, Z.-N. *Chem. Commun.* **2007**, 2744.

(25)   Ward, M. D. *Coord. Chem. Rev.* **2007**, *251*, 1663.

(26)   Torelli, S.; Imbert, D.; Cantuel, M.; Bernardinelli, G.; Delahaye, S.; Hauser, A.; Bünzli, J.-C. G.; Piguet, C. *Chem.-Eur. J.* **2005**, *11*, 3228.

(27) Bassett, A. P.; Van Deun, R.; Nockemann, P.; Glover, P. B.; Kariuki, B. M.; Van Hecke, K.; Van Meervelt, L.; Pikramenou, Z. *Inorg. Chem.* **2005**, *44*, 6140.

(28) Ronson, T. K.; Lazarides, T.; Adams, H.; Pope, S. J. A.; Sykes, D.; Faulkner, S.; Coles, S. J.; Hursthouse, M. B.; Clegg, W.; Harrington, R. W.; Ward, M. D. *Chem.-Eur. J.* **2006**, *12*, 9299.

(29) Senechal-David, K.; Pope, S. J. A.; Quinn, S.; Faulkner, S.; Gunnlaugsson, T. *Inorg. Chem.* **2006**, *45*, 10040.

(30) Herrera, J.-M.; Pope, S. J. A.; Meijer, A. J. H. M.; Easun, T. L.; Adams, H.; Alsindi, W. Z.; Sun, X.-Z.; George, M. W.; Faulkner, S.; Ward, M. D. *J. Am. Chem. Soc.* **2007**, *129*, 11491.

(31) Banerjee, S.; Huebner, L.; Romanelli, M. D.; Kumar, G. A.; Riman, R. E.; Emge, T. J.; Brennan, J. G. *J. Am. Chem. Soc.* **2005**, *127*, 15900.

(32) Desiraju, G. R. *Acc. Chem. Res.* **1996**, *29*, 441.

(33) Ye, Z.; Tan, M.; Wang, G.; Yuan, J. *Anal. Chem.* **2004**, *76*, 513.

(34) Wong, K.-L.; Kwok, W.-M.; Wong, W.-T.; Phillips, D. L.; Cheah, K.-W. *Angew. Chem., Int. Ed.* **2004**, *43*, 4659.

(35) Piszczek, G.; Maliwal, B. P.; Gryczynski, I.; Dattelbaum, J.; Lakowicz, J. R. *J. Fluoresc.* **2001**, *11*, 101.

(36) Piszczek, G.; Gryczynski, I.; Maliwal, B. P.; Lakowicz, J. R. *J. Fluoresc.* **2002**, *12*, 15.

(37) Sabbatini, N.; Guardigli, M.; Lehn, J. M. *Coord. Chem. Rev.* **1993**, *123*, 201.

(38) Hebbink, G. A.; Klink, S. I.; Grave, L.; Oude Alink, P. G. B.; van Veggel, F. C. J. M. *ChemPhysChem* **2002**, *3*, 1014.

(39) Yang, C.; Fu, L.-M.; Wang, Y.; Zhang, J.-P.; Wong, W.-T.; Ai, X.-C.; Qiao, Y.-F.; Zou, B.-S.; Gui, L.-L. *Angew. Chem., Int. Ed.* **2004**, *43*, 5010.

(40)   Hayes, A. V.; Drickamer, H. G. *J. Chem. Phys.* **1982**, *76*, 114.

(41)   Sato, S.; Wada, M. *Bull. Chem. Soc. Jpn.* **1970**, *43*, 1955.

(42)   Förster, T. *Discuss. Faraday Soc.* **1959**, *No. 27*, 7.

(43)   Förster, T. *Ann. Phys. (Leipzig)* **1948**, *2*, 55.

(44)   Dexter, D. L. *J. Chem. Phys.* **1953**, *21*, 836.

(45)   Faulkner, S.; Beeby, A.; Carrie, M. C.; Dadabhoy, A.; Kenwright, A. M.; Sammes, P. G. *Inorg. Chem, Commun.* **2001**, *4*, 187.

(46)   Horrocks, W. D., Jr.; Bolender, J. P.; Smith, W. D.; Supkowski, R. M. *J. Am. Chem. Soc.* **1997**, *119*, 5972.

(47)   Hebbink, G. A.; Grave, L.; Woldering, L. A.; Reinhoudt, D. N.; van Veggel, F. C. J. M. *J. Phys. Chem. A* **2003**, *107*, 2483.

(48)   Stein, G.; Wurzberg, E. *J. Chem. Phys.* **1975**, *62*, 208.

(49)   Siebrand, W. *J. Chem. Phys.* **1967**, *46*, 440.

(50)   Beeby, A.; Clarkson, I. M.; Dickins, R. S.; Faulkner, S.; Parker, D.; Royle, L.; de Sousa, A. S.; Williams, J. A. G.; Woods, M. *J. Chem. Soc., Perkin Trans. 2* **1999**, 493.

(51)   Petoud, S.; Bünzli, J.-C. G.; Glanzman, T.; Piguet, C.; Xiang, Q.; Thummel, R. P. *J. Lumines.* **1999**, *82*, 69.

(52)   Werts, M. H. V.; Woudenberg, R. H.; Emmerink, P. G.; van Gassel, R.; Hofstraat, J. W.; Verhoeven, J. W. *Angew. Chem., Int. Ed.* **2000**, *39*, 4542.

(53)   Klink, S. I.; Alink, P. O.; Grave, L.; Peters, F. G. A.; Hofstraat, J. W.; Geurts, F.; van Veggel, F. C. J. M. *J. Chem. Soc., Perkin Trans. 2* **2001**, 363.

(54)   Ziessel, R. F.; Ulrich, G.; Charbonniere, L.; Imbert, D.; Scopelliti, R.; Bünzli, J.-C. G. *Chem.-Eur. J.* **2006**, *12*, 5060.

(55)   Pope, S. J. A.; Coe, B. J.; Faulkner, S.; Bichenkova, E. V.; Yu, X.; Douglas, K. T. *J. Am. Chem. Soc.* **2004**, *126*, 9490.

(56)   Koullourou, T.; Natrajan, L. S.; Bhavsar, H.; Pope, S. J. A.; Feng, J.; Narvainen, J.; Shaw, R.; Scales, E.; Kauppinen, R.; Kenwright, A. M.; Faulkner, S. *J. Am. Chem. Soc.* **2008**, *130*, 2178.

(57)   Klink, S. I.; Keizer, H.; van Veggel, F. C. J. M. *Angew. Chem., Int. Ed.* **2000**, *39*, 4319.

(58)   Hasegawa, Y.; Ohkubo, T.; Sogabe, K.; Kawamura, Y.; Wada, Y.; Nakashima, N.; Yanagida, S. *Angew. Chem., Int. Ed.* **2000**, *39*, 357.

(59)   Mancino, G.; Ferguson, A. J.; Beeby, A.; Long, N. J.; Jones, T. S. *J. Am. Chem. Soc.* **2005**, *127*, 524.

(60)   Goncalves e Silva, F. R.; Malta, O. L.; Reinhard, C.; Güdel, H.-U.; Piguet, C.; Moser, J. E.; Bünzli, J.-C. G. *J. Phys. Chem. A* **2002**, *106*, 1670.

(61)   Albrecht, M.; Osetska, O.; Froehlich, R.; Bünzli, J.-C. G.; Aebischer, A.; Gumy, F.; Hamacek, J. *J. Am. Chem. Soc.* **2007**, *129*, 14178.

(62)   He, H.; Guo, J.; Zhao, Z.; Wong, W.-K.; Wong, W.-Y.; Lo, W.-K.; Li, K.-F.; Luo, L.; Cheah, K.-W. *Eur. J. Inorg. Chem.* **2004**, 837.

(63)   Foley, T. J.; Harrison, B. S.; Knefely, A. S.; Abboud, K. A.; Reynolds, J. R.; Schanze, K. S.; Boncella, J. M. *Inorg. Chem.* **2003**, *42*, 5023.

(64)   Shavaleev, N. M.; Moorcraft, L. P.; Pope, S. J. A.; Bell, Z. R.; Faulkner, S.; Ward, M. D. *Chem. Commun.* **2003**, 1134.

(65)   Davies, G. M.; Aarons, R. J.; Motson, G. R.; Jeffery, J. C.; Adams, H.; Faulkner, S.; Ward, M. D. *J. Chem. Soc., Dalton Trans.* **2004**, 1136.

2.0 SYNTHESIS, STRUCTURAL AND NEAR-INFRARED EMITTING PROPERTIES OF LANTHANIDE COMPLEXES FORMED WITH TROPOLONATE LIGANDS

Part of this chapter has been published as Zhang, J.; Badger, P. D.; Geib, S. J.; Petoud, S. *Angew. Chem., Int. Ed.* **2005**, 44, 2508 and Zhang, J.; Badger, P. D.; Geib, S. J.; Petoud, S. *Inorg. Chem.* **2007**, 6473.

As discussed in Chapter 1, to develop highly luminescent lanthanide complexes, lanthanide cations must be well-protected by the ligand(s) from nonradiative deactivations.[1] The ligand(s) must provide eight to ten coordination numbers to satisfy the requirement of Ln^{3+} in solution. Either a multidentate ligand (e.g. DPTA) or several bidentate/tridentate ligands could be used.[2] In addition, given the hard Lewis acid character of Ln^{3+}, it is more favorable to use hard Lewis base ligands, best being oxygen donor ligands, to form strong bonds between the metal cations and the ligand(s). Lastly, from an energy transfer point of view, the energy of the triplet state of the ligand should match the excited energy level of Ln^{3+}.

Ligands incorporating conventional chelators (8-hydroxyquinoline,[3,4] β-diketone,[5,6] bipyridine[7] etc), organic fluorescent dyes,[8] luminescent ruthenium bipyridine complexes,[9,10] and porphyrins[11,12] have been used as the sensitizer for NIR luminescent lanthanide complexes. Most molecules reported so far have limited luminescence output owing to low efficiency of intramolecular ligand-to-Ln^{3+} energy transfer and/or insufficient protection of Ln^{3+} against

nonradiative deactivation processes. To develop NIR luminescent complexes with better quantum yields, it is necessary to investigate other ligand systems. Furthermore, the sensitization of other lanthanide cations, such as Ho^{3+} or Tm^{3+}, is of high interest as supplementary emission wavelengths would then be also available for use in multiplex assay.

Tropolone (2-hydroxycyclohepta-2,4,6-trienone) and its derivatives have been studied in various fields such as medicinal and material sciences because of their biological activities[13] and their ability to form metallomesogens,[14,15] respectively. Tropolone derivatives have also been used as dynamic molecular systems for intramolecular proton tunneling[16,17] and proton transfer due to their structural tautomerism.[18] All these properties result from the molecular and electronic structure of the tropolone, a seven-membered nonbenzenoid aromatic ring compound. Its pK_a value of 6.7[19] allows for complete deprotonation at physiological conditions. Like the benzenoid catecholato ligand,[20-22] tropolone is a versatile bidentate chelating agent, suitable as a chelating group for d-block and f-block metal ions. It is considered that tropolone could be different with the other conventional ligands because of its seven-membered ring system.

In most tropolonate metal complexes, the deprotonated hydroxyl group and the carbonyl oxygen are involved in the coordination to the metal ion, resulting in a bidentate complex (Figure 2.1). This forms a thermodynamically favored five-membered chelating ring. Muetterties et al. were among the first to study tropolonate lanthanide coordination complexes.[23] They pointed out that compact shape, skeletal rigidity, and small bite angle of tropolonate make it a very suitable ligand for complexes with high coordination number. Using specific synthetic conditions, they were able to control the nature of two types of complexes (ML_3 and ML_4 formula). Three types of counterions have been described for the ML_4 systems: Na^+, Li^+, and NH_4^+. The molecular formulas of these complexes were obtained from elemental analysis since it was a common

technique available at that time. Information on the coordination geometry of the cation in these lanthanide complexes was not available since they had not been analyzed by X-ray crystallography.
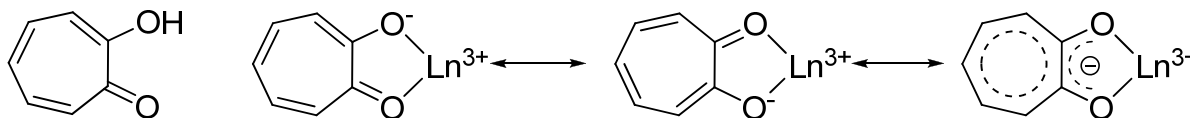
Figure 2.1: Structure of tropolone and its coordination mode in Ln^{3+} complexes

One of the main reasons of our interest for tropolonate ligand is that the tropolonate has a favorable electronic structure to act as an antenna because the energy of its triplet state (16,800 cm^{-1})[36] is compatible for efficient energy transfer to the low accepting levels of several Ln^{3+} that emit in the NIR.[7,12,24-25] Through the choice of the appropriate counterions and synthetic conditions, we were able to reproducibly prepare complexes with the ML_4 stoichiometry, and for the first time, the structure of seven different lanthanide complexes were isolated and analyzed. Through X-ray crystal analysis, we have been able to systematically compare the solid-state structures of these seven complexes. It is important to note that there are few reported examples of crystallographically characterized lanthanide complexes formed with the same ligand coordinating a series of Ln^{3+}.[46,47] The solid-state structural analysis was completed by the investigation of the complex species formed in solution through absorption spectrophotometric titrations, electrospray ionization mass spectroscopy, NMR, and luminescence techniques. The results of this investigation indicated that the coordination around Ln^{3+} is different in solution and in the solid state. More importantly, it is found that tropolonate is an excellent sensitizer for several NIR emitting Ln^{3+}, such as Yb^{3+}, Nd^{3+}, Er^{3+}, Ho^{3+}, and Tm^{3+}.

2.1   EXPERIMENTAL SECTION

2.1.1   Materials

All reagents were used as received, unless otherwise stated. Tropolone, $LnCl_3 \cdot nH_2O$ (Ln = La, Nd, Eu, Gd, Er, and Yb, 99.9% or 99.99%, n = 6 or 7), $YCl_3 \cdot 6H_2O$ (99.99%), and KOH standard solution in methanol (0.103 M) were purchased from Aldrich. $LnCl_3 \cdot nH_2O$ (Ln = Pr, Sm, Tb, Dy, Ho, Tm, and Lu, 99.9% or 99.99%, n = 6 or 7) were purchased from Strem Chemicals. All deuterated NMR solvents were purchased from Cambridge Isotope Labs and used as received.

2.1.2   Methods

Infrared spectra were recorded on a Perkin-Elmer Spectrum BX FT-IR instrument. Elemental analyses were performed by Atlantic Microlab, Inc. (Norcross, GA). ^{1}H NMR spectra were recorded on a Bruker DPX-300 spectrometer at 300 MHz. MS-ESI were measured on an Agilent HP 1100 series LC-MSD instrument. UV-vis absorption spectra were recorded on a Perkin-Elmer Lambda 9 spectrophotometer.

2.1.3   Spectrophotometric titrations

Spectrophotometric titrations were performed with a Perkin-Elmer Lambda 9 spectrophotometer connected to an external computer. All titrations were performed in a thermostated (25.0 ± 0.1 °C) cuvette in DMSO at constant ionic strength μ = 0.01 M (tetrabutylammonium perchlorate). In a typical experiment, 2.00 mL of a ligand (potassium tropolonate) solution in DMSO (initial total

ligand concentration 5×10^{-5} M) was titrated with lanthanide chloride solutions in DMSO (stock solution concentration: 1×10^{-4} M). After each addition of the lanthanide salt solution, the UV-vis spectrum the solution was measured. Factor analysis and mathematical treatment of the spectrophotometric data were performed with the SPECFIT program.[37]

2.1.4 Luminescence measurements

Emission and excitation spectra were measured using a Jobin Yvon Horiba Fluorolog-322 spectrofluorometer equipped with a Hamamatsu R928 detector for the visible domain and an Electro-Optical Systems, Inc. DSS-IGA020L detector for the NIR domain. The NIR luminescence quantum yields were measured by using the $^4G_{5/2}\rightarrow{}^6H_{9/2}$ transition of a Sm(2-hydroxyisophthalamide macrobicycle) previously reported ($\Phi = 7.3\times10^{-4}$) as reference.[81] The use of a Sm^{3+} complex allows for a simple method of cross calibrating the visible detector with the NIR detector of the Fluorolog-322. Spectra were corrected for the instrumental function for both excitation and emission. Values were calculated using the following equation:

$$\frac{\Phi_x}{\Phi_r} = \frac{A_{r_{\lambda_x}}}{A_{x_{\lambda_x}}} \frac{I_{\lambda_r}}{I_{\lambda_x}} \frac{\eta_x^2}{\eta_r^2} \frac{D_x}{D_r},$$ where subscript r stands for the reference and x for the sample; A is the absorbance at the excitation wavelength, I is the intensity of the excitation light at the same wavelength, η is the refractive index($\eta = 1.478$ in DMSO), and D is the measured integrated luminescence intensity.

Time-resolved measurements were conducted with a Jobin Yvon Spex Fluorolog-3 spectrofluorimeter equipped with a phosphorimeter module and Xenon flash lamp. The emission spectra were then collected, with increasing delay times until the phosphorescence band was the

26

main band on a spectrum (delay time: 0.1 ms). The emission spectra were corrected for the background and instrumental function.

The luminescence lifetime measurements were performed by excitation of solutions in 1 cm quartz cells using a nitrogen laser (Oriel model 79110, wavelength 337.1 nm, pulse width at half-height 15 ns, 5-30 Hz repetition rate). Emission from the sample was collected at a right angle to the excitation beam by a 3″ plano-convex lens. Emission wavelengths were selected by means of quartz filters. The signal was monitored by a cooled photomultiplier (Hamamatsu R316) coupled to a 500 MHz bandpass digital oscilloscope (Tektronix TDS 754D). The signals (15,000 points each trace) from at least 500 flashes were collected and averaged. Background signals were similarly collected and subtracted from sample signals. Lifetimes are averages of at least three independent determinations. Data were fitted to exponential decay by Origin 7.0 data analysis software. Ligand-centered triplet state lifetimes were performed by excitation of solid samples in a quartz tube at 77 K using the nitrogen laser described previously. Emission from the samples was collected at a right angle to the excitation beam, and the emission wavelengths were selected by means of a Spex FL1005 double monochromator. The signal was monitored by a Hamamatsu R928 photomultiplier coupled to a 500 MHz bandpass digital oscilloscope (Tektronix TDS 620B). The signals (15000 points each trace) from at least 500 flashes were collected and averaged.

2.1.5   X-ray crystallography

Crystals suitable for X-ray diffraction were coated with Fluorolube® then mounted on a glass fiber and coated with epoxy cement. X-ray data were collected on a Bruker Apex diffractometer using graphite-monochromatized Mo K_α radiation (λ = 0.71073 Å). Data collection was

controlled using the Bruker SMART program, and the data processing was completed with the SHELXTL program package. Graphical representations were obtained with the help of Diamond 3.0 software packages. All hydrogen atoms were calculated and placed in idealized positions (d_{C-H} = 0.96 Å).

2.1.6   Synthesis of complexes and preparation of single crystals

To a solution of tropolone (48.8 mg, 0.04 mmol) in MeOH (10 mL) was added 3.88 mL (0.04 mmol) of a 0.103 M KOH solution in methanol with stirring. To the resulting solution was added $LnCl_3 \cdot nH_2O$ (0.01 mmol) (Ln = La, Pr, Nd, Sm, Eu, Gd, Tb, Dy, Ho, Er, Tm, Yb, and Lu) or $YCl_3 \cdot 6H_2O$ in methanol (10 mL). The solution was stirred for 3 h, and the resulting precipitate was filtered, washed three times with methanol, and dried in vacuo over P_2O_5 for 48 h. Single crystals of $KLn(Trop)_4DMF$ (Trop = $C_7H_5O_2^-$, tropolonate) were obtained from slow diffusion of diethyl ether into DMF solutions of $KLn(Trop)_4$.

2.2   RESULTS AND DISCUSSION

2.2.1   Synthesis

The lanthanide complexes were synthesized in methanol using a 1:4 (metal/ligand) stoichiometry. Tropolone ligands were deprotonated by adding 1 equiv of KOH in methanol prior to addition of lanthanide chloride salt in the reaction mixture. Muetterties et al.[23] synthesized $[Ln(Trop)_4]^-$ complexes by reacting the $Ln(Trop)_3$ complex with NaTrop or LiTrop in a mixture of methanol

and water. Our method is more straightforward and rapid: the total synthesis duration is 3 h, a significantly shorter time compared to the reaction time of the Muetterties method (15 h and 2 days for $NaLn(Trop)_4$ and $LiLn(Trop)_4$, respectively) and leads to the isolation of the potassium salt, in comparison to the sodium and lithium salt for the Muetterties method. The difference in the nature of the counterion can have a significant role in the structures of the resultant complexes, as described recently the for rare-earth quinolinate system.[33] Although the same recrystallization method was systematically used for all the lanthanide tropolonate complexes, we were only able to isolate crystals suitable for X-ray diffraction for Tb^{3+} to Lu^{3+} but not for the larger Ln^{3+}.

2.2.2 Elemental analysis and IR absorption characterization

As used previously by Muetterties,[23] the analysis of the solid material has been obtained through elemental analysis. Results (Table 2.1) indicate that complexes with the ML_4 formula have been isolated. All the complexes have been found to have K^+ as counterion for the $[Ln(Trop)_4]^-$ anion.

The IR absorption spectra of tropolone, tropolonate (as potassium salt), and all the lanthanide complexes were recorded. The results are summarized in Table 2.1. The H-bonded OH stretching vibration of tropolone is assigned to the broad band located between 3,200 and 2,500 cm^{-1}. This band is not present in the spectra of the potassium tropolonate and lanthanide complexes, providing a strong indication of a complete deprotonation of the OH group. The band around 1,620 cm^{-1} present in the tropolone spectrum was assigned to the C=O bond stretching band. Upon deprotonation, this stretching band shifts to lower energy by 13 cm^{-1}. This change can be explained by the resonance of the deprotonated tropolonate anion (Figure 2.1) which gives the C=O bond the mixed character of single and double bonds, therefore decreasing the stretching energy. Upon coordination, this vibration red-shifts by an additional 10 cm^{-1} due to a further

29

decrease of the double bond character described above, which indicates that the oxygen atom of carbonyl group is involved in the complexation of Ln^{3+}. The stretching vibrations of C-O in tropolone disappear in potassium tropolonate and lanthanide complexes because the two CO vibrations are equivalent by resonance. Crystallography data also substantiate the equivalency of these two bonds (vide infra). The bond length of C=O in tropolone is 1.261 Å. In the complexes, the average CO bond length is longer (1.278(4) Å). A similar effect was observed for the C=C stretching vibration, which appears at 1,542, 1,530, and 1,508 cm^{-1} in tropolone, potassium tropolonate, and lanthanide tropolonate, respectively.

Table 2.1: Elemental analytical and IR spectral data for all the isolated complexes

Compound	Elemental analysis (%)[a]		IR (υ_{max}/cm^{-1})[b]				
	C	H	$\upsilon_{C=O}$	$\upsilon_{C=C}$	δ_{C-H} (in plane)	δ_{C-H} (out of plane)	υ_{Ln-O}
$C_7H_6O_2$	—	—	1614	1548	1241	711	—
$C_7H_5O_2K$	—	—	1601	1530	1233	734, 716	—
$C_{28}H_{20}O_8KLa$	50.37(50.77)	3.00(3.04)	1593	1508	1221	729	481
$C_{28}H_{20}O_8KPr$	50.59(50.61)	2.98(3.03)	1592	1507	1223	731	485
$C_{28}H_{20}O_8KNd$	50.12(50.36)	3.06(3.02)	1592	1507	1225	732	487
$C_{28}H_{20}O_8KSm$	49.59(49.90)	2.94(2.99)	1591	1507	1225	733	490
$C_{28}H_{20}O_8EuK$	49.62(49.78)	2.95(2.98)	1592	1508	1226	733	492
$C_{28}H_{20}O_8GdK$	49.50(49.40)	2.89(2.96)	1592	1508	1227	734	494
$C_{28}H_{20}O_8KTb$	49.30(49.28)	2.95(2.95)	1592	1508	1227	734	495
$C_{28}H_{20}O_8DyK$	48.78(49.02)	2.92(2.94)	1592	1510	1228	735	498
$C_{28}H_{20}O_8HoK$	48.23(48.85)	2.93(2.93)	1592	1510	1229	736	499
$C_{28}H_{20}O_8ErK$	48.52(48.68)	2.86(2.92)	1592	1511	1228	737	500
$C_{28}H_{20}O_8KTm$	47.75(48.56)	2.98(2.91)	1592	1512	1229	737	502
$C_{28}H_{20}O_8KYb$	48.47(48.28)	2.92(2.89)	1592	1512	1229	737	504
$C_{28}H_{20}O_8KLu$	47.87(48.15)	2.85(2.89)	1592	1512	1230	737	505
$C_{28}H_{20}O_8KY$	54.95(54.91)	3.23(3.29)	1592	1509	1229	735	500

a Data in parenthesis are theoretical values.
b The assignment was based on the previous IR results.[38,39].

The IR absorption bands of the tropolone ligand located at 1,241 and 711 cm^{-1} result from the in-plane and out-of-plane vibrations of C-H bonds, respectively.[38,39] Upon deprotonation and complexation, these C-H vibrations shift. These changes could be attributed to the change in rigidity of the tropolone ring upon coordination. The metal-oxygen bond vibration was identified in the IR spectra around 480-500 cm^{-1}. The frequency of this bond is an indication of the covalency of the M-O bond and has a higher value for heavier lanthanide cations.[40-42] This result is consistent with the previous study for lanthanide benzoates[43] and lanthanide 8-hydroxyquinoline complexes[44] for which an increase in covalency of the M-O bond in the heavier Ln^{3+} identified by IR spectroscopy were also described.

2.2.3 NMR analysis

The ^{1}H NMR spectra of tropolone, potassium tropolonate, and the diamagnetic Lu^{3+} complex KLu(Trop)$_4$ were measured in DMSO-d_6. The chemical shift data are given in Table 2.2, and the ^{1}H NMR spectra are shown in Figure 2.2.

Table 2.2: ^{1}H NMR data for tropolone, KTrop, and KLu(Trop)$_4$ in DMSO-d_6

Compounds	δ_{H3}	δ_{H1}	δ_{H2}
Tropolone	7.04 (t)	7.22 (d)	7.41 (dd)
KTrop	6.02 (t)	6.35 (d)	6.73 (dd)
KLu(Trop)$_4$	6.68 (t)	6.86 (d)	7.25 (dd)
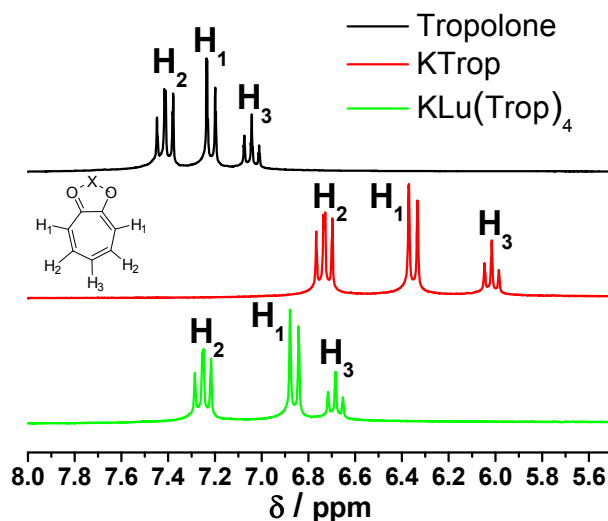
Figure 2.2: ^{1}H NMR spectra of tropolone, KTrop, and KLu(Trop)$_4$ at 298 K in DMSO-d_6

Due to the strong intramolecular hydrogen bonds present in tropolone, the proton from the OH group appears as a broad band with a chemical shift of 10.2 ppm (not shown in Figure 2.2). After deprotonation, all the ring protons in tropolone shift to higher field. A similar effect was also observed by Poh et al. in a tropolone-triethylamine system.[45] When coordinated with Lu^{3+}, proton signals are shifted back to lower field because of the electron withdrawing effect of Lu^{3+}, which decreases the electronic density on the protons.

2.2.4   Crystal structure

X-ray quality crystals have been obtained for KLn(Trop)$_4$ with Ln = Tb, Dy, Ho, Er, Tm, Yb, Lu, allowing for a systematic analysis of the structure of the complexes and of the coordination geometry around the different Ln^{3+} of the series. There are few reported examples of crystallographically characterized lanthanide complexes formed with the same ligand with a series

of Ln^{3+}. Of those few are the Ce^{3+}, Pr^{3+}, Nd^{3+}, Gd^{3+}, and Yb^{3+} complexes of the heptadentate ligand 2,2',2''- tris(salicylideneimino)triethyl-amine.[46,47]

The crystallographic data for the tropolonate complexes are summarized in Table 2.3. With the exception of the Tb^{3+} complex, all the crystal structures are isomorphous. The structure of the Yb^{3+} complex is shown in Figure 2.3 as an example. The first sphere of coordination around each Ln^{3+} is similar for all the different complexes analyzed. Each Ln^{3+} is coordinated by four bidentate tropolonate ligands, and the resulting coordination number is 8. The average Ln-O bond length in each of these complexes ranges from 2.31 to 2.37 Å, steadily decreasing from Tb^{3+} to Lu^{3+} (Figure 2.4), which can be explained by the decrease in the respective effective ionic radii of the central Ln^{3+} (1.04 Å for Tb^{3+} and 0.977 Å for Lu^{3+}, values obtained using Shannon[48] calculations for a coordination number of 8). The counterion K^+ bridges two $[Ln(Trop)_4]^-$ units being coordinated by six oxygen atoms, three from each unit of the complex, with an average K-O bond length of 2.8(1) Å. In addition, a DMF solvent molecule is coordinated to K^+ by its carbonyl oxygen atom, leading to a total coordination number of 7 for K^+ (Figure 2.5 and Figure 2.6). Through the bridging K^+, coordination polymeric chains are formed in the solid state, which have $K[Ln(Trop)_4]DMF$ as the smallest common motif for the repeated unit. Figure 2.7 shows the polymeric chain of the complexes. The average distance between the closest Ln^{3+} and K^+ cations is fairly small at 3.88(2) Å (Table 2.4).
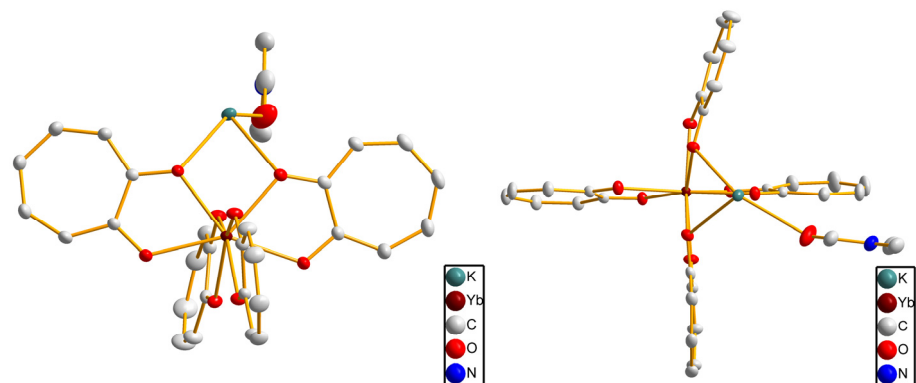
Figure 2.3: ORTEP representations of the molecular structure of K[Yb(Trop)$_4$]DMF. (50% probability ellipsoids, H

atoms have been omitted for clarity)
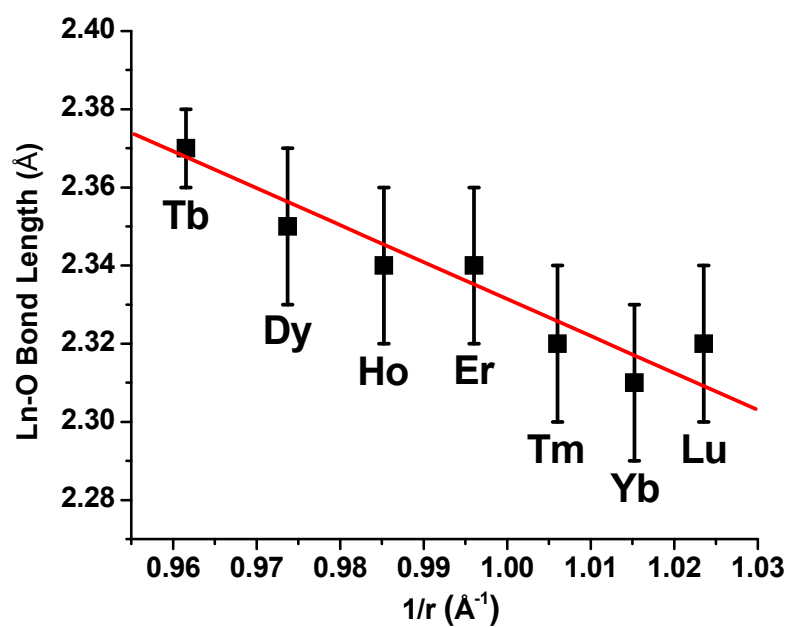
Figure 2.4: Ln-O bond length in K[Ln(Trop)$_4$]DMF vs. the reciprocal of the effective ionic radii of 8 coordinated

Ln^{3+}

Table 2.3: Summary of crystal data for K[Ln(Trop)$_4$]DMF (Ln = Tb, Dy, Ho, Er, Tm, Yb, Lu)

Complex	C$_{31}$H$_{27}$O$_9$KTb	C$_{31}$H$_{27}$O$_9$DyK	C$_{31}$H$_{27}$O$_9$KHo	C$_{31}$H$_{27}$O$_9$ErK	C$_{31}$H$_{27}$O$_9$KTm	C$_{31}$H$_{27}$O$_9$KYb	C$_{31}$H$_{27}$O$_9$KLu
CCDC number	252900	252901	252902	252903	252904	252899	252905
M	755.56	759.14	761.57	763.90	765.57	769.68	771.61
Space group	$P2_1/n$	P-1	P-1	P-1	P-1	P-1	P-1
a(°)	12.7566(12)	7.3048(5)	7.2622(4)	7.2758(10)	7.296(3)	7.2409(3)	7.2465(4)
b(°)	13.2771(12)	11.0879(8)	10.9440(6)	10.9867(16)	11.077(4)	10.9079(4)	10.9035(5)
c(°)	18.9393(18)	20.1174(15)	19.9951(12)	20.037(3)	20.107(7)	19.8683(7)	19.8822(10)
α(°)	90.00	79.3790(10)	80.0340(10)	79.993(3)	79.576(6)	80.0870(10)	80.1350(10)
β(°)	95.984(2)	84.2300(10)	84.0010(10)	84.103(3)	84.340(7)	84.1570(10)	84.1030(10)
γ(°)	90.00	78.8070(10)	78.8730(10)	78.941(3)	78.757(6)	78.8690(10)	78.8180(10)
V(Å^3)	3190.3(5)	1567.48(19)	1531.60(15)	1544.1(4)	1564.2(10)	1512.93(10)	1514.40(13)
Z	4	2	2	2	2	2	2
μ/mm^{-1}	2.399	2.569	2.773	2.906	3.022	3.283	3.452
T/K	295(2)	295(2)	150(2)	150(2)	150(2)	100(2)	150(2)
Data collection range, θ/deg	1.84-32.53	1.90-32.51	1.92-32.47	2.03-32.58	2.01-25.00	1.93-32.52	1.93-32.49
Reflections collected	40368	20601	13209	19971	11424	19668	19694
Independent reflections (R_{int})	11227(0.0588)	10708(0.0531)	9463(0.0211)	10444(0.0246)	5128(0.0152)	10293(0.0140)	10268(0.0577)
Data/Parameters	11227/388	10708/388	9463/388	10444/472	5128/388	10293/496	10268/388
Goodness of fit on F^2	0.941	0.861	1.083	1.096	1.004	1.272	1.035
R_1 [$I{\geq}2\sigma(I)$] [a]	0.0521	0.0342	0.0399	0.0276	0.0193	0.0209	0.0291
wR_2 [a]	0.1190	0.0666	0.0954	0.0660	0.0559	0.0544	0.0725

a $R_1 = \Sigma||F_0| - |Fc||/\Sigma|F_0|$; $wR_2 = \{\Sigma[w(||F_0|^2 - |F_c|^2|)^2]/\Sigma[w(F_0^4)]\}^{1/2}$
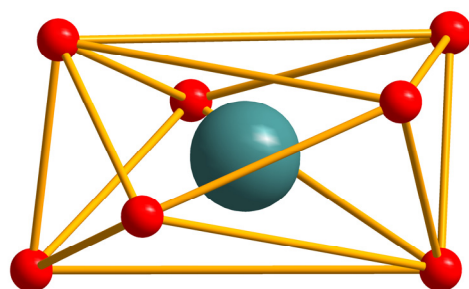
Figure 2.5: Coordination polyhedron around K$^+$ in K[Yb(Trop)$_4$]DMF
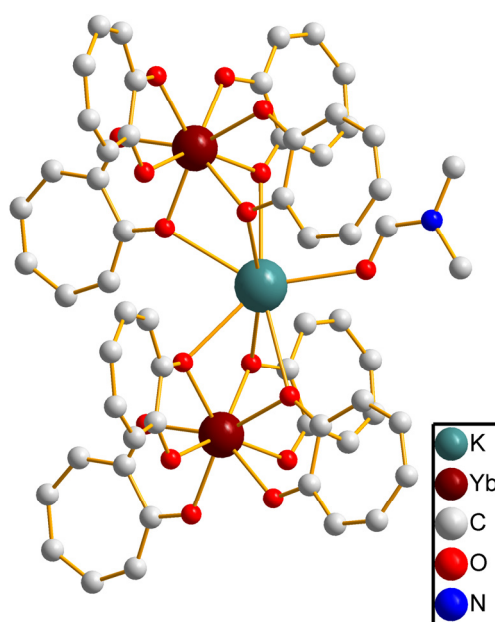
Figure 2.6: Coordination environment around K$^+$ in K[Yb(Trop)$_4$]DMF. (H atoms have been omitted for clarity)
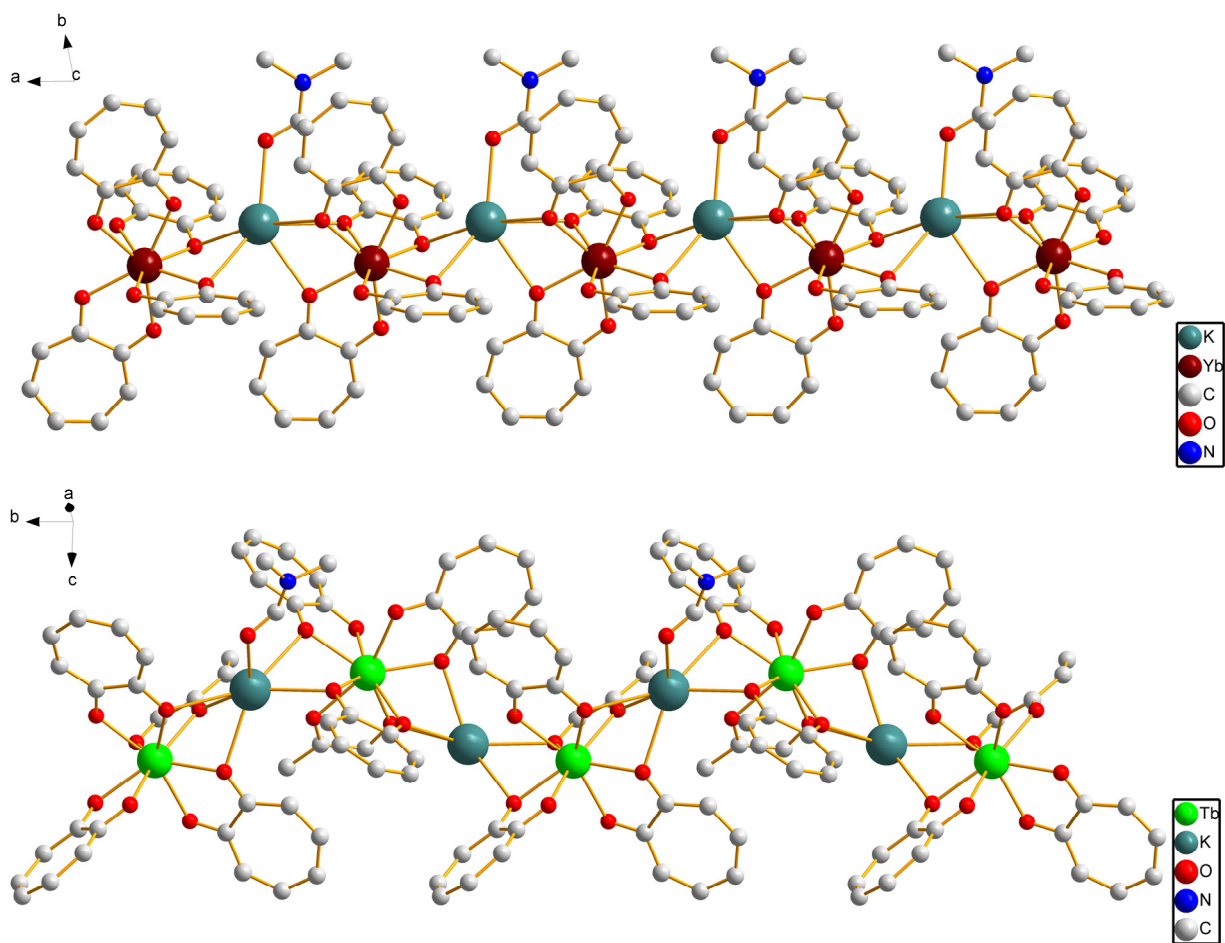
Figure 2.7: Structure of K[Yb(Trop)₄]DMF (top) and K[Tb(Trop)₄]DMF (bottom) showing the polymeric chain

Table 2.4: Selected bond lengths, Ln-K distances, and distance between tropolone rings with π-π stacking interactions in different K[Ln(Trop)₄]DMF complexes

	Tb	Dy	Ho	Er	Tm	Yb	Lu
Ln-O(Å)	2.37(1)	2.35(2)	2.34(2)	2.34(2)	2.32(2)	2.31(2)	2.32(2)
K-O(μ) (Å)	2.796	2.811	2.788	2.795	2.803	2.774	2.779
K-O(C=O) (Å)	2.784(5)	2.656(3)	2.651(4)	2.659(2)	2.650(3)	2.6464(17)	2.643(2)
Ln-Ln(Å)	7.251	7.3048(5)	7.2622(4)	7.2758(10)	7.296(3)	7.2409(3)	7.2465(4)
K-K(Å)	7.244	7.3048(5)	7.2622(4)	7.2758(10)	7.296(3)	7.2409(3)	7.2465(4)
Ln-K(Å)	3.8935(10)	3.8875(6)	3.8760(7)	3.8693(7)	3.8736(15)	3.8470(4)	3.8496(5)
Ln-K'(Å)	3.9273(10)	3.8954(6)	3.8603(7)	3.8813(6)	3.8933(13)	3.8593(4)	3.8630(5)
Distance 1(Å)ᵃ		3.3	3.3	3.3	3.3	3.3	3.2
Distance 2(Å)ᵃ		3.9	3.7	3.7	3.7	3.6	3.6

a. For π-π stacking interaction (Figure 2.9)

The main difference between the structures of the Tb^{3+} complex and the complexes formed with the other Ln^{3+} are the relative positions of Ln^{3+} vs. K^+. The views of the polymer chains for the two types of complexes are presented in Figure 2.7. Although both polymer chains have a zigzag motif for the alternating Ln···K···Ln···K···Ln sequence, their arrangements can be clearly distinguished by the relative position of K^+ with respect to the Ln···Ln···Ln sequence. In the structures of K[Ln(Trop)$_4$]DMF (Ln = Dy-Lu), K^+ are isotactic (on the same side of Ln···Ln···Ln), but in the Tb^{3+} complex, the K^+ ions are syndiotactic (located alternatively on both sides of Tb···Tb···Tb) (Figure 2.7). The difference of Ln···K···Ln···K···Ln sequences in the Tb^{3+} complex caused by the different packing mo of [Ln(Trop)$_4$]⁻ units is probably due to the larger ionic radius of the Tb^{3+}.

Hydrogen bonds and π-π stacking interactions. Although C-H···O hydrogen bonds are typically weak interactions (<12 kJ/mol), they play an important role in supramolecular chemistry and crystal packing.[49] Several types of C-H···O hydrogen bonds have been identified for all seven crystal structures. Figure 2.8 illustrates the different types of hydrogen bonds observed in the Yb^{3+} (four types, see Table 2.5) and Tb^{3+} complexes (two types, see Table 2.5). The distances and angles between the donor and acceptor atoms are reported in Table 2.5 and are all in the range of typical C-H···O hydrogen bonds.[50]

π-π stacking interactions are another type of weak interaction that can contribute to the crystal organization. There are typically two types of π-π stacking interactions: face-to-face and slipped.[41] Both of them were identified in the complexes from Dy^{3+} to Lu^{3+} complexes. As an example, in the Ho^{3+} complex, the distance between the tropolonate rings (C8-C14) in adjacent polymeric chains is 3.293 Å. The distance between the rings (C15-C21) is 3.695 Å. (Figure 2.9). Because the planes are crystallographically identical, the dihedral angles are zero. The distances in all of the complexes are listed in Table 2.4.
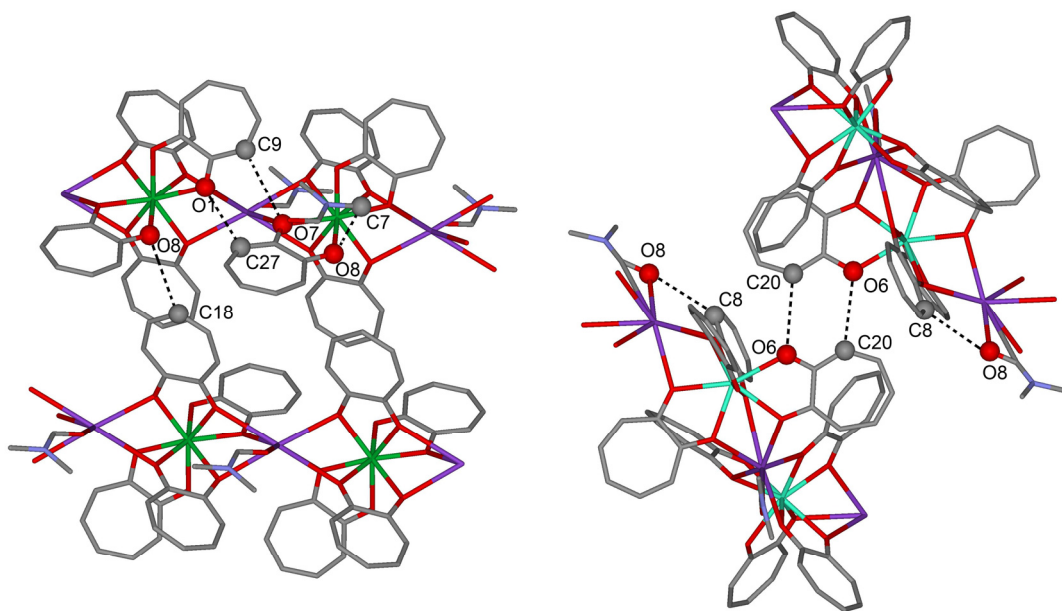
Figure 2.8: C–H···O hydrogen bonds in K[Yb(Trop)$_4$]DMF (left) and K[Tb(Trop)$_4$]DMF (right)
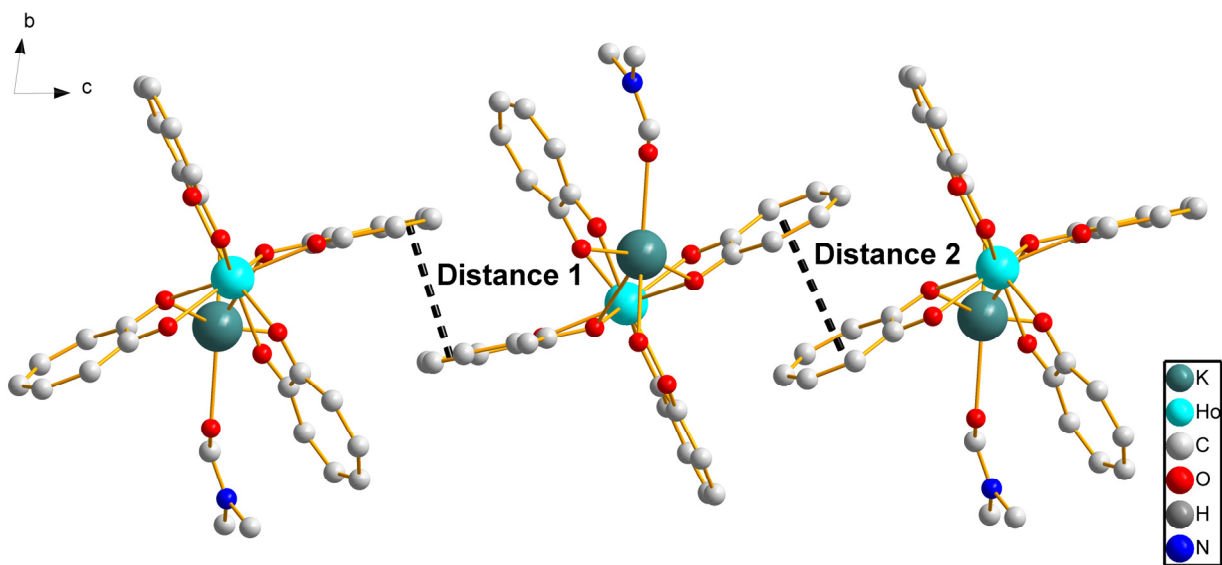
Figure 2.9: π-π interactions present in K[Ho(Trop)$_4$]DMF

39

Table 2.5: Summary of hydrogen bonds information in the K[Ln(Trop)₄]DMF

	Donor–H···Acceptor	Distance D–H (Å)	Distance H···A (Å)	Distance D···A (Å)	Angle D–H···A (°)
Tb	C(8)–H(8A) ···O(8)	0.93	2.47	3.306	149
	C(20)–H(20A) ···O(6)[a]	0.93	2.47	3.324	153
Symmetry code: a = 1-*x*, 1-*y*, 1-*z*					
Dy	C(2)–H(2A) ···O(6)[a]	0.93	2.47	3.327	153
	C(26)–H(26A) ···O(1)[b]	0.93	2.51	3.372	155
	C(42)–H(42A) ···O(9)	0.96	2.32	2.753	107
	C(43)–H(43B) ···O(2)[c]	0.96	2.57	3.460	154
Symmetry codes: a = -1+*x*, *y*, *z*; b = 1+*x*, *y*, *z*					
Ho	C(9)–H(9A) ···O(7)[a]	0.95	2.44	3.326	155
	C(18)–H(18A) ···O(8)[b]	0.95	2.51	3.338	145
	C(27)–H(27A) ···O(1)[c]	0.95	2.40	3.274	152
	C(32)–H(32A) ···O(10)	0.98	2.35	2.773	105
	C(33)–H(33C) ···O(8)[d]	0.98	2.50	3.381	150
Symmetry codes: a = 1+*x*, *y*, *z*; c = -1+*x*, *y*, *z*					
Er	C(9)–H(9A) ···O(7)[a]	0.92	2.46	3.331	158
	C(18)–H(18A) ···O(8)[b]	0.89	2.58	3.362	147
	C(27)–H(27A) ···O(1)[c]	0.91	2.42	3.285	158
	C(32)–H(32A) ···O(10)	0.98	2.36	2.785	106
	C(33)–H(33C) ···O(8)[d]	0.98	2.50	3.389	151
Symmetry codes: a = 1+*x*, *y*, *z*; c = -1+*x*, *y*, *z*					
Tm	C(12)–H(12A) ···O(6)[a]	0.95	2.47	3.339	156
	C(26)–H(26A) ···O(3)[b]	0.95	2.45	3.322	153
	C(42)–H(42A) ···O(5)[c]	0.98	2.55	3.453	153
	C(43)–H(43A) ···O(9)	0.98	2.36	2.783	106
Symmetry codes: a = -1+*x*, *y*, *z*					
Yb	C(9)–H(9) ···O(7)[a]	0.94	2.40	3.3012	160
	C(18)–H(18) ···O(8)[b]	0.92	2.52	3.3285	146
	C(27)–H(27) ···O(1)[c]	0.98	2.34	3.2596	156
	C(7)–H(7A) ···O(8)[d]	1.03	2.44	3.3605	149
Symmetry codes: a = 1+*x*, *y*, *z*					
Lu	C(2)–H(2A) ···O(6)[a]	0.95	2.39	3.2605	153
	C(26)–H(26A) ···O(1)[b]	0.95	2.41	3.2987	156
	C(34)–H(34A) ···O(2)[c]	0.95	2.52	3.3282	144
	C(42)–H(42A) ···O(9)	0.98	2.36	2.7891	105
	C(43)–H(43B) ···O(2)[d]	0.98	2.47	3.3589	150
Symmetry codes: a = -1+*x*, *y*, *z*; b = 1+*x*, *y*, *z*					

2.2.5   Geometry analysis of the complexes and of the coordination around Ln^{3+} in the solid state

Since seven crystal structures of the tropolonate complexes formed with different lanthanide cations were obtained, which has been rarely reported in the literature, we were able to collect a large amount of structural information on these complexes and to perform a systematic and comparative analysis of the coordination geometry around Ln^{3+}. In order to compare the tropolonate lanthanide complexes presented here with tropolonate complexes formed with other metal cations having a coordination number of 8, the Cambridge Structure Database (CSD) was searched and six structures were identified with the coordination motif $[M(Trop)_4]$ ($M = Zr^{4+}$, Nb^{5+}, Hf^{4+}, Sn^{4+}, Sc^{3+}).[51-56]

Evaluation of the geometry of these complexes was performed in two steps. First, the coordination polyhedron around the metal cation was identified using the analysis method from Kepert.[57] Second, the deviation of the experimental coordination polyhedron from the ideal polyhedron was quantified.

Crystallographic data show that the coordination number of the central cation in all the analyzed tropolonate lanthanide complexes is 8. A typical example of the coordination polyhedron around Ln^{3+} in $KLn(Trop)_4$ is depicted in Figure 2.10. Two different types of ideal coordination polyhedron have a minimal energy for this coordination number: square antiprism (D_{4d}) and dodecahedron (D_{2d}). For coordination complexes formed with four bidentate ligands, the normalized bite (b) value is used as quantitative criteria to attribute if the coordination geometry around Ln^{3+} is closer to a square antiprismatic or to a dodecahedral coordination geometry. Empirical relationships between the coordination geometry of tetra-bidentate complexes and their normalized bite have been put forth by Kepert.[57] The normalized bite is defined as the ratio of the distance of the two

oxygen atoms in the bidentate ligands (d_{O-O}) to the bond length of M-O (d_{M-O}): d_{O-O}/d_{M-O}.

Complexes with b < 1.1 are classified as adopting (D_{2d}) dodecahedral coordination geometries, where complexes with b values comprised between 1.15 and 1.20 possess intermediate D_2 stereochemistries. Complexes formed with bidentate ligands with b > 1.3 can be classified as having D_4 square antiprismatic coordination geometries. A theoretical model of a dodecahedron is represented in Figure 2.11. The results of these calculations for the tropolonate complexes formed with both Ln^{3+} (this work) and other metal ions are reported in Table 2.6. All the lanthanide tropolonate complexes presented here have b values between 1.07 and 1.10, which allows us to conclude, according to the Kepert criteria, that they adopt D_{2d} dodecahedral coordination geometries. For the other six tropolonate complexes formed with other metal cations, the b values fall within 1.12-1.17 and indicate the D_2 intermediate stereochemistries. In the existing literature, the coordination polyhedron observed for the Nb^{5+} and Sn^{4+} complexes were assigned to an irregular bicapped trigonal prism distorted toward a dodecahedron by their authors.[55,56]
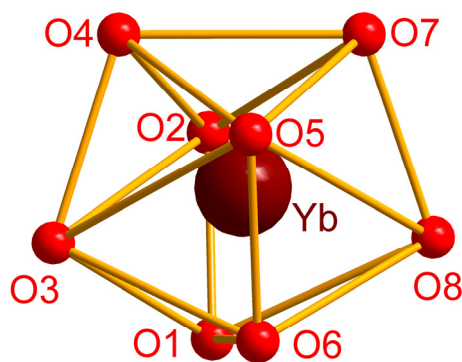
Figure 2.10: Coordination polyhedron around Yb^{3+} in [Yb(Trop)$_4$]$^-$
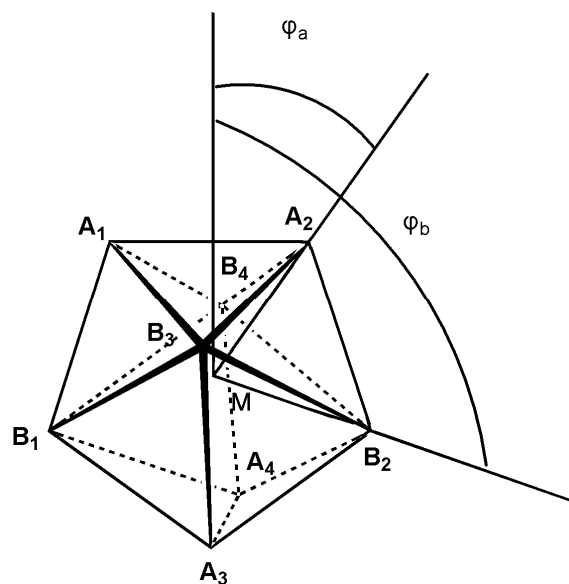
Figure 2.11: Dodecahedron model for the geometrical analysis

Table 2.6: Results of geometrical analysis of dodecahedra in M(Trop)$_4$

	Tb	Dy	Ho	Er	Tm	Yb	Lu	Sc[51]	Sc[52]	Zr[53]	Hf[54]	Sn[55]	Nb[56]	Ideal dodecahedron
φ_a (°)[a]	36	39	39	39	39	39	39	36	36	37	36	36	36	35.2
φ_b (°)[a]	101	104	105	105	105	106	105.	105	105	105	106	107	106	106.5
a[b]	1.00	0.99	1.00	0.99	0.99	0.99	0.99	1.00	1.00	1.01	1.00	1.01	1.00	1.03
θ (°)[c]	178	172	172	172	173	173	173	172	172	173	179	178	178	180
ω_i (°)[d]	0	3	3	3	9	21	3	18	9	1	2	6	4	0
	2	1	1	1	2	10	2	11	15	2	5	7	5	0
	6	7	17	5	2	2	6	6	6	3	2	20	10	0
	3	19	6	3	5	1	12	8	9	1	2	19	10	0
d_{O-O} (Å)	2.54	2.55	2.56	2.56	2.55	2.54	2.55	2.50	2.50	2.46	2.49	2.55	2.43	
d_{M-O} (Å)	2.37	2.35	2.34	2.34	2.32	2.31	2.32	2.21	2.21	2.18	2.18	2.17	2.09	
b[e]	1.07	1.08	1.09	1.09	1.10	1.10	1.10	1.13	1.13	1.12	1.14	1.17	1.16	
r_M (Å)[f]	1.04	1.027	1.015	1.004	0.994	0.985	0.977	0.87	0.87	0.84	0.83	0.81	0.74	

a. φ_a and φ_b are the average values of the angles between $\mathbf{R_1}$-$\mathbf{R_2}$ and A_i (i = 1, 2, 3, 4) and B_i (i = 1,2 3,4) respectively. The error in the angles is typically 1°.
b. a is the ratio of the bond length |M-A| to |M-B|
c. θ is the angle between $\mathbf{R_1}$ and $\mathbf{R_2}$
d. ω_i are the angles between the **Ln-O** vectors belonging to the same tropolonate ligand
e. b is the ratio between d_{O-O} and d_{M-O}
f. r_M is the effective ionic radii (calculated according to Shannon for a coordination number 8[48])

It can be observed from the comparison of the d_{O-O}, d_{M-O}, and b values, reported in Table 2.6 and shown in Figure 2.12, that there is an almost monotonous linear relationship between the d_{M-O} distances and the sizes of the metal cations; the smaller the size of central metal cation, the shorter the d_{M-O} distance. The relationship between the oxygen-oxygen distances, d_{O-O} and the size of the metal cations adopts two different regimes for lanthanides and for the other metal cations. This relationship is almost linear for Ln^{3+}. Two important changes in slopes are observed for the other cations with two abrupt changes, the slope is strongly positive from Zr^{4+} to Sn^{4+} and becomes negative from Sn^{4+} to Nb^{5+} (Figure 2.12). This indicates that parameters that control the coordination geometry around metal cations are significantly different for Ln^{3+} and other metal cations, even if they form the same type of complexes with tropolonate ligands with the same coordination numbers. This is attributed to the difference in the nature of the orbitals of these metal cations.
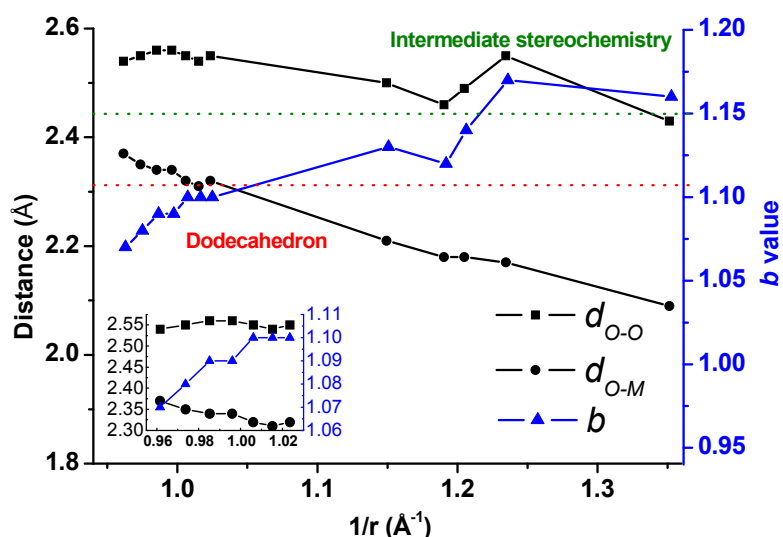
Figure 2.12: Average distances between oxygen atoms in tropolonate ligand (d_{O-O}), M-O bond lengths (d_{M-O}), and normalized bite b values for different tropolonate complexes

We have demonstrated that, according to the Kepert definition, for all the ML_4 lanthanide tropolonate complexes for which crystal structures have been isolated, Ln^{3+} adopt a dodecahedral coordination geometry. A shape analysis[82] was undertaken to quantify the level of distortion from the ideal coordination polyhedron. For each lanthanide complex analyzed, the coordination sphere around the cation has been analyzed using geometrical considerations assuming that the S_4 improper axis of rotation was maintained for all the complexes formed (Figure 2.13). Three parameters are relevant to confirm the dodecahedral shape: (i) the angle between $\mathbf{R_{M\text{-}A}}$ (vector of the M-A bond) and the S_4 axis (φ_a), (ii) the angle between $\mathbf{R_{M\text{-}B}}$ (vector of the M-B bond) and the $S4$ axis (φ_b), and (iii) the ratio, a, between bond length |M-A| and |M-B|. For an ideal dodecahedron, these three theoretical values are 35.2°, 106.5°, and 1.03, respectively. To quantify the presence of the pseudo-S_4 improper rotation axis, the sum of vectors M-A_1, M-A_2, M-B_3, and M-B_4 was defined as vector $\mathbf{R_1}$, the sum of vectors M-B_1, M-B_2, M-A_3, and M-A_4 was defined as vector $\mathbf{R_2}$, and the vector $\mathbf{R_1\text{-}R_2}$ is defined as the pseudo-S_4 axis (Figure 2.13). The angle between $\mathbf{R_1}$ and $\mathbf{R_2}$ is defined as θ. The projections of Ln^{3+} and the eight oxygen atoms of the coordination sphere onto a plane perpendicular to the $\mathbf{R_1\text{-}R_2}$ direction were then calculated. The angle, ω_i, located between the vectors Ln-O belonging to the same ligand ($\mathbf{Ln\text{-}A_i}$ and $\mathbf{Ln\text{-}B_i}$) is the direct quantification of the deformation of the pseudo-dodecahedron from its ideal geometry (ideal $\omega = 0°$). The assignments for the oxygen atom present in different complexes are shown in Table 2.7. The values for φ, θ, and ω_i are reported in Table 2.6.
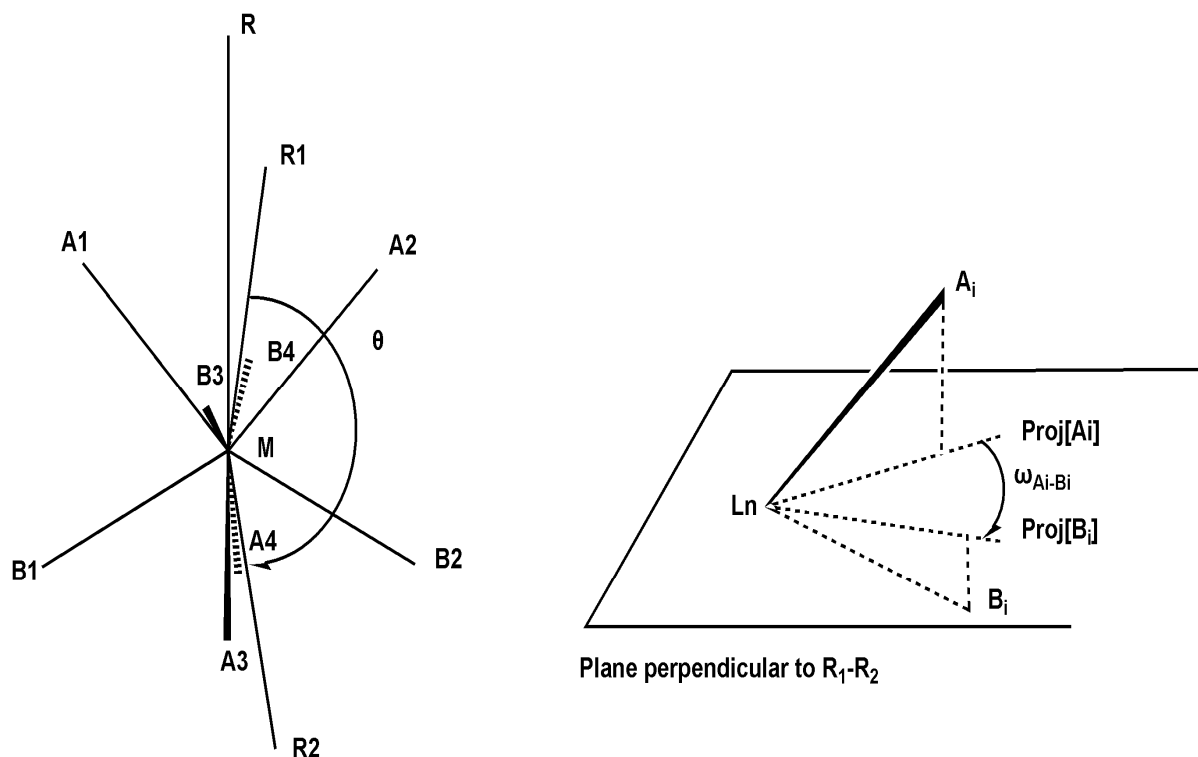
Figure 2.13: Definition of the angles and vectors used in the geometrical analysis

Table 2.7: Definition of atoms in the geometrical analysis for $KLn(Trop)_4$

	Tb	Dy	Ho	Er	Tm	Yb	Lu
A_1	O5	O6	O7	O7	O3	O7	O6
B_1	O6	O5	O8	O8	O4	O8	O5
A_2	O7	O8	O4	O4	O8	O4	O8
B_2	O8	O7	O3	O3	O7	O3	O7
A_3	O2	O4	O2	O1	O2	O1	O4
B_3	O1	O3	O1	O2	O1	O2	O3
A_4	O3	O1	O5	O6	O6	O6	O1
B_4	O4	O2	O6	O5	O5	O5	O2

It can be concluded from this treatment of the experimental data that the geometries of coordination polyhedron in the tropolonate lanthanide complexes possess some distortion relative to the ideal dodecahedron. This could be explained by the shape of the molecule in the crystal

packing, which is affected by the presence of K^+ and the DMF solvent molecule. In the crystals, K^+ is coordinated to the oxygen atoms in the deprotonated tropolonate ligands and the DMF is coordinated to K^+ (see above). This induces one of the tropolonate planes to deviate significantly from its ideal position, and as a consequence, two of the four dihedral angles deviate from the ideal values of 90°, one of the dihedral angles being larger and the other one being smaller (Table 2.8).

Table 2.8: Dihedral angles between four tropolonate planes in KLn(Trop)$_4$

	Tb	Dy	Ho	Er	Tm	Yb	Lu
Angle 1(°)	105	92.	92	92	93	92	92
Angle 2(°)	80	102	104	104	103	103	104
Angle 3(°)	96	74	72	72	74	74	72
Angle 4(°)	88	89	89	89	88.	88	89

2.2.6   Structure comparison to lanthanide complex with 1-hydroxy-2-pyridinone

Tedeschi et al.[58] recently reported the crystal structure of lanthanide complexes with 1-hydroxy-2-pyridinone (HOPO) as shown in Figure 2.14. HOPO is a cyclic hydroxamic acid, which can be used as a bidentate ligand. It is very similar to tropolone in structure, except it is six-membered ring. They prepared ML$_4$ complexes of Eu^{3+} and Gd^{3+} with HOPO.
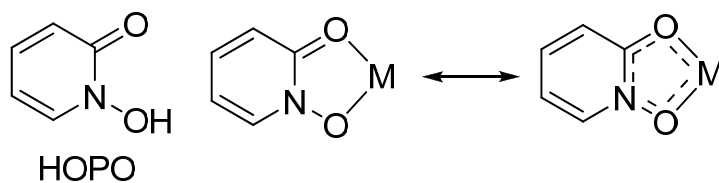
Figure 2.14: Structure of HOPO and its coordination mode with metal cation

The structure of Eu^{3+} complex with HOPO[72] is shown in Figure 2.15. There are two crystallographically unequivalent Eu^{3+} in each unit cell. Four HOPO ligands are coordinated to each Eu^{3+}, and the coordination number is eight. Using the formula mentions before, the b value can be calculated to be 1.09, which indicates that the coordination polyhedron is also best described as a dodecahedron. Na^+ was used as the counterion instead of K^+. Both of the Na^+ ions are six coordinated. Na(1) is coordinated with five oxygen atoms from HOPO, one from water. Na(2) is coordinated with four oxygen atoms, and two from water. The distance between two Eu^{3+} is 7.046 Å, which is shorter than the typical distance observed in tropolone complexes (about 7.26 Å), partially due to the smaller size of Na^+. According to Shannon's radii, six coordinated Na^+ is 1.16 Å, seven coordinated K^+ is 1.60 Å.[48]
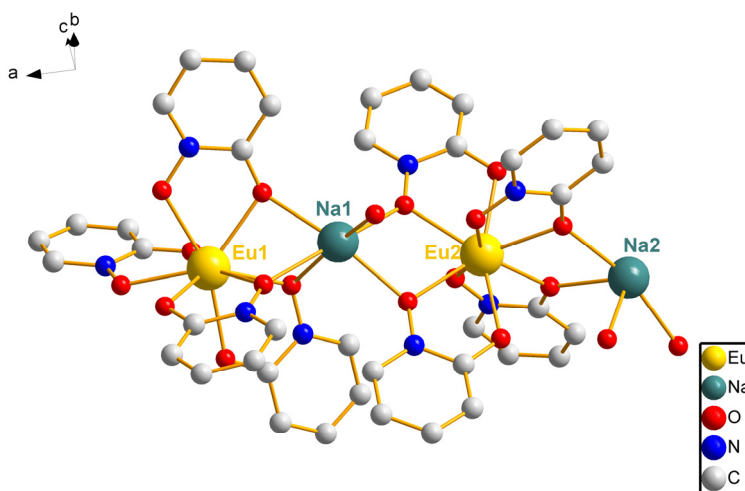
Figure 2.15: Structure of Eu^{3+} complex formed with HOPO

The average bite angles, (angle of O-M-O in bidentate ligand) are 65.7º and 66.0º for HOPO complexes of Eu^{3+} and Gd^{3+} respectively. These values are not very different with the bite angle in tropolone complexes (65.1º-67.0º). So the effect of seven-membered ring on the bite angle is very

limited. There are two types of coordination mode in both complexes of tropolonate and HOPO (Figure 2.16) for O atoms. The first type is the ligand coordinates with one Ln^{3+} and two alkaline cations. The other type is that the ligand only coordinates with one Ln^{3+} and one alkaline cation. In the crystal structure of tropolonate complexes, for every ML_4 unit, two ligands are type **a**, the other two are type b (Figure 2.7). In the HOPO complexes, for every $(ML_4)_2$ unit, only one ligand has the type **a** coordination mode, and the other seven ligands have type **b** coordination mode (Figure 2.15).
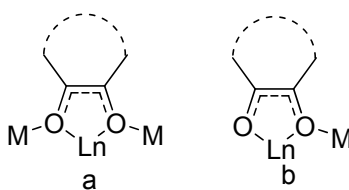
Figure 2.16: Coordination modes **a** and **b**

2.2.7   ESI-MS

Electrospray ionization mass spectra (ESI-MS) were recorded for different lanthanide complexes $KLn(Trop)_4$ (Ln = La, Pr, Nd, Sm, Eu, Gd, Tb, Dy, Ho, Er, Tm, Yb, Lu) in a mixture solvent of DMF and methanol. The results show rather similar peak patterns in both positive and negative spectra. Typical examples of spectra are depicted in Figure 2.17. The detailed results are listed in Table 2.9. In the negative ion mode spectra, the presence of the $[Ln(Trop)_4]^-$ peak (Figure 2.17) indicate the formation of ML_4 complex in solution. Other peaks were also observed on the spectra such as the free tropolonate anion with a lower abundance whose presence can be attributed to the partial dissociation of the ML_4 complex in the chosen experimental conditions. It is important to notice that the ML_3 species cannot be detected in this experiment because it is not ionized. In the

positive ion mode spectra, several types of ions were observed: $[Ln(Trop)_2]^+$, $[Ln(Trop)_2+DMF]^+$, $[Ln(Trop)_3+Na]^+$, $[Ln(Trop)_3+K]^+$, $[Ln(Trop)_4+2Na]^+$, $[Ln(Trop)_4+Na+K]^+$, and $[Ln(Trop)_4+2K]^+$. In addition, the signal of di- and trinuclear species such as $[Ln_2(Trop)_5]^+$, $[Ln_2(Trop)_6+Na]^+$, $[Ln_2(Trop)_6+K]^+$, $[Ln_3(Trop)_8]^+$, $[Ln_3(Trop)_9+Na]^+$, and $[Ln_3(Trop)_9+K]^+$ were also detected. Selected spectra for the different species are shown in Figure 2.18. This may indicate that there is significant interaction between the $Ln(Trop)_n$ units when the $KLn(Trop)_4$ complex is present at high concentration (10^{-3} M). Other phenomena such as fragmentation, ligand exchange, and clustering reactions during the mass spectral experiments could also account for the diverse ionic species observed. Tedeschi et al.[58] also observed a polynuclear pattern of peaks in ESI-MS with the 1,2-HOPO lanthanide complexes that they studied. Analysis obtained from spectrophotometric titrations (vide infra) did not indicate the presence of di- and trinuclear species.
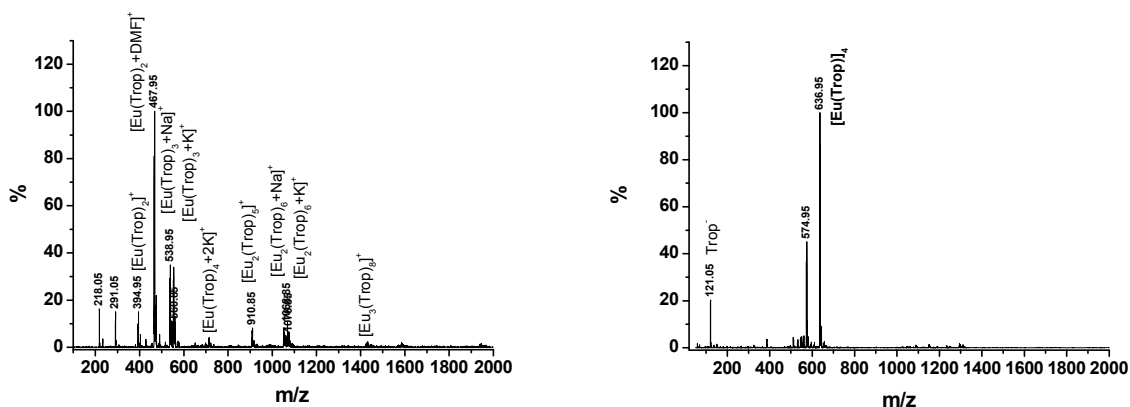
Figure 2.17: ESI-MS spectra of $KEu(Trop)_4$
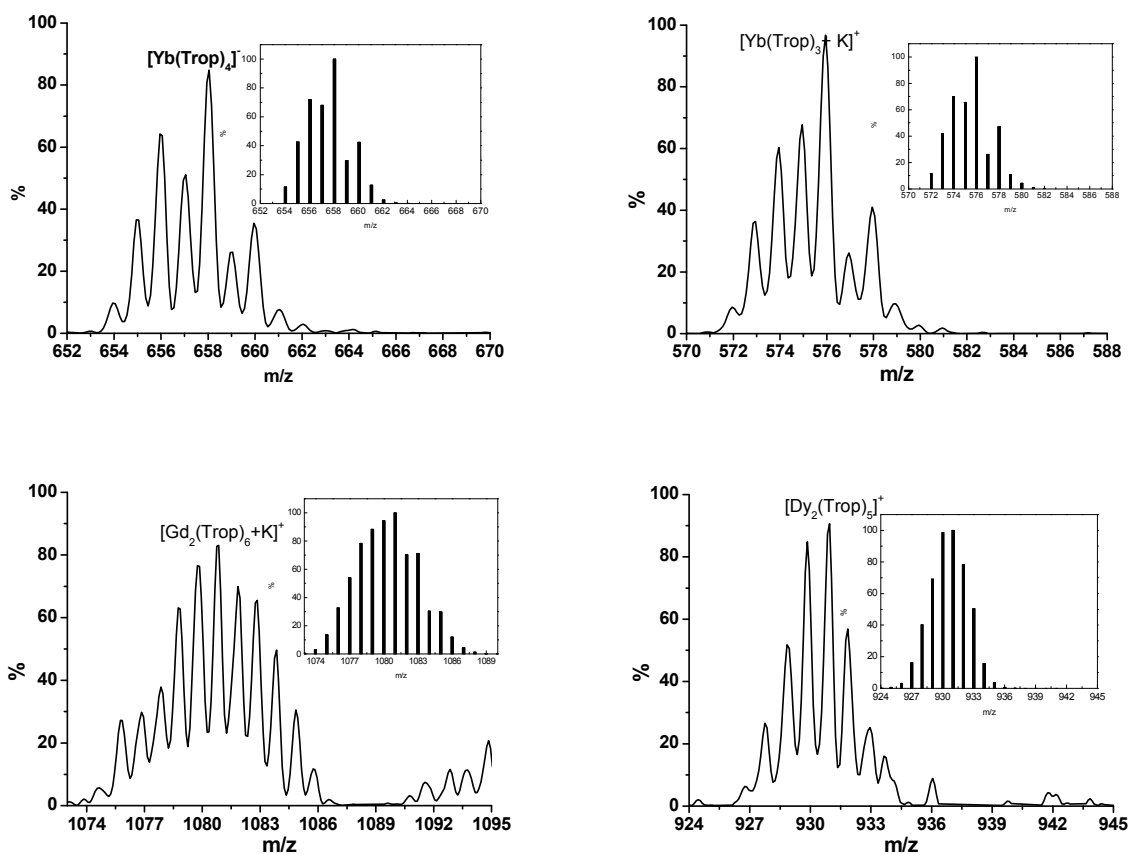
Figure 2.18: Selected ESI-MS peak patterns obtained for different tropolonate complexes

2.2.8   Spectrophotometric titration

To determine the number and nature of species formed in solution and the corresponding stability constants for the lanthanide tropolonate complexes, spectrophotometric titrations were performed for La^{3+}, Nd^{3+}, Sm^{3+}, Gd^{3+}, Ho^{3+}, Er^{3+}, Yb^{3+}, and Lu^{3+}. A typical example of experimental data for the titration of the Yb^{3+} complex is depicted in Figure 2.19. In this experiment, the lanthanide salt is added to a solution of deprotonated ligand (potassium tropolonate).

	[Ln(Trop)$_2$]$^+$	[Ln(Trop)$_2$+DMF]$^+$	[Ln(Trop)$_3$+Na]$^+$	[Ln(Trop)$_3$+K]$^+$	[Ln(Trop)$_4$+2Na]$^+$	[Ln(Trop)$_4$+Na+K]$^+$	[Ln(Trop)$_4$+2K]$^+$	[Ln$_2$(Trop)$_5$]$^-$	[Ln$_2$(Trop)$_6$+Na]$^+$	[Ln$_2$(Trop)$_6$+K]$^+$	[Ln$_3$(Trop)$_8$]$^+$	[Ln$_3$(Trop)$_9$+Na]$^+$	[Ln$_3$(Trop)$_9$+K]$^+$	[Ln(Trop)$_4$]$^-$
La	381	454	525	541			701	883	1027	1043	1385		1545	623
Pr	383	456	527	543			703	887	1031	1047	1391			625
Nd	384	457	530	546			706	893		1053	1400		1560	628
Sm	394	467	538	554		698	714	906	1050	1066	1421		1581	636
Eu	395	468	539	555		699	715	909	1053	1069	1425		1585	637
Gd	400	473	544	560		704	720	921	1065	1081	1441	1585	1601	642
Tb	401	474	545	561		705	721	923	1067	1083	1445		1605	643
Dy	406	479	550	566	694	710	726	931	1075	1091	1457	1601	1617	648
Ho	407	480	551	567	695	711	727	935	1079	1095				649
Er		481	554	570		714	730	939	1083	1099	1470	1614	1630	652
Tm	411	484	555	571				943	1087	1103	1475	1619	1635	653
Yb	416	489	560	576	704	720	736	951	1095	1111	1488	1631	1648	658
Lu	417	490	561	577	705	721	737	955	1099	1115	1493	1637	1653	659
Y	331	404	475	491			651	783	927	943	1235	1379	1395	573
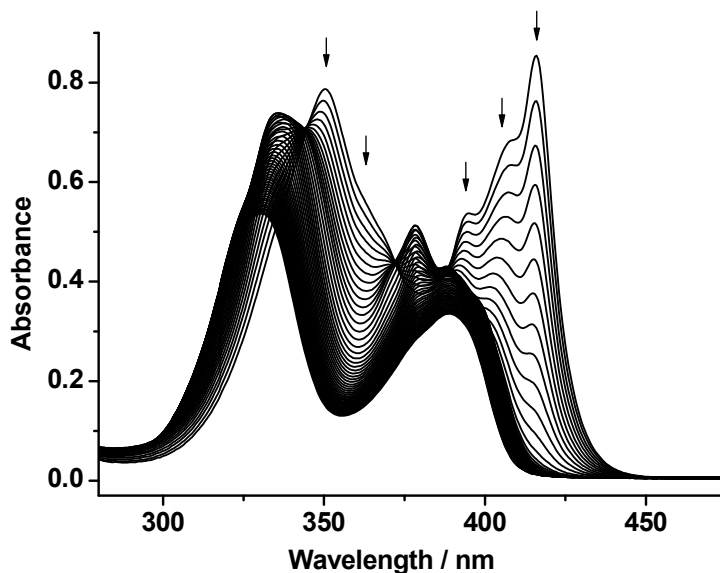
Figure 2.19: Example of absorption spectra collected during a spectrophotometric titration of Trop$^-$ solution with Yb^{3+} in DMSO, arrows indicate continuous changes in signal (upon the addition of Yb^{3+})

Factor analysis indicated the presence of five independent colored species in the solution (Figure 2.20). For each Ln^{3+}, experimental data were successfully fitted with a model where four

complexes are successfully formed in solution: ML, ML$_2$, ML$_3$, and ML$_4$ (this model is compatible with the factor analysis results). Stability constants for ML$_3$ and ML$_4$ were obtained on the basis of this model (Table 2.10) at the condition of fixing the values of log K_1 and log K_2 to values larger than 9.[60] This can be explained by the relatively high stability of the ML$_1$ and ML$_2$ complexes in solution. At the concentrations in which the experiments were conducted, insufficient information on these species is present to allow for accurate calculation with the Specfit software.

Table 2.10: Calculated formation constants for Ln(Trop)$_3$ and [Ln(Trop)$_4$]$^-$ complexes

	La	Nd	Sm	Gd	Ho	Er	Yb	Lu
Log K_3	5.6(3)	5.7(3)	5.7(3)	5.6(3)	6.0(3)	5.9(3)	6.02(3)	6.1(3)
Log K_4	4.8(3)	4.8(3)	4.5(3)	4.7(3)	4.8(3)	4.8(3)	4.4(3)	4.5(3)

The calculated formation constant of ML$_3$ and ML$_4$ shows different trends that depend on the size of Ln^{3+} (eight coordinated[48]) (Figure 2.21). Log K_3 increases as the size of Ln^{3+} decreases. This is the typical trend observed for Ln^{3+} where no steric hindrance is present between ligands upon complex formation, as the interaction between Ln^{3+} and the ligand is mainly electrostatic.[60] The strength of this interaction increases with the atomic number of Ln^{3+}. As the atomic number increases, the charge density on Ln^{3+} increases, leading to larger log K_3 values. log K_4 values for the different Ln^{3+} of the series show a different trend by steadily decreasing as the size of Ln^{3+} decreases. This can be explained by the steric hindrance generated between the four ligands when ML$_4$ is formed. This steric hindrance increases with smaller Ln^{3+} since the ligands must be located at closer proximity when the effective radii of Ln^{3+} decrease.
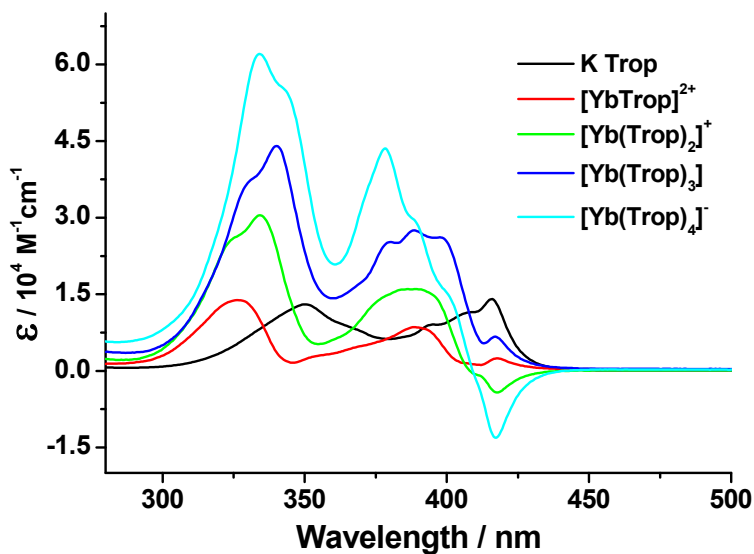
Figure 2.20: Calculated absorption spectra (Specfit software) of five components in solution

Unlike preorganized tridentate ligands such as substituted bis(benzimidazolyl)pyridines[60] and N_4O_3 tripodal aminephenol ligands,[61] bidentate tropolonate ligands do not induce a size-discrimination effect (size selectivity) based on the size of Ln^{3+} upon formation of the ML_4 complexes. This can be explained by the lack of ligand preorganization. For example, three bis(benzimidazolyl)pyridine ligands[60] form ML_3 complexes with Ln^{3+} wrapping around the central cation and forming a cavity with a specific size to accommodate Ln^{3+}. Tropolonate is only a bidentate ligand with a lower level of preorganization, which may explain the steady decrease of the stability with the decrease of the size of the metal cation instead of observing a peak of size selectivity.
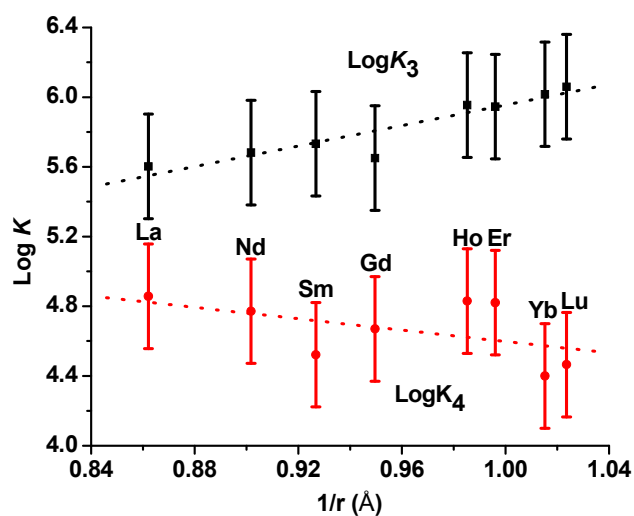
Figure 2.21 Plot of the calculated values of log K_3 and log K_4 obtained from Specfit vs. the reciprocal of the Shannon's effective ionic radii of Ln^{3+}

In summary, these measurements have demonstrated that the tropolonate ligands react with all the lanthanide cations of the series to form ML_1, ML_2, ML_3, and ML_4 complexes successively. The ML_4 species that has been observed in the solid state from the X-ray diffraction experiments is also formed in solution under specific conditions (mainly stoichiometry and concentration).

2.2.9   Absorption and excitation spectra

The absorption and excitation spectra of the Yb^{3+} complex are depicted in Figure 2.22. These spectra are representative for the absorption and excitation spectra of all of the luminescent lanthanide complexes. The resemblance of the excitation spectra with the absorption spectra provides evidence that the metal emission is sensitized through the ligand.
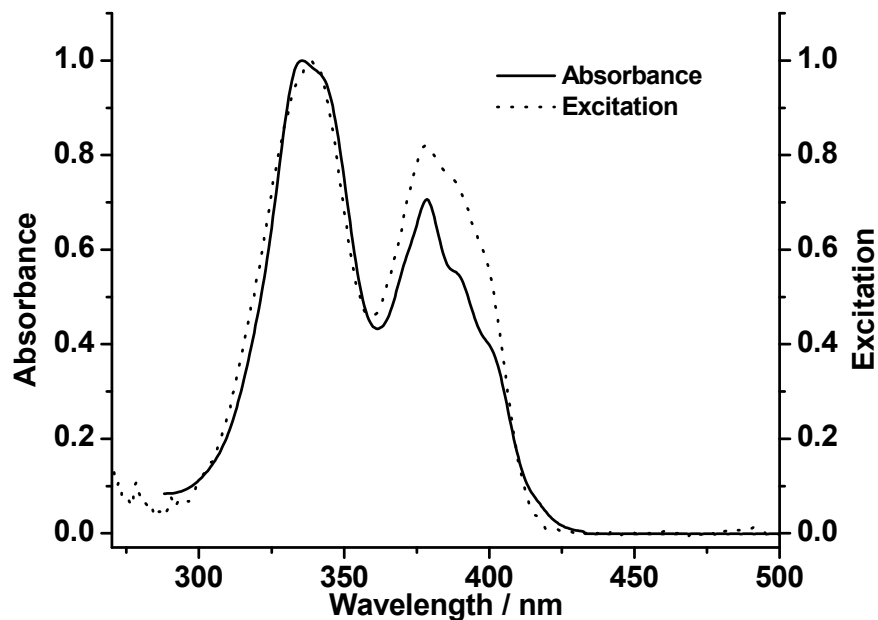
Figure 2.22: Normalized absorption and excitation spectra of [Yb(Trop)$_4$]$^-$ (10^{-5} M in DMSO, λ_{em} = 977 nm)

Upon formation of the corresponding ML$_4$ complexes, several Ln^{3+} could be sensitized through the tropolonate ligands (Figure 2.23). Corresponding with ligand-to-Ln^{3+} energy transfer, the intensity of the fluorescence decreased for the tropolonate ligand which is centered in the visible region at 425 nm, while the luminescence of the corresponding Ln^{3+} appeared as sharp emission lines in the NIR range. For the Nd^{3+} complex, emission bands were observed at 897, 1056, and 1331 nm and are attributed to the $^4F_{3/2} \rightarrow ^4I_{9/2}$, $^4F_{3/2} \rightarrow ^4I_{11/2}$, and $^4F_{3/2} \rightarrow ^4I_{13/2}$ transitions respectively. For the Yb^{3+} complex, there is only one emission band affected by crystal-field splitting which is assigned to the $^2F_{5/2} \rightarrow ^2F_{7/2}$ transition. An observed emission band at 1524 nm is attributed to the $^4I_{13/2} \rightarrow ^4I_{15/2}$ transition for Er^{3+}.
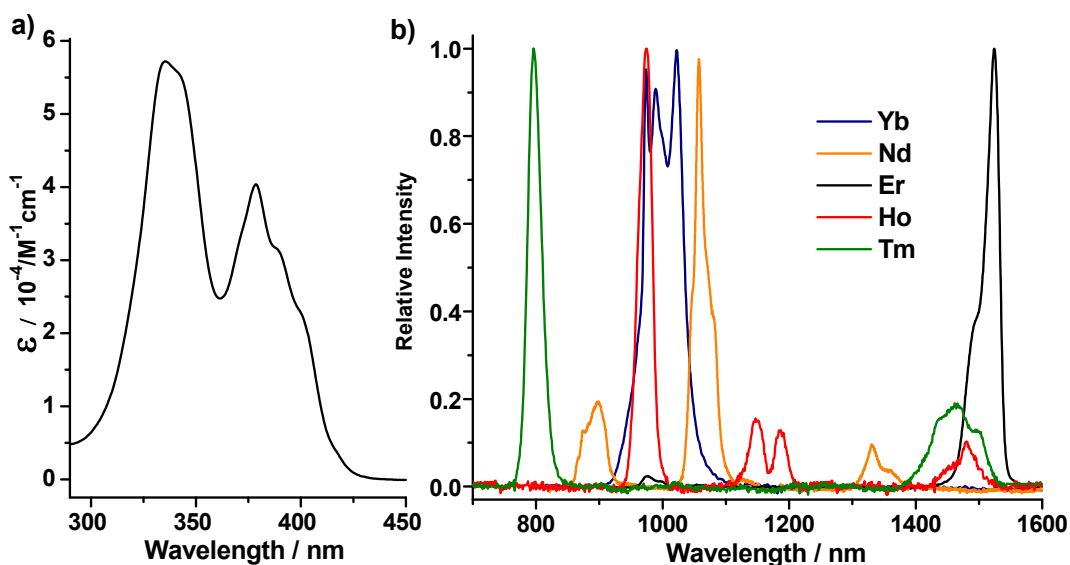
Figure 2.23: a) Absorption spectrum of [Yb(Trop)$_4$]$^-$ and b) normalized emission spectra of [Ln(Trop)$_4$]$^-$ with Ln = Yb, Nd, Er, Ho, and Tm (10^{-5} M in DMSO, λ_{ex} = 340 nm, 298 K)

To the best of our knowledge, the emission of a Ho^{3+} complex in solution is reported here for the first time. Four emission bands were observed. The emission bands at 975 and 1479 nm are assigned to $^5F_5 \rightarrow {}^5I_7$ and $^5F_5 \rightarrow {}^5I_6$ transitions respectively. The emission bands at 1148 and 1187 nm are assigned to the same $^5I_6 \rightarrow {}^5I_8$ transition split into two components. Ho^{3+} luminescence has been observed and studied in the solid state (inorganic crystals and glasses). Reisfeld et al.[62] studied luminescence of Ho^{3+} in barium zirconium fluoride glass at room temperature. A series of transitions from 383 nm to 991 nm were reported. Recently, Stouwdam et al.[63] synthesized and studied the luminescent properties of Ho^{3+} doped LaF$_3$ nanoparticles which are dispersible in organic solvent. They observed two Ho^{3+} NIR transition: $^5F_5 \rightarrow {}^5I_7$ and $^5I_6 \rightarrow {}^5I_8$. Zang et al.[64] reported the photoluminescence and electroluminescence of a Ho^{3+} organic complex in solid film. To our best of knowledge, our result is the first observation of a discrete luminescence of a Ho^{3+} complex in non-anhydrous solution. There is one visible emission band at 651 nm

57

($^5F_5 \rightarrow {}^5I_8$), which can be observed using both VIS and NIR detector by our fluorimeter. (Figure 2.24)
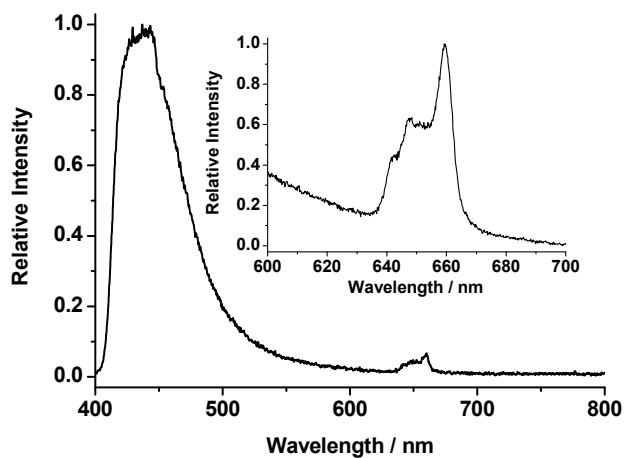
Figure 2.24: Uncorrected luminescence spectra of [Ho(Trop)$_4$]$^-$ measured by the visible detector of the fluorimeter (inset: measured by NIR detector) (10^{-5} M in DMSO, λ_{ex} = 340 nm, 298 K)

The emission bands of the Tm^{3+} complex observed at 796 and 1465 nm are assigned to $^3F_4 \rightarrow {}^3H_6$ and $^3F_4 \rightarrow {}^3H_4$ transitions respectively. In contrast to Ho^{3+}, the luminescence of Tm^{3+} complexes in solution has been described previously. Sharma et al.[65] described the transitions of Tm^{3+} from a β-diketone complexes. Although low in intensity, transition $^3F_4 \rightarrow {}^3H_6$ around 790 nm was observed. Meshkova et al.[66] obtained comparable results. Reinhard et al.[62] studied the high resolution luminescence spectra of a Tm^{3+} complex of 2,6-pyridine-dicarboxylate in single crystals at 15 K. Recently, Li et al.[67] reported the electroluminescence of a β-diketone complex of Tm^{3+}. Two NIR transitions of Tm^{3+} were observed. Our result is consistent with the previous work.

The ligand-centered emission does not completely disappear when Ln^{3+} is added. This indicates that the ligand-to-Ln^{3+} energy transfer process is not complete and the further optimization is possible.

The fact that the tropolonate ion can sensitize not only Yb^{3+}, Nd^{3+}, and Er^{3+} but also Ho^{3+} and Tm^{3+} indicates that it is a very promising and versatile sensitizer for Ln^{3+} that have acceptor levels located at relatively low energies. The narrow emission bands of Ln^{3+} allow the simultaneous detection of several Ln^{3+} during the same experiment by using a single excitation wavelength, a useful feature for multiplex assays.

To quantify the intramolecular ligand-to-Ln^{3+} energy transfer as well as quenching processes that take place in the different lanthanide complexes, luminescence quantum yields upon ligand excitation were measured in various solvents (Table 2.11). Quantum yield values reported for the Yb^{3+} complex compare well to those reported for other Yb^{3+} complexes and are among the highest values.[12,29,30,68-71] There is a significant difference between measurements made in deuterated and non-deuterated solvents, which indicates the presence of a non-radiative deactivation process. This dependency on the nature of the solvent suggests that Ln^{3+} are not completely protected from the solvent by the four tropolonate ligands in solution. Nevertheless, the ligand-to-Ln^{3+} energy-transfer process and the protection offered by the coordinated ligands are sufficient to allow the measurement of the quantum yields of the Yb^{3+} complex in water. The quantum yield values recorded for $[Ln(Trop)_4]^-$ with Ln = Nd, Er, Ho, and Tm are lower than those recorded with Ln = Yb, but are still easily measurable with a fluorimeter using a Xenon lamp as a source of excitation.

Table 2.11: Absolute emission quantum yields (Φ) for [Ln(Trop)$_4$]$^-$ in organic and aqueous media

| Ln | Solvent | deuterated | | non-deuterated | | $k_{q, solv}$ (s^{-1}) |
		QY	Lifetime (μs)	QY	Lifetime (μs)	
	DMSO	$2.2 \cdot 10^{-2}$(3)	18.13(6)	$1.9 \cdot 10^{-2}$(1)	12.43(9)	2.53×10^4
Yb	Methanol	$1.6 \cdot 10^{-2}$(2)	13.02(1)	$1.3 \cdot 10^{-3}$(2)	1.62(3)	5.40×10^5
	Water	$7.4 \cdot 10^{-3}$(1)	10.03(6)	$2.4 \cdot 10^{-4}$(3)	0.75(1)	1.23×10^6
Nd[a]	DMSO	$3.6 \cdot 10^{-3}$(7)	1.65(1)	$2.1 \cdot 10^{-3}$(1)	1.10(4)	3.03×10^5
Er[a]	DMSO	$3.2 \cdot 10^{-4}$(4)		$1.7 \cdot 10^{-4}$(1)		
Tm[b]	DMSO	$5.7 \cdot 10^{-5}$(2)		$3.8 \cdot 10^{-5}$(2)		
Ho[b]	DMSO	$2.4 \cdot 10^{-5}$(1)		$2.3 \cdot 10^{-5}$(2)		

a. λ_{ex} = 340 nm was used for quantum yield determinations.
b. Quantum yields were measured using [Yb(Trop)$_4$]$^-$ as reference.
c. Quantum yields were measured using [Er(Trop)$_4$]$^-$ as reference.

2.2.10 Fluorescence and phosphorescence

Gd^{3+} has no energy levels below 32,000 cm^{-1}, and therefore usually cannot accept any energy from the ligand excited states. So it is regarded as a "silent" cation and used to study the electronic state of ligand when coordinated to Ln^{3+}. The fluorescence and phosphorescence spectra of Gd^{3+} complex are depicted in Figure 2.25. The excitation and absorption spectra are similar (not shown here). The shift between the fluorescence band (431 nm, 23,200 cm^{-1}) and phosphorescence band (587 nm, 17,000 cm^{-1}) is 156 nm (6,160 cm^{-1}). Due to the low temperature, there are some structured bands in the phosphorescence spectrum. The triplet state measured here is consistent with the value previously reported by Croteau et al. (595 nm, 16,800 cm^{-1}).[72]

The quantum yields of the ligand fluorescence were also measured by using quinine sulfate as reference (Table 2.12). The non-luminescent Y^{3+}, La^{3+} complexes have comparable quantum yields to the "free" ligand (KTrop), which are higher than those observed in the complexes. This is due to the heavy atom (paramagnetic) effects.[73-74] An external heavy atom effect can be induced by a

heavy (paramagnetic) metal ion in close proximity of a chromophore, and increases the intersystem crossing yield of the chromophore, which results in a decrease of the fluorescence intensity and a concomitant increase in the phosphorescence intensity. This effect has been attributed to an enhanced spin-orbit coupling of the system which relaxes the selection rules for electronic transitions, but also to an exchange interaction of metal-unpaired electrons with the σ-electrons of the organic chromophore. The small differences in the fluorescence quantum yields with different Ln^{3+} can be explained by variation in atomic weight and magnetic moment of Ln^{3+}.[75]

Table 2.12: Quantum yield of singlet states of Trop⁻ in [Ln(Trop)$_4$]⁻

Ln	K	La	Lu	Y	Gd	Yb	Nd	Er	Ho	Tm
QY$_{abs}$[a]	0.0221	0.0176	0.0073	0.0127	0.0080	0.0021	0.0022	0.0020	0.0025	0.0023
QY$_{rel}$[b]	1.25	1.00	0.41	0.72	0.45	0.12	0.13	0.11	0.14	0.13

a. Absolute quantum yield measured by using quinine sulfate in 0.5 M H_2SO_4 as standard (Φ = 0.54), error 10%
b. Relative quantum yield calculated by using [La(Trop)$_4$] as reference.
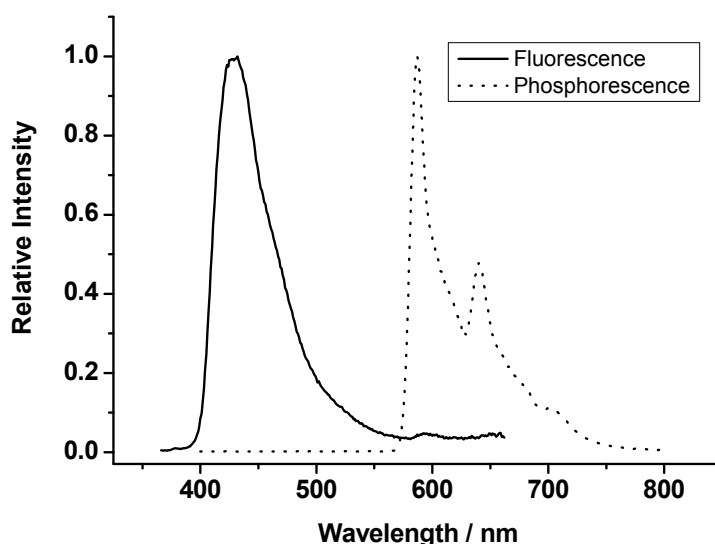
Figure 2.25: Fluorescence (10⁻⁵ M in DMSO, λ_{ex} = 340 nm, 298 K) and phosphorescence spectra (10⁻⁵ M in DMSO, decay time 0.1ms, λ_{ex} = 340 nm, 77 K) of [Gd(Trop)$_4$]⁻

61

Information on the structure of [Ln(Trop)$_4$]$^-$ obtained on the basis of the crystal structure data indicates that, in the solid state, lanthanide cations are coordinated with four tropolonate ligands and are well protected from solvent molecules since no solvent molecules are in the first coordination sphere of Ln^{3+}. To evaluate the situation in solution, Ln^{3+}-centered luminescence lifetimes measured upon ligand excitation have been recorded in different solvents in order to determine the nature of the coordination environment around Ln^{3+} when the [Ln(Trop)]$_4^-$ complex is in solution.

The hydration state of Ln^{3+} in a coordination complex can be estimated by using an empirical formula (eq 1) developed by Horrocks et al.,[76-77] where q is the number of the water molecules bound to Ln^{3+} and k_{H2O} and k_{D2O} are the rate constants of the excited states of the Ln^{3+} in H$_2$O and D$_2$O, respectively. A is a proportionality constant related to the sensitivity of the Ln^{3+} to vibronic quenching by OH oscillators. Beeby et al.[78] revised it to eq 2 for Eu^{3+}, Tb^{3+}, and Yb^{3+} complexes in water, where the outer-sphere quenchers are taken into account by adding a correction factor, B.

$$q = A(k_{H2O}-k_{D2O}) \tag{1}$$

$$q = A(k_{H2O} - k_{D2O}) - B \tag{2}$$

More recently, Davies et al.[79] and Beeby et al.[80] modified this formula for the determination of q for Yb^{3+} and Nd^{3+} complexes in MeOH solutions, respectively.

For the Yb^{3+} complex

$$q = k_{H2O} - k_{D2O}-0.1 = 1/\tau_{H2O} - 1/\tau_{D2O} - 0.1 \tag{3}$$

$$q = 2 (k_{CH3OH} - k_{CD3OD}) - 0.1 = 2 (1/\tau_{CH3OH} - 1/\tau_{CD3OD}) - 0.1 \tag{4}$$

(All the rate constants are expressed in units of μs.) Applying these formulas for the tropolonate Yb^{3+} complex, q values were calculated as 1.13 in water ($\tau_{H2O} = 0.75 \pm 0.01$ μs,

$\tau_{D2O} = 10.0 \pm 0.1$ µs) and 0.98 in methanol ($\tau_{CH3OH} = 1.62 \pm 0.03$ µs, $\tau_{CD3OD} = 13.02 \pm 0.01$ µs).

Due to the limited solubility of these complexes in methanol and water, they were dissolved in a mixture of DMSO (5% by volume) and methanol or water, respectively. These values consistently indicate that in both solvents, one water molecule is bound to Ln^{3+} in the first sphere of coordination. The structure in solution therefore has to be different from the structure observed in the solid state, where no coordinated solvent molecules were present in the first coordination sphere. The four tropolonate ligands in $[Ln(Trop)_4]^-$ do not efficiently protect Ln^{3+} from nonradiative deactivations induced by coordinated water molecules in solution. This system of coordination complexes is an example where the structure observed in the solid state does not reflect the structure of the complex in solution.

2.3   CONCLUSION

In this Chapter, the structures of ML_4 complexes formed between tropolonate ligands and lanthanide cations in the solid state were systematically studied and compared. It was observed that for the $KLn(Trop)_4DMF$ analyzed (Ln^{3+} = Tb^{3+}, Dy^{3+}, Ho^{3+}, Er^{3+}, Tm^{3+}, Yb^{3+}, Lu^{3+}), four tropolonate ligands coordinate to Ln^{3+}, the coordination number around Ln^{3+} being 8 and the coordination polyhedron being best described as a slightly distorted dodecahedron. The systematic analysis of the experimental data obtained from the X-ray crystal structures shows that the coordination geometries around different Ln^{3+} are similar for all the different complexes.

The crystal packing of the molecules was similar for Ln^{3+} = Dy^{3+}, Ho^{3+}, Er^{3+}, Tm^{3+}, Yb^{3+}, Lu^{3+}. A change in the packing mode of the molecules in the crystal has been observed for the largest lanthanide cation of our series (Tb^{3+}). We explain this change by the increase in size of

Ln^{3+} which generates a modification in the coordination mode of the potassium counterion and in the resulting crystal packing of the molecules.

In solution, spectrophotometric titrations confirmed that the ML_1, ML_2, ML_3, and ML_4 species are successively formed in solution. The stability constant values of the ML_3 complexes increase as the radii of Ln^{3+} decrease. This behavior has been typically observed for complexes where bonds are mainly of electrostatic nature. However, this situation is quite different for the ML_4 complexes, where the stability constant values of ML_4 steadily decrease as the size of Ln^{3+} decreases. This can be explained by the steric hindrance generated by the four tropolonate ligands around Ln^{3+} upon formation of the ML_4 complex.

Quantitative luminescence measurements indicated that tropolonate ligands are able to sensitize several lanthanide cations that emit in the near-infrared domain. Also, the luminescence of Ho^{3+} in a lanthanide complex in solution is reported here for the first time. Quantum yields of the complexes formed with Yb^{3+} are comparable to the highest reported quantum yields of other lanthanide complexes that emit in the NIR domain in organic solvents. In aqueous solution, water has a very strong deactivating effect on the luminescence of Ln^{3+} owing to the coordination to Ln^{3+} of water molecules, which were not present in the solid state.

Luminescence lifetimes of the Yb^{3+} complex in H_2O/D_2O and MeOH/MeOH-d_4 indicate that the coordination geometries around Ln^{3+} in the ML_4 complexes in solution are different than those in the solid state. These measurements provide evidence of the presence of one water/methanol molecule in the first coordination sphere. However, no solvent molecule was observed as being bound to Ln^{3+} in the crystal structure. This demonstrates that coordination chemists must be careful in using X-ray data to explain the solution behavior of coordination complexes.

Owing to the flexibility of the approach, limitations can be removed by preparing a multidentate ligand that connects several chelating tropolone units to a common backbone. The backbone will function 1) to improve protection of Ln^{3+} from nonradiative deactivation by preventing the access of water molecules to Ln^{3+} and 2) to increase the stability of the complex in solution, a useful feature when the complex is used at low concentrations. Emission spectra of the complexes indicate that for all the studied lanthanide complexes here, there is a significant amount of residual ligand emission. This is an indication of incomplete energy transfer from the ligand to Ln^{3+}.

2.4   REFERENCES

(1)   Beeby, A.; Clarkson, I. M.; Dickins, R. S.; Faulkner, S.; Parker, D.; Royle, L.; de Sousa, A. S.; Williams, J. A. G.; Woods, M. *J. Chem. Soc., Perkin Trans. 2* **1999**, 493.

(2)   Parker, D.; Williams, J. A. G. *J. Chem. Soc., Dalton Trans.* **1996**, 3613.

(3)   Comby, S.; Imbert, D.; Vandevyver, C.; Bünzli, J.-C. G. *Chem.-Eur. J.* **2007**, *13*, 936.

(4)   Comby, S.; Imbert, D.; Chauvin, A.-S.; Bünzli, J.-C. G. *Inorg. Chem.* **2006**, *45*, 732.

(5)   Hasegawa, Y.; Ohkubo, T.; Sogabe, K.; Kawamura, Y.; Wada, Y.; Nakashima, N.; Yanagida, S. *Angew. Chem., Int. Ed.* **2000**, *39*, 357.

(6)   Bassett, A. P.; Van Deun, R.; Nockemann, P.; Glover, P. B.; Kariuki, B. M.; Van Hecke, K.; Van Meervelt, L.; Pikramenou, Z. *Inorg. Chem.* **2005**, *44*, 6140.

(7)   Quici, S.; Cavazzini, M.; Marzanni, G.; Accorsi, G.; Armaroli, N.; Ventura, B.; Barigelletti, F. *Inorg. Chem.* **2005**, *44*, 529.

(8)   Werts, M. H. V.; Woudenberg, R. H.; Emmerink, P. G.; van Gassel, R.; Hofstraat, J. W.; Verhoeven, J. W. *Angew. Chem., Int. Ed.* **2000**, *39*, 4542.

(9)   Klink, S. I.; Keizer, H.; van Veggel, F. C. J. M. *Angew. Chem., Int. Ed.* **2000**, *39*, 4319.

(10)   Miller, T. A.; Jeffery, J. C.; Ward, M. D.; Adams, H.; Pope, S. J. A.; Faulkner, S. *J. Chem. Soc., Dalton Trans.* **2004**, 1524.

(11)   He, H.; Guo, J.; Zhao, Z.; Wong, W.-K.; Wong, W.-Y.; Lo, W.-K.; Li, K.-F.; Luo, L.; Cheah, K.-W. *Eur. J. Inorg. Chem.* **2004**, 837.

(12)   Foley, T. J.; Harrison, B. S.; Knefely, A. S.; Abboud, K. A.; Reynolds, J. R.; Schanze, K. S.; Boncella, J. M. *Inorg. Chem.* **2003**, *42*, 5023.

(13)   Erdtman, H.; Gripenberg, J. *Nature* **1948**, *161*, 719.

(14)   Chipperfield, J. R.; Clark, S.; Elliott, J.; Sinn, E. *Chem. Commun.* **1998**, 195.

(15)   Elliott, J. M.; Chipperfield, J. R.; Clark, S.; Sinn, E. *Inorg. Chem.* **2002**, *41*, 293.

(16)   Redington, R. L. *J. Chem. Phys.* **2000**, *113*, 2319.

(17)   Tanaka, K.; Honjo, H.; Tanaka, T.; Kohguchi, H.; Ohshima, Y.; Endo, Y. *J. Chem. Phys.* **1999**, *110*, 1969.

(18)   Tanaka, K.; Nagahiro, R.; Ohba, S.; Eishima, M. *Tetrahedron Lett.* **2001**, *42*, 925.

(19)   Doering, W. v. E.; Knox, L. H. *J. Am. Chem. Soc.* **1951**, *73*, 828.

(20)   Carey, G. H.; Martell, A. E. *J. Am. Chem. Soc.* **1967**, *89*, 2859.

(21)   Pierpont, C. G.; Buchanan, R. M. *Coord. Chem. Rev.* **1981**, *38*, 45.

(22)   Albrecht, M. *Chem. Soc. Rev.* **1998**, *27*, 281.

(23)   Muetterties, E. L.; Wright, C. M. *J. Am. Chem. Soc.* **1965**, *87*, 4706.

(24)   Bünzli, J.-C. G.; Piguet, C. *Chem. Soc. Rev.* **2005**, *34*, 1048.

(25)   Bünzli, J.-C. G. *Acc. Chem. Res.* **2006**, *39*, 53.

(26)   Aime, S.; Barge, A.; Batsanov, A. S.; Botta, M.; Castelli, D. D.; Fedeli, F.; Mortillaro, A.; Parker, D.; Puschmann, H. *Chem. Commun.* **2002**, 1120.

(27)   Torelli, S.; Imbert, D.; Cantuel, M.; Bernardinelli, G.; Delahaye, S.; Hauser, A.; Bünzli, J.-C. G.; Piguet, C. *Chem.-Eur. J.* **2005**, *11*, 3228.

(28)   Imbert, D.; Cantuel, M.; Bünzli, J.-C. G.; Bernardinelli, G.; Piguet, C. *J. Am. Chem. Soc.* **2003**, *125*, 15698.

(29)   Pope, S. J. A.; Coe, B. J.; Faulkner, S.; Bichenkova, E. V.; Yu, X.; Douglas, K. T. *J. Am. Chem. Soc.* **2004**, *126*, 9490.

(30)   Hebbink, G. A.; Grave, L.; Woldering, L. A.; Reinhoudt, D. N.; van Veggel, F. C. J. M. *J. Phys. Chem. A* **2003**, *107*, 2483.

(31)   Pope, S. J. A.; Coe, B. J.; Faulkner, S.; Laye, R. H. *J. Chem. Soc., Dalton Trans.* **2005**, 1482.

(32)   Davies, G. M.; Pope, S. J. A.; Adams, H.; Faulkner, S.; Ward, M. D. *Inorg. Chem.* **2005**, *44*, 4656.

(33)   Van Deun, R.; Fias, P.; Nockemann, P.; Schepers, A.; Parac-Vogt, T. N.; Van Hecke, K.; Van Meervelt, L.; Binnemans, K. *Inorg. Chem.* **2004**, *43*, 8461.

(34)   Lenaerts, P.; Driesen, K.; Van Deun, R.; Binnemans, K. *Chem. Mater.* **2005**, *17*, 2148.

(35)   Bertolo, L.; Tamburini, S.; Vigato, P. A.; Porzio, W.; Macchi, G.; Meinardi, F. *Eur. J. Inorg. Chem.* **2006**, 2370.

(36)   Murov, S. L.; Carmichael, I.; Hug, G. L. *Handbook of Photochemistry*; 2nd ed.; Marcel Dekker, Inc, 1993

(37)   Gampp, H.; Maeder, M.; Meyer, C. J.; Zuberbuehler, A. D. *Talanta* **1985**, *32*, 1133.

(38)   Selbin, J.; Ortego, J. D. *J. Inorg. Nucl. Chem.* **1968**, *30*, 313.

(39)   Bagnall, K. W.; Bhandari, A. M.; Brown, D.; Lidster, P. E.; Whittaker, B. *J. Chem. Soc., Dalton Trans.* **1975**, 1249.

(40)   Bünzli, J.-C. G.; Yersin, J. R.; Mabillard, C. *Inorg. Chem.* **1982**, *21*, 1471.

(41)   Bünzli, J. C. G.; Klein, B.; Pradervand, G. O.; Porcher, P. *Inorg. Chem.* **1983**, *22*, 3763.

(42)   Bünzli, J.-C. G.; Mabillard, C.; Yersin, J. R. *Inorg. Chem.* **1982**, *21*, 4214.

(43)   Taylor, M. D.; Carter, C. P.; Wynter, C. I. *J. Inorg. Nuc. Chem.* **1968**, *30*, 1503.

(44)   Aly, H. F.; Abdel Kerim, F. M.; Kandil, A. T. *J. Inorg. Nuc. Chem.* **1971**, *33*, 4340.

(45)   Poh, B.-L.; Siow, H.-L. *Aust. J. Chem.* **1980**, *33*, 491.

(46)   Bernhardt, P. V.; Flanagan, B. M.; Riley, M. J. *Aust. J. Chem.* **2000**, *53*, 229.

(47)   Bernhardt, P. V.; Flanagan, B. M.; Riley, M. J. *Aust. J. Chem.* **2001**, *54*, 229.

(48)   Shannon, R. D. *Acta Crystallogr., Sect. A* **1976**, *A32*, 751.

(49)   Desiraju, G. R. *Acc. Chem. Res.* **1996**, *29*, 441.

(50)   Jeffrey, G. A.; Maluszynska, H.; Mitra, J. *Int. J. Biol. Macromol.* **1985**, *7*, 336.

(51)   Anderson, T. J.; Neuman, M. A.; Melson, G. A. *Inorg. Chem.* **1974**, *13*, 1884.

(52)   Davis, A. R.; Einstein, F. W. B. *Inorg. Chem.* **1974**, *13*, 1880.

(53)   Davis, A. R.; Einstein, F. W. B. *Acta Crystallogr., Sect. B* **1978**, *B34*, 2110.

(54)   Tranqui, D.; Tissier, A.; Laugier, J.; Boyer, P. *Acta Crystallogr., Sect. B* **1977**, *B33*, 392.

(55)   Kira, M.; Zhang, L. C.; Kabuto, C.; Sakurai, H. *Organometallics* **1998**, *17*, 887.

(56)   Davis, A. R.; Einstein, F. W. B. *Inorg. Chem.* **1975**, *14*, 3030.

(57)   Kepert, D. L. *Prog. Inorg. Chem.* **1978**, *24*, 179.

(58)   Tedeschi, C.; Azema, J.; Gornitzka, H.; Tisnes, P.; Picard, C. *J. Chem. Soc., Dalton Trans.* **2003**, 1738.

(59)   Flanagan, J. H., Jr.; Khan, S. H.; Menchen, S.; Soper, S. A.; Hammer, R. P. *Bioconjugate Chem.* **1997**, *8*, 751.

(60)   Petoud, S.; Bünzli, J.-C. G.; Renaud, F.; Piguet, C.; Schenk, K. J.; Hopfgartner, G. *Inorg. Chem.* **1997**, *36*, 5750.

(61)   Caravan, P.; Hedlund, T.; Liu, S.; Sjoeberg, c. S.; Orvig, C. *J. Am. Chem. Soc.* **1995**, *117*, 11230.

(62)   Reinhard, C.; Güdel Hans, U. *Inorg. Chem.* **2002**, *41*, 1048.

(63)   Stouwdam, J. W.; van Veggel, F. C. J. M. *Nano Lett.* **2002**, *2*, 733.

(64)   Zang, F. X.; Li, W. L.; Hong, Z. R.; Wei, H. Z.; Li, M. T.; Sun, X. Y.; Lee, C. S. *Appl. Phys. Lett.* **2004**, *84*, 5115.

(65)   Sharma, P. K.; van Doorn, A. R.; Staring, A. G. J. *J. Lumines.* **1994**, *62*, 219.

(66)   Meshkova, S. B.; Topilova, Z. M.; Bol'shoi, D. V.; Nazarenko, N. A. *J. Appl. Spectrosc.* **2000**, *67*, 893.

(67)   Zang, F. X.; Hong, Z. R.; Li, W. L.; Li, M. T.; Sun, X. Y. *Appl. Phys. Lett.* **2004**, *84*, 2679.

(68)   Goncalves e Silva, F. R.; Malta, O. L.; Reinhard, C.; Güdel, H.-U.; Piguet, C.; Moser, J. E.; Bünzli, J.-C. G. *J. Phys. Chem. A* **2002**, *106*, 1670.

(69)   Iwamuro, M.; Wada, Y.; Kitamura, T.; Nakashima, N.; Yanagida, S. *Phys. Chem. Chem. Phys.* **2000**, *2*, 2291.

(70)   Werts, M. H. V.; Verhoeven, J. W.; Hofstraat, J. W. *J. Chem. Soc., Perkin Trans. 2* **2000**, 433.

(71)   Beeby, A.; Dickins, R. S.; Faulkner, S.; Parker, D.; Williams, J. A. G. *Chem. Commun.* **1997**, 1401.

(72)   Croteau, R.; Leblanc, R. M. *Photochem. Photobiol.* **1978**, *28*, 33.

(73)   Tobita, S.; Arakawa, M.; Tanaka, I. *J. Phys. Chem.* **1984**, *88*, 2697.

(74)   Tobita, S.; Arakawa, M.; Tanaka, I. *J. Phys. Chem.* **1985**, *89*, 5649.

(75)   Guldi, D. M.; Mody, T. D.; Gerasimchuk, N. N.; Magda, D.; Sessler, J. L. *J. Am. Chem. Soc.* **2000**, *122*, 8289.

(76)   Horrocks, W. D., Jr.; Sudnick, D. R. *J. Am. Chem. Soc.* **1979**, *101*, 334.

(77)   Horrocks, W. D., Jr.; Sudnick, D. R. *Acc. Chem. Res.* **1981**, *14*, 384.

(78)   Beeby, A.; Clarkson, I. M.; Dickins, R. S.; Faulkner, S.; Parker, D.; Royle, L.; de Sousa, A. S.; Williams, J. A. G.; Woods, M. *J. Chem. Soc., Perkin Trans. 2* **1999**, 493

(79)   Davies, G. M.; Aarons, R. J.; Motson, G. R.; Jeffery, J. C.; Adams, H.; Faulkner, S.; Ward, M. D. *J. Chem. Soc., Dalton Trans.* **2004**, 1136.

(80)   Beeby, A.; Burton-Pye, B. P.; Faulkner, S.; Motson, G. R.; Jeffery, J. C.; McCleverty, J. A.; Ward, M. D. *J. Chem. Soc., Dalton Trans.* **2002**, 1923.

(81)   Petoud, S.; Cohen, S. M.; Bünzli, J.-C. G.; Raymond, K. N. *J. Am. Chem. Soc.* **2003**, *125*, 13324.

(82)   Piguet, C.; Bernardinelli, G.; Bocquet, B.; Schaad, O.; Williams, A. F. *Inorg. Chem.* **1994**, *33*, 4112.

3.0   DESIGN, SYNTHESIS AND LUMINESCENCE PROPERTIES OF

LANTHANIDE COMPLEXES FORMED WITH OCTADENTATE LIGANDS WHICH

INCORPORATE FOUR DERIATIVE OF TROPOLONE CHELATING UNITS

In chapter 2, we have demonstrated that tropolone is a useful chelator and sensitizer for several NIR luminescent lanthanide cations. Nevertheless, there are two important drawbacks for practical applications in this initial design. Firstly, tropolonate (Trop$^-$) is a bidentate ligand. To satisfy the requirement of the high coordination number of Ln^{3+}, four Trop$^-$ ligands are needed. This requirement could be problematic for these complexes to be used at low concentration due to the dissociation of the ML$_4$ complexes (entropic factor). Secondly, it has been shown that in the ML$_4$ tropolonate complexes, the four ligands provide only a limited protection to the central Ln^{3+}. Particularly, we have demonstrated that one solvent/water molecule is bound to Ln^{3+} when the complex is in solution. As discussed previously, the protection of Ln^{3+} is important for NIR luminescent lanthanide complex. NIR emitting Ln^{3+} are more sensitive to non-radiative quenching from the coordinated solvent molecules due to the smaller energy gap between their excited and ground states. It is therefore desirable to increase the stability of complexes and the protection of the ligands for Ln^{3+}.

To increase the stability of lanthanide complexes, the use of ligands with high denticity is a widely use strategy to override the entropy effect.[1] For example, DTPA derivatives[1], *m-*

terphenyl-based ligands[2], calix[4]arene derivatives[3] have been used as multidentate ligands for the NIR luminescent Ln^{3+}.

Two octadentate ligands L_1 and L_2 have been designed by the incorporation of four tropolone units connected through a common backbone (Figure 3.1). These octadentate ligands could satisfy the requirement of high coordination number of Ln^{3+} and use a derivative of tropolonate chromophore as the sensitizer for Ln^{3+}. The addition of a methylene group on the seven-membered ring is expected not to modify the electronic structure of tropolonate significantly, hence retaining its efficiency of sensitization. More importantly, by connecting the four tropolone units to a common backbone, the entropy effect should increase the thermodynamic stability of the resulted complex. The protection of Ln^{3+} is expected to be improved through the proposed backbone by preventing the physical access of water/solvent molecules to Ln^{3+}. As an example, this strategy has been used recently by Comby et al. in 8-hydroxyquinolinate-based podates for NIR emitting Ln^{3+}.[4,5] It is expected that ligand L_2 will be suitable for bio-applications because of the ease of attachment of biological molecules to the carboxylic acid group on the backbone.

In this chapter, the synthesis and characterization of the ligand L_1, L_2, and the corresponding lanthanide complexes of L_1 are described. Photophysical properties of these complexes are also described.
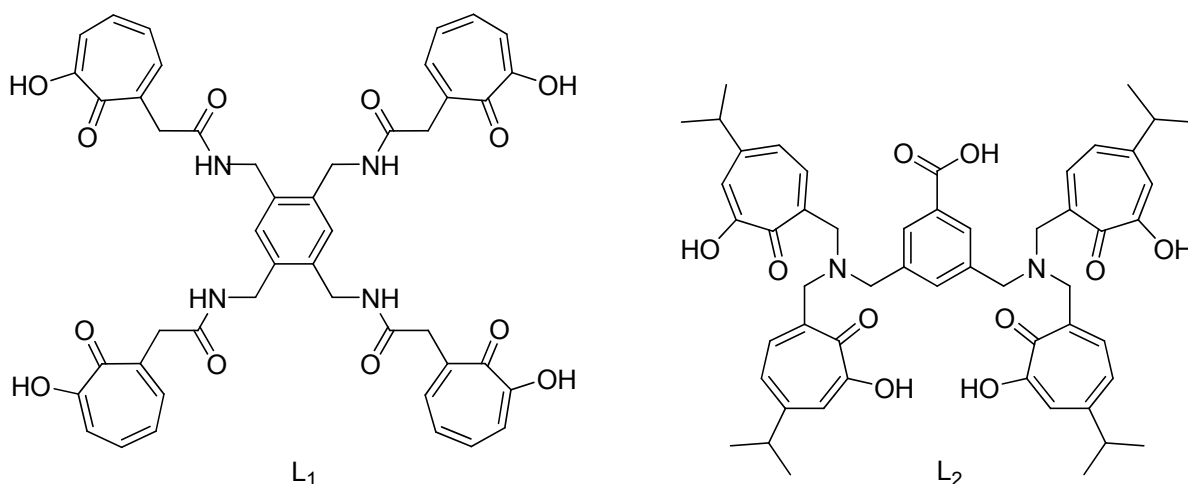
Figure 3.1: Molecular structure of designed octadentate ligand L_1 and L_2

3.1 EXPERIMENTAL SECTION

3.1.1 Chemicals

All chemicals were used as received. $LnCl_3 \cdot nH_2O$ (Ln = Gd and Yb, n = 6 or 7, 99.99%), 1,2,4,5-tetrakisbromomethylbenzene, NaN_3, 5% Pd on carbon, bromine, ethyl acetoacetate, benzenesulfonyl chloride, ethyl malonate, hinokitiol, 27% HCHO, $SOCl_2$, N-bromosuccinimide, methyl-3,5-dimethylbenzoate, benzoyl peroxide, BBr_3 were purchased from Aldrich. Cyclohepanone and selenium dioxide were bought from Alfa Aesar. All solvents were used as received, unless otherwise stated. All deuterated NMR solvents were purchased from Cambridge Isotope Labs and used as received.

3.1.2 Methods

Infrared spectra were recorded on a Perkin-Elmer Spectrum BX FT-IR instrument. UV-vis absorption spectra were recorded on a Perkin-Elmer Lambda 9 spectrophotometer.^{1}H NMR spectra were recorded on a Bruker DPX-300 spectrometer at 300 MHz. MS-ESI were measured on an Agilent HP 1100 series LC-MSD instrument.

3.1.3 Luminescence measurements

Emission and excitation spectra were measured using a Jobin Yvon Horiba Fluorolog-322 spectrofluorometer equipped with a Hamamatsu R928 detector for the visible domain and an Electro-Optical Systems, Inc. DSS-IGA020L detector for the NIR domain. The NIR luminescence quantum yields were measured by using $KYb(Trop)_4$ complex ($\Phi = 1.9 \times 10^{-2}$ in DMSO) as reference.[6] Spectra were corrected for the instrumental function for both excitation and emission. Values were calculated using the following equation: $\dfrac{\Phi_x}{\Phi_r} = \dfrac{A_{r_{\lambda_x}}}{A_{x_{\lambda_x}}} \dfrac{I_{\lambda_r}}{I_{\lambda_x}} \dfrac{\eta_x^2}{\eta_r^2} \dfrac{D_x}{D_r}$, where

subscript r stands for the reference and x for the sample; A is the absorbance at the excitation wavelength, I is the intensity of the excitation light at the same wavelength, η is the refractive index ($\eta = 1.478$ in DMSO), and D is the measured integrated luminescence intensity. Time-resolved measurements were conducted with a Jobin Yvon Horiba Fluorolog-3 spectrofluorimeter equipped with a phosphorimeter module and Xenon flash lamp. The emission spectra were then collected, with increasing delay times until the phosphorescence band was the main band on a spectrum (at delay 0.1 ms). The emission spectra were corrected for the background and instrumental function.

The luminescence lifetime measurements were performed by excitation of solutions in 1 cm quartz cells using a nitrogen laser (Oriel model 79110, wavelength 337.1 nm, pulse width at half-height 15 ns, 5-30 Hz repetition rate). Emission from the sample was collected at a right angle to the excitation beam by a 3″. plano-convex lens. Emission wavelengths were selected by means of quartz filters. The signal was monitored by a cooled photomultiplier (Hamamatsu R316) coupled to a 500 MHz bandpass digital oscilloscope (Tektronix TDS 754D). The signals (15,000 points each trace) from at least 500 flashes were collected and averaged. Background signals were similarly collected and subtracted from sample signals. Lifetimes are averages of at least three independent determinations. Data were fitted to exponential decay by Origin 7.0 data analysis software. Ligand-centered triplet state lifetimes were performed by excitation of solid samples in a quartz tube at 77 K using the nitrogen laser described previously. Emission from the samples was collected at a right angle to the excitation beam, and the emission wavelengths were selected by means of a Spex FL1005 double monochromator. The signal was monitored by a Hamamatsu R928 photomultiplier coupled to a 500 MHz bandpass digital oscilloscope (Tektronix TDS 620B). The signals (15000 points each trace) from at least 500 flashes were collected and averaged.

3.1.4   X-ray crystallography

Crystals suitable for X-ray diffraction were coated with Fluorolube® then mounted on a glass fiber and coated with epoxy cement. X-ray data were collected on a Bruker Apex diffractometer using graphite-monochromatized Mo K_α radiation (λ = 0.71073 Å). Data collection was controlled using the Bruker SMART program, and the data processing was completed with the SHELXTL program package. Graphical representations were obtained with the help of Diamond

3.0 software packages. All hydrogen atoms were calculated and placed in idealized positions (d_{C-H} = 0.96 Å).

3.1.5 Synthesis of ligand L_1

The synthesis route of ligand L_1 is shown in Figure 3.2.
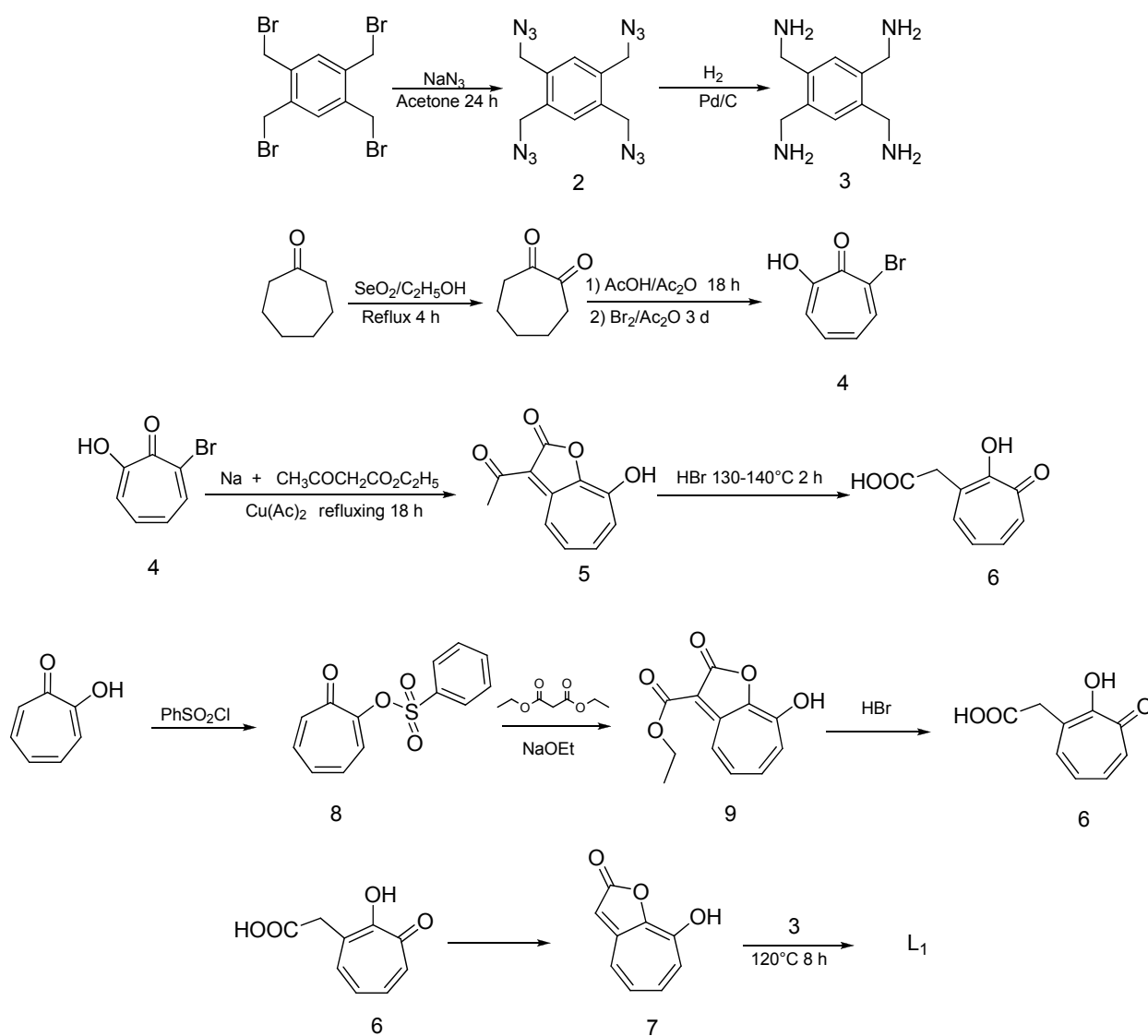
Figure 3.2: Synthesis route of ligand L_1
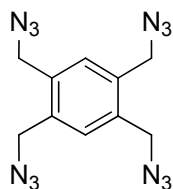
1,2,4,5-Tetrakis(azidomethyl)-benzene (2). [Caution: This step is dangerous; the pure compound is explosive and should not be heated. A blast shield should also be used.]. 1,2,4,5-Tetrakisbromomethyl-benzene (5.18 g, 11.5 mmol) was dissolved in acetone (300 mL). Sodium azide (10.77 g, 165.7 mmol) was added and the mixture was refluxed for 24 h under nitrogen atmosphere whilst stirring. The reaction mixture was cooled to room temperature and diluted with ether (100 mL) and water (100 mL). The organic layer was separated and washed with 200 mL of saturated sodium chloride, dried over Na_2SO_4, and the solvent removed in vacuo (without heating) to give the title compound as a colorless crystal (3.26 g, 95%). This material was used without further purification and characterization. The single crystal structure of this compound is analyzed and depicted in Figure 3.3. The crystallographic data is listed in Table 3.1.
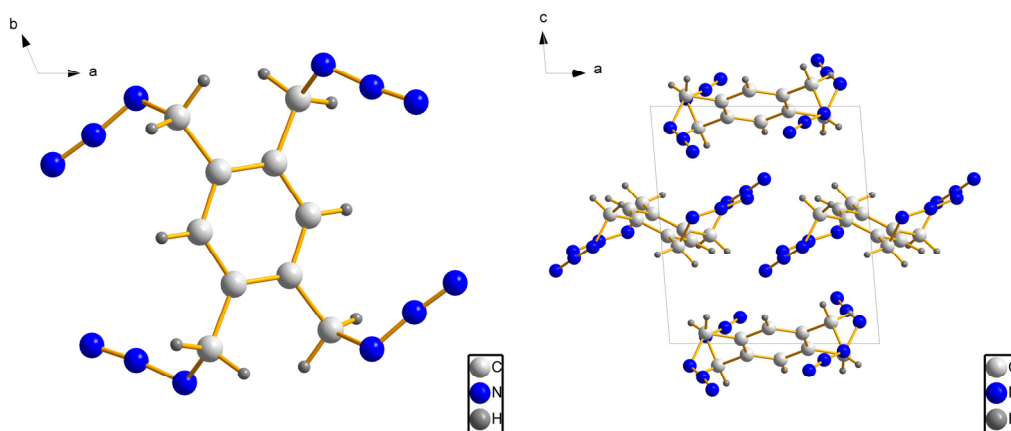
Figure 3.3: Crystal structure of compound **2** (left) and its packing diagram (right)
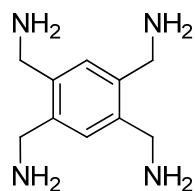
1,2,4,5-Tetrakis(aminomethyl)-benzene (3). 2.00 g of **2** (6.71 mmol) was dissolved in CH$_3$OH (150 mL) and Pd/C (0.5 g) was added. The reaction was carried out under hydrogen for 12 h. The solution was filtered and evaporated under vacuum to give the title compound (1.23 g, 95%). ^{1}H NMR (DMSO-d_6, 300 MHz): δ 2.70 (s, 8H, -NH_2), 3.73 (s, 8H, -CH_2NH$_2$), 7.26 (s, 2H, Ar-H).
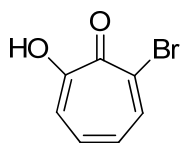
2-Bromo-7-hydroxy-2,4,6-cycloheptatrien-1-one (4).[7] To a solution of cycloheptanone (6.80 g, 60.7 mmol) dissolved in ethanol (14 mL), selenium dioxide (6.66 g, 60.0 mmol) was added. After refluxing the solution for 4 h, insoluble materials were removed by filtration. The resulting mixture was distilled under reduced pressure (110 °C/15 mmHg) for purification to give 5.112 g of 1, 2-cycloheptadione as a yellow oily substance. To this 1, 2-cycloheptadione (5.15 g, 40.8 mmol), acetic acid (2 mL) and acetate anhydride (0.2 mL) were added. After stirring the resulting solution at room temperature for 18 h followed by cooling to 0 °C, a solution of bromine (4.1 mL) and acetic acid (4 mL) was gradually added dropwise thereto. This mixture was allowed to react at room temperature for 3 days. The resulting precipitate was recovered by filtration. A suspension of this precipitate in water was adjusted to pH 3-4 with a

solution of 20% sodium hydroxide. The precipitate was then recovered by filtration to give a crude crystal of **4**. Recrystallized from cyclohexane gave the title compound as yellow needles (0.976 g, 8%). The single crystal structure of **4** was analyzed and depicted in Figure 3.4. The crystallographic data is listed in Table 3.1. Mp: 104-105 °C. EI-MS: m/z [M]$^+$ 199.947647 (Calc. 199.947291 for $C_7H_5O_2Br$). ^{1}H NMR (CD_3COCD_3, 300 MHz): δ 7.00 (t, J = 10 Hz, 1H), 7.38 (d, J = 10.5 Hz, 1H), 7.55 (t, J = 10 Hz, 1H), 8.32 (d, J = 9.6 Hz, 1H). IR (KBr, cm^{-1}): 3568 (O-H), 3215 (C-H), 1603, 1591 (C=O), 1544, 1477, 1458, 1413, 1361, 1306, 1242, 1204, 1076, 994, 957, 897, 778, 749.
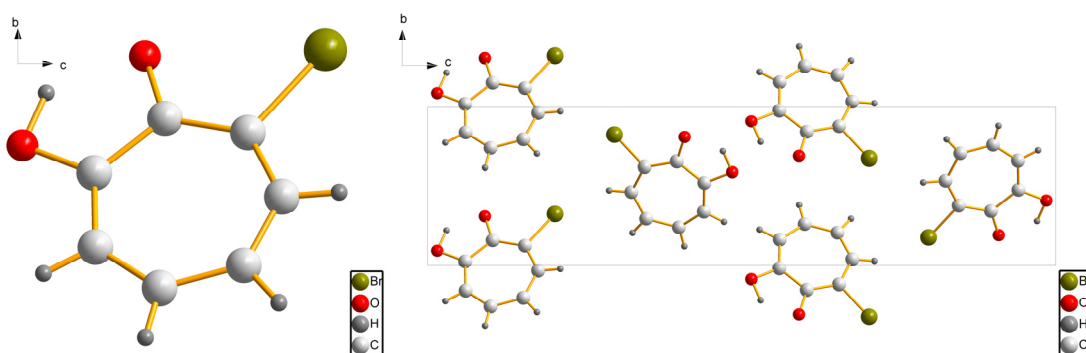
Figure 3.4: Crystal structure of compound **4** (left) and its packing diagram (right)
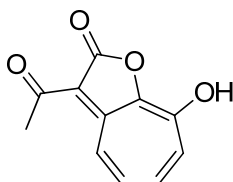
3-Acetyl-8-hydroxy-1-oxaazulan-2-one (5).[8] To a solution of ethyl sodioacetoacetate prepared by dissolving sodium (12.0 g, 0.522 mol) in a mixture of ethyl acetoacetate (90 g, 0.9 mol) and dry dioxane (160 mL), 20.0 g of **4** (20.0 g, 0.100 mol) and copper acetate (400 mg, 2.2

mmol) were added. The mixture was then refluxed for 18 h. After the addition of water (200 mL), the mixture was shaken with ether (200 mL) and the aqueous layer was acidified with 6 M hydrochloric acid and allowed to stand overnight. The crystals thereby formed were collected and washed with CHCl$_3$ to give the product. Recrystallization from a large amount of acetone gave **5** as yellow silky needles (19.1 g, 94%). Mp: 285-287 °C (decomp.). EI-MS: *m/z* [M]$^+$ 204.041960 (Calc. 204.042259 for C$_{11}$H$_8$O$_4$). ^{1}H NMR (CD$_3$COCD$_3$, 300 MHz): δ 2.46 (s, 3H, -C*H*$_3$), 7.59-7.76 (m, 3H, Ar-*H*), 9.20 (d, *J* = 11 Hz, 1H, Ar-*H*). IR (KBr, cm^{-1}): 3424 (O-H), 3056 (C-H), 1736 (C=O), 1623 (C=O), 1587, 1506, 1465, 1392, 1357, 1311, 1285, 1242, 1190, 1147, 1091, 1024, 929, 780, 748, 702, 662, 613.
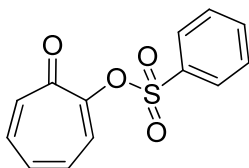
7-Oxocyclohepta-1,3,5-trienyl benzenesulfonate (8).[9] Into a stirred solution of tropolone (2.4 g, 19.67 mmol) in dry pyridine (12 mL) benzenesulfonyl chloride (4.0 g, 20.65 mmol) was added dropwise at 0 °C. The mixture was then allowed to stand for 12 h at room temperature and poured into water. Crystals were collected, washed with water and dried in vacuo. Recrystallization from EtOH, gave the product **8** (4.81 g, 93.2%). EI-MS: *m/z* [M]$^+$ 262.0306 (Calc. 262.0300 for C$_{13}$H$_{10}$O$_4$S). ^{1}H NMR (CDCl$_3$, 300 MHz): δ 7.12-7.40 (m, 5H), 7.59-7.86 (m, 4H), 8.19-8.22 (m, 1H). IR (Thin film, cm^{-1}): 3066 (C-H), 1636, 1602, 1367, 1189, 1111, 1089, 1033, 949, 801, 736, 594.
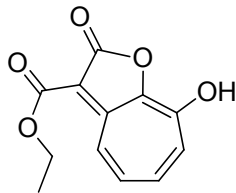
Ethyl 8-hydroxy-2-oxo-2H-cyclohepta[b]furan-3-carboxylate (9).[9] To a stirred solution of **8** (0.524 g, 2.00 mmol) and ethyl malonate (0.64 g, 4.00 mmol) in anhydrous EtOH (15 mL), 6 mL of 1 M NaOEt solution was added at 0 °C. After being stirred for additional 3 h, the mixture was allowed to stand overnight, then poured into water and shaken with benzene. The aqueous layer was acidified with 6 M HCl and crystals thereby formed were collected and recrystallized from EtOH to give the product **9** (0.400 g, 85%). EI-MS: m/z [M]$^+$ 234.0519 (Calc. 234.0528 for $C_{12}H_{10}O_5$). ^{1}H NMR (CDCl$_3$, 300 MHz): δ 1.42 (t, J = 6.9 Hz, 3H), 4.42 (q, J = 6.9 Hz, 2H), 7.35-7.55 (m, 3H), 8.93 (d, J = 11.1 Hz, 1H). IR (KBr, cm^{-1}): 3441 (O-H), 2981, 1744, 1720, 1623, 1506, 1459, 1322, 1203, 1145, 1092, 1024, 800.
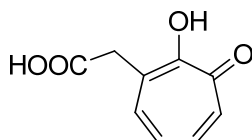
2-Hydroxy-3-oxo-1,4,6-cycloheptatriene-1-acetic acid (6).[8] (Method **I**) 4.0 g of **5** (19.6 mmol) and concentrated hydrobromic acid (30 mL) were heated at 130-140 °C for 2 h. The resulting mixture was poured into ice-water (50 g) and adjusted to pH 3 with a potassium hydroxide solution. The crystals thereby obtained were collected by filtration, affording compound **6** (2.7 g, 76%). (Method **II**) A mixture of **9** (3.95 g, 17.78 mmol) and concentrated HBr (25 mL) was heated to 130-140 °C for 2 h. The mixture was poured into ice-water (40 g)

and adjusted to pH 3 with a 2 M KOH solution; the crystals thereby obtained were collected by filtration. The compound was recrystallized to afford the product **6** (2.4 g, 75%). The single crystal structure of this compound was analyzed and is depicted in Figure 3.5. The crystallographic data are listed in Table 3.1. Mp: 174-177 °C (decomp.). EI-MS: *m/z* [M]$^+$ 180.0432 (Calc. 180.0422 for $C_9H_8O_4$). ^{1}H NMR (CD$_3$COCD$_3$, 300 MHz): δ 3.81 (s, 2H, C*H$_2$*-COOH), 7.12 (t, *J* = 10 Hz, 1H), 7.35 (d, *J* = 10.5 Hz, 1H), 7.45 (t, *J* = 10 Hz, 1H), 7.73 (d, *J* = 9.0 Hz, 1H), 10.23 (b, 1H). IR (KBr, cm^{-1}): 3447, 3225, 2942, 1701 (C=O, acid), 1610 (C=O, ring), 1595, 1540, 1472, 1420, 1388, 1318, 1270, 1241, 1216, 1181, 947, 858, 726, 701, 650.
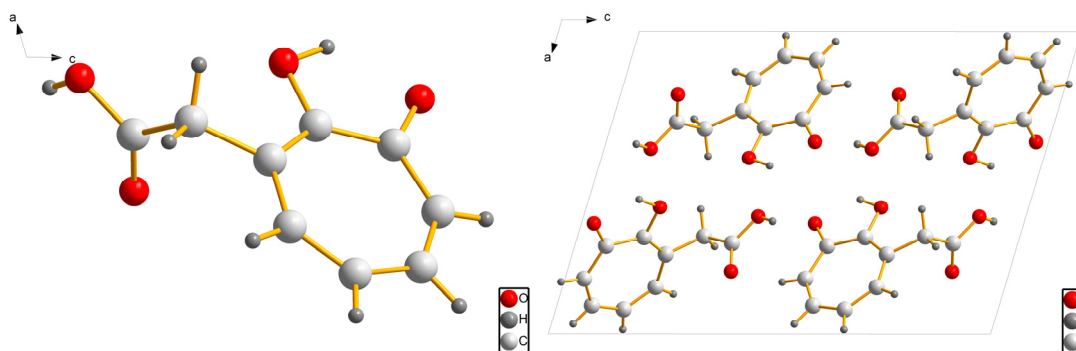
Figure 3.5: Crystal structure of compound **6** (left) and its packing diagram (right)
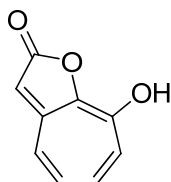
8-Hydroxy-2*H*-cyclohepta[*b*]furan-2-one (7). (Method **I**[8]) A solution of 0.40 g **6** (1.96 mmol) in concentrated sulfuric acid (1 mL) was poured into ice-water to give the title compound **7** (0.22 g, 60%). (Method **II**) To 25 mL anhydrous THF solution of **6** (0.09 g, 0.5 mmol), 0.1235

g of N,N'-Dicyclohexylcarbodiimide (DCC) in 5 mL THF was added. The reaction mixture was stirred for 24 h at room temperature. The resulted precipitate was filtered, and the filtrate was evaporated to dryness and the solid recrystallized in methanol to give 0.07 g (86%) of the title compound **7**. Mp: 223-224 °C (decomp.). EI-MS: *m/z* [M]$^+$ 162.1. ^{1}H NMR (CD$_3$COCD$_3$, 300 MHz): δ 5.54 (s, 1H, -C*H*-CO), 6.94-7.12 (m, 3H), 7.50 (d, *J* = 11.4 Hz, 1H).

L_1
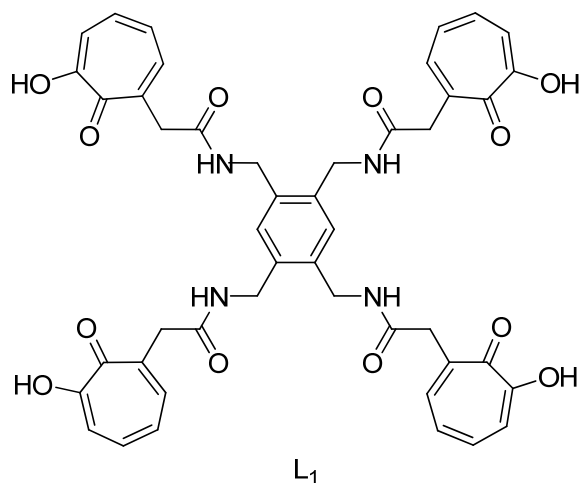
N,N',N'',N'''-[1,2,4,5-Phenylenetetra(methylene)]tetrakis-(2-hydroxy-3-oxo-1,4,6-cyclo-heptatriene-1-)acetamide (L$_1$). 32.4 mg (0.2 mmol) of **7** and 9.7 mg (0.05 mmol) of **3** were dissolved in dry DMF (10 mL). The reaction mixture was heated to 120ºC for 6 h. The DMF was then evaporated and the resulted solid was dispersed in methanol, filtered, and washed with methanol three times to give the title compound (25.3 mg, 60%). MS-ESI: *m/z* [M + Na]$^+$ 865.2. ^{1}H NMR (DMSO-d_6, 300 MHz): δ 3.65 (s, 8H, -C*H$_2$*-CONH), 4.30 (d, *J* = 5.4 Hz, 8H, Ar-C*H$_2$*-NH), 7.01 (t, *J* = 10 Hz, 4H), 7.22-7.26 (m, 6H), 7.33 (t, *J* = 10 Hz, 4H), 7.60 (d, *J* = 9.3 Hz, 4H), 8.42 (t, *J* = 5.4 Hz, 4H, -N*H*-), 10.18 (b, 4H). IR (KBr, cm^{-1}): 3284 (NH), 3081, 2924,

1644 (C=O of amide), 1610 (C=O of ring), 1595, 1540, 1472, 1420, 1388, 1318, 1270, 1241, 1216, 1181, 947, 858, 726, 701, 650.

Table 3.1: Crystallographic data of **2**, **4**, and **6**

Compound	**2**	**4**	**6**
Formula	$C_{10}H_{10}N_{12}$	$C_7H_5BrO_2$	$C_9H_8O_4$
M	298.30	201.02	180.15
Space group	P-1	P2(1)2(1)2(1)	P2(1)/c
a(Å)	8.9042(14)	4.1965(16)	11.0878(17)
b(Å)	8.9042(14)	6.476(3)	4.9539(8)
c(Å)	9.4803(16)	25.733(10)	15.509(2)
α(°)	93.089(2)	90	90
β(°)	93.089(2)	90	106.722(3)
γ(°)	112.71	90	90
V(Å^3)	690.06(19)	699.3(5)	815.9(2)
Z	2	4	4
μ/mm^{-1}	0.103	5.805	0.117
T/K	150(2)	298(2)	273(2)
Data collection range, θ/deg	2.16-25.00	1.58-32.54	1.92-32.50
Reflections collected	5501	8914	10009
Independent reflections (R_{int})	2432 (0.3865)	2460(0.0285)	2815 (0.1379)
Data/Parameters	2432 / 0 / 199	2460 / 0 / 96	2815 / 0 / 123
Goodness of fit on F^2	0.886	0.915	0.860
R_1 [$I{\geq}2\sigma(I)$] [a]	0.0745	0.0398	0.0655
wR_2 [a]	0.2472	0.1218	0.1598

a. $R_1 = \Sigma||F_0| - |Fc||/\Sigma|F_0|$; $wR_2 = \{\Sigma[w(||F_0|^2 - |F_c|^2|)^2]/\Sigma[w(F_0^4)]\}^{1/2}$

3.1.6   Synthesis of lanthanide complexes of ligand L$_1$

Synthesis of the lanthanide complexes were carried in high dilution conditions. KOH in methanol (0.010 mmol) was added to a solution of L$_1$ (2.1 mg, 0.0025 mmol) in 150 mL

methanol. The resulting solution was then refluxed and a solution of 0.0025 mmol $LnCl_3 \cdot nH_2O$ (Ln = Gd and Yb) in 150 mL methanol was added slowly over a period of time of 6 h. The solution was kept under reflux for an additional 6 h and the total volume of solvent reduced to 20 mL by evaporation. The resulted precipitate was filtered, washed three times with methanol and dried in vacuo over P_2O_5 for 48 h. ESI-MS for Yb^{3+} complex: 1014.0 (L_1+Yb-2H), 1036.1 (L_1+Yb-3H+Na), and 1052.0 (L_1+Yb-3H+K).

3.1.7 Synthesis of ligand L_2

The synthesis route of ligand L_2 is shown is Figure 3.6.
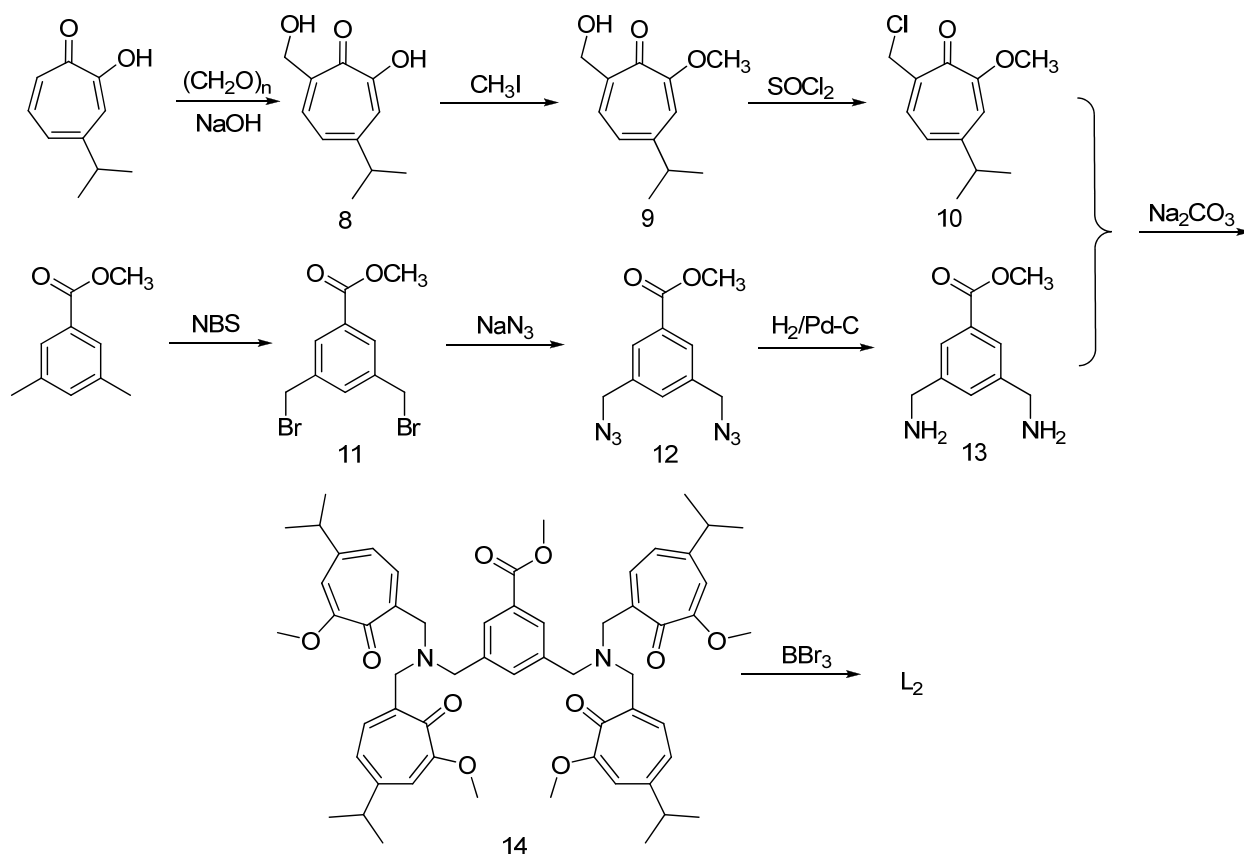
Figure 3.6: Synthesis route of ligand L_2
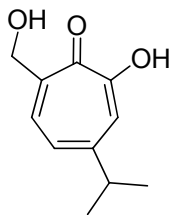
(2*E*,4*Z*,6*Z*)-2-Hydroxy-7-(hydroxymethyl)-4-isopropylcyclohepta-2,4,6-trienone

(8).[10] To a mixture of HThup (10.0 g, 60.9 mmol) and 8.7 mL 50% aqueous KOH were added 9.5 mL 27% HCHO and 10 mL water. The resulting mixture was heated for 5 h at 60-65 °C. The mixture was then evaporated at reduced pressure to give a yellow solid. This solid was purified by recrystallization from H_2O-Acetone, and by neutralization with 3M H_2SO_4 to give 7.3 g of the product **8** as an oil (61.7%). EI-MS: *m/z* [M]$^+$ 194.0944 (Calc. 194.0943 for $C_{10}H_{12}O_2$). ^{1}H NMR (CD$_3$COCD$_3$, 300 MHz): δ 1.28 (d, *J* = 6.9 Hz, 6H), 2.95 (m, *J* = 6.9 Hz, 1H), 4.72 (s, 2H), 7.15 (d, *J* = 10.2 Hz, 1H), 7.36 (s, 1H), 7.84 (d, *J* = 10.2 Hz, 1H). IR (Thin film, cm^{-1}): 3392 (O-H), 3221, 2964, 2930, 2874, 1614, 1544 (C=O), 1482, 1390, 1243, 1045, 711, 658.
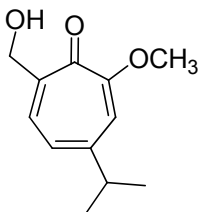
(2*E*,4*Z*,6*Z*)-7-(Hydroxymethyl)-4-isopropyl-2-methoxycyclohepta-2,4,6-trienone   (9).

To a solution of **8** (1.55 g, 8.00 mmol) dissolved in 10 mL acetone, CH$_3$I (1.20 g, 8.45 mmol) and K$_2$CO$_3$ (1.50 g, 10.87 mmol) were added. The mixture was kept reflux for 15 h. When TLC indicated the completion of the reaction, the mixture was filtered and evaporated to dryness. Flash chromatography on silica gel (ethyl acetate) allowed to obtain the product **9** (1.16 g, yield

70%). EI-MS: *m/z* [M]$^+$ 208.1099 (Calc. 208.1099 for $C_{12}H_{16}O_3$). ^{1}H NMR (CD$_3$COCD$_3$, 300 MHz): δ 1.27 (d, *J* = 6.9 Hz, 6H), 2.93 (m, *J* = 6.9 Hz, 1H), 3.91 (s, 3H), 4.44 (s, 1H), 4.57 (s, 2H), 6.89 (s, 1H), 6.92 (d, *J* = 9.3 Hz, 1H), 7.63 (d, *J* = 9.3 Hz, 1H). IR (Thin film, cm^{-1}): 3380 (O-H), 2962, 1600, 1565, 1549 (C=O), 1495, 1271, 1230, 1194, 1172, 1013, 845, 655.
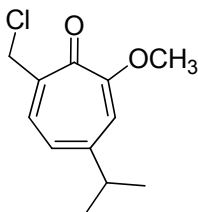
(2E,4Z,6E)-7-(Chloromethyl)-4-isopropyl-2-methoxycyclohepta-2,4,6-trienone (10).
To a solution of **9** (0.60 g, 2.88 mmol) dissolved in 20 mL of benzene, SOCl$_2$ (0.4 g, 3.36 mmol) was added dropwise under stirring and the solution turned cloudy. The solution turned clear after 1-2 h of additional stirring and TLC indicated the completion of the reaction. The solvent and the excess SOCl$_2$ were evaporated. Flash chromatography on silica gel (1:2 hexane/ethyl acetate) gave the product **10** (0.48 g, yield 74%). EI-MS: *m/z* [M]$^+$ 226.0762 (Calc. 226.0761 for $C_{12}H_{15}O_2Cl$). ^{1}H NMR (CD$_3$COCD$_3$, 300 MHz): δ 1.19 (d, *J* = 6.9 Hz, 6H), 2.80 (m, *J* = 6.9 Hz, 1H), 3.88 (s, 3H), 4.63 (s, 2H), 6.64 (s, 1H), 6.74 (d, *J* = 9.3 Hz, 1H), 7.53 (d, *J* = 9.6 Hz, 1H). IR (Thin film, cm^{-1}): 2964, 1598, 1583, 1503, 1233, 1050, 935.
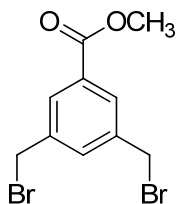
Methyl 3,5-bis(bromomethyl)benzoate (11).[11] A solution of methyl 3,5-dimethylbenzoate (1.68 g, 10.23 mmol), N-bromosuccinimide (3.56 g, 20.00 mmol), and benzoyl peroxide (500 mg, 2.06 mmol) in CCl_4 (15 mL) was refluxed for 3 h. After the cooling of the solution, the precipitate (succinimide) was separated and washed with CCl_4. The filtrate was washed with H_2O, dried ($MgSO_4$), and evaporated to dryness. The thick residue was suspended in petroleum ether and refrigerated. The product crystallized to yield the title compound **11** (2.7 g, 85%). Mp: 65-69 °C. EI-MS: m/z [M]$^+$ 319.9041 (Calc. 319.9048 for $C_{10}H_{10}O_2Br_2$). ^{1}H NMR (CDCl$_3$, 300 MHz): δ 3.93 (s, 3H), 4.49 (s, 4H), 7.61 (s, 1H), 7.99 (s, 2H). IR (KBr, cm^{-1}): 2951w, 1727, 1604, 1450, 1436, 1319, 1229, 995, 771, 698, 598.
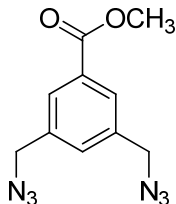
Methyl 3,5-bis(azidomethyl)benzoate (12). [Caution: This step is dangerous; the pure compound is explosive and should not be heated. A blast shield should also be used.]. Compound **11** (2.05 g, 6.37 mmol) was dissolved in acetone (100 mL) and sodium azide (3.00 g, 46.15 mmol) was added to this solution. The mixture was then refluxed for 24 h under nitrogen atmosphere whilst stirring. The reaction mixture was allowed to cool to room temperature and diluted with ether (30 mL) and water (50 mL). The organic layer was separated and washed with 70 mL of saturated sodium chloride, dried over Na_2SO_4, and the solvent removed in vacuo (without heating) to give the title compound as a colorless solid **12** (1.44 g, 92%). This material was used without further purification. EI-MS: m/z [M]$^+$ 246.0875 (Calc. 246.0865 for

$C_{10}H_{10}N_6O_2$). ^{1}H NMR (CDCl$_3$, 300 MHz): δ 4.04 (s, 3H), 4.61 (s, 4H), 7.72 (s, 1H), 8.10 (s, 2H). IR (Thin film, cm^{-1}): 2953w, 2102, 1723, 1609, 1435, 1308, 1224, 862, 767.
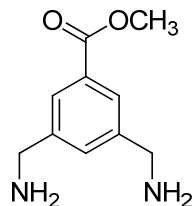
Methyl 3,5-bis(aminomethyl)benzoate (13). Compound **12** (0.50 g, 2.03 mmol) was dissolved in CH$_3$OH (50 mL) and Pd/C (0.2 g) was added. The reaction was carried out under hydrogen overnight. The solution was filtered and evaporated under vacuum to give the title compound **13** (0.37 g, 95%). EI-MS: *m/z* [M]$^+$ 194.1049 (Calc. 194.1055 for $C_{10}H_{14}N_2O_2$). ^{1}H NMR (CD$_3$OD, 300 MHz): δ 3.98 (s, 4H), 4.00 (s, 3H), 7.68 (s, 1H), 8.03 (s, 2H). IR (Thin film, cm^{-1}): 3421, 3312, 3252, 2954, 2035, 1719, 1600, 1431, 1313, 1229, 1116, 940, 767, 633.
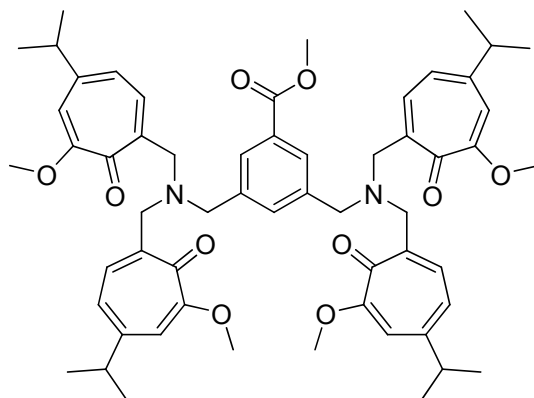
Methyl-3,5-bis((bis((((1Z,3Z,5E)-4-isopropyl-6-methoxy-7-oxocyclohepta-1,3,5-trienyl)methyl)amino)methyl)benzoate (14). To a solution of **10** (0.384 g, 1.98 mmol)

dissolved in 20 mL CH$_3$CN, Na$_2$CO$_3$ (0.80 g, 7.55 mmol) was added. The mixture was heated to 60-70 °C. A DMF/CH$_3$CN solution of **13** was then added dropwise to this reaction mixture within half an hour. The solution was kept at 60-70 °C overnight. TLC showed the completion of reaction; the mixture was filtered and the filtrate was evaporated. Flash chromatography on silica gel (3:1 ethyl acetate/methanol) allowed the separation of the product **14** (0.55 g, yield 37%). Q-TOF-MS: *m/z* [M+Na]$^+$ 977.4916 (Calc. 977.4928 for C$_{58}$H$_{70}$N$_2$O$_{10}$Na). ^{1}H NMR (CDCl$_3$, 300 MHz): δ 1.21 (d, *J* = 6.9 Hz, 24H), 2.79 (m, *J* = 6.9 Hz, 4H), 3.71 (s, 4H), 3.74 (s, 8H), 3.86 (s, 3H), 3.90 (s, 12H), 6.65 (s, 4H), 6.80 (d, *J* = 9.6 Hz, 4H), 7.65 (s, 1H), 7.88 (d, *J* = 9.6 Hz, 4H), 7.89 (s, 2H). ^{13}C NMR (CDCl$_3$, 75 MHz): δ 23.5, 38.6, 52.0, 56.1, 56.4, 58.8, 113.5, 124.1, 127.8, 130.2, 132.3, 135.0, 140.1, 143.6, 152.4, 162.6, 167.1, 179.1. IR (Thin film, cm^{-1}): 3052, 2962, 1722, 1598, 1580, 1574, 1504, 1462, 1266, 1226, 1195, 1172, 1039, 732.

L$_2$
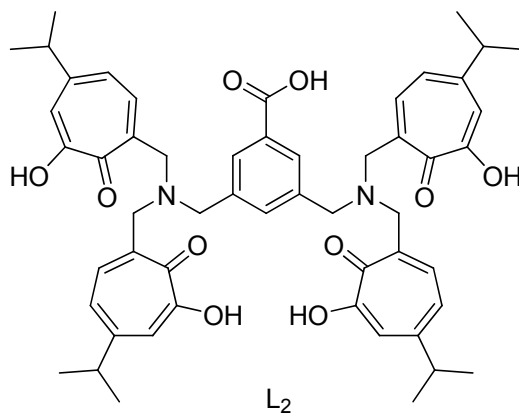
3,5-Bis((bis(((1Z,3Z,5E)-6-hydroxy-4-isopropyl-7-oxocyclohepta-1,3,5-trienyl)methyl)amino)methyl)benzoic acid (L$_2$). To a solution of **14** (0.55 g, 0.58 mmol) dissolved in 50 mL CH$_2$Cl$_2$, BBr$_3$ (2.62 g, 10.46 mmol) was added dropwise at -78 °C. The mixture was kept at this temperature for 4 h, and then reacted for an additional 24 h at room

temperature. The mixture was quenched with water on ice bath and evaporated to dryness. Water was added, the solid filtered and dried to give the product L_2 (0.392 g, 77%). Q-TOF-MS: m/z [M+H]$^+$ 885.4300 (Calc. 885.4326 for $C_{53}H_{61}N_2O_{10}$). ^{1}H NMR (CD$_3$OD, 300 MHz): δ 1.23 (d, J = 6.9 Hz, 24H), 2.89 (m, J = 6.9 Hz, 4H), 4.62-4.86 (m, 12H), 7.00 (d, J = 9.9 Hz, 4H), 7.21 (s, 4H), 7.73 (d, J = 9.6 Hz, 4H), 8.14 (s, 2H), 8.21 (s, 1H). IR (KBr, cm^{-1}): 3423, 2966, 1709, 1607, 1545, 1464, 1441, 1409, 1328, 1286, 1252, 1218, 1189, 1128, 956, 738.

3.2   RESULTS AND DISCUSSION

3.2.1   Synthesis of ligand L_1 and its lanthanide (Yb^{3+} and Gd^{3+}) complexes

The synthetic sequence leading to L_1 from 1,2,4,5-tetrakis(bromomethyl)-benzene and cycloheptone or tropolone is depicted in Figure 3.2. 1,2,4,5-tetrakis(bromomethyl)-benzene was treated with NaN$_3$ in acetone for 24 h to give 1,2,4,5-tetrakis(azidomethyl)-benzene (**2**) in 95% yield. **2** was reduced under H$_2$ by using Pd/C as the catalyst at room temperature to give 1,2,4,5-tetrakis(aminomethyl)-benzene (**3**) quantatively.

Two methods were used to synthesize compound 6. Method **I**: Cycloheptanone was oxidized by SeO$_2$ in ethanol to give 1,2-cycloheptadione, followed by treating with Br$_2$ in acetic acid and acetate hydride for 3 d to give 2-bromo-7-hydroxy-2,4,6-cycloheptatrien-1-one (**4**). The yield for this step was only 8%. **4** was treated with ethyl sodioacetoacetate in dry dioxane for 18 h followed by acidification to give 3-acetyl-8-hydroxy-1-oxaazulan-2-one (**5**) in 94% yield. **5** was heated in HBr for 2 h to give 2-hydroxy-3-oxo-1,4,6-cycloheptatriene-1-acetic acid (**6**) in 76% yield. Due the low yield during the synthesis of compound **4**, method **II** was used to

synthesize **6**. Tropolone was used as the starting material in this method: tropolone was treated with benzenesulfonyl chloride in dry pyridine for 12 h at room temperature, followed by recrystallization from EtOH to give 7-oxocyclohepta-1,3,5-trienyl benzenesulfonate (**8**) in 93.2% yield. **8** was treated with ethyl malonate and NaOEt in EtOH followed by acidification with 6 M HCl to give ethyl 8-hydroxy-2-oxo-2*H*-cyclohepta[*b*]furan-3-carboxylate (**9**) in 85% yield. **9** was heated in HBr for 2 h to give 2-hydroxy-3-oxo-1,4,6-cycloheptatriene-1-acetic acid (**6**) in 75% yield.

Two methods were used to synthesize compound 8-hydroxy-2*H*-cyclohepta[*b*]furan-2-one (**7**). Method I: **6** was treated in 1M H_2SO_4 to give **7** in 60% yield. The yield of this step is not high and the byproduct is difficult to remove. So method **II** was used to synthesize **7**. 6 was treated with DCC in dry THF for 24 h at room temperature, followed by recrystallization of the raw product in methanol to give **7** in 86% yield. L_1 was obtained by heating **7** with **3** in 4:1 molar ratio in DMF at 120 °C for 6h in 60% yield.

Lanthanide complexes of L_1 were synthesized in methanol at highly dilutied concentration to avoid the formation of intermolecular species. The result from ESI-MS indicates the formation of ML type complex.

3.2.2 Synthesis of ligand L_2

The synthetic sequence leading to L_2 from methyl-3,5-dimethylbenzoate and hinokitiol is depicted in Figure 3.6. Hinokitiol (HThup) was treated with HCHO in aqueous KOH followed by acidification to give (2*E*,4*Z*,6*Z*)-2-hydroxy-7-(hydroxymethyl)-4-isopropylcyclohepta-2,4,6-trienone (**8**) in 61.7% yield. **8** was treated with CH3I in acetone to give the methyl protected product (2*E*,4*Z*,6*Z*)-7-(hydroxymethyl)-4-isopropyl-2-methoxycyclohepta-2,4,6-trienone (**9**) in

70% yield. **9** was treated with $SOCl_2$ in dry benzene to give (2*E*,4*Z*,6*E*)-7-(chloromethyl)-4-isopropyl-2-methoxycyclohepta-2,4,6-trienone (**10**) in 74% yield.

Methyl 3,5-dimethylbenzoate was treated with N-bromosuccinimide in CCl_4 for 3 h to give methyl 3,5-bis(bromomethyl)benzoate (**11**). **11** was treated with NaN_3 in acetone for 24 h followed by reduction under H_2 by using Pd/C as catalyst to give methyl 3,5-bis(aminomethyl)benzoate (**13**) in 95% yield.

10 was reacted with **13** in a mixture solvent of DMF and CH_3CN for 24 h to give full protected ligand L_2: methyl-3,5-bis((bis(((1*Z*,3*Z*,5*E*)-4-isopropyl-6-methoxy-7-oxocyclohepta-1,3,5-trienyl)methyl)amino)methyl)benzoate (**14**) in 37% yield. The methyl groups were removed by treating **14** with BBr_3 in CH_2Cl_2 for 24 h to give L2 in 77% yield.

3.2.3   Modeling of lanthanide complex with L_1: $[Ln(L_1)]^-$

The modeling of the lanthanide complex formed with L_1 was performed with the help of the software CAChe.[12] The structure of the $[LnL_1]^-$ was refined by performing an optimized geometry calculation in molecular mechanics using augmented *MM3* parameters. The resulting predicted structure is shown in Figure 3.7. The ligand acts as an octadentate ligand, coordinating Ln^{3+} with its eight oxygen atoms from the four tropolonate units. This figure also indicates that the access to Ln^{3+} by the solvent molecules is prevented through the ligand design (good protection of Ln^{3+}).
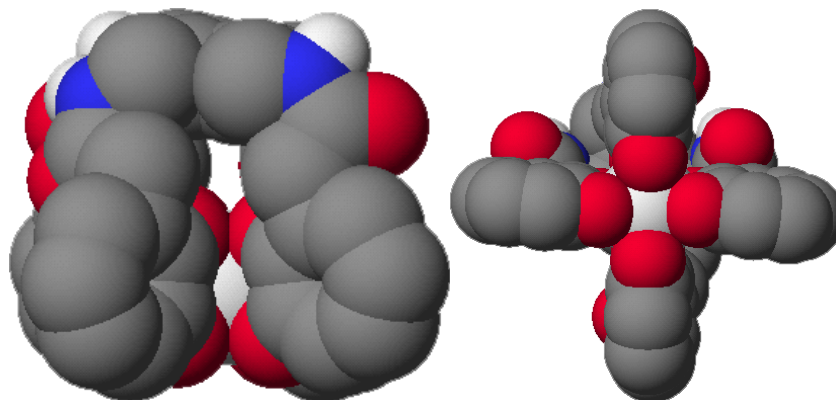
Figure 3.7: Two different views of the optimized structure (CAChe, *MM3* molecular mechanics) of [Ln(L$_1$)]$^-$

3.2.4   Absorption, excitation and emission spectra of [Yb(L$_1$)]$^-$

As we expected, the absorption spectrum of [Yb(L$_1$)]$^-$ in DMSO is similar to the spectrum of [Yb(Trop)$_4$]$^-$ in the same solvent (Figure 3.8). In both cases, the apparent maxima of the envelope of the absorption bands are located around 337 nm and 385 nm. These bands are attributed to the $^1\pi \rightarrow \pi^*$ transition located on the four Trop$^-$ units in the octadentate ligand. The linkage of the derivatives of tropolonates to the common backbone does not affect significantly their electronic structure. The similarity between the absorption spectra of [Yb(L$_1$)]$^-$ and [Yb(Trop)$_4$]$^-$ also indicate that there is no electronic communication between the Trop$^-$ moieties in ligand L$_1$.

The excitation spectrum of [Yb(L$_1$)]$^-$ (Figure 3.9) was measured upon monitoring the emission narrow band of Yb^{3+} centered at 979 nm. This excitation spectrum is similar in shape to the absorption spectrum of [Yb(L$_1$)]$^-$ (Figure 3.8), which indicates that this ligand sensitizes the luminescence of Yb^{3+} through the chromophoric tropolonate units. Upon excitation of the ligand at 340 nm, the characteristic sharp emission splitted band of Yb^{3+} centered around 980 nm was

observed (Figure 3.9). The crystal field splitting was observed (three main bands with apparent maxima at 979, 992 and 1023 nm), which is similar to that observed for KYb(Trop)$_4$ in DMSO (Figure 2.23).
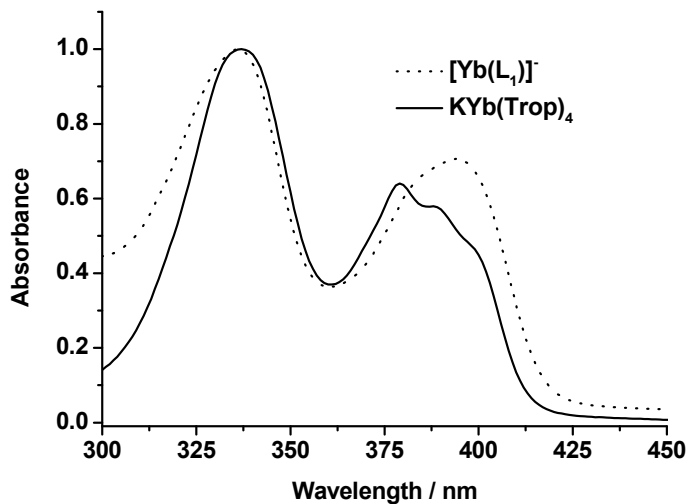
Figure 3.8: Normalized absorption spectra of [Yb(L$_1$)]$^-$ and KYb(Trop)$_4$ in DMSO (10^{-5} M, 298 K)
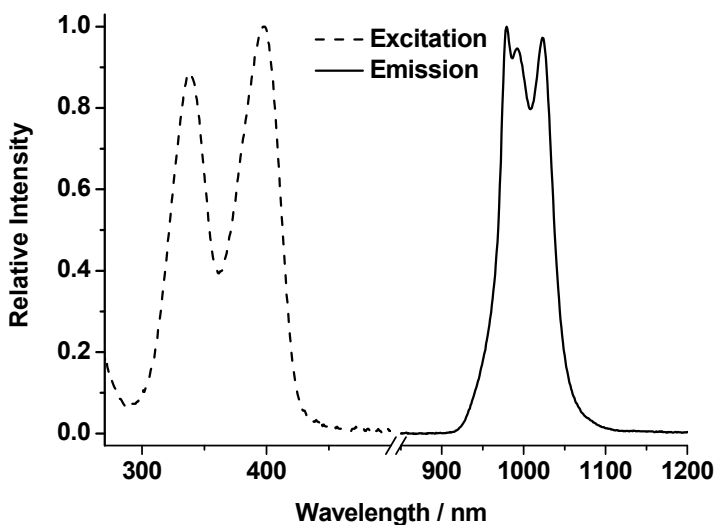
Figure 3.9: Normalized emission (λ_{ex} = 340 nm) and excitation spectra (λ_{em} = 980 nm) of [Yb(L$_1$)]$^-$ (10^{-5} M, 298 K)

3.2.5 Overall quantum yield and luminescence lifetime of Yb^{3+} in $[Yb(L_1)]^-$

Quantum yields of the sensitized emission of Yb^{3+} complex in different solvents were determined by using $KYb(Trop)_4$ as reference. The luminescence lifetimes were also measured in different solvents. All the results are tabulated in Table 3.2.

Table 3.2: Quantum yields (Φ) and luminescence lifetimes (τ) of $[Yb(L_1)]^-$ in different solvents

Solvent	Deuterated		Non-deuterated		$k_{q, solv}$ $(s^{-1})^c$
	Φ^a	τ $(\mu s)^b$	Φ^a	τ $(\mu s)^b$	
DMSO	3.6×10^{-2}	15.84(3)	2.0×10^{-2}	12.68(4)	$1.57\cdot10^4$
Methanol^d	4.1×10^{-2}	15.5(2)	6.1×10^{-3}	5.13(8)	$1.30\cdot10^5$
Water^d	1.8×10^{-2}	13.8(2)	2.9×10^{-3}	2.77(2)	$2.88\cdot10^5$

a. Quantum yields were measured using $[Yb(Trop)_4]^-$ as reference, estimated error 10%.
b. Luminescence lifetimes are the average values of three independent measurements. λ_{ex} = 337 nm (nitrogen laser).
c. k_q,solv is the quenching rate of the solvent. $k_{q,solv} = 1/\tau_H - 1/\tau_D$.
d. Mixture of solvents was used: 3% DMSO was used due to the limited solubility of complex.

All the quantum yield values measured in different solvents for $[Yb(L_1)]^-$ are larger than those reported for the $KYb(Trop)_4$ complex. It is important to notice that the quantum yield of $[Yb(L_1)]^-$ in water is about 12 times higher than that in $KYb(Trop)_4$, which can be viewed as a result of improved protection. This result indicates that the introduction of the backbone provides a better protection to Ln^{3+}, assuming the energy transfer is comparable with the $KLn(Trop)_4$ tropolonate complexes. This hypothesis is supported by the result of the measurements and calculations of q values. According to the empirical formula developed by Beeby et al.[13] and Davies et al.[14], the q values for $[Yb(L_1)]^-$ were calculated to be 0.06 and 0.09 in methanol and water respectively. These two values can be interpreted as the absence of water/solvent molecules bound in first sphere of coordination to Ln^{3+}, a different result in comparison to the measurements obtained for $KYb(Trop)_4$ where similar measurements indicated the presence of

96

one molecule of water bound to Ln^{3+} in first sphere of coordination. Therefore, no significant source of non-radiative deactivation due to O-H, N-H, and C-H vibration are present, which is consistent with the higher quantum yield of $[Yb(L_1)]^-$.

3.2.6   Ligand-centered visible luminescence

The fluorescence spectrum of $[Yb(L_1)]^-$ at room temperature and phosphorescence spectrum of $[Gd(L_1)]^-$ at 77 K in DMSO were recorded and are shown in Figure 3.10. These fluorescence and phosphorescence spectra are very similar to those observed for the corresponding $KLn(Trop)_4$ complex. Both phosphorescence spectra contain two sharp bands with apparent maxima of electronic envelope at 590 nm (16,950 cm^{-1}) and 640 nm (15,630 cm^{-1}). This result indicates that the energies of the singlet and triplet electronic states of the ligand are not significantly affected by the attachment of a backbone to the tropolonate chelating group. The phosphorescence lifetimes of triplet states in both complexes are long, 5.5 ± 0.1 ms (587 nm and 640 nm) for $KGd(Trop)_4$ and 5.8 ± 0.3 ms (589 nm and 641 nm) for $[Gd(L_1)]^-$. These phosophorescence lifetime results indicate that the depopulation rate of the triplet states for both complexes are also similar as a result of similar electronic structures of the tropolonate moieties.

3.2.7   Dilution experiment

The lanthanide complexes formed with the octadentate ligand L_1 are hypothesized to have higher stability than the corresponding $KLn(Trop)_4$ complexes due to entropic effects. Due to the low solubility of $[Ln(L_1)]^-$, it would have been difficult to evaluate stability constants through the classical spectrophotometric titrations. Therfore, we have evaluated the stability of this complex

97

through dilution experiments. Since lanthanides are very labile metal cations, more dissociation will happen if the lanthanide complex is more diluted, depending on the stability constant of the complex. The more dissociated complex, the less luminescence should be detected due to the sensitizing antennae not being connected to Ln^{3+} and the quenching from the solvent molecules deactivating its excited states. Therefore, the relative thermodynamic stability can be estimated by measuring the decay of the luminescence intensity upon dilution of the two systems. The luminescence intensity decreases upon dilution of the complexes until the limit of instrumental detection were measured and are reported in Figure 3.11 and Table 3.3.
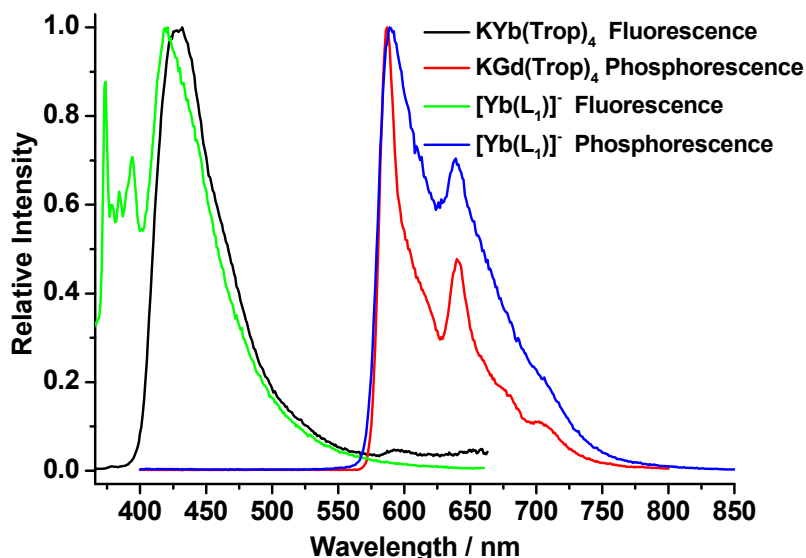
Figure 3.10: Normalized fluorescence spectra of $[Yb(L_1)]^-$ and $KYb(Trop)_4$ at 298 K and phosphorescence spectra for $[Gd(L_1)]^-$ and $KGd(Trop)_4$ at 77 K and 0.1 ms delay time (DMSO, 10^{-5} M, λ_{ex} = 340 nm)
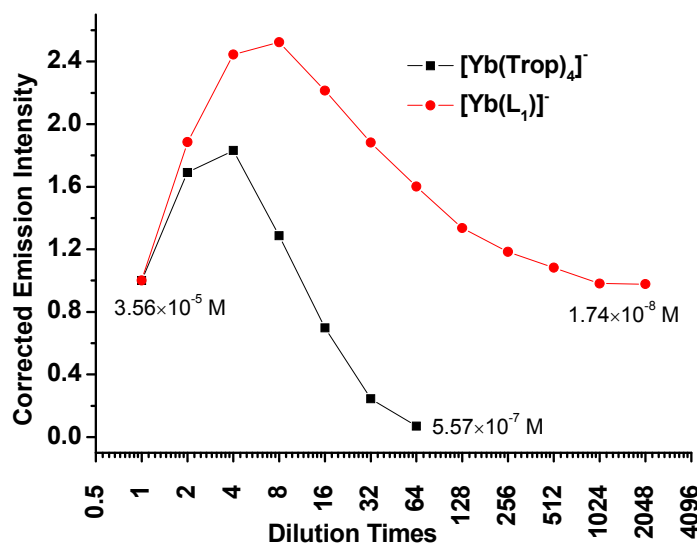
Figure 3.11: Corrected Yb^{3+}-centered luminescence intensity vs. dilution times. (Corrected intensity = measured intensity × dilution factor).

Table 3.3: Corrected luminescence intensities of complexes [Yb(Trop)$_4$]$^-$ and [Yb(L$_1$)]$^-$ in DMSO

Dilution factor	Concentration (M)	[Yb(Trop)$_4$]$^-$		[Yb(L$_1$)]$^-$	
		Intensity[a]	Corrected intensity[b]	Intensity[a]	Corrected intensity[b]
1	3.56×10^{-5}	1.0000	1.0000	1.0000	1.0000
2	1.78×10^{-5}	0.8460	1.6920	0.9426	1.8852
4	8.91×10^{-6}	0.4578	1.8312	0.6111	2.4444
8	4.46×10^{-6}	0.1608	1.2864	0.3155	2.5240
16	2.23×10^{-6}	0.0436	0.6976	0.1384	2.2144
32	1.11×10^{-6}	0.0076	0.2432	0.0588	1.8816
64	5.57×10^{-7}	0.0011	0.0704	0.0250	1.6000
128	2.79×10^{-7}			0.0104	1.3312
256	1.39×10^{-7}			0.0046	1.1776
512	6.96×10^{-8}			0.0021	1.0752
1024	3.48×10^{-8}			0.0010	1.0240
2048	1.74×10^{-8}			0.0005	1.0240

a. The initial absorbance of both solutions was kept as A = 2.0. The initial emission intensity was normalized to 1.
b. The dilution effect was corrected by multiplying the observed intensity value by the dilution factor.

For both complexes an increase in luminescence intensity can be observed for the initial 2-3 dilutions. This can be attributed to the "inner filter effect" due to the high absorbance of the initial solution (A = 2.0, in 1 cm cell) at the excitation wavelength (340 nm). When subsequent dilutions are carried out, the corrected luminescence intensities of both complexes decrease. This can be explained as follows: firstly, the solvent was not completely dry (typically, a freshly opened bottle of DMSO solvent contains at least 400 ppm of water (which represents a concentration of about 5.6×10^{-3} M), so the molar ratio of water to Yb^{3+} complex increases when the solution of complexes is more diluted. For example, the initial molar ratio of water to Ln^{3+} complex is about 168 to 1, after dilution 6, the ratio is 10,763 to 1, and 344,408 to 1 after dilution 11. The increasing ratio of water molecules to Ln^{3+} due to the increasing dilution leads to a higher luminescence quenching probability. This quenching could happen through the first or second coordination sphere mechanisms. Secondly, the complex might partially dissociate at lower concentration since the water molecules can act as a competing ligand, which is more pronounced for $KYb(Trop)_4$.

The observation of the signal arising from Yb^{3+} in $[Yb(L_1)]^-$ at significantly lower concentration than $[Yb(Trop)_4]^-$ is a strong indication of the higher stability of $[Yb(L_1)]^-$ in comparison to $[Yb(Trop)_4]^-$. The signal of $[Yb(Trop)_4]^-$ vanished completely after the 32nd dilution. The signal of $[Ln(L_1)]^-$ can still be observed at dilution factor of 2048 and tends to plateau. At 10^{-8} M, the luminescence of Yb^{3+} is still observable using a Xenon lamp as a source of excitation and further experiments will allow us to determine the absolute lower limit of detection that also depends on the fluorimeter.

3.3   CONCLUSION

This chapter describes the synthesis and characterization of two new octadentate ligands (L_1 and L_2) and the photophysical properties of the Gd^{3+} and Yb^{3+} complexes formed with ligand L_1. Dilution experiments indicate that, by using a common backbone to connect four tropolone chelating units to form an octadentate ligand, the stability of the resulted complex $[Yb(L_1)]^-$ was increased significantly in comparison to $KYb(Trop)_4$. The luminescence signal of the $[Yb(L_1)]^-$ was observable at low concentration (10^{-8} M). This achievement is important for biological applications since concentration of most luminescent reporters typically must be in a range of concentration between 10^{-8} to 10^{-10} M.

Similar photophysical properties of tropolonate and L_1 were observed, which indicates that the attachment to a backbone does not significantly affect the electronic structure of $Trop^-$. The octadentate ligand offers a better protection to Ln^{3+} for $[Ln(L_1)]^-$ in solution compared to $KYb(Trop)_4$. Calculations from the measured luminescence lifetimes indicate that no water molecules are bound to Ln^{3+}, and the non-radiative deactivation of the excited states of Ln^{3+} from high energy O-H vibration was minimized. We have demonstrated here through the modification of the ligand by incorporation of a common backbone and the formation of an octadentate ligand, that we have been able to remove or decrease two limitations of the previously described of $KLn(Trop)_4$ for bioanalytical and imaging applications in solution: i) the limited stability and ii) the incomplete protection of Ln^{3+} from the solvent molecules. The presence of the backbone does not modify significantly the photophysical properties of the resulting $[Yb(L_1)]^-$ complex. On the basis of the complexes formed with four bidentate ligands, it is possible to predict part of the luminescence properties of the complexes formed with the octadentate ligand that requires more effort for its synthesis

3.4　REFERENCES

(1)　　a) Petoud, S.; Cohen, S. M.; Bünzli, J.-C. G.; Raymond, K. N. *J. Am. Chem. Soc.* **2003**, *125*, 13324; b) Petoud, S.; Müller, G.; Moore, E. G.; Xu, J.; Sokolnicki, J.; Riehl, J. P.; Le, U. N.; Cohen, S. M.; Raymond, K. N. *J. Am. Chem. Soc.* **2007**, *129*, 77.

(2)　　a) Pope, S. J. A.; Coe, B. J.; Faulkner, S. *Chem. Commun.* **2004**, 1550; b) Wolbers, M. P. O.; van Veggel, F. C. J. M.; Snellink-Ruel, B. H. M.; Hofstraat, J. W.; Guerts, F. A. J.; Reinhoudt, D. N. *J. Chem. Soc., Perkin Trans. 2* **1998**, 2141.

(3)　　Wolbers, M. P. O.; van Veggel, F. C. J. M.; Peters, F. G. A.; Van Beelen, E. S. E.; Hofstraat, J. W.; Geurts, F. A. J.; Reinhoudt, D. N. *Chem.-Eur. J.* **1998**, *4*, 772.

(4)　　Comby, S.; Imbert, D.; Chauvin, A.-S.; Bünzli, J.-C. G. *Inorg. Chem.* **2006**, *45*, 732.

(5)　　Comby, S.; Imbert, D.; Vandevyver, C.; Bünzli, J.-C. G. *Chem.-Eur. J.* **2007**, *13*, 936.

(6)　　Zhang, J.; Badger, P. D.; Geib, S. J.; Petoud, S. *Angew. Chem., Int. Ed.* **2005**, *44*, 2508.

(7)　　Kondo, E.; Hayashi, Y.; Konishi, T.; Hattori, T.; Shoji, J., Tropolone and derivatives as anti-mycoplasma agents, and their preparation, U.S., 4,950,686, 1990

(8)　　Takase, K. *Bull. Chem. Soc. Jpn.* **1964**, *37*, 1460.

(9)　　Nozoe, T.; Takase, K.; Kato, M.; Nogi, T. *Tetrahedron* **1971**, *27*, 6023.

(10)　　Nozoe, T.; Mukai, T.; Takase, K. *Science Repts. Tohoku Univ.* **1952**, *36*, 40.

(11)　　Markovac, A.; LaMontagne, M. P. *J. Med. Chem.* **1980**, *23*, 1198.

(12)　　CAChe WorkSystem Pro., 6.1.12.33., Fujitsu Limited Inc., USA, 2004

(13)　　Beeby, A.; Burton-Pye, B. P.; Faulkner, S.; Motson, G. R.; Jeffery, J. C.; McCleverty, J. A.; Ward, M. D. *J. Chem. Soc., Dalton Trans.* **2002**, 1923.

(14)　　Davies, G. M.; Aarons, R. J.; Motson, G. R.; Jeffery, J. C.; Adams, H.; Faulkner, S.; Ward, M. D. *J. Chem. Soc., Dalton Trans.* **2004**, 1136.

4.0 STRUCTURAL AND NEAR-INFRARED LUMINESCENCE PROPERTIES OF LANTHANIDE COMPLEXES FORMED WITH LIGANDS DERIVED FROM TROPOLONATE

Since *f-f* transitions are Laporte forbidden[1], free Ln^{3+} have low extinction coefficients, and their direct excitation is not efficient. Therefore, it is advantageous to sensitize these cations with suitable chromophores ("antenna effect").[2] Several ligand/chromophore systems have been tested for the sensitization of NIR emitting Ln^{3+}. The substituents of molecules can dramatically affect their electronic structures and properties such as the energies of their singlet and triplet states as well as the luminescent properties of the corresponding lanthanide complexes. As an example, Werts et al.[3] studied the photophysical properties of NIR emitting lanthanide complexes formed with ligands derived from DTPA (diethylene triamine pentaacetic acid) that incorporate two different sensitizers: eosin and fluorescein. Eosin is a tetrabromo-derivative of fluorescein, and it has a triplet energy level located at lower energy than fluorescein. Eosin-derived complexes of Yb^{3+} and Nd^{3+} have higher quantum yields in comparison to their respective fluorescein analogues.[3] Different results were obtained by Hebbink et al.[4] in their study of the sensitization of NIR Ln^{3+} (Yb^{3+}, Nd^{3+}, and Er^{3+}) by using triphenyl-based ligands attached to fluorescein, eosin and erythrosine as the antenna groups. These authors observed that all the complexes formed with the ligand incorporating fluorescein have the highest quantum yield values. Van Deun et al.[5] and Iwamuro et al.[6] tested the 8-hydroxyquinoline and its chloro and bromo

derivatives as ligands and chromophoric components to study the NIR luminescent complexes formed with Er^{3+} and Nd^{3+} respectively. Both authors found that the incorporation of a halogen atom in the chromophore strongly increases the quantum yields (increase of 30% and 150% respectively). They attributed this effect to the heavy-atom effect.[7-9] Similar result has been observed by Albrecht et al.[7] The quantum yields of the complexes (Yb^{3+}, Nd^{3+}, and Er^{3+}) formed with bromo substituted ligand are almost three times higher compared to the complexes formed with the unsubstituted ligand.

One strategy to obtain better rationalization of the ligand-to-Ln^{3+} energy transfer is to establish the relationship between the structure of ligand and the luminescence properties of the complex. We have previously reported that tropolonate (Trop⁻) is an efficient sensitizer for five different NIR emitting lanthanide cations.[8] In the present work, we have extended our research work to a broader selection range of ligands belonging to the tropolonate family. Six derivatives of tropolonate ligands and their corresponding lanthanide complexes were synthesized and characterized (Figure 4.1). The NIR luminescence properties of the resulting complexes were studied and compared with those of the Trop⁻ complexes. These six derivatives are: 3-isopropyltropolone (2-hydroxy-4-isopropylcyclohepta-2,4,6-trienone, **HThup**), 2-bromotropolone (2-bromo-7-hydroxy-cyclohepta-2,4,6-trienone, **HBrTP**), 5-nitrotropolone (2-hydroxy-5-nitrocyclohepta-2,4,6-trienone, **HNTP**), and 5-aminotropolone (5-amino-2-hydroxycyclohepta-2,4,6-trienone, **HMTP**) 4,5-benzotropolone (6-hydroxy-7*H*-benzo[7]annulen-7-one, **2-HBTP**), 3,4-benzotropolone (6-hydroxy-5*H*-benzo[7]annulen-5-one, **1-HBTP**). The systematic study of the photophysical properties of the luminescent lanthanide complexes formed with ligands having similar parent structure but different substituents is a useful systematic methodology to obtain a better understanding of the energy transfer from the

sensitizer to Ln^{3+} as well as of the parameters that control it. The choice of these six substituting groups was made on the criteria of modifying significantly the electronic structure of tropolonate and the resulting complexes in different directions. The nitro substituent is a strong electron withdrawing group, and its introduction is hypothesized to decrease the electronic density of the seven-membered ring, which is expected to modify the energy positions and populations of the singlet and triplet states. As a result, the intra-molecular energy transfer between the ligand and the Ln^{3+} in the complexes should be modified.[9] On the other hand, the amino substituent is a strong electron-donating group, and is hypothesized to have the opposite effect on the electronic density of the Trop⁻ ring compared with the nitro group. The bromo group and isopropyl group are somewhat in the middle in terms of the effect of electron density on the tropolonate ring. The bromo group is both inductive electron withdrawing and resonance electron donating, and the isopropyl is a weak electron donating group. In addition, the bromo group is expected to generate a heavy atom effect[10-12], which will increase the population of its triplet state by enhancing the intersystem crossing process. Both 2-HBTP and 1-HBTP are benzotropolones. In both bidentate ligands, the aromatic resonance structure of tropolone is further extended, which is typically hypothesized to decrease the energy gap between ground and excited states of the molecule, lowering the energy of the corresponding singlet and triplet states. We will study systematically the effect of these six substituting groups on the electronic structure of Trop⁻ and on the photophysical properties of their corresponding lanthanide complexes.
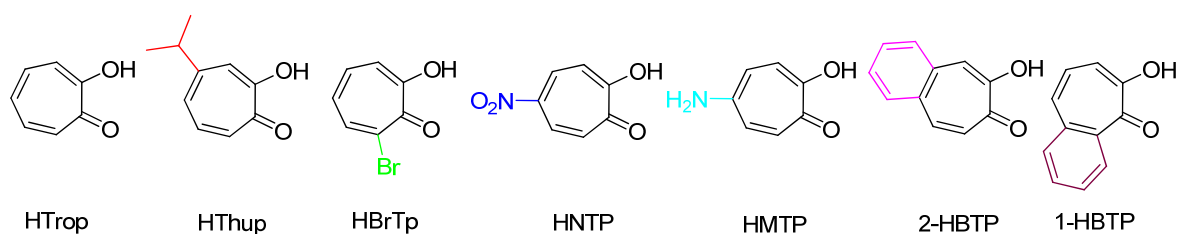
Figure 4.1: Chemical structures and abbreviated names of the ligands discussed in this chapter

4.1 EXPERIMENTAL SECTION

4.1.1 Materials

All reagents were used as received, unless otherwise stated. Tropolone (HTrop), β-Thujaplicin (HThup), cycloheptanone, selenium dioxide, bromine, phthalaldehyde, methoxyacetone, benzosuberone, anhydrous ethereal HCl, n-butyl nitrite, $LnCl_3 \cdot nH_2O$ (Ln = Nd, Gd, Er, Tm, and Yb, 99.9% or 99.99%, n = 6 or 7 depending on the Ln), and KOH standardized solution in methanol (0.100 M) were purchased from Aldrich. Synthesis of HBrTP has been described in chapter 3 in this dissertation.

4.1.2 Methods

Infrared spectra were recorded on a Perkin-Elmer Spectrum BX FT-IR instrument. Elemental analyses were performed by Atlantic Microlab, Inc. (Norcross, Georgia). ^{1}H NMR spectra were recorded on a Bruker DPX-300 spectrometer at 300 MHz. MS-ESI were measured on an Agilent HP 1100 series LC-MSD instruments. UV-vis absorption spectra were recorded on a Perkin-Elmer Lambda 9 spectrophotometer.

4.1.3 Luminescence measurements

Emission and excitation spectra were measured using a modified Jobin Yvon Horiba Fluorolog-322 spectrofluorimeter equipped with a Hamamatsu R928 detector for the visible domain and a DSS-IGA020L detector (Electro-Optical Systems, Inc.) for the NIR domain. Time-resolved

measurements were conducted with a Jobin-Yvon Spex Fluorolog-3 spectrofluorimeter equipped with a phosphorimeter module and Xenon flash lamp. The emission spectra were then collected, with increasing delay times until the phosphorescence band was the main band on a spectrum (at delay 0.1 ms). The emission spectra were corrected for the background and instrumental response. The NIR luminescence relative quantum yields were measured by using a KYb(Trop)$_4$ complex ($\Phi = 1.9 \times 10^{-2}$ in DMSO) as a reference.[8] Spectra were corrected for the instrumental function for both excitation and emission. Quantum yield values were calculated using the

following equation: $\dfrac{\Phi_x}{\Phi_r} = \dfrac{A_{r_{\lambda_x}}}{A_{x_{\lambda_x}}} \dfrac{I_{\lambda_r}}{I_{\lambda_x}} \dfrac{\eta_x^2}{\eta_r^2} \dfrac{D_x}{D_r}$, where the subscript r stands for the reference and x for

the sample; A is the absorbance at the excitation wavelength, I is the intensity of the excitation light at the same wavelength, η is the refractive index($\eta = 1.478$ in DMSO), and D is the measured integrated luminescence intensity. The luminescence lifetime measurements were performed by excitation of solutions in 1 cm quartz cells using a Nd:YAG Continuum Powerlite 8010 Laser at 354 nm (3rd harmonic) as excitation source. Emission was collected at a right angle to the excitation beam, the emission wavelength selected with a Spectral Products CM 110 1/8 meter monochromator. The signal was monitored by a cooled photomultiplier (Hamamatsu R316-2) coupled to a 500 MHz bandpass digital oscilloscope (Tektronix TDS 754D). The signals to be treated (at least 15,000 points resolution for each trace) were averaged from at least 500 individual decay curves. Luminescence decay curves were imported into Origin 7.0 scientific data analysis software. The decay curves were analyzed using the Advanced Fitting Tool module. Reported luminescence lifetimes are averages of at least three independent determinations.

4.1.4 X-ray crystallography

Crystals suitable for X-ray diffraction were coated with Fluorolube® then mounted on a glass fiber and coated with epoxy cement. X-ray data were collected on a Bruker Apex diffractometer using graphite monochromatized Mo K_α radiation ($\lambda = 0.71073$ Å). Data collection was controlled using the Bruker SMART program, and the data processing was completed with the SHELXTL program package. Graphical representations were obtained with the help of Diamond 3.0 software packages. All hydrogen atoms were calculated and placed in idealized positions ($d_{C-H} = 0.96$ Å).

4.1.5 Synthesis of HNTP

The synthesis route of HNTP is shown in Figure 4.2.
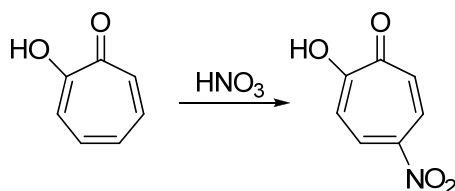
Figure 4.2: Synthesis of HNTP

HNTP was synthesized according the method described by Doering *et al.*[13]. A solution of tropolone (1.00 g, 8.20 mmol) in 40 mL of water was treated with 40 mL of cold 1:1 nitric acid. Crystallization occurred within 10 to 15 min. The title compound HNTP was immediately centrifuged and washed twice with cold water and dried (0.48 g, 35 %). Mp: 191 °C. EI-MS: *m/z* [M]$^+$ 167.021789 (Calc. 167.021858). ^{1}H NMR (CD$_3$COCD$_3$, 300 MHz): δ 7.40 (d, *J* = 12 Hz,

2H), 8.58 (d, J = 12 Hz, 2H). IR (KBr, cm^{-1}): 3204, 3055, 1612, 1565, 1525, 1457, 1419, 1313, 1266, 1230, 1201, 1089, 1041, 887, 865, 828, 752, 752, 725, 698, 559, 492.

4.1.6   Synthesis of HMTP

The synthesis route of HMTP is shown in Figure 4.3.
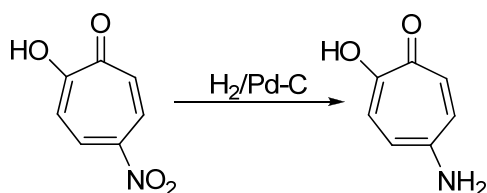
Figure 4.3: Synthesis of HMTP

HMTP was synthesized according the method described by Elliott *et al.*[14] HNTP (2.32 g, 15.36 mmol) was suspended in ethanol (100 mL). 5% Pd/C (20 mg) was added as a catalyst and the reaction was stirred under a hydrogen atmosphere at room temperature for 24 h. The resulted dark-green solution was filtered to reclaim the catalyst, and the solvent was removed to give the title compound HMTP as an orange powder (1.75 g, 92 %). Mp: 178-179 °C. EI-MS: *m/z* [M]$^{+}$ 137.048168 (Calcd. 137.047679 for $C_7H_7O_2N$). ^{1}H NMR (CD$_3$OD, 300 MHz): δ 6.89 (d, J = 12.6 Hz, 2H), 7.28 (d, J = 12 Hz, 2H). IR (KBr, cm^{-1}): 3422, 3338, 3208, 1662 (C=O), 1529, 1513, 1443, 1423, 1318, 1249, 1212, 1141, 953, 893, 845, 776, 665, 624, 580, 495.

4.1.7 Synthesis of 2-HBTP

The synthesis route of 2-HBTP is shown in Figure 4.4.
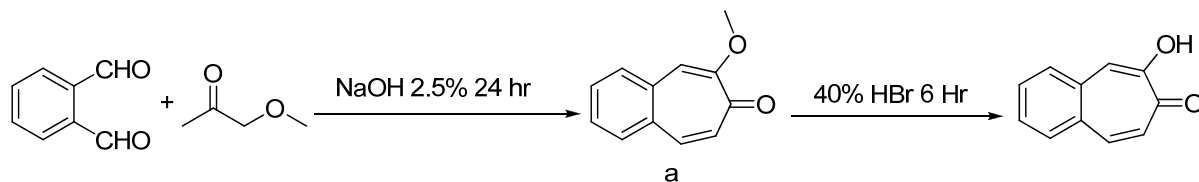
Figure 4.4: Synthesis of 2-HBTP
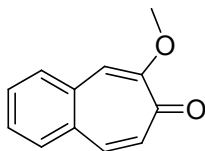
6-Methoxy-7*H*-benzo[7]annulen-7-one (a).[15] To a solution of phthalaldehyde (15.0 g, 0.112 mol) and methoxyacetone (10.0 g, 0.114 mol) in 1.5 L of water, 40 mL of a 2.5% aqueous sodium hydroxide solution was added dropwise under stirring. The stirring was maintained for 24 h, and the mixture was acidified, saturated with sodium chloride and extracted with $CHCl_3$. After drying the solution and removing the solvent in vacuo, a red gum remained. After column chromatography (SiO_2, CH_2Cl_2/ethyl acetate, 9/1), the title compound **a** was afforded as a yellow solid (12 g).Yield: 58 %. Mp: 89 °C. EI-MS: *m/z* $[M]^+$ 186.068292 (Calc. 186.068080 for $C_{12}H_{10}O_2$). ^{1}H NMR (CD_3COCD_3, 300 MHz): δ 6.84 (d, J = 12.6 Hz, 1H), 7.28 (s, 1H), 7.52-7.57 (m, 1H), 7.61-7.62 (m, 1H), 7.69 (d, J = 13.2 Hz, 1H), 7.83 (d, J = 7.5 Hz, 1H), 7.89 (d, J = 7.5 Hz, 1H). IR (KBr, cm^{-1}): 3056, 2937, 1622, 1600, 1543, 1288, 1256, 1227, 1178, 1143, 988, 868, 754, 647, 501.
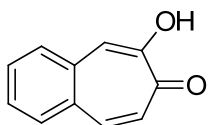
6-Hydroxy-7*H*-benzo[7]annulen-7-one (2-HBTP).[15] 1.20 g (6.45 mmol) of **a** was refluxed for 6 h with 100 mL of 40% hydrobromic acid. The mixture was then cooled, diluted with 300 mL of water, and extracted with $CHCl_3$. The extract was washed with 5% KOH, and the resulting bright yellow alkaline solution was acidified. The acidic solution was extracted with $CHCl_3$. The extract was dried by removing the solvent in vacuo. The solid residue was recrystallized from ethanol to give the title compound 2-HBTP (1.10 g, yield: 97%). The single crystal structure of this compound was analyzed and the result is depicted in Figure 4.5. The crystallographic data are listed in Table 4.1. Mp: 158-160 °C. EI-MS: *m/z* [M]$^+$ 172.052775 (Calc. 172.052430 for $C_{11}H_8O_2$). ^{1}H NMR (CD$_3$COCD$_3$, 300 MHz): δ 7.17 (d, *J* = 12.6 Hz, 1H), 7.53 (t, *J* = 7.5 Hz, 1H), 7.56 (s, 1H, O*H*), 7.63 (t, *J* = 7.5 Hz, 1H), 7.72 (d, *J* = 7.8 Hz, 1H), 7.77 (d, *J* = 7.8 Hz, 1H), 7.84 (d, *J* = 12.6 Hz, 1H), 8.07 (s, 1H). IR (KBr, cm^{-1}): 3290, 3048, 1624, 1624, 1609, 1567, 1532, 1457, 1423, 1350, 1304, 1252, 1182, 1157, 986, 957, 917, 867, 845, 818, 755, 693, 587, 530, 504.
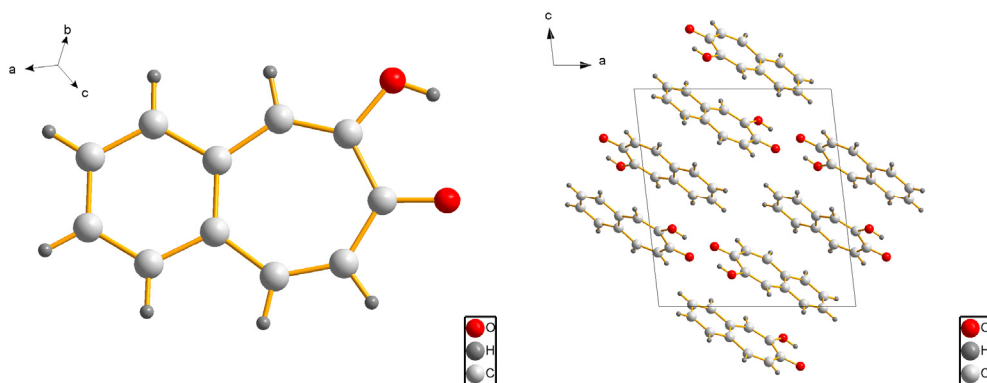
Figure 4.5: Crystal structure of 2-HBTP (left) and its packing diagram (right)

Compound	$C_{11}H_8O_2$	Z	4
M	172.17	μ/mm^{-1}	0.096
Space group	P2(1)/n	T/K	295(2)
a(Å)	10.8045(11)	Data collection range, θ/deg	2.40-32.45
b(Å)	6.3744(7)	Reflections collected	10370
c(Å)	11.9942(13)	Independent reflections (R_{int})	2904(0.0237)
α(°)	90	Data/Parameters	2904 / 0 / 119
β(°)	96.528(2)	Goodness of fit on F^2	0.837
γ(°)	90	R_1 [$I{\geq}2\sigma(I)$] [a]	0.0567
V(Å^3)	820.71(15)	wR_2 [a]	0.2212

a $R_1 = \Sigma||F_0| - |Fc||/\Sigma|F_0|$; $wR_2 = \{\Sigma[w(||F_0|^2 - |F_c|^2|)^2]/\Sigma[w(F_0^4)]\}^{1/2}$

4.1.8   Synthesis of 1-HBTP

The synthesis route of 1-HBTP is shown in Figure 4.6.
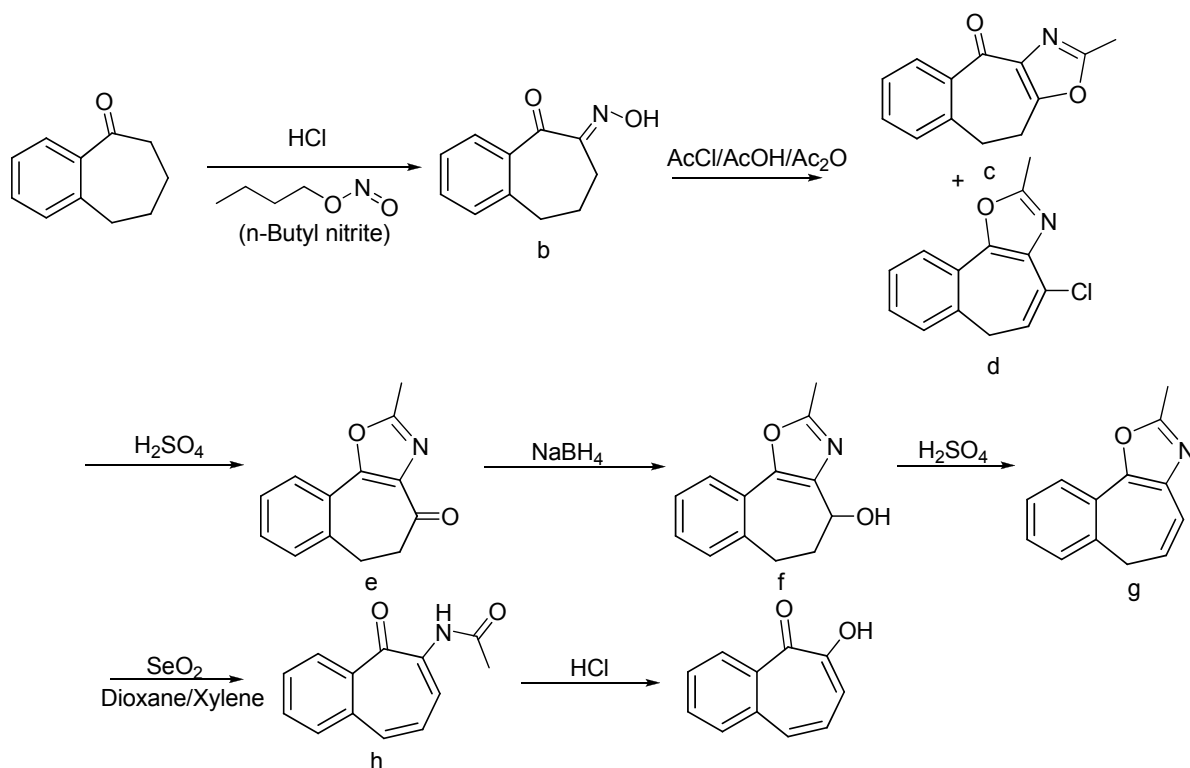
Figure 4.6: Synthesis of 1-HBTP
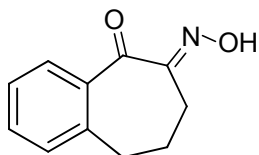
(*E*)-6-(Hydroxyimino)-6,7,8,9-tetrahydro-5*H*-benzo[7]annulen-5-one **(b).**[16]

Benzosuberone (10 g, 0.061 mol) was dissolved in 2 L of anhydrous ethereal HCl (3.7 g) solution. While maintaining the solution temperature at 15-20°C, 6.5 g (0.063 mol) of *n*-butyl nitrite was added over 50 min. At 5°C, 40 mL of petroleum ether was added, whereupon 8.23 g (70%) of the product **b** was obtained as light yellow solid through extraction of the mother liquor with 2 M NaOH followed by adjusting the pH to 7.0 with 2 M HCl. Mp: 135-138 °C. EI-MS: *m/z* [M]$^+$ 189.0796 (Calc. 189.0790 for C$_{11}$H$_{11}$NO$_2$). ^{1}H NMR (CDCl$_3$, 300 MHz): δ 2.04 (m, 2H), 2.72 (m, 2H), 2.88 (m, 2H), 7.16 (t, *J* = 7.4 Hz, 1H), 7.37 (t, *J* = 7.5 Hz, 1H), 7.51 (t, *J* = 7.3 Hz, 1H), 7.84 (d, *J* = 7.7 Hz, 1H). IR (KBr, cm^{-1}): 3236 (O-H), 2947, 2865, 1698, 1621, 1600, 1452, 1302, 962, 899, 873, 772, 714, 656.
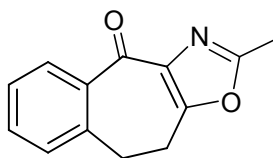
2-Methyl-9,10-dihydro-4*H*-benzo[5,6]cyclohepta[1,2-*d*]oxazol-4-one **(c).**[16] AcCl (0.645 mL, 11 mmol) was added dropwise (within 1 h) to a solution of 0.397 g (2.1 mmol) of **b** in 4.2 mL of AcOH and 0.44 mL of Ac$_2$O at 85°C. After stirring for 1 h at 85°C, the mixture was poured on ice-NaOH and extracted with CHCl$_3$ to yield 0.463 g of thick oil from which (400 mL of ethyl acetate) 0.182 g (41%) of **c** recrystallized. Mp: 178-179 °C. EI-MS: *m/z* [M]$^+$ 213.0793

(Calc. 213.0790 for $C_{13}H_{11}NO_2$). ^{1}H NMR (CDCl$_3$, 300 MHz): δ 2.47 (s, 3H), 3.15 (m, 4H), 7.34 (d, J = 8.2 Hz, 1H), 7.36 (t, J = 7.3 Hz, 1H), 7.43 (t, J = 6.9 Hz, 1H), 7.96 (d, J = 7.4 Hz, 1H). ^{13}C NMR (CDCl$_3$, 75 MHz): δ 13.8, 26.0, 33.2, 127.6, 130.2, 130.5, 132.5, 136.0, 138.0, 138.3, 160.5. IR (KBr, cm^{-1}): 3068, 3033, 2942, 1672, 1609, 1492, 1417, 1377, 1245, 1067, 988, 883, 781, 759, 681, 586, 463.
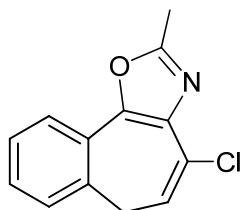
2-Methyl-4-chloro-6H-benzo[3,4]cyclohepta[1,2-d]oxazole (d).[16] The oil obtained by evaporation of the mother liquor during the last step was crystallized from diethyl ether to yield 0.20 g (46%) of **d**. Mp: 88-99 °C. EI-MS: *m/z* [M]$^+$ 231.0451 (Calc. 231.0451 for $C_{13}H_{10}NOCl$). ^{1}H NMR (CDCl$_3$, 300 MHz): δ 2.64 (s, 3H), 3.20 (d, J = 7.4 Hz, 1H), 5.89 (t, J = 7.4 Hz, 2H), 7.26 (m, 1H), 7.54 (m, 2H), 7.65 (m, 1H). IR (KBr, cm^{-1}): 3060, 2931, 1709, 1682, 1628, 1598, 1253, 1233, 1071, 764, 734.
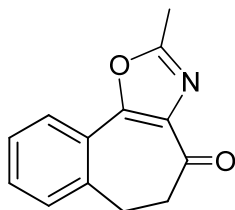
2-Methyl-5,6-dihydro-4H-benzo[3,4]cyclohepta[1,2-d]oxazol-4-one (e).[16] The crude product mixture of **c** and **d** (2.00 g) obtained as described above was dissolved in 4.2 mL of

concentrated H_2SO_4. After 18 h at room temperature, the prodcution of HCl ceased and the mixture was poured on ice. Upon neutralization (2 M NaOH), 1.62 g of **e** (84% based on **c**) precipitated. Mp: 106-107 °C. EI-MS: m/z [M]$^+$ 213.0792 (Calc. 213.0790 for $C_{13}H_{11}NO_2$). ^1H NMR (CDCl$_3$, 300 MHz): δ 2.42 (s, 3H), 2.62-2.90 (m, 4H), 7.14-7.27 (m, 3H), 7.64 (m, 1H). ^{13}C NMR (CDCl$_3$, 75 MHz): δ 13.9, 29.5, 40.2, 126.1, 126.5, 127.6, 129.9, 130.5, 134.5, 139.5, 154.9, 161.1, 192.6. IR (KBr, cm^{-1}): 3062, 2952, 2897, 2842, 1676, 1599, 1491, 1374, 1248, 1069, 881, 772, 754, 680, 582.
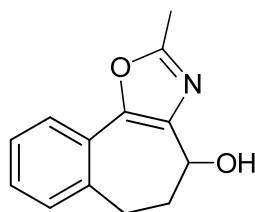
4-Hydroxy-2-methyl-9,10-dihydro-4*H*-benzo[5,6]cyclohepta[1,2-*d*]oxazole (f).[16] To a solution of 0.426 g (2.00 mmol) of **e** in 4.20 mL of CH_2Cl_2-EtOH (1:4) at 5°C was added 0.058 g (1.2 mmol) of NaBH$_4$. After stirring for 5 h at 5°C, 4.20 mL of NaOH (1 M) was carefully added and the mixture worked up with CH_2Cl_2. Crystallization from 3.0 mL of *i*-PrOH yielded 0.42 g (98%) of **f**. Mp: 134-135 °C. EI-MS: m/z [M]$^+$ 215.0944 (Calc. 215.0946 for $C_{13}H_{13}NO_2$). ^1H NMR (CDCl$_3$, 300 MHz): δ 1.95 (m, 1H), 2.31 (m, 1H), 2.55 (s, 3H), 2.84-3.10 (m, 2H), 4.94 (t, J = 4.5 Hz, 1H), 7.21-7.35 (m, 3H), 7.76 (d, J = 7.5 Hz, 1H). IR (KBr, cm^{-1}): 3307, 3070, 2927, 1760, 1709, 1585, 1493, 1445, 1375, 1294, 1276, 1073, 1050, 762, 673.
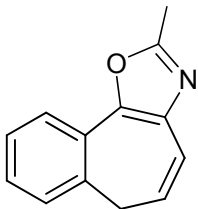
2-Methyl-6*H*-benzo[3,4]cyclohept[1,2-*d*]oxazole (g).[16] To a solution of 8.4 g of **f** (39 mmol) in 5.6 mL of DMSO was added 0.093 mL of concentrated H_2SO_4 and the mixture heated to 180°C for 4 h. After cooling, dilution with water, and neutralization of the acid, **g** was obtained by extraction (CHCl$_3$) as colorless oil (6.2 g, 80%). EI-MS: *m/z* [M]$^+$ 197.0840 (Calc. 197.0841 for C$_{13}$H$_{11}$NO). ^{1}H NMR (CDCl$_3$, 300 MHz): δ 2.58 (s, 3H), 3.19 (d, *J* = 6.9 Hz, 2H), 5.78 (m, 1H), 6.58 (d, *J* = 9.9 Hz, 1H), 7.27-7.45 (m, 3H), 7.66-7.69 (m, 1H). IR (KBr, cm^{-1}): 3043, 2960, 2871, 1674, 1632, 1575, 1490, 1448, 1283, 1262, 1208, 1190, 1023, 812, 767, 735, 697.
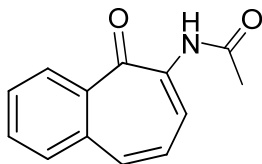
***N*-(5-oxo-5*H*-benzo[7]annulen-6-yl)-acetamide (h).**[17] To a solution of 9.9 g of **g** (50 mmol) in 50 mL dioxane, was added 5.58 g (50 mmol) SeO$_2$ and the mixture was refluxed for 4 h. The resulted solution was then cooled to room temperature and filtered. 100 mL of water was added to the filtrate to precipitate the product **h** (10.7 g, 95%). Mp: 75-76 °C. EI-MS: *m/z* [M]$^+$ 213.0785 (Calc. 213.0790 for C$_{13}$H$_{11}$NO$_2$). ^{1}H NMR (CDCl$_3$, 300 MHz): δ 2.44 (s, 3H), 7.09 (m,

1H), 7.44 (m, 1H), 7.77-7.91 (m, 3H), 8.91-9.03 (m, 2H), 9.38 (s, 1H). IR (KBr, cm^{-1}): 3335, 3034, 1696, 1586, 1565, 1501, 1478, 1463, 1377, 1239, 796, 745, 704, 599, 551.
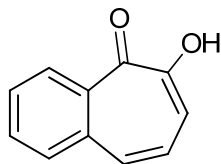
6-Hydroxy-5*H***-benzo[7]annulen-5-one (1-HBTP).**[17] 2.13 g of **h** (10 mmol) was added to 20 mL HCl (2 M) solution. The mixture was heated to 100 °C for 4 h. The product was obtained quantitatively as a yellow solid. Mp: 82-84 °C. EI-MS: *m/z* [M]$^{+}$ 172.0526 (Calc. 172.0524 for C$_{11}$H$_8$O$_2$). ^{1}H NMR (CDCl$_3$, 300 MHz): δ 7.09 (m, 1H), 7.37 (m, 1H), 7.52 (m, 1H), 7.82-7.98 (m, 3H) 8.80 (s, 1H, br), 9.06 (m, 1H). IR (KBr, cm^{-1}): 3430, 1634, 1590, 1547, 1487, 1416, 1352, 1232, 1166, 1063, 792, 743, 670, 441.

4.1.9   Synthesis of complexes and preparation of single crystals

General method: to a solution of ligand (0.04 mmol) in MeOH (10 mL) was added 4.00 mL (0.04 mmol) KOH solution in methanol (0.100 M) with stirring. To the resulting solution was added LnCl$_3$·nH$_2$O (0.01 mmol) (Ln = La, Pr, Nd, Gd, Er, and Yb) in methanol (10 mL). The solution was stirred for 3 h and the resulting precipitate was filtered, washed three times with methanol and dried in vacuo over P$_2$O$_5$ for 48 h. Single crystals were obtained either through evaporation of the complexes in solution of CH$_3$CN or ethanol, or slow diffusion of ethyl ether into a solution of the complexes in DMF.

4.2   RESULTS AND DISCUSSION

4.2.1   Synthesis and characterization of ligands

Ligand BrTP was synthesized according to the method described in chapter 3. Ligand HNTP, HMTP, 2-HBTP, and 1-HBTP were synthesized according to literature methods. Tropolone was treated in 1:1 HNO_3 for 15 min to give HNTP in 35% yield. HNTP was treated with H_2 by using Pd/C as catalyst to give HMTP in 92% yield.

The synthetic sequence leading to 2-HBTP from phthalaldehyde is depicted in Figure 4.4. Phthalaldehyde was reacted with methoxyacetone in aqueous NaOH solution to give 6-methoxy-7*H*-benzo[7]annulen-7-one (**a**) in 58% yield. **a** was treated with 40% HBr to give 2-HBTP in 97% yield.

The synthetic sequence leading to 1-HBTP from Benzosuberone is depicted in Figure 4.6. Benzosuberone was treated with *n*-butyl nitrite to give (*E*)-6-(hydroxyimino)-6,7,8,9-tetrahydro-5*H*-benzo[7]annulen-5-one (**b**) in 70% yield. **b** was treated with acetyl chloride for 1h at 85 °C to give a mixture of 2-methyl-9,10-dihydro-4*H*-benzo[5,6]cyclohepta[1,2-*d*]oxazol-4-one (**c**) and 2-methyl-4-chloro-6*H*-benzo[3,4]cyclohepta[1,2-*d*]oxazole (**d**). This mixture was treated in concentrated H_2SO_4 for 18 h at room temperature followed by neutralization with 2 M NaOH to give 2-methyl-5,6-dihydro-4*H*-benzo[3,4]cyclohepta[1,2-*d*]oxazol-4-one (**e**) in 84% yield. **e** was reduced by using $NaBH_4$, followed by dehydration reaction in concentrated H_2SO_4 to give 2-methyl-6*H*-benzo[3,4]cyclohept[1,2-*d*]oxazole **g** in 80% yield. **g** was treated with SeO**2** followed by 2 M HCl to give final product 1-HBTP in 95% yield.

During the synthesis of 1-HBTP, 2-D NMR technique HMQC was used to identify compound **c** and **e**. Those two molecules are isomers. IR and 1-D ^{1}H NMR (Figure 4.7) and ^{13}C NMR did not provide sufficient information to unambiguously identify those two compounds.

Heteronuclear Multiple Quantum Coherence (HMQC) and Heteronuclear Multiple Bond Coherence (HMBC) are 2-dimensional inverse H-C correlation techniques that allow for the determination of carbon (or other heteroatom) to hydrogen connectivity. HMQC is selective for direct C-H coupling and HMBC will provide information on longer range couplings (2-4 bond coupling). HMBC was used to identify these two compounds, due to the relative positions of the carbonyl carbon atom with the nearby hydrogen atom. For compound **c**, the correlation is only possible between the carbonyl carbon with one hydrogen atom on the nearby benzene ring (Figure 4.8). For compound **e**, the correlation can only take place between the carbonyl carbon with the hydrogen atoms connected to the alkyl carbons on the seven member ring (Figure 4.9).
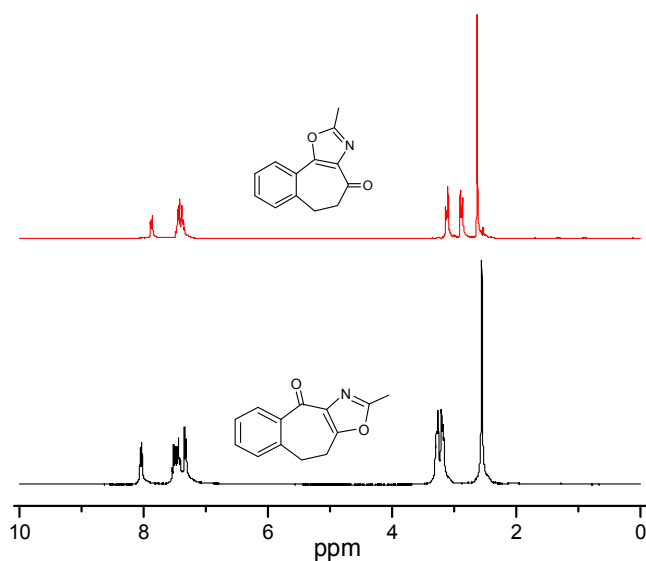
Figure 4.7: ^{1}H NMR spectra of compounds **c** and **e**

4.2.2 Synthesis and characterization of complexes

All the complexes were synthesized by using a similar method. A lanthanide chloride solution in methanol was added to a methanolic solution of the potassium salt of the corresponding deprotonated ligand. A 4:1 ligand to metal stoichiometry was used in each case. The resulting solid complexes were collected, washed and dried to give the final product. Elemental analysis and ESI-MS (Table 4.2) shows that the complexes all have the ML_4 molecular formula as it had been previously observed for the Trop⁻ complexes.
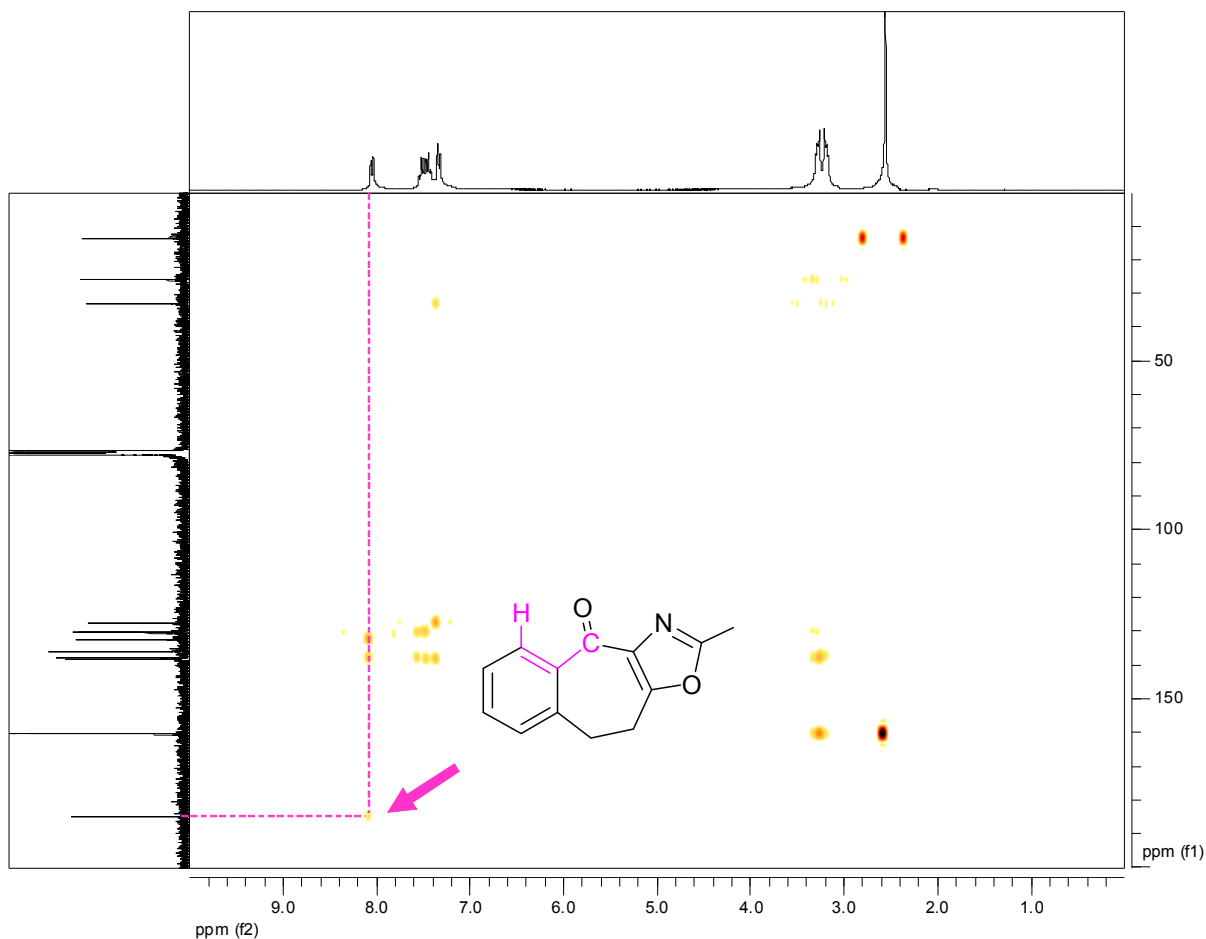
Figure 4.8: HMQC 2-D NMR spectrum of compound **c**
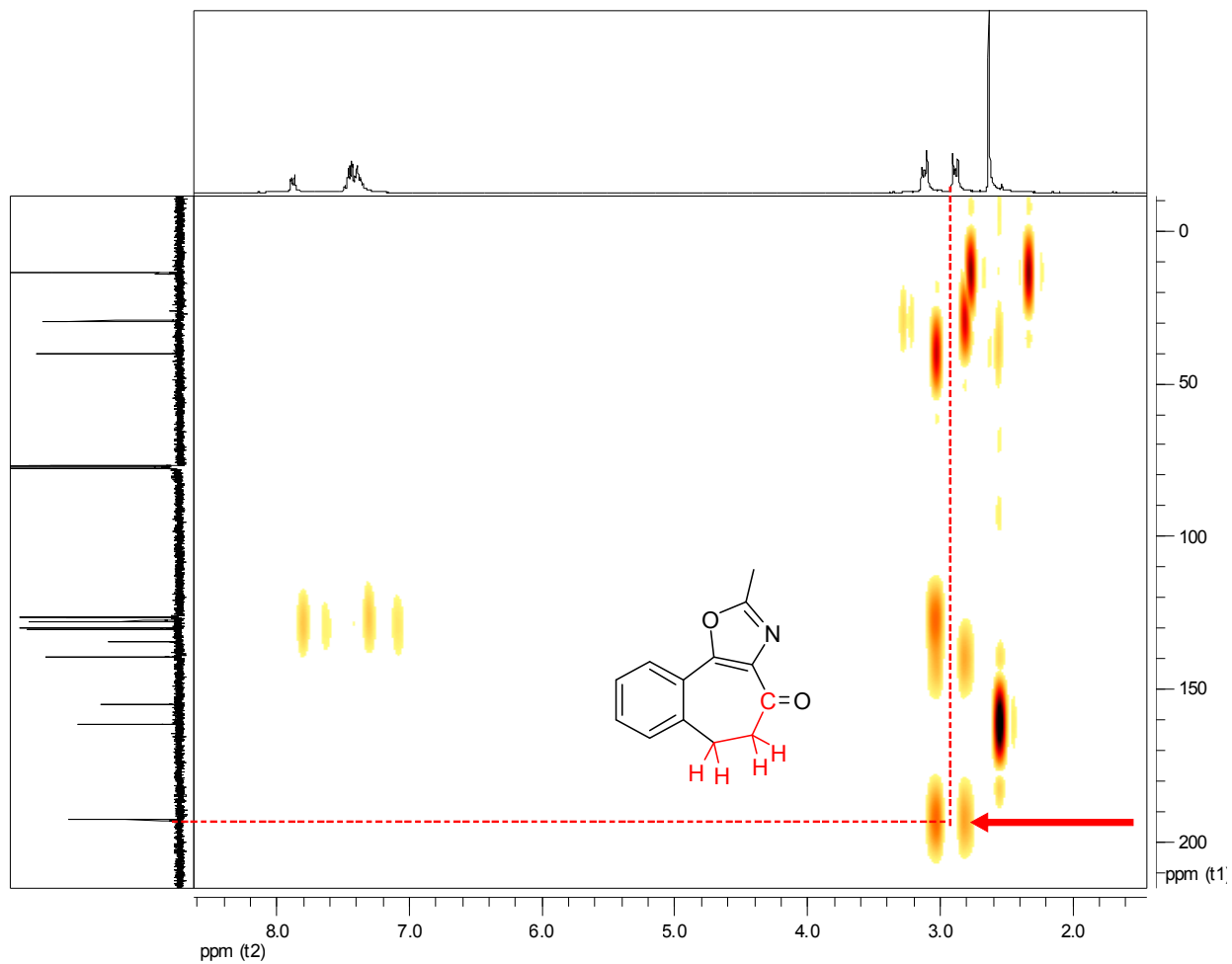
Figure 4.9: HMQC 2-D NMR spectrum of compound e

Table 4.2: Elemental analytical and ESI-MS data for all the isolated complexes

Formula	Ln	Elemental Analysis			ESI-MS		
		C	H	N	Positive Ions		Negative Ions
KLn(Thup)$_4$·H$_2$O	Pr	56.23(56.47)	5.38(5.45)	-	669.0 [Pr(Thup)$_3$+K]$^+$	1097.1 [Pr$_2$(Thup)$_5$]$^+$	793.2 [Pr(Thup)$_4$]$^-$
	Nd	56.06(56.25)	5.31(5.43)	-	672.5 [Nd(Thup)$_3$+K]$^+$	1103.7 [Nd$_2$(Thup)$_5$]$^+$	796.5 [Nd(Thup)$_4$]$^-$
	Gd	55.18(55.40)	5.23(5.35)	-	648.0 [Nd(Thup)$_3$+H]$^+$	1131.1 [Gd$_2$(Thup)$_5$]$^+$	810.2 [Gd(Thup)$_4$]$^-$
	Er	55.01(54.77)	5.28(5.29)	-	a		
	Yb	54.83(54.41)	5.06(5.25)	-	a		
KLn(BrTP)$_4$	Nd	33.95(34.20)	1.58(1.64)	-	a		944.2 [Nd(BrTP)$_4$]$^-$
	Gd	33.76(33.75)	1.69(1.62)	-	a		957.2 [Gd(BrTP)$_4$]$^-$
	Er	33.17(33.42)	1.48(1.60)	-	a		967.0 [Er(BrTP)$_4$]$^-$
	Yb	33.29(33.23)	1.78(1.59)	-	a		973.5 [Yb(BrTP)$_4$]$^-$
KLn(NTP)$_4$	Pr	39.78(39.83)	2.00(1.91)	6.30(6.63)	551.3 [Pr(NTP)$_2$]$^+$+DMSO		805.0 [Pr(NTP)$_4$]$^-$
	Nd	39.44(39.67)	2.07(1.90)	6.58(6.61)	554.2 [Nd(NTP)$_2$]$^+$+DMSO		808.3 [Nd(NTP)$_4$]$^-$
	Gd	39.39(39.07)	1.92(1.87)	6.37(6.51)	563.0 [Gd(NTP)$_2$]$^+$+DMF		821.8 [Gd(NTP)$_4$]$^-$
	Er	38.56(38.62)	1.99(1.85)	6.09(6.43)	578.3 [Er(NTP)$_2$]$^+$+DMSO		832.2 [Er(NTP)$_4$]$^-$
	Yb	38.33(38.37)	1.87(1.84)	6.27(6.39)	584.2 [Yb(NTP)$_2$]$^+$+DMSO		838.0 [Yb(NTP)$_4$]$^-$
KLn(MTP)$_4$	Nd	45.89(46.21)	3.22(3.32)	7.47(7.70)	a		
	Gd	45.09(45.39)	3.12(3.27)	7.23(7.56)	a		
	Er	44.64(44.79)	3.38(3.22)	7.60(7.46)	a		
	Yb	44.23(44.45)	3.52(3.20)	7.19(7.40)	a		
KLn(2-BTP)$_4$·2H$_2$O	Nd	58.87(58.46)	3.16(3.57)		a		
	Gd	57.96(57.63)	3.29(3.52)		a		
	Er	57.31(57.00)	3.11(3.48)		a		
	Yb	56.56(56.65)	3.12(3.46)		a		
KLn(1-BTP)$_4$·2H$_2$O	Nd	58.40(58.46)	3.17(3.57)		a		
	Gd	57.32(57.63)	3.25(3.52)		a		
	Er	57.19(57.00)	3.23(3.48)		a		
	Yb	56.81(56.65)	3.20(3.46)		a		

a. Not measured.

4.2.3 Crystal structure

Slow diffusion of ethyl ether into a solution of solid complex KPr(NTP)$_4$ in DMF yielded yellow crystals of K[Pr(NTP)$_4$DMF] (**1**). By slow evaporation of a solution of KGd(NTP)$_4$ and KYb(NTP)$_4$ in CH$_3$CN, yellow crystals were isolated as K[Gd(NTP)$_4$CH$_3$CN] (**2**) and [KCH$_3$CN [Yb(NTP)$_4$]]K[Yb(NTP)$_4$]·CH$_3$CN (**3**) respectively. By slow evaporation of a solution of KPr(Thup)$_4$ and KNd(Thup)$_4$ in ethanol, colorless crystals were isolated as K[Pr(Thup)$_4$]C$_2$H$_5$OH (**4**) and K[Nd(Thup)$_4$]C$_2$H$_5$OH (**5**). The crystallography data of all the five crystals are summarized in Table 4.3.

Crystal structural description of 1. The compound crystallizes in the monoclinic system, space group P$_{2(1)c}$, with a = 10.2231(6) Å, b = 23.3932(16) Å, c = 14.0586(8) Å, β = 108.0380(10)°, and Z = 4. In the crystal structure of **1**, the central Pr^{3+} is coordinated with four bidentate NTP$^-$ ligands and one DMF solvent molecule. The total coordination number of Pr^{3+} is therefore nine and the coordination polyhedron is best described as a distorted tricapped trigonal prism (Figure 4.10). Selected bond lengths are listed in Table 4.3. The structural analysis reveals significant differences in comparison to the crystal structure of lanthanide complexes formed with Trop$^-$ that we have previously reported[18], for which the coordination number is eight for all the Ln^{3+} analyzed. DMF is part of the structural assembly of the complex, being coordinated to Pr^{3+} in the first coordination sphere. The counter ion, K$^+$, functions as a bridging ion connecting two discrete adjacent ML$_4$ units together and allowing the formation of a 1-D coordination polymer along the c axis (Figure 4.11).

It is interesting to observe that in the crystal structure, one of the four nitro groups (O11-N2-O12) is coordinated to the K$^+$ from an adjacent polymer chain in a bidentate motif (see Table

4.4 for symmetry code), as shown in Figure 4.12. Each K^+ has a coordination number of 8, six O atoms belonging to the NTP⁻ ligands and two O atoms from the nitro group. Due to this type of inter-chain coordination interaction, two-dimensional (2-D) coordination polymers are formed along the *ac* plane (Figure 4.12). The overall crystal structure is composed of this type of 2-D coordination polymer planes. A view of the packing of the crystal structure is shown in Figure 4.13.

Table 4.3: Summary of crystallography data

Complex	1	2	3	4	5
Formula	$C_{30}H_{23}KN_5O_{17}Pr$	$C_{30}H_{19}GdKN_5O_{16}$	$C_{30}H_{16}KN_5O_{16}Yb$	$C_{44}H_{54}KO_{10}Pr$	$C_{44}H_{54}KNdO_{10}$
CCDC number	680892	680894	680893	680891	680890
M	917.55	901.85	914.62	922.88	926.21
Space group	P2(1)/c	P2(1)/c	P2(1)/n	Pna2(1)	Pna2(1)
$a(°)$	10.2231(6)	10.216(4)	10.945(2)	15.0224(7)	14.8507(7)
$b(°)$	27.3932(16)	23.070(10)	28.071(5)	17.0810(8)	16.7937(8)
$c(°)$	14.0586(8)	14.003(6)	23.789(4)	18.1690(9)	17.9314(9)
$\alpha(°)$	90	90	90	90	90
$\beta(°)$	108.0380(10)	108.739(8)	100.020(4)	90	90
$\gamma(°)$	90	90	90	90	90
$V(Å^3)$	3743.5(4)	3126(2)	7197(2)	4662.1(4)	4472.1(4)
Z	4	4	8	4	4
μ/mm^{-1}	1.493	2.345	2.792	1.185	1.307
T/K	150(2)	150(2)	295(2)	150(2)	150(2)
Data collection range, θ/deg	1.49-28.32	1.77-27.50	1.69-25.00	1.64-27.50	1.66-27.50
Reflections collected	38661	30027	53893	30571	42066
Independent reflections (R_{int})	9325 (0.0791)	7164(0.2222)	12633(0.1104)	5526(0.0452)	5297 (0.0912)
Data/Parameters	9325 / 0 / 496	7164 / 0 / 470	5128/388	5526 / 0 / 296	5297 / 0 / 327
Goodness of fit on F^2	0.924	0.965	1.039	1.150	0.810
$R_1 [I \geq 2\sigma(I)]$ [a]	0.0518	0.1060	0.0658	0.0628	0.0485
wR_2 [a]	0.1353	0.2757	0.1595	0.1712	0.1368

a $R_1 = \Sigma||F_0| - |Fc||/\Sigma|F_0|$; $wR_2 = \{\Sigma[w(||F_0|^2 - |F_c|^2|)^2]/\Sigma[w(F_0^4)]\}^{1/2}$
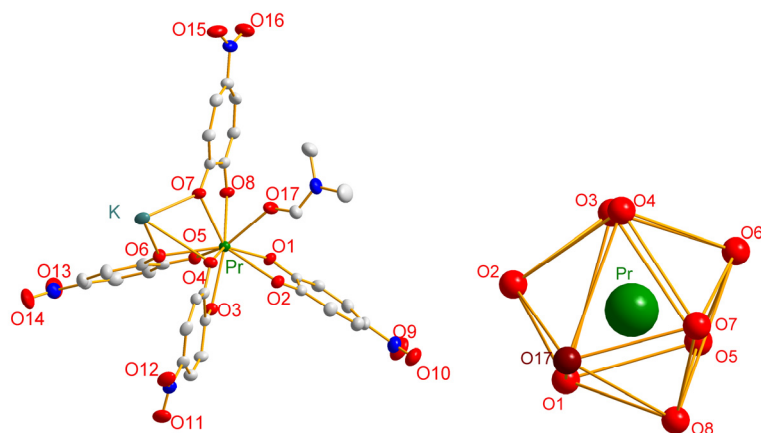
Figure 4.10: Left: ORTEP representations of the molecular structure of **1** (30% probability ellipsoids, H atoms have been omitted for clarity); Right: Coordination polyhedron of Pr^{3+} in **1**

Table 4.4: Selected bond lengths (Å) for **1**

Pr-O(1)	2.471(3)	K-O(1)A	2.693(3)
Pr-O(2)	2.557(3)	K-O(7)	2.726(3)
Pr-O(3)	2.514(3)	K-O(5)A	2.732(3)
Pr-O(4)	2.419(3)	K-O(6)	2.758(3)
Pr-O(5)	2.466(3)	K-O(12)B	2.788(4)
Pr-O(6)	2.539(3)	K-O(8)A	2.835(3)
Pr-O(7)	2.488(3)	K-O(11)B	3.116(4)
Pr-O(8)	2.530(3)	K-O(4)	3.142(3)
Pr-O(17) (from DMF)	2.527(4)		

Symmetry codes: A: *x*, -*y*+1/2, *z*+1/2; B: *x*+1, *y*, *z*
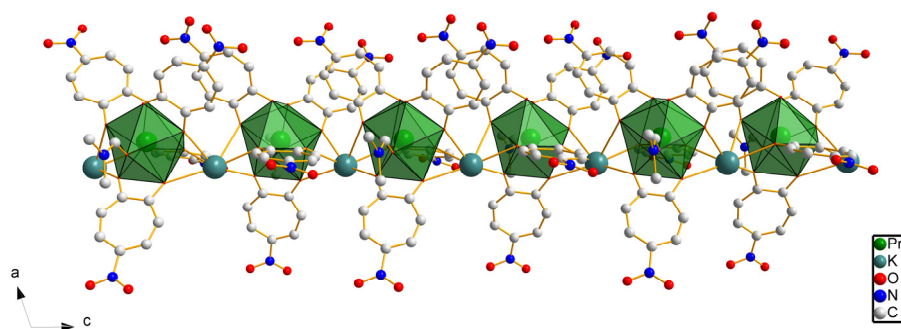
Figure 4.11: Structure of **1** showing the 1D coordination polymer chain along the *c* axis
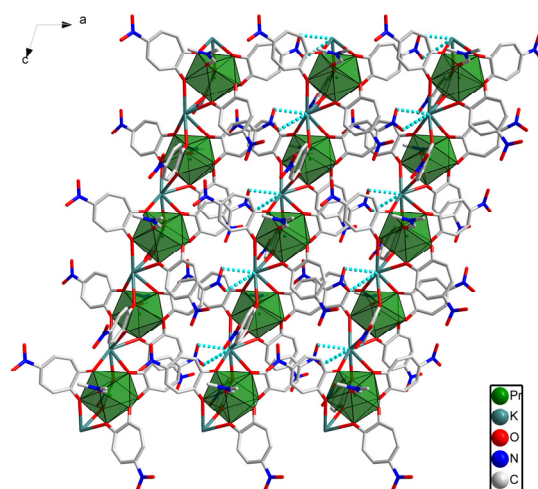
Figure 4.12: Structure of **1** showing the NO$_2$ coordination in the *ac* plane
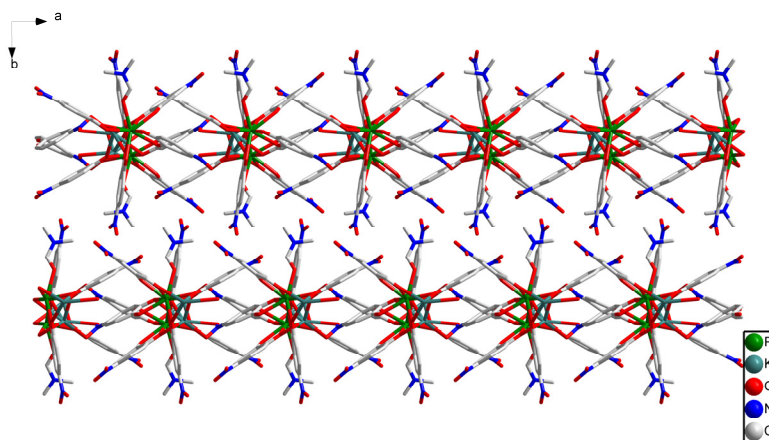
Figure 4.13: Crystal packing diagram of **1**

Crystal structural description of 2. The compound crystallizes in the monoclinic system, space group P$_{2(1)c}$, with *a* = 10.216(4) Å, *b* = 23.070(10) Å, *c* = 14.003(6) Å, *β* = 108.739(8)°, and *Z* = 4. A similar coordination motif was found in the crystal structure of **2**. Four bidentate NTP$^-$ ligands and a molecule of CH$_3$CN are coordinated in their first coordination sphere to Gd^{3+}. The total coordination number is nine, and the polyhedron is best described as a

126

distorted tricapped trigonal prism (Figure 4.14). Selected bond lengths are listed in Table 4.5. The K^+ functions as a bridging ion to connect two adjacent ML_4 units, and 1-D coordination polymers are also formed in this structure along c axis (Figure 4.15).
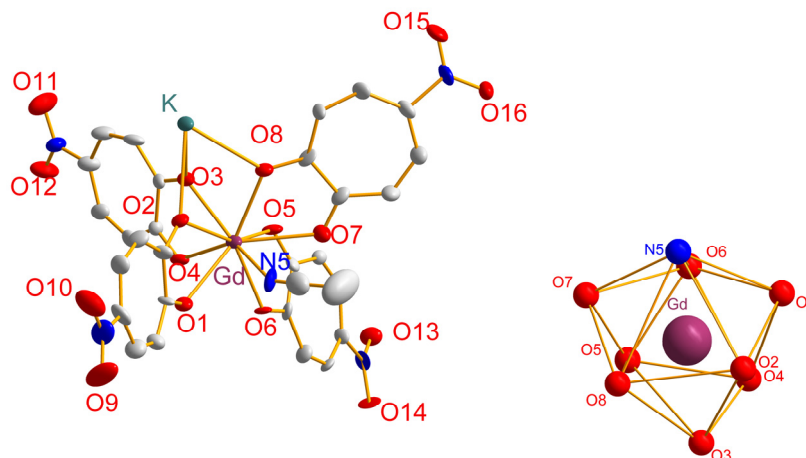
Figure 4.14: Left: ORTEP representations of the molecular structure of **2** (30% probability ellipsoids, H atoms have been omitted for clarity); Right: Coordination polyhedron of Gd^{3+} in **2**

Table 4.5: Selected bond lengths (Å) for **2**

Gd-O(1)	2.445(10)	K-O(8)	2.687(9)
Gd-O(2)	2.447(10)	K-O(4)A	2.765(9)
Gd-O(3)	2.371(10)	K-O(2)	2.772(10)
Gd-O(4)	2.451(10)	K-O(14)B	2.782(10)
Gd-O(5)	2.439(10)	K-O(1)A	2.809(10)
Gd-O(6)	2.354(8)	K-O(3)	2.813(10)
Gd-O(7)	2.540(10)	K-O(13)B	3.091(10)
Gd-O(8)	2.414(9)	K-O(6)A	3.180(10)
Gd-N(5) (from CH$_3$CN)	2.561(14)	K-O(12)C	3.234(13)

Symmetry codes: A: x, $-y+1/2$, $z+1/2$, B: x-1, $-y+1/2$, $z+1/2$, C: $-x$, y-1/2, $-z+3/2$
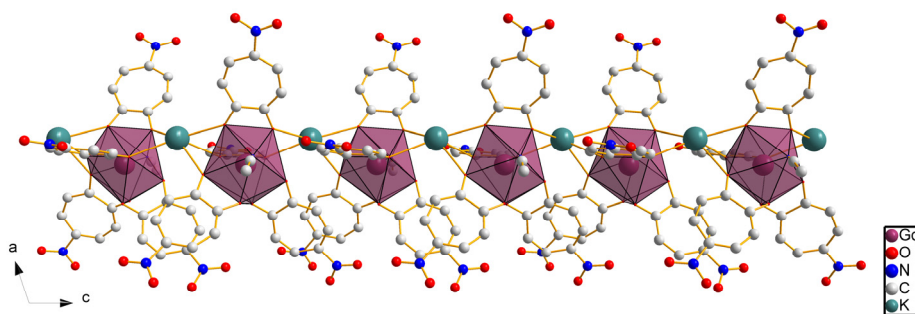
Figure 4.15: Structure of **2** showing the coordination polymer chain along the *c* axis

Like the organization observed in the crystal structure of **1**, one of the four nitro groups (O13-N3-O14) is coordinated to the K^+ from an adjacent polymer chain (see Table 4.5 for symmetry code) in a bidentate motif (Figure 4.16 left). Through the presence of this inter-chain coordination interaction, 2-D coordination polymers are formed in the *ac* plane (Figure 4.16 left). In addition, an O atom (O11) belonging to another nitro group (O11-N2-O12) is also coordinated with the K^+ from an adjacent polymer chain (monodentate motif, see Table 4.5 for symmetry code) (Figure 4.16 right). This additional coordination interaction further converts the 2-D plane structure into a 3-D coordination network, as shown in the packing structure shown in Figure 4.17. The K^+ is coordinated with six O atoms from NTP^- ligands and three O atoms from the nitro groups, and the total coordination number is nine.
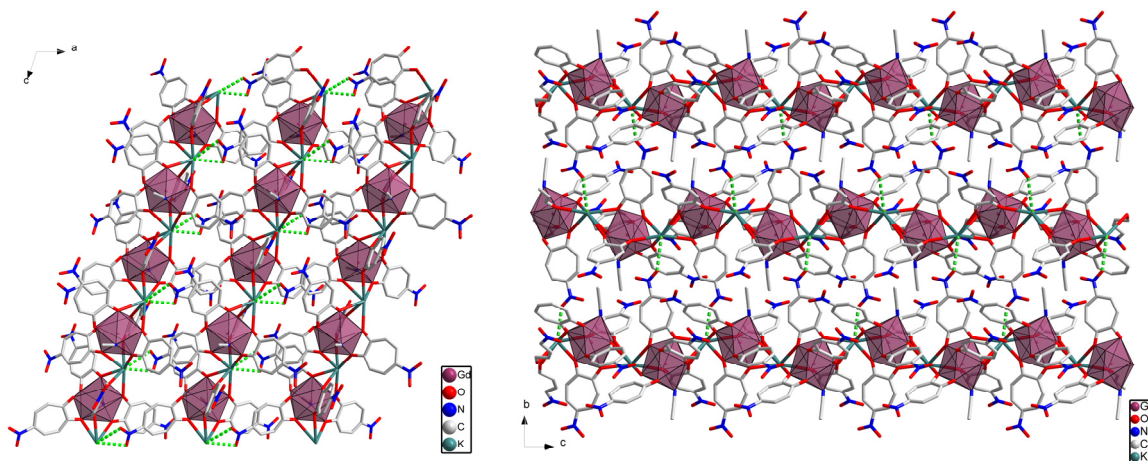
Figure 4.16: Structure of **2** showing the NO$_2$ coordination in the *ac* plane (Left) and *bc* plane (Right)
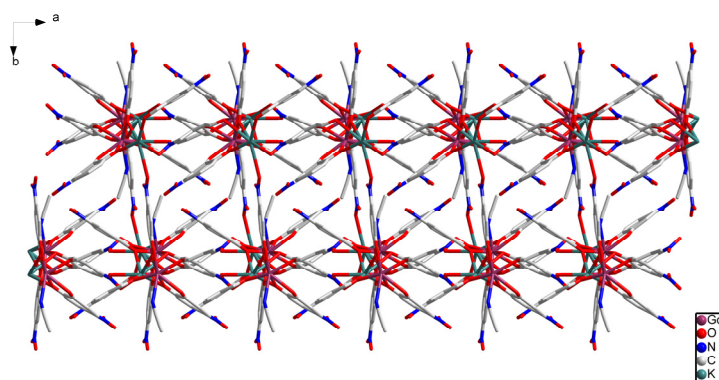
Figure 4.17: Crystal packing diagram of **1**

Crystal structural description of 3. The compound crystallizes in the monoclinic system, space group P$_{2(1)n}$, with a = 10.945(2) Å, b = 28.071(5) Å, c = 23.789(4) Å, β = 100.020(4)°, and $Z = 4$. Two crystallographically unequivalent Yb^{3+} are present in each unit cell. Both of them are coordinated to four NTP$^-$ ligands with a coordination number eight (Figure 4.18). In contrast to what has been observed in the structures of Pr^{3+} and Gd^{3+} complexes (see **1** and **2**), no molecule of solvent is directly bound to Yb^{3+}, which is fundamentally different. For each of the two Yb^{3+}, the polyhedron that describes the best coordination geometry is

129

dodecahedron, as characterized by the value of the normalized bite value b.[19] The b values are 1.09 and 1.11 for Yb(1) and Yb(2) respectively, similar to that reported for $[Yb(Trop)_4]^-$ (b = 1.10).[18] Two molecules of CH_3CN are present in the crystal. One of them is coordinated to K(2). The other CH_3CN molecule is present as a crystallization solvent molecule. Selected bond lengths are listed in Table 4.6. The K^+ functions as a bridging ion to connect two adjacent ML_4 units, and 1-D coordination polymers are formed in this structure along c axis (Figure 4.19).

Like the structure of $[Yb(Trop)_4]^-$, all of the bond lengths of Yb-O for both Yb(1) and Yb(2) in **3** are close to each other with a small standard deviation value (Table 4.9). The average of the bond lengths is 2.32(2) Å and 2.31(2) Å for Yb(1)-O and Yb(2)-O respectively. These two values are close to that observed in $[Yb(Trop)_4]^-$, which indicates that the decrease of the electronic density on the tropolonate ring due to the presence of the electron withdrawing NO_2 group does not induce a change in the coordinating strength of the NTP^-. This result is different from the previously reported observation of the bonds lengths in lanthanide complexes formed with a family of bis-benzimidazole ligands possessing different substituents.[9] In that work, a significant decrease of bond lengths of the Ln-N bonds was observed for the lanthanide complexes formed with the bis-benzimidazole ligand with a NO_2 group in position-4 of the pyridine in comparison to the corresponding complex formed with the unsubstituted ligand. The explanation of this difference in bond length was attributed to the decrease of the electron density on the aromatic ring due to the presence of the electron withdrawing NO_2 group.
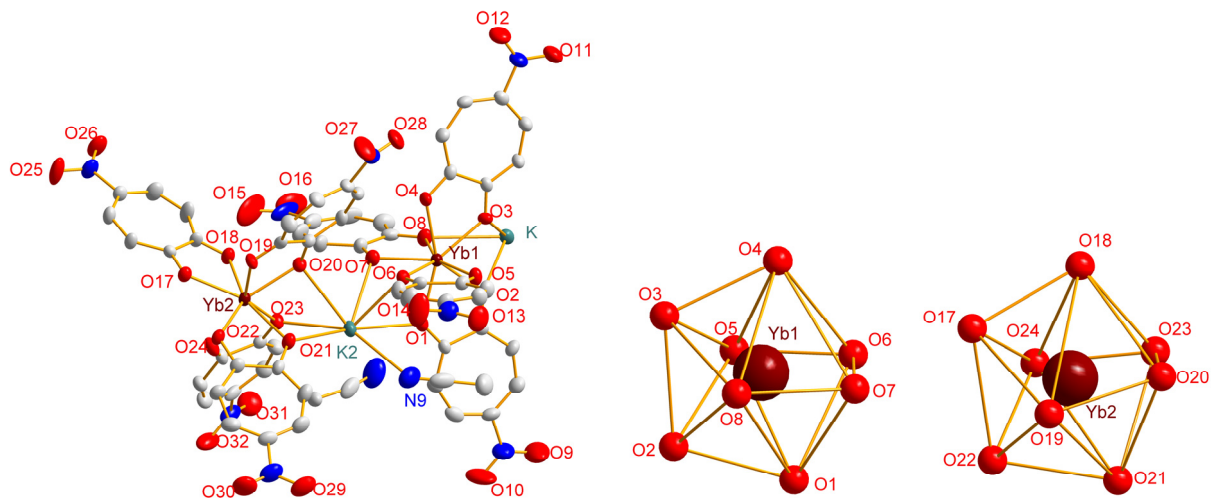
Figure 4.18: Top: ORTEP representations of the molecular structure of **3** (30% probability ellipsoids, H atoms have been omitted for clarity); Bottom: Coordination polyhedron of Yb^{3+} in **3**

Table 4.6: Selected bond lengths (Å) for **3**

Yb(1)-O(1)	2.319(8)	K(1)-O(17)A	2.828(7)
Yb(1)-O(2)	2.310(7)	K(1)-O(29)B	2.844(10)
Yb(1)-O(3)	2.282(7)	K(1)-O(2)	2.878(7)
Yb(1)-O(4)	2.337(7)	K(1)-O(3)	2.910(7)
Yb(1)-O(5)	2.315(7)	K(1)-O(22)A	2.977(7)
Yb(1)-O(6)	2.322(7)	K(1)-O(19)A	3.011(7)
Yb(1)-O(7)	2.307(7)	K(1)-O(8)	3.037(8)
Yb(1)-O(8)	2.329(7)	K(1)-O(12)C	3.143(9)
		K(1)-O(11)C	3.319(10)
Yb(2)-O(17)	2.282(7)	K(2)-O(23)	2.749(7)
Yb(2)-O(18)	2.314(7)	K(2)-O(6)	2.771(7)
Yb(2)-O(19)	2.321(6)	K(2)-O(21)	2.839(7)
Yb(2)-O(20)	2.269(7)	K(2)-O(7)	2.960(8)
Yb(2)-O(21)	2.322(7)	K(2)-O(20)	2.971(7)
Yb(2)-O(22)	2.313(7)	K(2)-O(28)C	3.097(10)
Yb(2)-O(23)	2.325(6)	K(2)-N(9)	3.099(15)
Yb(2)-O(24)	2.320(7)	K(2)-O(27)C	3.127(11)

Symmetry codes: A: -x+3/2, y+1/2, -z+1/2; B: x+1/2, -y+3/2, z+1/2; C: x-1, y, z
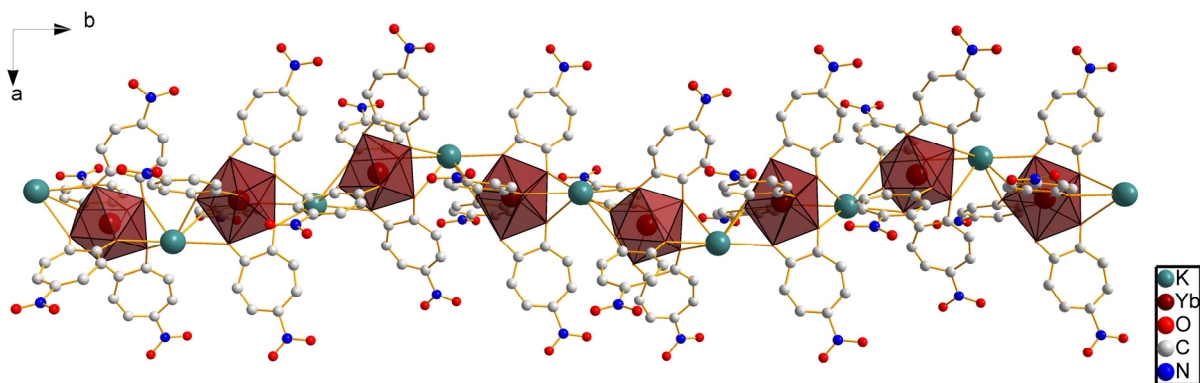
Figure 4.19: Structure of **3** showing the coordination polymer chain along the *b* axis

Coordination bonds formed between NO_2 and K^+ are also present in this structure with two different coordination motifs. One NO_2 group (O11-N2-O12) from the NTP⁻ ligand coordinated to Yb(1) is coordinated to K(1) in a bidentate motif (Figure 4.20 left, see Table 4.6 for symmetry code). Another NO_2 group (O27-N6-O28) from the NTP⁻ ligand bound to Yb(2) is coordinated to K(2) in a bidentate motif (Figure 4.20 left, see Table 4.6 for symmetry code). This intermolecular coordination interaction connects the 1-D coordination polymer chains into a 2-D coordination polymer along the *ab* plane. In addition, one O atom (O29) from the NO_2 group (O29-N7-O30) is coordinated to K(1) in a monodentate motif (Figure 4.20 right, see Table 4.6 for symmetry code). These additional coordination bonds link the 2-D planar structure into a 3-D coordination network, as illustrated in the packing diagram in Figure 4.21. K(1) is coordinated with six O atoms from NTP⁻ ligands and three oxygen atoms from two nitro groups (one in a bidentate motif and one in a monodentate motif). The coordination number is nine. K(2) is coordinated with six O atoms from NTP⁻ ligands, two oxygen atoms from one nitro group, and one nitrogen atom from the solvent molecule CH_3CN. The coordination number is also nine.
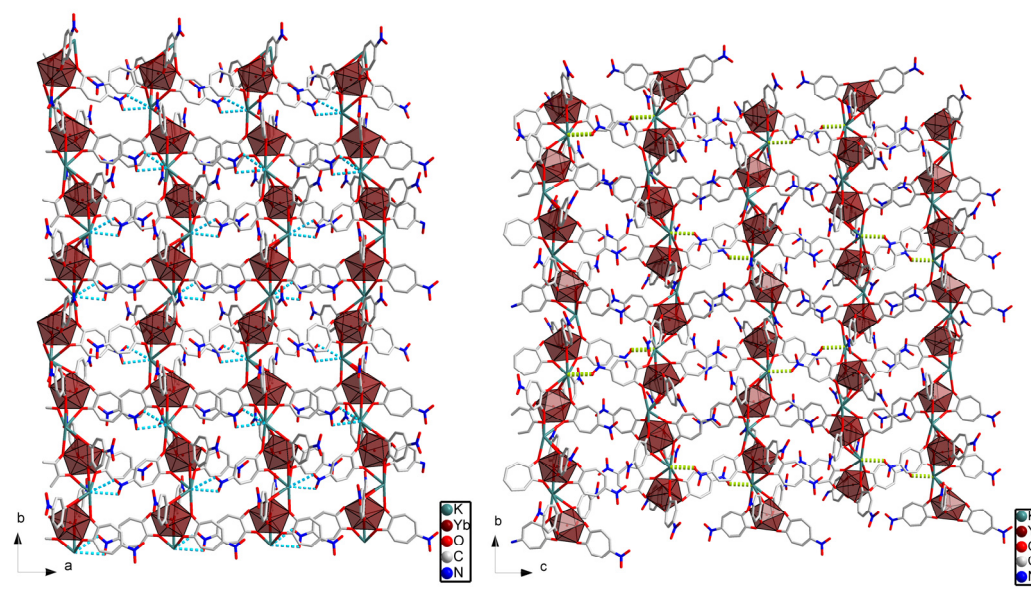
Figure 4.20: Structure of **3** showing the NO$_2$ coordination in the *ab* plane (Left) and *bc* plane (Right)
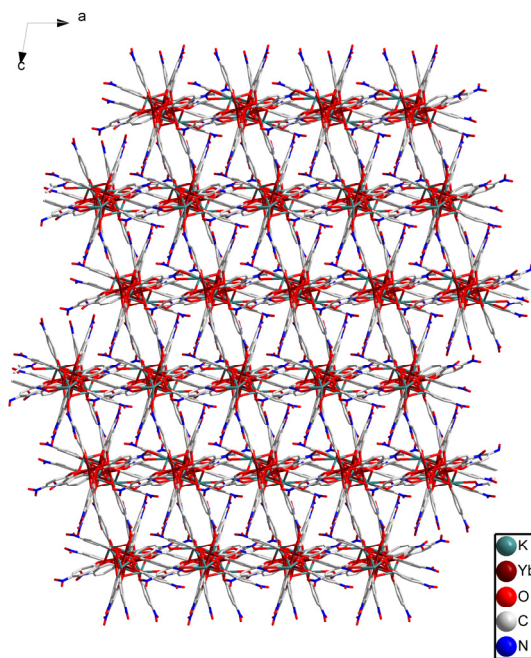
Figure 4.21: Crystal packing diagram of **3**

Crystal structural description of 4 and 5. The coordination motifs in the crystal structures of **4** and **5** are similar. The compound **4** crystallizes in the orthorhombic system, space group $P_{na2(1)}$, with a = 15.0224(7) Å, b = 17.0810(8) Å, c = 18.1690(9) Å, and Z = 4. The compound **5** crystallizes in the orthorhombic system as well, space group $P_{na2(1)}$, with a = 14.8507(7) Å, b = 16.7937(8) Å, c = 17.9314(9) Å, and Z = 4. Selected bond lengths of **4** and **5** are listed in Table 4.7 and Table 4.8 respectively. In both structures, the Ln^{3+} are coordinated with four $Thup^-$ ligands and the coordination number is therefore eight (Figure 4.22 and Figure 4.23). The calculation of the normalized bite from the crystallographic data reveals b values of 1.04 and 1.05 for **4** and **5** respectively. They are smaller than 1.10, so the coordination polyhedrons for both structures are best described as dodecahedron.[19] An ethanol molecule from the crystallization solvent is coordinated to K^+ which functions as bridging ions to connect two adjacent ML_4 units. As a result, 1-D coordination polymers are formed along the c axis in both structures (Figure 4.24 and Figure 4.25). The K^+ is coordinated with five O atoms from $Thup^-$ ligands and one oxygen atom from the ethanol molecule. The total coordination number is six.

Unlike what observed in the structures of the lanthanide complexes formed with $Trop^-$[18] and NTP^-, there are important variations of the bond lengths of Ln-O in **4** and **5**. This can be visualized as the presence of two asymmetrical bindings. To analyze and quantify these differences, we have grouped two sets of bond lengths and averaged their respective values in order to minimize the standard deviation of these averages (Table 4.9). The average bond length of the four bonds from two of the four ligands containing O(1), O(2), O(5), and O(6) are significantly longer [2.57(5) Å and 2.55(8) Å in **4** and **5** respectively] (Table 4.9) than the bond length of the four bonds from the other two ligands containing O(3), O(4), O(3)A, O(4)A [2.35(4) Å and 2.32(4) Å in **4** and **5** respectively] (Table 9). As a result, two of the four $Thup^-$

ligands are closer to Ln^{3+}, and the other two are further. This is different compared with the other structures of the complexes formed with NTP^- and $Trop^-$, in which all the ligands are at approximately similar distances to the central Ln^{3+}, as shown by the relatively small standard deviation of their Ln-O bond lengths (Table 4.9). The Ln-O bond lengths in **4** and **1** can be directly compared since both of them are Pr^{3+} complexes. The difference between the longer Pr-O bond length [2.57(5) Å] in **4** and the average Pr-O bond length in **1** [2.50(5) Å] is smaller than the difference between the shorter Pr-O bond length [2.35(4) Å] in **4** and the average bond length [2.50(5) Å] in **1**. This could be attributed to the packing motif in the crystal structure (Figure 4.26 and Figure 4.27).
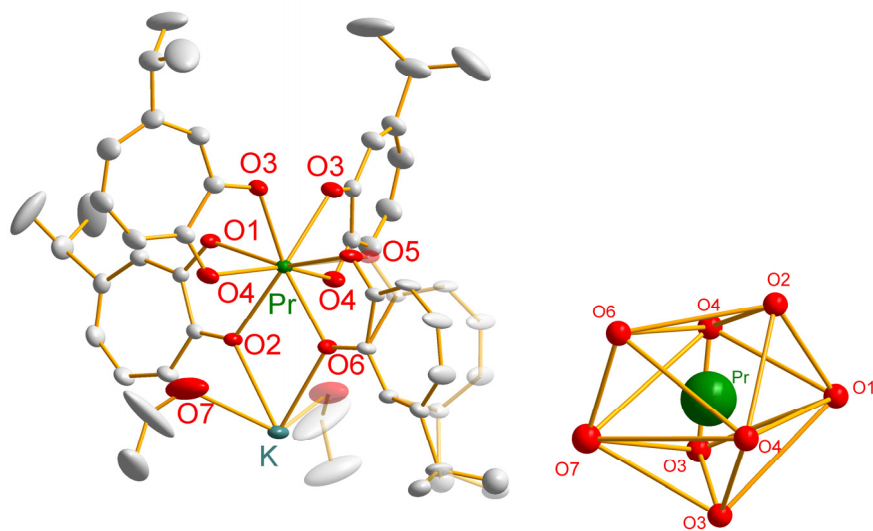
Figure 4.22: Left: ORTEP representations of the molecular structure of **4** (30% probability ellipsoids, H atoms have been omitted for clarity); Right: Coordination polyhedron of Pr^{3+} in **4**
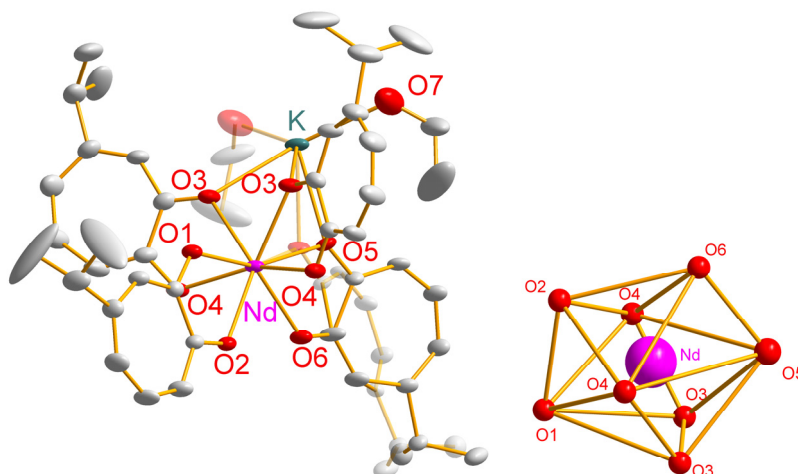
Figure 4.23: Left: ORTEP representations of the molecular structure of **5** (30% probability ellipsoids, H atoms have been omitted for clarity); Right: Coordination polyhedron of Nd^{3+} in **5**

Table 4.7: Selected bond lengths (Å) for **4**

Pr-O(1)	2.619(5)	K-O(6)	2.702(5)
Pr-O(2)	2.520(4)	K-O(5)B	2.707(5)
Pr-O(3)	2.383(3)	K-O(7)	2.826(9)
Pr-O(4)	2.309(4)	K-O(2)	2.824(4)
Pr-O(3)A	2.383(3)	K-O(3)C	2.860(4)
Pr-O(4)A	2.309(4)	K-O(3)B	2.860(4)
Pr-O(5)	2.619(7)		
Pr-O(6)	2.536(4)		

Symmetry codes: A: *x*, -*y*+3/2, *z*; B: *x*+1/2, *y*, -*z*+1/2; C: *x*+1/2, -*y*+3/2, -*z*+1/2

Table 4.8: Selected bond lengths (Å) for **5**

Nd-O(1)	2.625(4)	K-O(6)	2.674(4)
Nd -O(2)	2.470(4)	K-O(5)B	2.686(5)
Nd -O(3)	2.357(3)	K-O(7)	2.735(5)
Nd-O(4)	2.286(3)	K-O(2)	2.772(4)
Nd-O(3)A	2.357(3)	K-O(3)C	2.812(4)
Nd-O(4)A	2.286(3)	K-O(3)B	2.812(4)
Nd-O(5)	2.619(6)		
Nd-O(6)	2.494(4)		

Symmetry codes: A: *x*, -*y*+3/2, *z*; B: *x*+1/2, *y*, -*z*+1/2; C: *x*+1/2, -*y*+3/2, -*z*+1/2

136
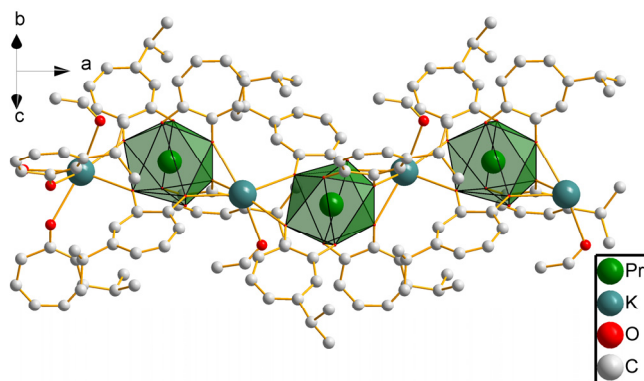
Figure 4.24: Structure of **4** showing the coordination polymer chain along the *a* axis
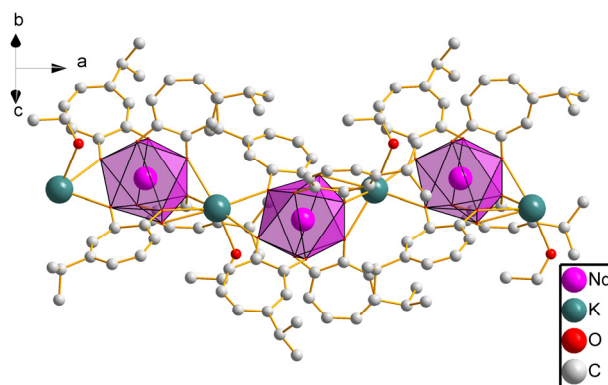
Figure 4.25: Structure of **5** showing the coordination polymer chain along the *a* axis
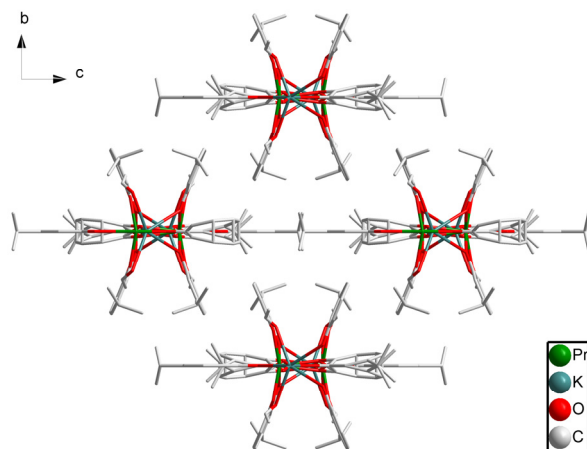
Figure 4.26: Crystal packing diagram of **4**

137
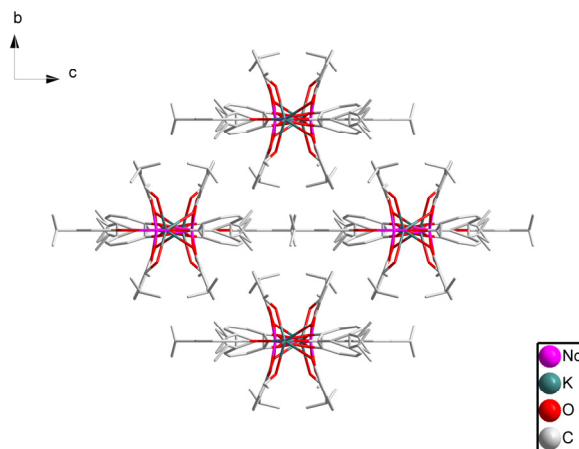
Figure 4.27: Crystal packing diagram of **5**

Table 4.9: Summary of the lengths (Å) of Ln-O bonds, and the coordination number (CN) of Ln^{3+} and K^+

Complex		Bond lengths of Ln-O bonds				CN of Ln^{3+}	CN of K^+	Distance of K-Ln
		Average	d_s	d_l	Δd			
KYb(Trop)$_4$[18]		2.31(2)	2.30(2)	2.325(3)	0.03	8	7	3.927, 3.894
KTb(Trop)$_4$[18]		2.37(1)	2.355(7)	2.376(6)	0.02	8	7	3.859, 3.847
1		2.50(5)	2.46(3)	2.53(1)	0.07	9	8	4.058, 3.942
2		2.43(6)	2.40(4)	2.47(5)	0.07	9	9	4.095, 3.958
3	Yb(1)	2.32(2)	2.30(1)	2.327(8)	0.02	8	9	4.077, 3.972
	Yb(2)	2.31(2)	2.30(2)	2.320(5)	0.02	8	9	4.039, 3.927
4		2.57(5)	2.42	2.50	0.08	8	6	4.177, 3.973
		2.35(4)						
5		2.55(8)	2.37	2.49	0.12	8	6	4.121, 3.885
		2.32(4)						

Summary of the analysis of the crystal structures

8 Coordination vs. 9 Coordination. The analysis of the single crystal structures provides some interesting pieces of information. Two types of coordination numbers have been observed for the NTP⁻ complexes: nine coordination for Pr^{3+} complex (**1**) and Gd^{3+} complex (**2**), and eight coordination for the Yb^{3+} complex (**3**). Since all the different Ln^{3+} have similar reactivities, the change of coordination number can only be explained by the size of these three Ln^{3+}, the sole parameter that differentiates them. Yb^{3+} has the smallest effective ionic radius of

138

0.985 Å for a coordination of 8 according to the definition of Shannon.[20] Pr^{3+} and Gd^{3+} have larger effective ionic radii: 1.179 Å and 1.107 Å for coordination number of 9 respectively.[20] In the Yb^{3+} complex, there is not enough room to accommodate the coordination of an additional molecule of solvent. As a consequence, Yb^{3+} is better protected by the four NTP$^-$ ligands from the coordination of molecules of solvent. It is interesting that in our previous work of the structural analysis of the lanthanide complexes formed with Trop$^-$, we have not been able to isolate crystals of sufficient quality with Ln^{3+} larger than Tb^{3+}. This negative result could be explained by a possible change in the coordination numbers of Ln^{3+} making the crystallization process more difficult.

A different situation is observed for the complexes formed with Thup$^-$. Both of the Pr^{3+} (**4**) and Nd^{3+} (**5**) complexes adopt a coordination number of eight. Therefore, the formation of nine coordinated species in the complexes of NTP$^-$ can not be solely explained by the size of Ln^{3+}. Nevertheless, the observation of nine coordinated complexes with NTP$^-$ allows us to conclude that it is possible to form nine-coordinated species, which was the conclusion from our previous study of the solution structure of Trop$^-$ complexes.[8,18] It was found that the eight coordinated [Yb(Trop)$_4$]$^-$, observed by X-ray structure analysis for the solid sample, was determined to be a nine coordinated complex in solution by the luminescent lifetime measurements and the calculation of the hydration state of Ln^{3+} (*q* value).[8,18]

To compare further and describe the similarities and differences between these five crystal structures, and how the coordination numbers of Ln^{3+} vary from eight to nine, a systematic analysis of the individual geometry of the different complexes has been performed. Firstly, four planes representing the four ligands are defined by using ten atoms (seven C atoms from the seven-membered ring and two coordinating O atoms from the ligand, see Table 4.11 for

the definitions) for each of them. Four dihedral angles (θ_1, θ_2, θ_3, and θ_4) formed between these four planes can then be calculated and compared. Secondly, four centers of mass based on the seven carbon atoms on each of the seven-membered ring (b1, b2, b3, b4) are calculated. Then two angles: φ_1 (angle of b1-Ln-b3) and φ_2 (angle of b2-Ln-b4) are calculated (Figure 4.28). The values are listed in Table 4.10. For comparison, the data of $[Yb(Trop)_4]^-$ is also listed.
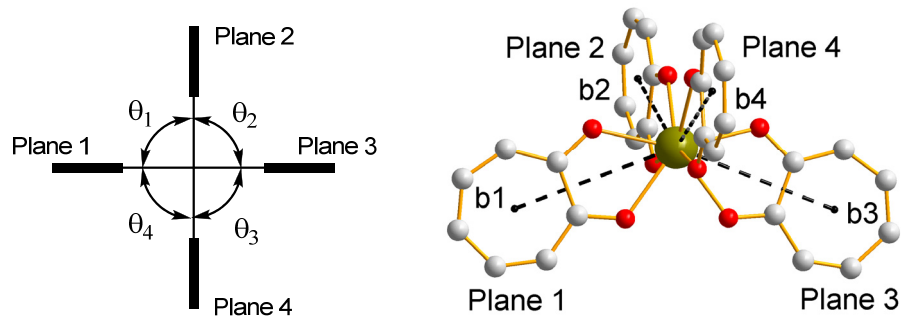
Figure 4.28. Definition of planes 1 to 4, dihedral angles θ_1 to θ_4, and barycenters b_1 to b_4

In complex **3**, four dihedral angles in both Yb(1) and Yb(2) centered ML_4 unit are close to 90°. The two angles (φ_1) and (φ_2) are also close to those in $[Yb(Trop)_4]^-$. This result indicates the similarity between the geometries of these two complexes. In fact, they have the same D_{2d} dodecahedron coordination geometry, as discussed previously.

Table 4.10: Summary of top and side views of the different structures, dihedral angles, φ_1 and φ_2

	Yb(Trop)$_4^-$ 8 coordinated	**3**: Yb(NTP)$_4^-$ 8 coordinated Yb1	**3**: Yb(NTP)$_4^-$ 8 coordinated Yb2
$\theta_1, \theta_2, \theta_3, \theta_4$ φ_1, φ_2	86.4, 79.2, 99.0, 93.8 141.9; 143.3	87.6, 91.0, 93.4, 88.0 137.9; 138.2	86.5, 98.8, 83.0, 89.1 142.3, 142.6
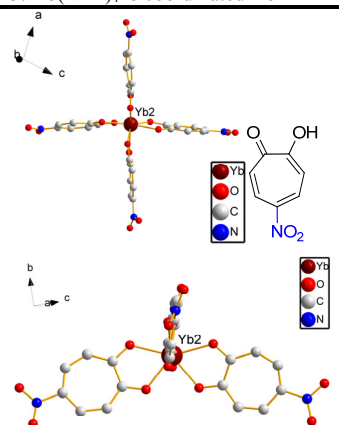
	1: Pr(NTP)$_4^-$ 9 coordinated	**2**: Gd(NTP)$_4^-$ 9 coordinated	**4**: Pr(Thup)$_4^-$ 8 coordinated	**4**: Nd(Thup)$_4^-$ 8 coordinated
$\theta_1, \theta_2, \theta_3, \theta_4$ φ_1, φ_2	124.9, 66.2, 70.0, 100.1 135.1; 119.5	124.4, 65.4, 69.4, 102.6 135.9; 118.5	106.2, 73.8, 73.8, 106.2 142.6, 121.7	105.3, 74.7, 74.7, 105.3 141.5, 122.3

In complexes **1** and **2**, the coordination number is increased from eight to nine by the coordination of an additional solvent molecule. As shown in Table 4.10, the solvent molecule is coordinated to Ln^{3+} from a position between plane 1 and plane 2. This induces two effects. Firstly, it causes plane 2 and plane 4 to bend toward plane 3. As a consequence, angles θ_1 and θ_4 increase, angles θ_2 and θ_3 decrease. Secondly, the value of the angle φ_2 is decreased from c.a. 140° to 120°, indicating that plane 2 and plane 4 are forced to get closer to give more space for the accommodation/coordination of the solvent molecule. It is interesting to notice that despite the difference between the sizes of the Pr^{3+} and Gd^{3+}, and the presence of different coordinated solvent molecules, all the angles examined for both structures are fairly similar.

Surprisingly, in the structures of eight coordinated Thup⁻ complexes **4** and **5**, even without the perturbation of the coordinated solvent molecules, the bent of the plane 2 and 4 is also observed to a smaller extent (θ_1 = 105-106°), compared with those in complex **1** and **2** (θ_1 = 124°).

Ln-O bond length. We have discussed the special situation of the Ln-O bond length in **4** and **5**, in which two of the four ligands are closer to Ln^{3+} than the other two ligands. After further scrutiny of the Ln-O bond lengths, we found that for each ligand, one of the Ln-O bond is longer than the other Ln-O bond (asymmetry at the level of the ligand). The average of the four longer bond lengths (d_l) is calculated and compared with the average of the four short bond lengths (d_s). The values are listed in Table 4.9. For comparison, the data of the structure of $[Yb(Trop)_4]^-$ and $[Tb(Trop)_4]^-$ are also included in Table 4.9.

It is interesting to notice that the difference (Δd) between the longer and the shorter bond is smaller for $[Yb(Trop)_4]^-$, $[Tb(Trop)_4]^-$, and both $[Yb(NTP)_4]^-$ units in **3**. This result indicates that in these three structures, not only the four ligands are evenly close to Ln^{3+}, as discussed

142

above, and that for each of the four ligands, two oxygen atoms are also located at equal distances to Ln^{3+}. This situation has not been observed for the 9 coordinated complex **1** and **2** or for the 8 coordinated complex **4** and **5**, in which Δd is large (0.07-0.12 Å). In **1** and **2**, although four ligands are evenly close to Ln^{3+}, the difference between the two bond lengths for each ligand is rather large. In complex **4** and **5**, there is not only an important difference in respect to the positions of the ligands to Ln^{3+}, but also a big difference between the two Ln-O bond lengths in each of the ligand.

Table 4.11: Definition of four planes in different structures

Complexes	Plane 1	Plane 2	Plane 3	Plane 4
KYb(Trop)₄DMF	Yb O5 C15 C16 C17 C18 C19 C20 C21 O6	Yb O4 C7 C6 C5 C4 C3 C2 C1 O3	Yb O1 C8 C9 C10 C11 C12 C13 C14 O2	Yb O7 C28 C27 C26 C25 C24 C23 C22 O8
1	Pr O7 C22 C23 C24 C25 C26 C27 C28 O8	Pr O1 C1 C2 C3 C4 C5 C6 C7 O2	Pr O3 C8 C9 C10 C11 C12 C13 C14 O4	Pr O5 C15 C16 C17 C18 C19 C20 C21 O6
2	Gd O1 C1 C2 C3 C4 C5 C6 C7 O2	Gd O7 C22 C23 C24 C25 C26 C27 C28 O8	Gd O5 C15 C16 C17 C18 C19 C20 C21 O6	Gd O3 C8 C9 C10 C11 C12 C13 C14 O4
3	Yb1 O3 C8 C9 C10 C11 C12 C13 C14 O4	Yb1 O5 C15 C16 C17 C18 C19 C20 C21 O6	Yb1 O1 C1 C2 C3 C4 C5 C6 C7 O2	Yb1 O7 C22 C23 C24 C25 C26 C27 C28 O8
	Yb2 O21 C43 C44 C45 C46 C47 C48 C49 O22	Yb2 O19 C36 C37 C38 C39 C40 C41 C42 O20	Yb2 O17 C29 C30 C31 C32 C33 C34 C35 O18	Yb2 O23 C50 C51 C52 C53 C54 C55 C56 O24
4	Pr O5 C20 C21 C22 C23 C24 C25 C26 O6	Pr O3 C10 C11 C12 C13 C14 C15 C16 O4	Pr O1 C1 C2 C3 C4 C5 C6 C7 O2	Pr O3 C10 C11 C12 C13 C14 C15 C16 O4
5	Nd O5 O6 C20 C26 C21 C25 C22 C23 C24	Nd O3 C10 C11 C12 C13 C14 C15 C16 O4	Nd O1 C1 C2 C3 C4 C5 C6 C7 O2	Nd O3 C10 C11 C12 C13 C14 C15 C16 O4

4.2.4 Ligand-centered luminescence in Gd^{3+} complexes

The photophysical properties of the different coordinated ligands were studied by the analysis of their corresponding Gd^{3+} complexes. This work allowed the determination of the energies of the singlet and triplet states of these ligands when coordinated to Ln^{3+} and how the different

substituents affect the electronic structure of the sensitizers. Gd^{3+} can not be sensitized by these ligands since its electronic levels are energetically not accessible (the energy gap between the ground and the first excited state of Gd^{3+} is too large).

The UV-vis absorption and steady state fluorescence spectra were measured in DMSO at room temperature to gather the information related to the singlet states. The time-resolved phosphorescence spectra were measured at 77 K in order to obtain information on the triplet states. The UV-vis absorption spectra with molar extinction coefficient of the Gd^{3+} complexes formed with the different ligands are reported in Figure 4.29, and the normalized UV-vis absorption, fluorescence, and phosphorescence spectra are shown in Figure 4.30. Information extracted from these spectra are summarized in Table 4.12. For comparison, the corresponding spectra recorded from tropolonate complexes are also included.
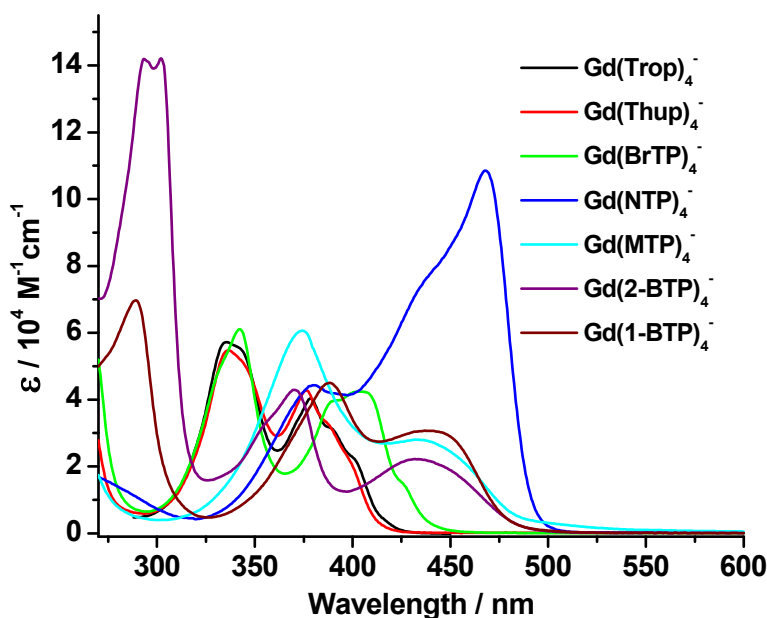
Figure 4.29: UV-vis absorption spectra of different Gd^{3+} complexes in DMSO

Table 4.12: Summary of the data obtained on $\pi\rightarrow\pi^*$, $^1\pi\pi^*$, and $^3\pi\pi^*$ as reported as maxima of electronic envelopes

of absorption, fluorescence (singlet states), and phosphorescence (triplet states) spectra of the ligands bound to Gd^{3+}

in DMSO (10^{-4} M)

Ligand	$\pi\rightarrow\pi^*$ E (cm^{-1}) and ε (M^{-1}cm^{-1})	$^1\pi\pi^*$ E (cm^{-1})	$^3\pi\pi^*$ E (cm^{-1})[a]
Trop$^-$	29,810 (57,170), 26,420 (40,400)	23,500[b]	17,200, 15,600, 14,300[b]
Thup$^-$	29,720 (54,760), 26,600 (42,600)	23,700[b]	17,090, 15,650, 14,270[b]
BTP$^-$	29,240 (61,060), 24,810 (42,400)	22,830[b]	17,150, 15,700, 14,310[b]
NTP$^-$	26,250 (44,350), 21,370 (109,000)	20,200[c]	15,800, 14,370[c]
MTP$^-$	26,740 (60,550), 23,070 (27,980)	20,410[d]	14,500, 13,140[d]
2-BTP$^-$	33,610 (139,200), 27,030 (42,940), 23,180 (22,170)	19,920[d]	14,510[d]
1-BTP$^-$	34,540 (69,730), 25,770 (45,030), 22,880 (30,710)	20 370[e]	18,730[e]

a. Measured at 77 K, delay time: 0.1 ms, integration time: 20 ms
b. $\lambda_{exc.}$ = 340 nm
c. $\lambda_{exc.}$ = 400 nm
d. $\lambda_{exc.}$ = 370 nm
e. $\lambda_{exc.}$ = 390 nm
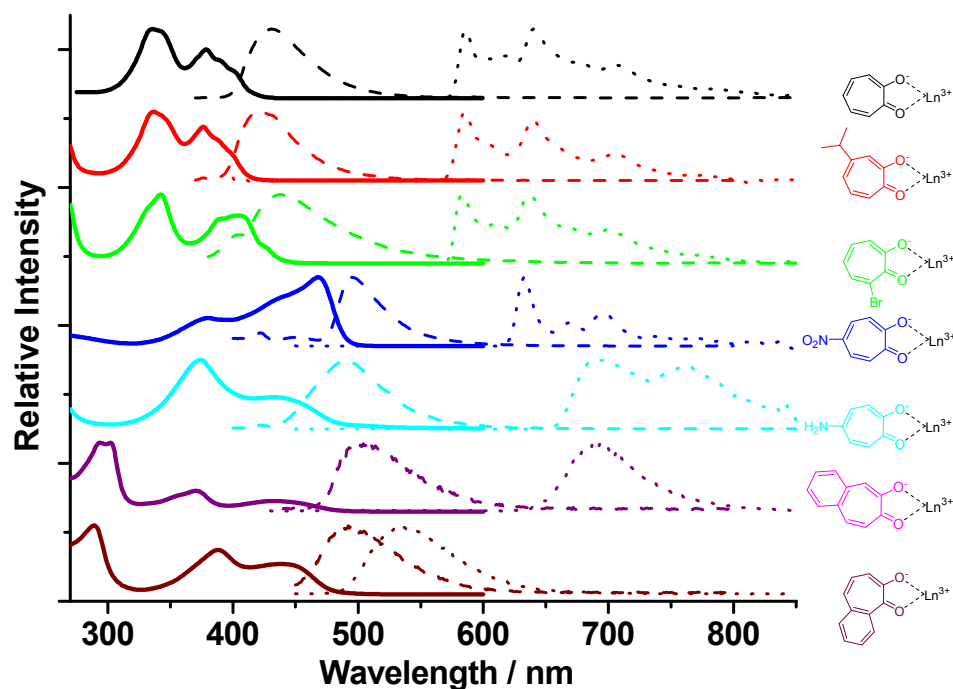
Figure 4.30: Combination of normalized UV-vis absorption (298 K, plain line), fluorescence (298 K, dash line),

phosphorescence (77 K, dot line) spectra for Gd^{3+} complexes formed with Trop$^-$, Thup$^-$, BrTP$^-$, NTP$^-$, MTP$^-$, 2-BTP$^-$,

and 1-BTP$^-$ in DMSO (see Table 4.12 for experimental conditions)

Thup⁻ and BrTP⁻. In general, the absorption spectra of the Gd^{3+} complexes formed with these ligands reveal the presence of a combination of bands and shoulders that can be attributed to $\pi \rightarrow \pi^*$ transitions with large extinction coefficients. For $Gd(Trop)_4^-$, $Gd(Thup)_4^-$, and $Gd(BrTP)_4^-$, the absorption spectrum appears to be constituted of two major bands. The $\pi \rightarrow \pi^*$ bands located at higher energy (29,810 cm^{-1} for Trop⁻, 29,720 cm^{-1} for Thup⁻, and 29,240 cm^{-1} for BrTP⁻) of all three ligands have fairly similar shapes and energies. The $\pi \rightarrow \pi^*$ band and shoulder located at lower energy of Thup⁻ is slightly shifted towards higher energy (180 cm^{-1}) in comparison to Trop⁻. This blue-shift effect can also be observed on the $^1\pi\pi^*$ transition (200 cm^{-1}). This result can be tentatively explained by the weak electron-donating effect of the isopropyl group that does not induce significant changes on the electronic structure of the ligand by the presence of the substituent. However, this blue-shift effect is not observed on the $^3\pi\pi^*$ transition, where a slight red-shift (110 cm^{-1}) is observed instead (Table 4.12).

For $Gd(BrTP)_4^-$, the $\pi \rightarrow \pi^*$ band and associated shoulder located at lower energy is red-shifted by about 1,610 cm^{-1} in comparison to $Gd(Trop)_4^-$. In addition, BrTP⁻ has a significantly larger extinction coefficient at lower energy (longer wavelength) than Trop⁻. The $^1\pi\pi^*$ transition of BrTP⁻ is also located at about 670 cm^{-1} lower in energy in comparison to Trop⁻. No meaningful difference can be observed between the phosphorescence spectra of $Gd(BrTP)_4^-$ and $Gd(Trop)_4^-$ as an indication that this electronic state is located at similar energies for both complexes.

NTP⁻ and MTP⁻. In contrast to the small changes of $\pi \rightarrow \pi^*$, $^1\pi\pi^*$, $^3\pi\pi^*$ observed in $Gd(Thup)_4^-$ and $Gd(BrTP)_4^-$, the presence of nitro and amino group induces significant changes of the electronic structure of both ligands in comparison to $Gd(Trop)_4^-$. Surprisingly, both groups which have opposite inducing electronic effects (electron withdrawing effect for the nitro group

and electron donating effect for the amino group) induce similar changes of the electronic structure of these ligands. The red-shift of all transitions in the absorbance, fluorescence, and phosphorescence spectra has been observed for $Gd(NTP)_4^-$ and $Gd(MTP)_4^-$. For the $\pi \rightarrow \pi^*$ transitions, the respective UV-vis absorption spectra can be interpreted as the nitro group inducing a larger red-shift (3,560 cm^{-1}, 5,050 cm^{-1}) of both observed apparent maxima of the bands in comparison to the amino group (3,070 cm^{-1}, 3,350 cm^{-1}). The band located at lower energy has a surprisingly larger extinction coefficient (108,500 $M^{-1}cm^{-1}$ at 470 nm), more than double the value for the band located at higher energy (44,350 $M^{-1}cm^{-1}$ at 381 nm). By comparison of the UV-vis spectra of $Gd(NTP)_4^-$ and $Gd(MTP)_4^-$, we can also conclude that this band may result from an additional electronic state of NTP^-. The $\pi \rightarrow \pi^*$ transition located at higher energy in the absorption spectrum of $Gd(MTP)_4^-$ has similar relative intensity in comparison to $Gd(Trop)_4^-$. There is no important difference between the energies of the $^1\pi\pi^*$ transitions of NTP^- and MTP^-, but the apparent maxima associated with the $^3\pi\pi^*$ transitions of MTP^- (14,500 cm^{-1} and 13,140 cm^{-1}) are located at lower energy region compared to those of NTP^- (15,800 cm^{-1}, 14,370 cm^{-1}).

2-BTP⁻ and 1-BTP⁻. Both 2-BTP⁻ and 1-BTP⁻ have three apparent maxima corresponding to their $\pi \rightarrow \pi^*$ transitions. The two bands located at lower energy for both ligands have similar relative intensity in comparison to Trop⁻, Thup⁻, BrTP⁻, and MTP⁻. This situation is attributed to the red-shift of the electronic structure of tropolonate induced by the conjugated resonate benzene aromatic ring. The third band located at the UV-vis range (33,610 cm^{-1} and 34,540 cm^{-1} for 2-BTP⁻ and 1-BTP⁻ respectively) can be assigned to the transition with higher energy, which is not observed in Trop⁻ due to the limitation of the solvent used: DMSO has a

cut-off wavelength at 262 nm. In fact, the transition with higher energy has been reported to be located around 230 nm in EtOH.[21]

The red-shift of the two bands at lower energy (4,040 cm^{-1} and 3,540 cm^{-1}) in 1-BTP^{-} is larger than the red-shift (2,780 cm^{-1} and 3,240 cm^{-1}) in 2-BTP^{-}, although singlet state of 2-BTP^{-} is located at lower energy (19,920 cm^{-1}) than the singlet state of 1-BTP^{-} (20,370 cm^{-1}). The more interesting result is the large difference between the energies of the triplet states of 2-BTP^{-} and 1-BTP^{-}. 2-BTP^{-} ligand has a low energy-lying triplet state located around 14,510 cm^{-1}. Surprisingly, the triplet state of 1-BTP^{-} is located at much higher energy (18,730 cm^{-1}), with a difference of 4,220 cm^{-1}. This result illustrates that a subtle change of the chemical structure of a chromophore can induce a major impact on its electronic structure and photophysical properties.

4.2.5 Lanthanide-centered luminescence

To analyze the ability of the different ligands to sensitize the lanthanide-centered NIR luminescence, emission spectra of Yb^{3+}, Nd^{3+}, and Er^{3+} complexes formed with all six ligands were measured in DMSO. For the complexes formed with each ligand, the luminescence excitation spectra were recorded upon monitoring the specific transitions of each Ln^{3+} (Yb^{3+}: $^{2}F_{5/2} \rightarrow {}^{2}F_{7/2}$, 980 nm; Nd^{3+}: $^{4}F_{3/2} \rightarrow {}^{4}I_{11/2}$, 1060 nm; Er^{3+}: $^{4}I_{13/2} \rightarrow {}^{4}I_{15/2}$, 1520 nm). The three luminescence excitation spectra have similar shapes and relative intensities, as shown in Figure 4.31. The excitation spectra of Yb^{3+} complexes are depicted in Figure 4.32 as examples. For comparison purpose, the absorption spectra of the Yb^{3+} complex of each ligand are also overlaid in Figure 4.32.

As shown in Figure 4.32, except for Yb(NTP)$_4^{-}$, the luminescence excitation spectra of the Yb^{3+} complexes are similar to their respective absorption spectra (good match between the

numbers and energy positions of the corresponding spectral bands). Considering the excitation spectra are similar for the complexes formed with each ligand, these data indicate that the energy absorbed by the $\pi \rightarrow \pi^*$ transitions of the Trop⁻, Thup⁻, MTP⁻, BrTP⁻, 2-BTP⁻, and 1-BTP⁻ ligands is transferred to different NIR emitting Ln^{3+} using a similar energetic pathway through the electronic states of the respective ligand.

The situation is significantly different in the NTP⁻ complexes. The absorption spectrum of $Yb(NTP)_4^-$ has two bands with apparent maxima of electronic envelope at 26,250 and 21,370 cm^{-1} (Figure 4.32). However, the observed apparent maximum of the excitation spectrum is located at 25,000 cm^{-1}, which indicates only the band located at higher energy of the absorption spectrum is able to sensitize Yb^{3+}. The second band located at lower energy of the spectrum that possesses a significantly larger absorption is surprisingly not active for the sensitization of Yb^{3+}. This additional band is also not active for the sensitization of Nd^{3+} and Er^{3+} since the excitation spectra of three complexes are similar (Figure 4.31).

Overall, we can conclude that the absorption spectra of the Yb^{3+} complexes formed with the seven different ligands are similar to the corresponding Gd^{3+} complexes. The observations and conclusions on these Yb^{3+} complexes can be generalized to Nd^{3+} and Er^{3+} studied in this work.

Through excitation of the $\pi \rightarrow \pi^*$ absorption bands of the coordinated ligands, the NIR luminescence emission spectra of Yb^{3+}, Nd^{3+}, and Er^{3+} complexes were recorded in DMSO solution. The Yb^{3+} complexes display an emission band ranging from 977 to 1,022 nm, which is assigned to the $^2F_{5/2} \rightarrow {}^2F_{7/2}$ transition. For the Nd^{3+} complex, three emission bands were observed at 880, 1,059, and 1,332 nm and are attributed to the transitions from the $^4F_{3/2}$ level to the $^4I_{9/2}$,

$^4I_{11/2}$, and $^4I_{13/2}$ sublevels respectively. For Er^{3+} complex, the emission band observed at 1,531 nm can be assigned to the transition arising from $^4I_{13/2}$ level to $^4I_{15/2}$ level.
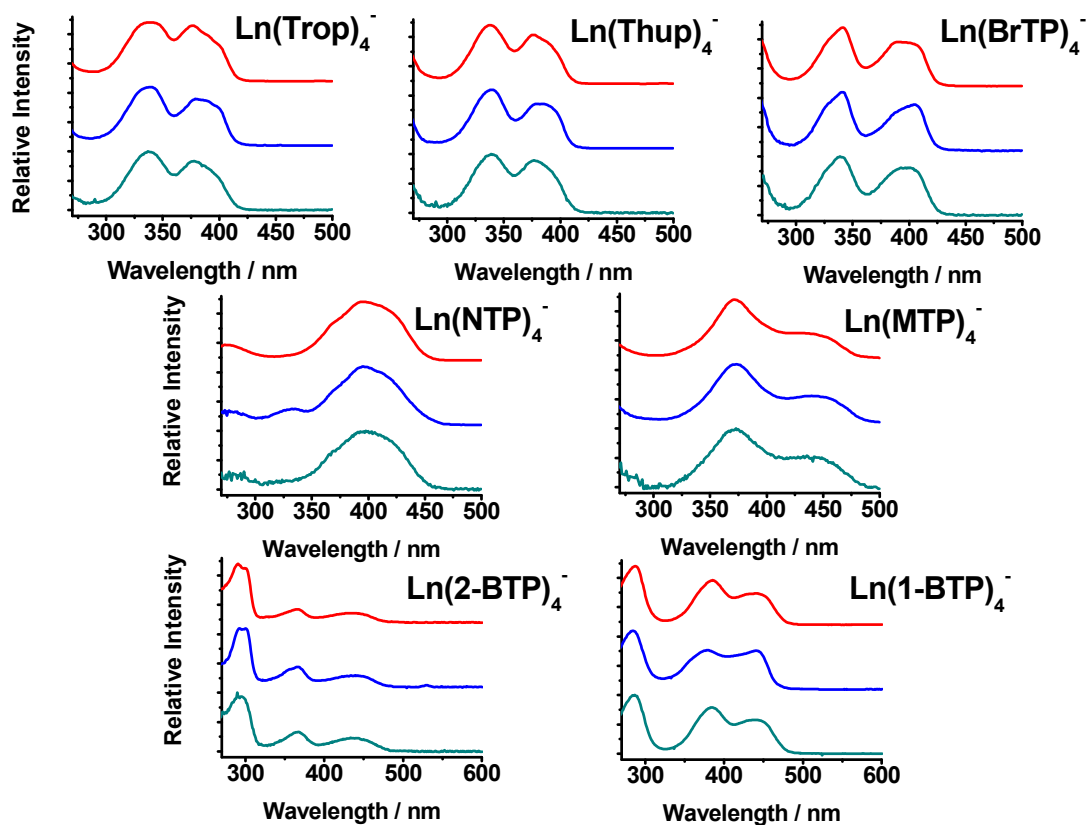
Figure 4.31: Luminescence excitation spectra for different complexes in DMSO (10^{-4} M, for Yb^{3+}, $\lambda_{em} = 980$ nm (red), for Nd^{3+}, $\lambda_{em} = 1060$ nm (blue), for Er^{3+}, $\lambda_{em} = 1520$ nm (dark cyan))
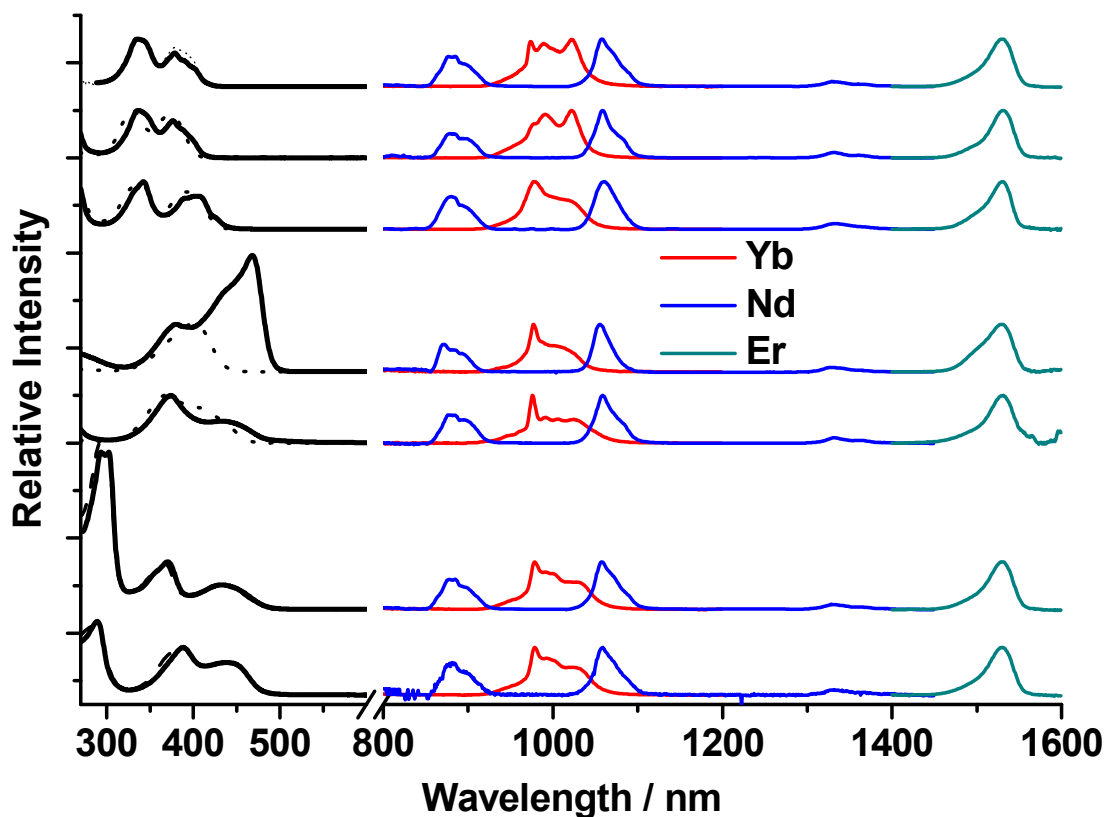
Figure 4.32: Normalized UV-vis absorption (plain line) and luminescence excitation spectra (dashed line) in DMSO (10^{-4} M, $\lambda_{em} = 980$ nm) of Yb^{3+} complexes (the UV-vis absorption spectra of KYb(NTP)$_4$ was normalized at 400 nm (corresponding to the maximum of its excitation spectra), luminescence emission spectra of Nd^{3+}, Er^{3+}, and Yb^{3+} complexes in DMSO (see Table 4.13 for experimental conditions)

In order to quantify the efficiency of the ligand-to-Ln^{3+} energy transfer and the quenching of the excited states of Ln^{3+} through non-radiative deactivations, quantum yields of the Nd^{3+}, Yb^{3+}, and Er^{3+} complexes formed with all six ligands were measured in DMSO and DMSO-d_6, and compared with those previously reported for the tropolonate complexes.[8] The results are listed in Table 4.13 and graphically summarized in Figure 4.33. To quantify the non-radiative

deactivations of the excited states of Ln^{3+}, the luminescence lifetimes of Yb^{3+} and Nd^{3+} complexes formed with all six ligands were also measured in DMSO and DMSO-d_6 and reported in Table 4.14. The luminescence lifetimes of Yb^{3+} complexes have also been recorded in CH_3OH and CD_3OD in order to obtain some information on the coordination environment around Ln^{3+} in these complexes in solution and to quantify the degree of protection against non-radiative deactivation provided by the ligands. This information was obtained by the calculation of the number of water/solvent molecules (hydration state value q) bound in first sphere of coordination of Ln^{3+}.[22,23] The result of tropolonate complexes[8] is also included for comparison and listed in Table 4.14.

The overall quantum yield of a lanthanide-containing molecular edifice is given by the following equation: $Q_{Ln}^{L} = \eta_{sens} \times Q_{Ln}^{Ln} = \eta_{sens} \times \dfrac{\tau_{obs}}{\tau_{rad}}$, whereby Q_{Ln}^{L} and Q_{Ln}^{Ln} are the overall and intrinsic quantum yields resulting from indirect and direct excitation, respectively, while η_{sens} represents the efficiency with which electromagnetic energy is transferred from the surroundings onto Ln^{3+}; τ_{obs} is the experimental lifetime of the Ln^{3+} excited state recorded on the specific emission bands of Ln^{3+} and the τ_{rad} is the radiative lifetime (Nd^{3+}, 0.25 ms[24]; Er^{3+}, 14 ms[25]; Yb^{3+}, 2 ms[25]). Because the rate of sensitization (intersystem crossing and energy transfer) is usually considered as much faster than the rate constant of radiative emission of Ln^{3+}, luminescence lifetimes were measured upon ligand excitation was used as τ_{obs}. Providing that the availability of Q_{Ln}^{L} and τ_{obs} values for different ligands, it is possible to calculate the relative η_{sens} values for six ligands by using $\dfrac{Q_{Ln}^{L_1}}{Q_{Ln}^{L_2}} = \dfrac{\eta_{sens}^{L_1}}{\eta_{sens}^{L_2}} \times \dfrac{\tau_{obs}^{L_1}}{\tau_{obs}^{L_2}}$, with the hypothesis that the complexes formed between a common Ln^{3+} and different ligands have the τ_{rad} values close enough to be

considered as the same (these τ_{rad} values typically depends on the coordination geometry around Ln^{3+}). The relative efficiencies of the ligand sensitization in different complexes were calculated and the results are summarized in Table 4.14.

In the next section, the structures of the complexes in solution are discussed followed by the detailed discussion of the quantum yields, luminescence lifetimes, and relative efficiency of sensitization results for each ligand. The diagram of the energy levels of the electronic states of Nd^{3+}, Er^{3+}, Yb^{3+}, and the singlet and triplet states of different ligands is depicted in Figure 4.34.
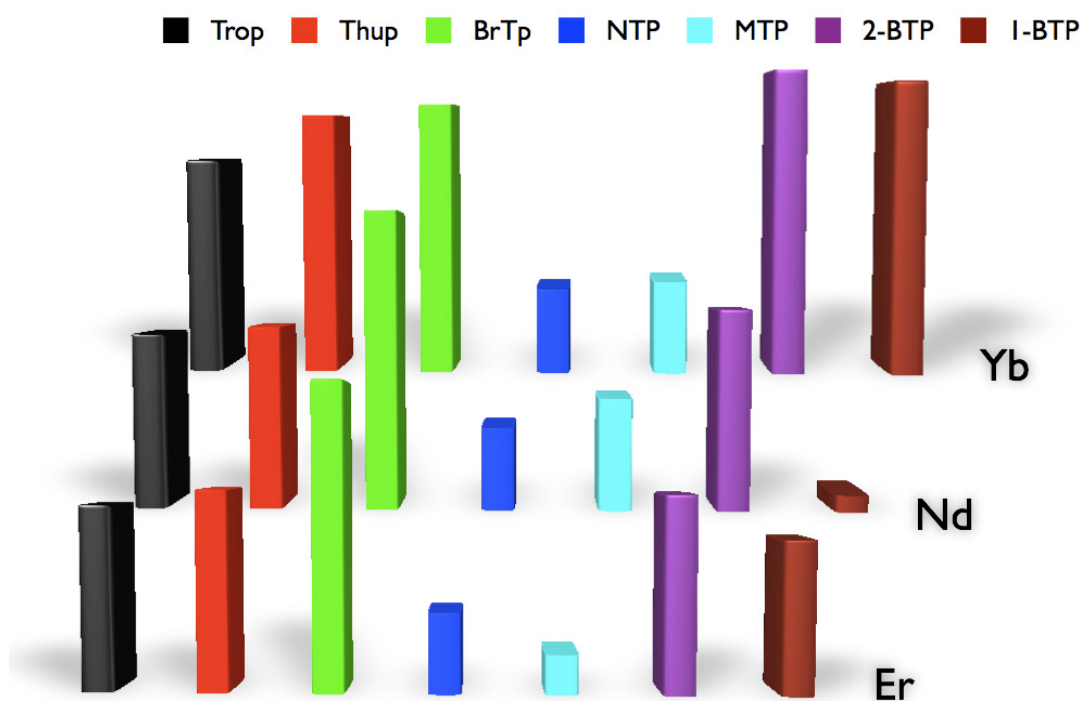
Figure 4.33: 3-D schematic quantitative representation of the relative quantum yields of all the complexes. For each lanthanide, the quantum yield values are normalized to the value obtained for the corresponding tropolonate complex

Table 4.13: Luminescence quantum yields (Q_{Ln}^L) of different complexes in DMSO

Ln	Ln(Trop)$_4$[b]		Ln(Thup)$_4$[b]		Ln(BrTP)$_4$[b]		Ln(NTP)$_4$[c]		Ln(MTP)$_4$[d]		Ln(2-BTP)$_4$[d]		Ln(1-BTP)$_4$[e]	
	Q_{Ln}^L[8]	Q_R[f]	Q_{Ln}^L	Q_R[f]	Q_{Ln}^L	Q_R[f]	Q_{Ln}^L	Q_R[f]	Q_{Ln}^L	Q_R[f]	Q_{Ln}^L	Q_R[f]	Q_{Ln}^L	Q_R[f]
Yb[a]	$1.9(1)\times10^{-2}$	1.00	$2.3(1)\times10^{-2}$	1.21	$2.4(1)\times10^{-2}$	1.26	$7.5(1)\times10^{-3}$	0.39	$8.2(1)\times10^{-3}$	0.43	$2.7(1)\times10^{-2}$	1.42	$2.6(1)\times10^{-2}$	1.37
Nd[a]	$2.1(1)\times10^{-3}$	1.00	$2.2(1)\times10^{-3}$	1.05	$3.6(2)\times10^{-3}$	1.71	$9.9(5)\times10^{-4}$	0.47	$1.3(1)\times10^{-3}$	0.64	$2.4(1)\times10^{-3}$	1.14	$2.0(1)\times10^{-4}$	0.095
Er[a]	$1.7(1)\times10^{-4}$	1.00	$1.8(1)\times10^{-4}$	1.06	$2.8(1)\times10^{-4}$	1.65	$7.3(4)\times10^{-5}$	0.43	$3.6(1)\times10^{-5}$	0.21	$1.8(1)\times10^{-4}$	1.06	$1.4(1)\times10^{-5}$	0.82

a. 10^{-4} M
b. λ_{ex} = 340 nm
c. λ_{ex} = 400 nm
d. λ_{ex} = 370 nm
e. λ_{ex} = 390 nm
f. Relative quantum yield by using corresponding tropolonate complexes as reference.
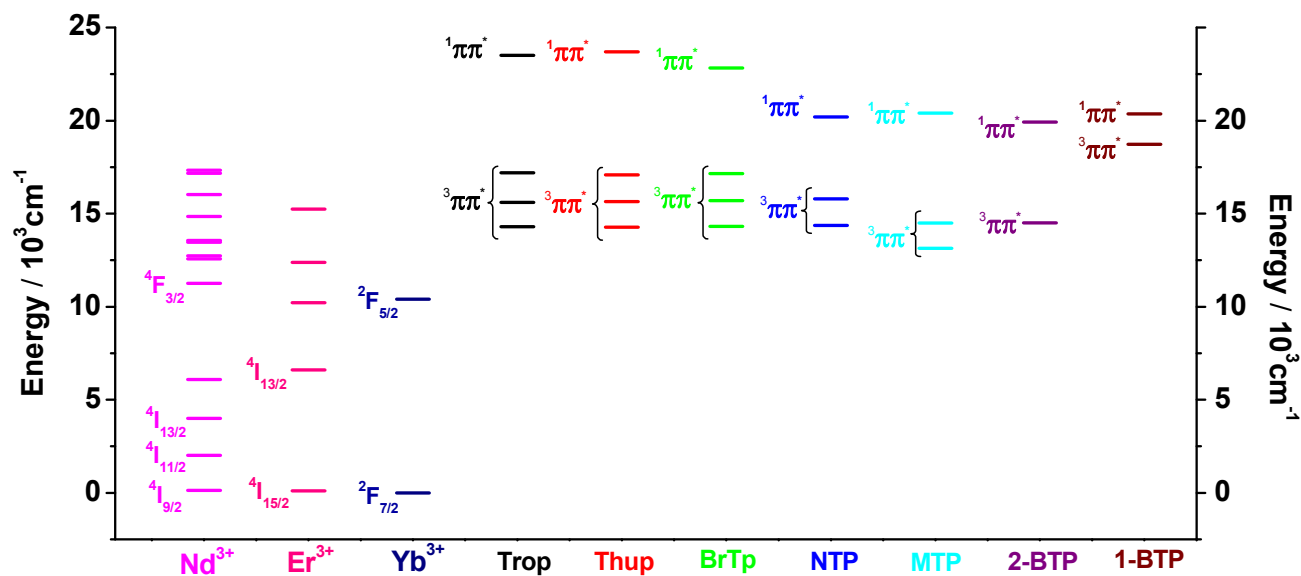
Figure 4.34: Diagram of the energy levels of Nd^{3+}, Er^{3+}, and Yb^{3+}, as well as singlet and triplet energy of different ligands

Ligand	Nd^{3+} complex			Yb^{3+} complex					q
	τ_{DMSO}	$\eta_{sensDMSO}$	$\tau_{DMSO-d6}$	τ_{DMSO}	$\eta_{sensDMSO}$	$\tau_{DMSO-d6}$	τ_{CH3OH}	τ_{CD3OD}	
Trop⁻	1.19(4)[8]	1.00	1.65(1)[8]	14.1(6)[8]	1.00	18.1(1)[8]	1.4(1)	17.6(4)	1.2
Thup⁻	1.17(1)	1.07	1.57(3)	13.2(2)	1.29	16.9(2)	1.23(1)	14.43(8)	1.4
BrTP⁻	1.65(1)	1.24	3.2(2)	13.8(1)	1.29	34(3)	1.6(1)	19.8(4)	1.0
NTP⁻	1.48(1)	0.38	3.34(2)	11.8(1)	0.47	27.3(1)	1.25(2)	15.20(1)	1.4
MTP⁻	0.85(1)	0.87	1.09(1)	6.32(1)	0.96	10.1(1)	0.95(4)	12.85(4)	1.8
2-BTP⁻	1.45(1)	0.94	2.00(1)	14.1(1)	1.42	19.8(1)	1.55(1)	17.45(3)	1.1
1-BTP⁻	NA	NA	NA	13.9(1)	1.39	20.9(1)	1.39(1)	16.3(4)	1.2

4.2.6 Coordination of Ln^{3+} in solution: hydration value q

The comparison between the luminescence lifetimes recorded in deuterated and non-deuterated solvents can be used to quantify the number of solvent molecules coordinated in the first sphere to Ln^{3+} in solution. The calculation of the hydration/solvation number is obtained by using an empirical formula (1) developed by Beeby et al.[23,26] In this formula, q is the number of water molecules bound to Ln^{3+} in the first sphere of coordination; k_H and k_D are the rate constants of excited states of Ln^{3+} in non-deuterated and deuterated solvent respectively. A is a proportionality constant related to the sensitivity of Ln^{3+} to vibrational quenching by OH oscillators, B is the correction factor for outer sphere water/solvent molecules.

$$q = A \ (k_H\text{-}k_D) \ \text{-}B \qquad\qquad (1)$$

For Yb^{3+} complex in methanol solution, A = 2 μs, B = 0.1, k_H = $1/\tau_H$ (in μs^{-1}) and k_D = $1/\tau_D$ (in μs^{-1})

Except for the MTP⁻ complex, all the calculated q values for different complexes are close to 1 (Table 4.14), indicating that in solution, one single solvent molecule is coordinated to Ln^{3+}. This is consistent with the q value we have previously measured for the Trop⁻ complexes.[8,18] These results globally indicate that the coordination of Ln^{3+} in all the different

complexes includes a molecule of bound solvent. The structures of the complexes in solution are therefore close to the structures observed in the crystal structure where a molecule of solvent is bound to Ln^{3+} in the first sphere of coordination, such as compound **1** and **2**. The larger q value (1.8) that has been obtained for the MTP$^-$ complex can be tentatively explained by the presence of the N-H vibrations of the amino group of the ligand that act as additional source of non-radiative deactivation.

Thup$^-$ complexes. All the Thup$^-$ complexes have higher quantum yields compared to the Trop$^-$ complexes (+21% for Yb^{3+}, +5% for Nd^{3+} and +6% for Er^{3+}), but slightly shorter luminescence lifetimes for both Yb^{3+} and Nd^{3+} complexes. The shorter luminescence lifetimes reveal the presence of a more efficient non-radiative deactivation process within these complexes in comparison to the Trop$^-$ complexes. From the calculated η_{sens} values, we can conclude that the presence of the isopropyl group on Trop$^-$ increases the efficiency of sensitization by 7% for Nd^{3+} and by 29% for Yb^{3+}. From the combination of the luminescence lifetimes and the η_{sens} values, it can be interpreted that the lower level of protection of Ln^{3+} is compensated by the higher efficiency of sensitization, which results in higher quantum yield values being obtained for Thup$^-$ complexes than for the corresponding Trop$^-$ complexes.

BrTP$^-$ complexes. The bromo group induced major increases of quantum yields for all three complexes (+26% for Yb^{3+}, +71% for Nd^{3+}, and +65% for Er^{3+}). Longer luminescence lifetimes were observed for Nd^{3+} complexes as an indication that the central Nd^{3+} is more efficiently protected in solution by BrTP$^-$ than Trop$^-$. The larger quantum yield values are consistent with the trend of results of Iwamuro's study of the bromo substituted 8-hydroxyquinoline Nd^{3+} complexes, in which the bromo group accounted for a 150% increase of the quantum yield. Interestingly, the η_{sens} value of $Nd(BrTP)_4^-$ is 24% larger than the value for

Nd(Trop)$_4^-$, indicating that the introduction of the bromo group, hypothesized to induce a heavy atom effect, increases the sensitization efficiency for Nd^{3+}. On the other hand, the sensitization efficiency of Yb(BrTP)$_4^-$ increases by about 29% compared to Yb(Trop)$_4^-$. This indicates that the heavy atom effect should be beneficial for the sensitization of Yb^{3+}, which is reflected by the significantly increased quantum yield value.

NTP$^-$ complexes. For both Nd(NTP)$_4^-$ and Yb(NTP)$_4^-$, the quantum yields are significantly smaller than those reported for the corresponding Trop$^-$ complexes. No large difference between the luminescence lifetimes for both Nd(NTP)$_4^-$ and Yb(NTP)$_4^-$ were observed (Table 4.14), indicating a similar level of protection of Ln^{3+}. The calculated η_{sens} values indicate that the efficiency of sensitization of nitro group to the NIR emitting Ln^{3+} is poor. For Nd(NTP)$_4^-$, the lower efficiency can be partially explained by the small energy gap between the donating triplet state of NTP$^-$ (15,800 cm^{-1}) and the accepting energy level ($^4F_{3/2}$) of Nd^{3+} located at 15,000 cm^{-1}. In such situation, a risk of Ln^{3+} to sensitizer energy back transfer[4] is pronounced.

MTP$^-$ complexes. All three MTP$^-$ complexes have significantly smaller quantum yields compared to the corresponding Trop$^-$ complexes (-57% for Yb^{3+}, -36% for Nd^{3+} and -79% for Er^{3+}) and shorter luminescence lifetimes. As mentioned before, the shorter lifetime can tentatively be explained by the fact that eight N-H vibrations are present within the four ligands coordinated to the central Ln^{3+} The *B* value in formula (1) does not include this quenching which comes directly from the sensitizer, and they can account for the additional second sphere quenchers. This quenching hypothesis is reinforced by the fact that the quenching is happening independently of the nature of Ln^{3+}. Interestingly, the η_{sens} of Yb(MTP)$_4^-$ is very similar higher than the value for Yb(Trop)$_4^-$. This indicates the MTP$^-$ could potentially be a good sensitizer for Yb^{3+} provided that the quenching can be removed, e.g., using NMe$_2$ group instead of the NH$_2$

group. The poor sensitization efficiency of Nd^{3+} can be tentatively explained by the energetically low lying triplet state of MTP^- (14,500 cm^{-1}) which is too close to the energy accepting level of Nd^{3+}, which could potentially result in thermally activated back energy transfer[4] to the ligand and non-radiative deactivation of the excited states of Nd^{3+}.

2-BTP⁻ complexes. The $Yb(2\text{-}BTP)_4^-$ complex has the highest quantum yield among the seven Yb^{3+} complexes with an increase of 42% in value compared to $Yb(Trop)_4^-$. The increase of quantum yields for $Nd(2\text{-}BTP)_4^-$ (14%) and $Er(2\text{-}BTP)_4^-$ (6%), on the other hand, is not as strong as $Yb(2\text{-}BTP)_4^-$. The η_{sens} for $Yb(2\text{-}BTP)_4^-$ is higher than that of $Yb(Trop)_4^-$, indicating that 2-BTP^- is a more efficient sensitizer for Yb^{3+} than $Trop^-$. This situation can be explained by the triplet state being at lower energy.

1-BTP⁻ complexes. The results of the analysis of the photophysical properties of $Ln(1\text{-}BTP)_4^-$ are interesting. For $Yb(1\text{-}BTP)_4^-$, both of the quantum yield and η_{sens} are comparable to that of $Yb(2\text{-}BTP)_4^-$. But the quantum yield for $Nd(1\text{-}BTP)_4^-$ is surprising small. In fact, the measurement of luminescent lifetime was unsuccessful because of the insufficient intensity of the NIR signal.

4.3   CONCLUSION

In this work, the synthesis, structure, and NIR luminescence properties of ML_4 complexes formed between six derivatives of tropolonate with Ln^{3+} (Ln = Nd, Er, and Yb) were systematically studied and compared. Six ligands (HThup, HBrTP, HNTP, HMTP, 2-HBTP, and 1-HBTP) all form ML_4 complexes with Ln^{3+}. Crystal structures of three NTP^- complexes (Pr^{3+}, Gd^{3+}, and Yb^{3+}) and two $Thup^-$ complexes (Pr^{3+} and Nd^{3+}) were isolated and resolved by using

X-ray structural analysis. In the resolved structures, Ln^{3+} are all coordinated with four ligands, and the K^+ is the bridging ion connecting two adjacent ML_4 units to a 1-D coordination polymer, similar to what has been previously observed in the structure of $Ln(Trop)_4^-$. We have observed two different coordination numbers (8 and 9) in the structures of NTP^- complexes: the additional coordination of a solvent molecule is the cause of the increase of the coordination number. This difference in coordination number is attributed to the change of the size of Ln^{3+}. But it was not observed in the structures of $Thup^-$ complexes that larger Ln^{3+} complexes have larger coordination number (9). In both Pr^{3+} and Nd^{3+} complexes, the lanthanide cations have a coordination number of eight. In addition to the changes at the molecular level, different packing schemes have also been observed in the crystal structures of the complexes formed with different Ln^{3+}. Depending on the absence or presence of the different interactions between the 1-D coordination polymers, 1-D coordination chain (compound **4** and **5**), 2-D coordination plane (compound **1**), and 3-D coordination network (compound **2** and **3**) are formed. This structural information indicates that the presence of the substituents can induce large variations of the structures of the resulting complexes at both molecular and intermolecular level. The presence of NO_2 (electron withdrawing group) does not appear to have a strong effect on the strengths of coordination bond formed between the oxygen atoms of the ligands and Ln^{3+}. Such results tend to indicate that the presence of these substituents does not affect significantly the electron density on the seven-membered ring.

The photophysical properties of these different complexes were systematically studied and compared to tropolonate complexes. Firstly, the calculation of hydration number (q) reveals the presence of the additional coordination of a solvent molecule for all the complexes in solution, which is consistent with the result previously obtained for tropolonate complexes. We

believe that the presence of N-H vibrations in MTP$^-$ ligand accounts for the relative larger calculated q value. The results of the quantum yields and luminescent lifetimes were measured on the solutions of the complexes and the efficiencies of sensitization were calculated. The isopropyl group does generate an improvement in the quantum yields, but the shorter luminescence lifetimes indicate it has a slight quenching effect to the excited states of Ln^{3+}. Complexes formed with BrTP$^-$ have higher quantum yields and longer luminescence lifetimes, indicating that bromo groups are a favorable parameter for the optimization of the sensitizers. It was surprising to observe that both electron attracting NO$_2$ and electron donating NH$_2$ group induce the same trend of red-shift effect for the $^1\pi\pi^*$ and $^3\pi\pi^*$ transitions in respect to the tropolonate complexes. Although the NO$_2$ group does not induce additional quenching of Ln^{3+} in NIR emitting lanthanide complexes, the sensitization efficiencies decrease greatly in NTP$^-$ complexes, indicating that NO$_2$ group is not a good choice for improvement of NIR luminescence. The NH$_2$ group is not a good choice either due to the smaller quantum yields and shorter lifetimes, which is attributed to the quenching effect from the N-H vibration on the ligand. This is an intrinsic problem for NTP$^-$, but it can be probably eliminated by replacing the N-H bonds by a N-C bond (e.g in NMe$_2$). Besides, improved sensitization efficiency is observed for Yb^{3+} complexes for NTP$^-$. This result indicates that the NH$_2$ group should be a good substituent at the condition that its quenching contribution is removed. After all, it does lower the triplet state of the ligand, which has been demonstrated to be beneficial for the sensitization of NIR emitting Ln^{3+}. The two isomeric ligands (2-BTP$^-$ and 1-BTP$^-$) have similar sensitization efficiency for Yb^{3+}, but significantly different for Nd^3. This result indicates that a small change in the structure of ligand could tremendously impact the energy transfer process in NIR emitting lanthanide complexes. Overall, Yb(2-BTP)$_4^-$ has the highest quantum yields among all the Yb^{3+}

complexes. Nd(BrTP)$_4$- and Er(BrTP)$_4$- have the highest quantum yield values among all the Nd^{3+} and Er^{3+} complexes respectively. The ligand BrTP$^-$ provides the most efficient protection for Ln^{3+}, as in indicated by its smallest q value. The order of the efficiency of sensitization for this series of ligands:

for Yb^{3+}, 2-BTP$^-$, 1-BTP$^-$ > BrTP$^-$, Thup$^-$ > Trop$^-$, MTP$^-$ >> NTP$^-$;

for Nd^{3+}, BrTP$^-$ > Thup$^-$, Trop$^-$, 2-BTP$^-$ > MTP$^-$ >> NTP$^-$.

4.4   REFERENCES

(1)   Bünzli, J.-C. G.; Piguet, C. *Chem. Soc. Rev.* **2005**, *34*, 1048.

(2)   Weissman, S. I. *J. Chem. Phys.* **1942**, *10*, 214.

(3)   Werts, M. H. V.; Hofstraat, J. W.; Geurts, F. A. J.; Verhoeven, J. W. *Chem. Phys. Lett.* **1997**, *276*, 196.

(4)   Hebbink, G. A.; Grave, L.; Woldering, L. A.; Reinhoudt, D. N.; van Veggel, F. C. J. M. *J. Phys. Chem. A* **2003**, *107*, 2483.

(5)   Van Deun, R.; Fias, P.; Driesen, K.; Binnemans, K.; Goerller-Walrand, C. *Phys. Chem. Chem. Phys.* **2003**, *5*, 2754.

(6)   Iwamuro, M.; Adachi, T.; Wada, Y.; Kitamura, T.; Nakashima, N.; Yanagida, S. *Bull. Chem. Soc. Jpn.* **2000**, *73*, 1359.

(7)   Albrecht, M.; Osetska, O.; Klankermayer, J.; Froehlich, R.; Gumy, F.; Bünzli, J.-C. G. *Chem. Commun.* **2007**, 1834.

(8)   Zhang, J.; Badger, P. D.; Geib, S. J.; Petoud, S. *Angew. Chem., Int. Ed.* **2005**, *44*, 2508.

(9)   Petoud, S.; Bünzli, J.-C. G.; Schenk, K. J.; Piguet, C. *Inorg. Chem.* **1997**, *36*, 1345.

161

(10)   Tobita, S.; Arakawa, M.; Tanaka, I. *J. Phys. Chem.* **1984**, *88*, 2697.

(11)   Tobita, S.; Arakawa, M.; Tanaka, I. *J. Phys. Chem.* **1985**, *89*, 5649.

(12)   Guldi, D. M.; Mody, T. D.; Gerasimchuk, N. N.; Magda, D.; Sessler, J. L. *J. Am. Chem. Soc.* **2000**, *122*, 8289.

(13)   Doering, W. v. E.; Knox, L. H. *J. Am. Chem. Soc.* **1951**, *73*, 828.

(14)   Elliott, J. M.; Chipperfield, J. R.; Clark, S.; Sinn, E. *Inorg. Chem.* **2001**, *40*, 6390.

(15)   Tarbell, D. S.; Bill, J. C. *J. Am. Chem. Soc.* **1952**, *74*, 1234.

(16)   Galantay, E. E.; Simpson, R.; Corriveau, G.; Denzer, M.; Knorr, D. C.; Strohschein, R. J.; Paolella, N. A.; Uike, Y.; Gogerty, J. H.; et al. *J. Med. Chem.* **1974**, *17*, 1316.

(17)   Galantay, E. E.; Simpson, W. R. J. *Chem. Commun.* **1970**, 754.

(18)   Zhang, J.; Badger, P. D.; Geib, S. J.; Petoud, S. *Inorg. Chem.* **2007**, 6473.

(19)   Kepert, D. L. *Prog. Inorg. Chem.* **1978**, *24*, 179.

(20)   Shannon, R. D. *Acta Crystallogr., Sect. A* **1976**, *A32*, 751.

(21)   Breheret, E. F.; Martin, M. M. *J. Lumin.* **1978**, *17*, 49.

(22)   Davies, G. M.; Aarons, R. J.; Motson, G. R.; Jeffery, J. C.; Adams, H.; Faulkner, S.; Ward, M. D. *J. Chem. Soc., Dalton Trans.* **2004**, 1136.

(23)   Beeby, A.; Burton-Pye, B. P.; Faulkner, S.; Motson, G. R.; Jeffery, J. C.; McCleverty, J. A.; Ward, M. D. *J. Chem. Soc., Dalton Trans.* **2002**, 1923.

(24)   Weber, M. J. *Phys. Rev.* **1968**, *171*, 283.

(25)   Miniscalo, W. J. *J. Lightwave Technol.* **1991**, *9*, 234.

(26)   Beeby, A.; Clarkson, I. M.; Dickins, R. S.; Faulkner, S.; Parker, D.; Royle, L.; de Sousa, A. S.; Williams, J. A. G.; Woods, M. *J. Chem. Soc., Perkin Trans. 2* **1999**, 493

5.0   AZULENE-MOIETY-BASED LIGAND FOR THE EFFICIENT SENSITIZATION OF FOUR NEAR-INFRARED LUMINESCENT LANTHANIDE CATIONS

Part of this chapter has been published as Zhang, J.; Petoud, S. *Chem.-Eur. J.* **2008**, 14, 1264.

Since most of the accepting energy levels of NIR emitting lanthanide cations are generally located at lower energy compared to visible emitting lanthanides, it is hypothesized that efficient sensitizing ligands for NIR emitting Ln^{3+} should have a triplet state located at relatively lower energy. Different sensitizers which have low energy-lying triplet states have been used, such as organic fluorophores,[1-3] the ligand-to-metal charge transfer (LMCT bands) from the transition metal (Ru, Os, Re) complexes,[4-6] and porphyrins.[7,8] We have previously studied the tropolonate (Trop⁻) ligand which possesses a triplet state located at an energy of 17,200 cm⁻¹ (580 nm) for the sensitization of five different NIR emitting Ln^{3+} for the first time.[9,10] We hypothesized that the tropolonate has such low energy-lying triplet states despite of its small size is related to its special seven-membered conjugated ring system. For this reason, we have decided to evaluate other ligands that possess similar seven-membered conjugated ring systems.

Azulene is a non-benzenoid aromatic molecule; its name is derived from the Spanish word "azul", meaning blue. It is a dark blue crystalline solid used in many cosmetics. Azulene is an isomer of naphthalene but its photophysical properties are significantly different. Its structure

consists of a cyclopentadiene ring fused with a cycloheptatriene ring, and can be therefore considered as a fusion product of a 6π electrons cyclopentadienide anion which is aromatic and the corresponding aromatic 6π electrons tropylium cation (Figure 5.1). Due to this particular electronic structure, azulene appears to be a versatile organic fragment with both an electron-rich five-membered ring that could act as a potential electron density donor and an electron-deficient seven-membered ring that could act as a potential electron density acceptor. Due to this rich electronic character, azulene and its derivatives have been attracting a growing interest in various areas of molecular materials, such as charge transfer complexes,[11,12] conducting polymers,[13,14] liquid crystals,[15,16] anion receptor/sensors,[17,18] optoelectronic molecular switches,[19] and nonlinear optical (NLO) material.[20-22]
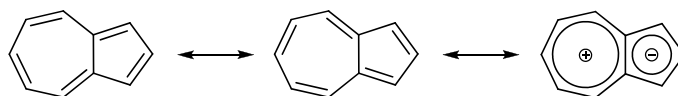
Figure 5.1: Molecular structure of azulene and its polar resonance form

For the sensitization of NIR emitting lanthanide cations, the azulene moiety is interesting since it possesses a triplet state located at significantly lower energy (13,600 cm^{-1})[23] in comparison to the tropolonate ligand (17,200 cm^{-1}). It is therefore hypothesized that azulene would have better sensitizing efficiency for several NIR emitting Ln^{3+} since its triplet state is located at lower energy and close to the energy of their accepting levels. In this work, we have designed and synthesized a new bidentate ligand that incorporates the azulene moiety (Figure 5.2): diethyl 2-hydroxyazulene-1,3-dicarboxylate (HAz), for the coordination and sensitization of NIR emitting Ln^{3+}. The synthesis of the ligand and several of its lanthanide complexes are reported in this chapter. The luminescent properties have been analyzed and quantified. The ligand Az$^-$ has been

demonstrated to act as an efficient sensitizer for several different Ln^{3+} emitting in the near-infrared: Yb^{3+}, Nd^{3+}, Er^{3+}, and Tm^{3+}. It is worth noting that Tm^{3+} luminescence arising from a complex in solution is rarely reported. Its luminescence is especially appealing for bioimaging, since the main NIR emission band is located around 800 nm, which corresponds to an absorption minimum for water and tissues.[24,25]
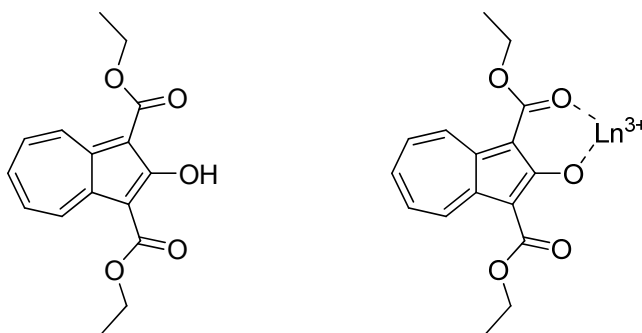
Figure 5.2: Molecular structure of HAz and the proposed bidentate coordination mode of Az⁻ with Ln^{3+}

5.1 EXPERIMENTAL SECTION

5.1.1 Materials

All reagents were used as received, unless otherwise stated. Tropolone, thionyl chloride, diethyl malonate, $LnCl_3 \cdot nH_2O$ (Ln = Nd, Gd, Er, Tm, and Yb, 99.9% or 99.99%, n = 6 or 7 depending on the Ln), and KOH standardized solution in methanol (0.100 M) were purchased from Aldrich. All deuterated NMR solvents were purchased from Cambridge Isotope Labs and used as received. KGd(Trop)$_4$ was prepared according to our published procedure.[9]

5.1.2 Methods

Infrared spectra were recorded on a Perkin-Elmer Spectrum BX FT-IR instrument. Samples were prepared with a drop of CH_2Cl_2 solution, and evaporated to dryness on KBr pellets. Elemental analyses were performed by Atlantic Microlab, Inc. (Norcross, Georgia). ^{1}H NMR spectra were recorded on a Bruker DPX-300 spectrometer at 300 MHz. MS-EI and MS-ESI were measured on a MicroMass AutoSpec and Agilent HP 1100 series LC-MSD instruments respectively. UV-vis absorption spectra were recorded on a Perkin-Elmer Lambda 9 spectrophotometer.

5.1.3 Spectrophotometric titrations

Spectrophotometric titrations were performed with a Perkin–Elmer Lambda 9 spectrophotometer connected to an external computer. All titrations were performed in a 1.00 cm thermostated (25.0 ± 0.1 °C) cuvette in CH_3OH or CH_3CN at constant ionic strength $\mu = 0.01$ M (tetrabutylammonium perchlorate). In a typical experiment, 2.00 mL of a ligand solution in CH_3OH (initial total ligand concentration 1×10^{-5} M) was titrated with $LnCl_3$ solutions (stock solution concentration: 2×10^{-5} M in CH_3OH). The kinetic of formation of the complexes was tested to take place within one min by monitoring the changes through UV-vis absorption spectra. For the titration experiments, two min after each addition of aliquot of the lanthanide salt stock solution to the ligand solution, the UV-vis spectrum of the resulting solution was recorded. Factor analysis and mathematical treatment of the spectrophotometric data were performed with the SPECFIT program.[26]

5.1.4 Luminescence measurements

Emission and excitation spectra were measured using a Jobin Yvon Horiba Fluorolog-322 spectrofluorometer equipped with a Hamamatsu R928 detector for the visible domain and an Electro-Optical Systems, Inc. DSS-IGA020L detector for the NIR domain. The NIR luminescence quantum yields were measured by using $KYb(Trop)_4$ complex ($\Phi = 1.9 \times 10^{-2}$ in DMSO) as reference.[9] Spectra were corrected for the instrumental function for both excitation and emission. Values were calculated using the following equation: $\dfrac{\Phi_x}{\Phi_r} = \dfrac{A_{r_{\lambda_x}}}{A_{x_{\lambda_x}}} \dfrac{I_{\lambda_r}}{I_{\lambda_x}} \dfrac{\eta_x^2}{\eta_r^2} \dfrac{D_x}{D_r}$, where

subscript r stands for the reference and x for the sample; A is the absorbance at the excitation wavelength, I is the intensity of the excitation light at the same wavelength, η is the refractive index ($\eta = 1.478$ in DMSO, $\eta = 1.344$ in acetonitrile, $\eta = 1.342$ in CD_3CN), and D is the measured integrated luminescence intensity. Time-resolved measurements were conducted with a Jobin Yvon Spex Fluorolog-3 spectrofluorimeter equipped with a phosphorimeter module and Xenon flash lamp. The emission spectra were then collected, with increasing delay times until the phosphorescence band was the main band on a spectrum (at delay 0.1 ms). The emission spectra were corrected for the background and instrumental function. The luminescence lifetime measurements were performed by excitation of solutions in 1 cm quartz cells using a Nd/YAG Continuum Powerlite 8010 Laser at 354 nm (third harmonic) as excitation source. Emission was collected at a right angle to the excitation beam, the emission wavelength selected with a Spectral Products CM 110 1/8 meter monochromator. The signal was monitored by a cooled photomultiplier (Hamamatsu R316-2) coupled to a 500 MHz bandpass digital oscilloscope (Tektronix TDS 754D). The signals to be treated (at least 15000 points resolution for each trace) were averaged from at least 500 individual decay curves. Luminescence decay curves were

imported into Origin 7.0 scientific data analysis software. The decay curves were analyzed using the Advanced Fitting Tool module. Reported luminescence lifetimes are averages of at least three independent determinations.

5.1.5   Synthesis of ligand HAz

The synthesis route of ligand HAz is shown in Figure. 5.3.
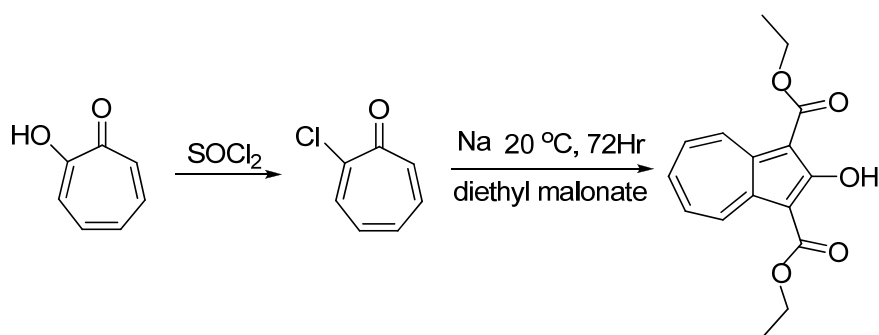
Figure 5.3: Synthesis route of HAz

2-Chlorocyclohepta-2,4,6-trien-1-one.[27,28] Tropolone (1.00 g, 8.20 mmol) was dissolved in dry benzene (25 mL) to give a colorless solution. Thionyl chloride (1.07 g, 8.99 mmol) was then added, which immediately give a white precipitate of tropolone hydrogen chloride; the precipitate dissolved after heating under reflux for 1.5 h to afford a dark-red solution. Excess thionyl chloride and benzene were evaporated and the brown residue was washed with hexane and evaporated. After chromatography (silica gel, 35% hexanes/ethyl acetate), 2-chlorotropone was obtained as a white solid (1.07 g, 94%). Mp: 64-65 °C. EI-MS: m/z [M]$^+$ 140.003216 (Calc. 140.002893 for C_7H_5ClO). ^1H NMR (CD$_3$COCD$_3$, 300 MHz): δ = 7.93 (d, J = 9.3 Hz, 1H), 7.41-7.34 (m, 1H), 7.25-7.04 (m, 3H). IR (KBr, cm^{-1}): 3568 (O-H), 3215 (C-

H), 1603 (C=O), 1591 (C=O), 1544, 1477, 1458, 1413, 1361, 1306, 1242, 1204, 1076, 994, 957, 897, 778, 749.

Diethyl 2-hydroxyazulene-1,3-dicarboxylate.[27] To a sodium ethoxide solution prepared from sodium (700 mg, 30.4 mmol) and absolute ethanol (50 mL), diethyl malonate (2.4 g, 15 mmol) and 2-chlorotropone (700 mg, 5.0 mmol) were added, and the mixture was allowed to stand for 72 h at room temperature. The reaction mixture turned into a gelatinous orange mass. Water was then added to this suspension, and the sodium salt of the targeted compound precipitated out. After collection by filtration, the precipitate was redissolved in glacial acetic acid. This solution was diluted with water and extracted with $CHCl_3$. The solvent was then evaporated and the residue was recrystallized from ethanol to give orange-yellow needles (720mg, 50%). Mp: 95 °C. EI-MS: m/z $[M]^+$ 288.100211 (Calc. 288.099774 for $C_{16}H_{16}O_5$). ^1H NMR (CD_3COCD_3, 300 MHz): δ = 1.45 (t, J = 7.2 Hz, 6H), 4.48 (q, J = 7.2 Hz, 4H), 7.84-7.93 (m, 3H), 9.44-9.47 (m, 2H), 11.68 (s, 1H). IR (KBr, cm^{-1}): 2978, 1671 (C=O), 1650 (C=O), 1597, 1533, 1476, 1435, 1333, 1284, 1204, 1176, 1032, 799, 735.

5.1.6 Synthesis of lanthanide complexes

To a solution of ligand HAz (115.2 mg, 0.04 mmol) in methanol (10 mL) was added 4.00 mL of a 0.100 M (0.04 mmol) KOH solution in methanol under stirring. The initially clear solution became cloudy due to the formation of the precipitate of the potassium salt of the deprotonated ligand. Methanol (10 mL) was added to the solution which was then heated until complete dissolution of the precipitates. $LnCl_3 \cdot nH_2O$ (0.01 mmol) (Ln = Pr, Nd, Gd, Ho, Er, Tm, Yb and Lu) in methanol (10 mL) was added to the resulting solution. This solution was stirred overnight

and the resulting yellow precipitate was collected by filtration, washed three times with methanol and dried in vacuo over P_2O_5 for 48 h.

Data for KPr(Az)$_4$: 39.4 mg, 59% isolated yield; ESI-MS (CH$_2$Cl$_2$ negative mode): *m/z* 1289.2 [M(Az)$_4$]$^-$, elemental analysis calcd (%) for C$_{64}$H$_{60}$O$_{20}$PrK·CH$_3$OH (1361.22): C 57.35, H 4.74; found: C 57.42, H 4.49; IR (KBr, cm^{-1}): 2978 (w), 1683 (s, C=O), 1615 (s, C=O), 1489 (s), 1454 (m), 1212 (m), 1147 (s), 803 (m).

Data for KNd(Az)$_4$: 42.3 mg, 64% isolated yield; ESI-MS (CH$_2$Cl$_2$ negative mode): *m/z* 1289.2 [M(Az)$_4$]$^-$; elemental analysis calcd (%) for C$_{64}$H$_{60}$O$_{20}$NdK·CH$_3$OH (1364.55): C 57.21, H 4.73; found: C 57.45, H 4.54; IR (KBr, cm^{-1}): 2977 (w), 1686 (s, C=O), 1615 (s, C=O), 1490 (s), 1454 (m), 1212 (m), 1148 (s), 803 (m).

Data for KGd(Az)$_4$: 39.2mg, 58% isolated yield; ESI-MS (CH$_2$Cl$_2$ negative mode): *m/z* 1306.2 [M(Az)$_4$]$^-$; elemental analysis calcd (%) for C$_{64}$H$_{60}$O$_{20}$GdK·CH$_3$OH (1377.56): C 56.67, H 4.68; found: C 56.45, H 4.39; IR (KBr, cm^{-1}): 2978 (w), 1683 (s, C=O), 1616 (s, C=O), 1494 (s), 1455 (m), 1213 (m), 1151 (s), 803 (m).

Data for KHo(Az)$_4$: 55.3 mg, 82% isolated yield; ESI-MS (CH$_2$Cl$_2$ negative mode): m/z 1313.2 [M(Az)$_4$]$^-$; elemental analysis calcd (%) for C$_{64}$H$_{60}$O$_{20}$HoK·CH$_3$OH (1385.24): C 56.36, H 4.66; found: C 56.24, H 4.43; IR (KBr, cm^{-1}): 2978 (w), 1683 (s, C=O), 1616 (s, C=O), 1495 (s), 1471 (s), 1456 (m), 1213 (m), 1152 (s), 803 (m).

Data for KEr(Az)$_4$: 47.4 mg, 70% isolated yield; ESI-MS (CH$_2$Cl$_2$ negative mode): *m/z* 1316.2 [M(Az)$_4$]$^-$; elemental analysis calcd (%) for C$_{64}$H$_{60}$O$_{20}$ErK·CH$_3$OH (1387.57): C 56.26, H 4.65; found: C 56.26, H 4.41; IR (KBr, cm^{-1}): 2978 (w), 1683 (s, C=O), 1616 (s, C=O), 1495 (s), 1471 (s), 1455 (m), 1213 (m), 1151 (s), 803 (m).

Data for KTm(Az)$_4$: 51.7 mg, 76% isolated yield; ESI-MS (CH$_2$Cl$_2$ negative mode): *m/z* 1317.2 [M(Az)$_4$]$^-$; elemental analysis calcd (%) for C$_{64}$H$_{60}$O$_{20}$TmK·CH$_3$OH (1389.24): C 56.20, H 4.64; found: C 56.18, H 4.38; IR (KBr, cm^{-1}): 2978 (w), 1683 (s, C=O), 1616 (s, C=O), 1495 (s), 1481 (s), 1456 (m), 1213 (m), 1153 (s), 803 (m).

Data for KYb(Az)$_4$: 45.0 mg, 66% isolated yield; ESI-MS (CH$_2$Cl$_2$ negative mode): *m/z* 1322.2 [M(Az)$_4$]$^-$; elemental analysis calcd (%) for C$_{64}$H$_{60}$O$_{20}$YbK·CH$_3$OH (1393.35): C 56.03, H 4.63; found: C 56.14, H 4.30; IR (KBr, cm^{-1}): 2976 (w), 1685 (s, C=O), 1620 (s, C=O), 1495 (s), 1481 (m), 1455 (m), 1213 (m), 1152 (s), 803 (m).

Data for KLu(Az)$_4$: 44.3 mg, 65% isolated yield; ESI-MS (CH$_2$Cl$_2$ negative mode): *m/z* 1323.2 [M(Az)$_4$]$^-$; elemental analysis calcd (%) for C$_{64}$H$_{60}$O$_{20}$LuK·CH$_3$OH (1395.28): C 55.95, H 4.62; found: C 56.02, H 4.49; IR (KBr, cm^{-1}): 2978 (w), 1683 (s, C=O), 1622 (s, C=O), 1495 (s), 1480 (s), 1455 (m), 1213 (m), 1152 (s), 803 (m).

5.2   RESULTS AND DISCUSSION

5.2.1   Formation of ML$_4$ complexes

The lanthanide complexes were prepared by mixing for 15 h the deprotonated ligand with stoichiometric amounts of LnCl$_3$ in methanol at room temperature. The result of the elemental analysis suggests the formation of complexes with KLn(Az)$_4$ as molecular formula for all the lanthanide complexes studied (Ln = Pr, Nd, Gd, Ho, Er, Tm, Yb, Lu). This indicates that only one of the C=O groups of the ligand is coordinated to Ln^{3+} forming a complex with ML$_4$ formula (the molecule acting as bidentate ligand, as shown in Figure 5.2). This conclusion was confirmed by

the FT-IR analysis. The IR absorption spectra of both the free ligand and the complex have two different C=O stretching bands with one common and one different vibration frequency (Figure 5.4). The presence of two different C=O vibrations in the free ligand can be explained by the formation of a hydrogen bond between the OH group with one of the C=O groups, which results in the red shift of the C=O stretching band. Similarly, the presence of different types of C=O vibrations in the coordinated ligand can be explained by one of the two C=O of the ligand being coordinated to Yb^{3+}. The bands located at higher energy that appears at 1,682 and 1,686 cm^{-1} can be assigned to the ligand and to the Yb^{3+} complex respectively. This vibration frequency can be assigned to the free C=O group, which is not involved in the formation of hydrogen or coordination bond. The vibration band located at lower wavenumber in the Yb^{3+} complex (1,620 cm^{-1}) is red-shifted by about 22 cm^{-1} compared to the value measured for the free ligand (1,642 cm^{-1}), confirming the formation of a coordination bond between this C=O and Ln^{3+}.
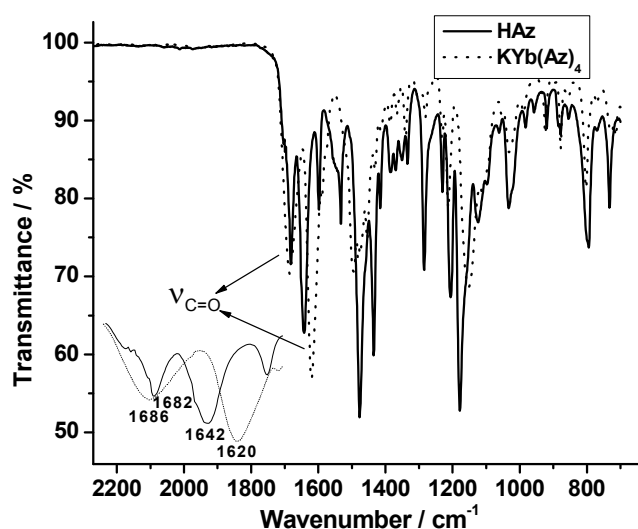
Figure 5.4: FT-IR spectra of HAz and $[Yb(Az)_4]^-$ complex

Electrospray mass spectroscopy (ES-MS) measurements provide an insight on the nature of the species of complexes formed in solution. In the negative ion mode, the molecular peak corresponding to the $[Ln(Az)_4]^-$ anion is observed. The presence of signal assigned to the free ligand indicates partial dissociation of the complexes in these experimental conditions. The ES-MS spectrum of the Nd^{3+} complex is depicted as an example in Figure 5.5. It is important to point out that the relative abundance reflected by intensities in the MS spectra can not be directly used to interpret the relative amount of the species of complexes present in solution but allow to conclude the presence of the $[Ln(Az)_4]^-$ species.
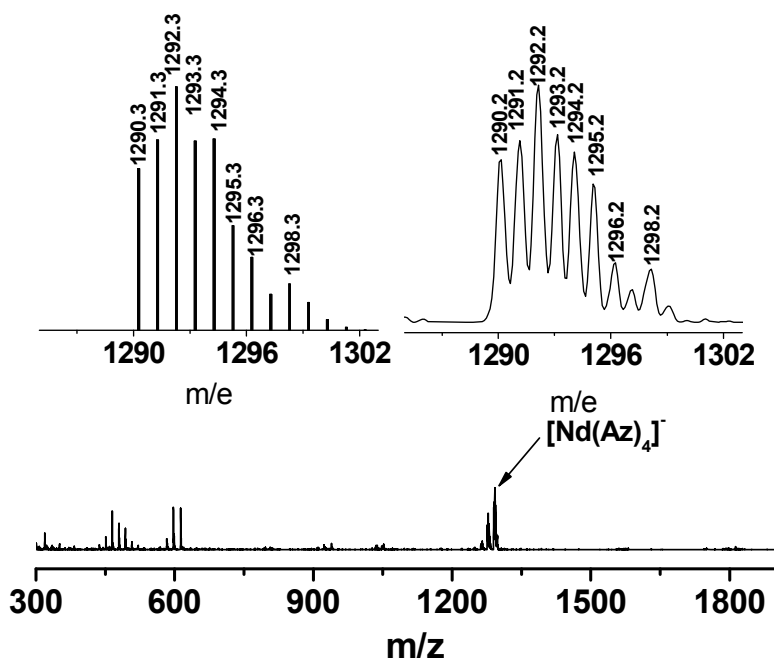
Figure 5.5: ES-MS spectrum in negative mode (10^{-4} M in CH_3CN/CH_2Cl_2) (bottom); prediction of the isotopic distribution of the ML_4 peak (top left); the zoomed region of the experimental ML_4 peak (top right)

173

5.2.2 Spectrophotometric titration

It has been shown by elemental analysis that the composition of the complexes corresponds to ML_4 when isolated in the solid state. To investigate the number and nature of the species formed between the ligand Az^- and Ln^{3+} in solution, UV-vis spectrophotometric titrations were performed with Nd^{3+}, Er^{3+}, Tm^{3+}, and Yb^{3+}. Spectra were collected varying the metal to ligand ratio in both CH_3CN and methanol solvents at constant ionic strength. UV-vis spectra recorded during the spectrophotometric titration of a solution of the deprotonated ligand Az^- by Tm^{3+} in CH_3CN are depicted as example in Figure 5.6. For all the four cations, a smooth evolution of the absorption spectra for Ln/Az^- in the range 0.1–1.0 with a single sharp endpoint for $Ln/Az^- = 4.0$ has been observed by monitoring the absorbance at 480 nm (Figure 5.6).

The software SPECFIT[26] was used to analyze the experimental data. Factor analysis indicated the presence of five independent colored species in solution. The data obtained from the titrations with the different cations were best fitted with a model where four complexes are successfully formed in solution (ML, ML_2, ML_3 and ML_4) and satisfactory stability constants were obtained using this model. Convergence of the fitting process to calculate $\log K_4$ values was only possible if the values of $\log K_1$, $\log K_2$, and $\log K_3$ were fixed to values of 9, 8, and 7 respectively for the titrations performed in both MeOH and CH_3CN solvents. This could be explained by the high stability of the ML_1, ML_2, and ML_3 species formed in solution. A complementary explanation could be the strong correlation of the UV-vis spectra of the individual species as indicated by the spectra of the individual ML_1, ML_2, ML_3, and ML_4 species calculated with the help of the Specfit software (Figure 5.7).

174
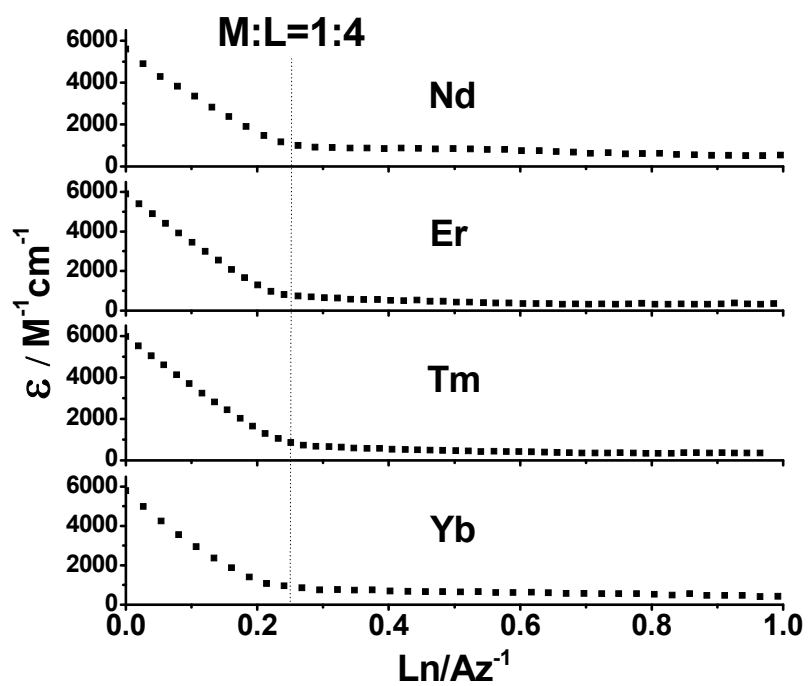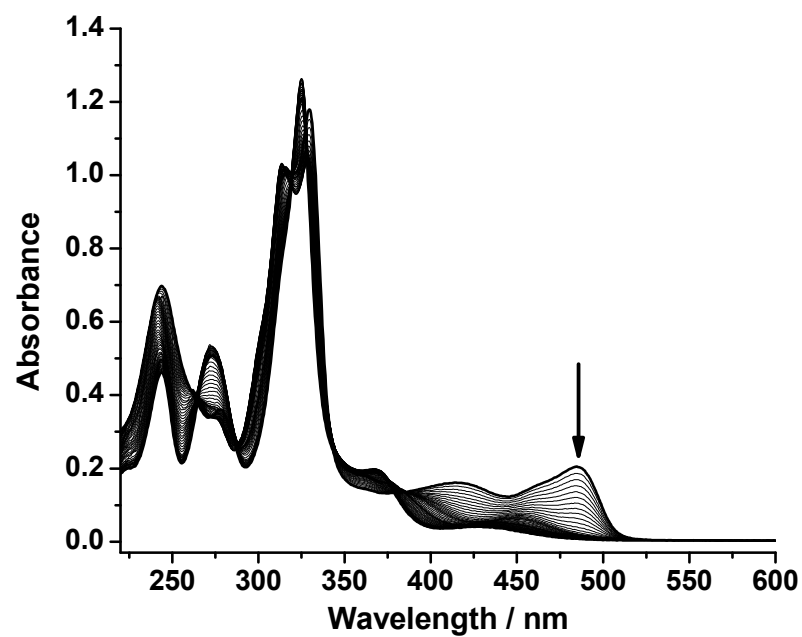
Figure 5.6: UV-vis spectra collected during the spectrophotometric titration of ligand Az⁻ in CH₃CN solution with

Tm³⁺ (top); variations of observed molar extinctions at 484 nm obtained with four Ln³⁺ (bottom)

LogK_4 stability constant values of 4.5 ± 0.3, 4.7 ± 0.3, 4.5 ± 0.3 and 4.1 ± 0.3 were obtained after fitting for Nd^{3+}, Er^{3+}, Tm^{3+}, and Yb^{3+} complex respectively in CH_3OH; 5.5 ± 0.3, 5.4 ± 0.3, 4.9 ± 0.3, and 4.9 ± 0.3 were obtained from measurements in CH_3CN. The overall higher values of logK_4 obtained in CH_3CN can be explained by this solvent being less coordinating than MeOH which posses an oxygen hard Lewis donor, resulting in lower competition between the ligand and this solvent. In addition, the titration spectra show a smooth evolution of the absorption spectra at 484 nm for Ln/Az^- in the range 0.1–1.0 with a single sharp end point for $Ln/Az^- = 1:4$ (Figure 5.6). This series of results lead to the conclusion that four different lanthanide complexes ML_1, ML_2, ML_3, and ML_4 are successfully formed in MeOH solution. The values of logK_4 for the ML_4 complexes are all comprised within the experimental error. A molecular modeling calculation (Figure 5.8) using *MM3* parameters (CAChe)[29] also indicates that it is possible for four ligands to coordinate a central lanthanide cation. The qualitative analysis of the modeled structure indicates that these four ligands provide a good protection for Ln^{3+} from non-radiative deactivations from the environment.

5.2.3 Photophysical properties of the ligand HAz

The UV-vis absorption spectrum of the free ligand HAz in CH_3CN is reported in Figure 5.9. This spectrum indicates the presence of several electronic transitions with apparent maxima at 237 nm, 261 nm and 311 nm with a shoulder located at 300 nm. There are two additional broader bands located at lower energy with an apparent maxima at 355 nm and 430 nm, which can be assigned to $S_0 \rightarrow S_2$ and $S_0 \rightarrow S_1$ transitions respectively (see below for the attribution of these bands).
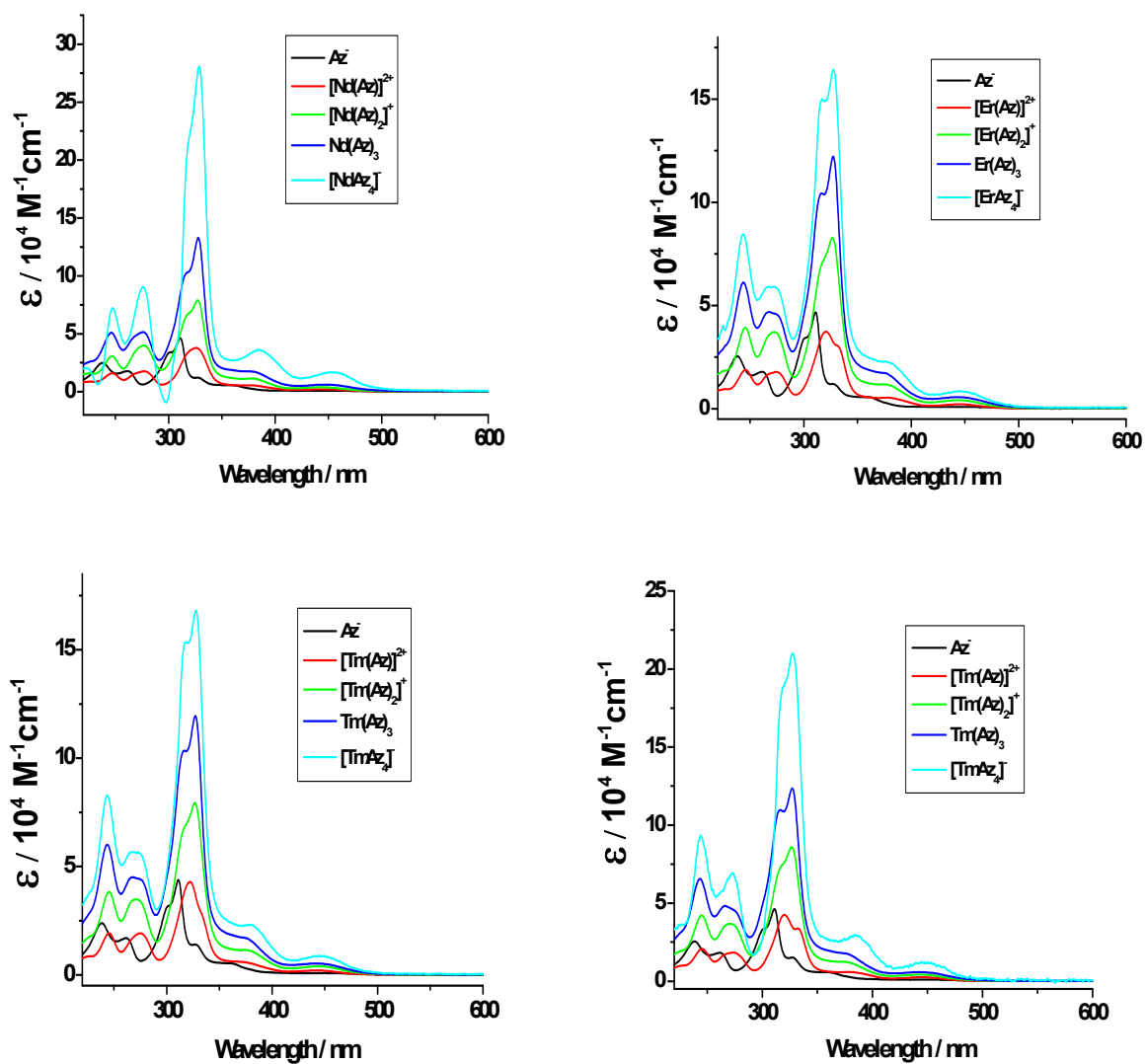
Figure 5.7: Calculated individual absorption spectra of ML, ML$_2$, ML$_3$, and ML$_4$ species by using Specfit program
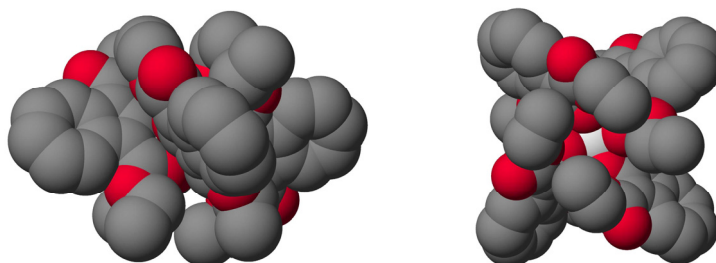
Figure 5.8: Two different views of the [Yb(Az)$_4$]$^-$ complex created with CAChe (*MM3* parameters)
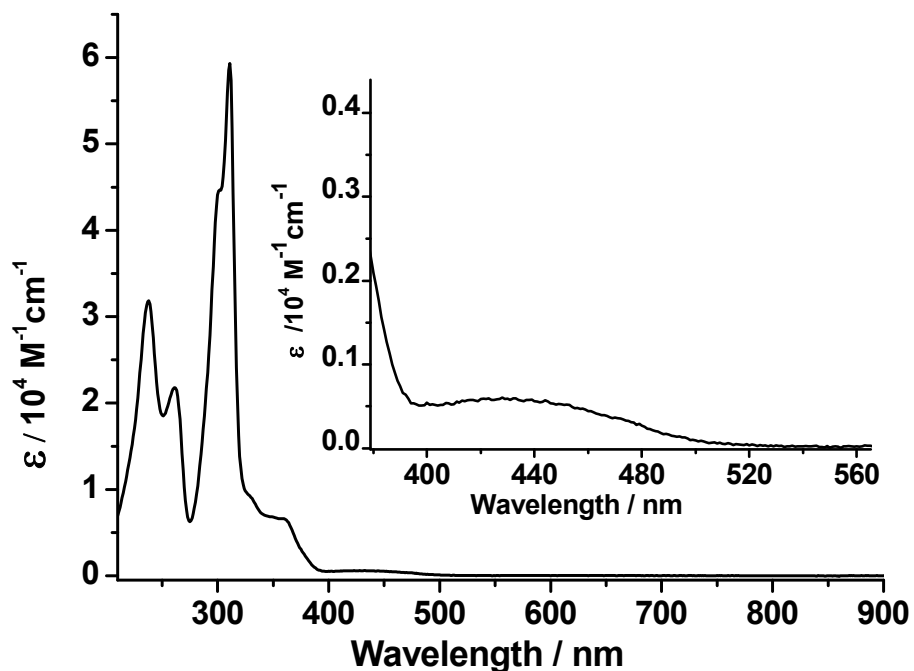
Figure 5.9: UV-vis spectrum of HAz in CH$_3$CN (2.3×10^{-5} M, 298 K) (Inset: zoomed region of the absorption band centered at 430 nm)

In contrast to the blue color of azulene, the ligand HAz is yellowish orange. It is known that the electronic structure and photophysical properties of derivatives of azulene are affected by their substituents.[30] This perturbation of the molecular orbitals of the azulene moiety can be rationalized by a qualitative pictorial description of the low lying molecular orbitals (Figure 5.10).[31] The HOMO, LUMO, and LUMO+1 orbitals of azulene, which correspond to S$_0$, S$_1$, and S$_2$ levels respectively, are depicted in Figure 5.10[31].
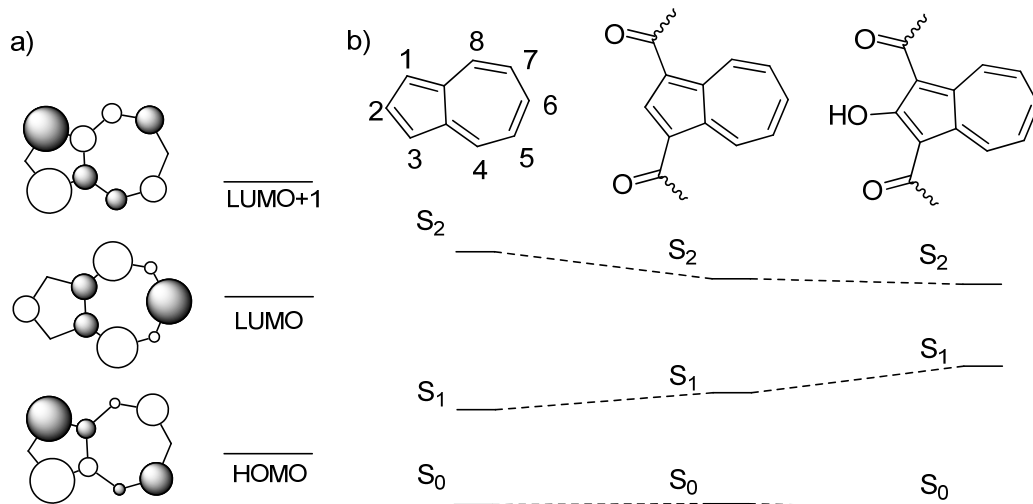
Figure 5.10: (a) Probability of location of the electron in the HOMO, LUMO and LUMO+1 of azulene; (b) Schematic illustration of effects of different substituents on the energies of electronic levels of azulene

For azulene, the small overlap between HOMO and LUMO leads to a transition located at lower energy of the S_1 state. The large electron-electron correlation energy for the LUMO+1 and HOMO considerably raises the energy of the second singlet excited state (S_2 level of azulene). As a result, the S_2 (raised in electronic energy level) and S_1 (lowered in electronic energy levels) couple together to create a unusually large gap resulting the so called "blue window" (360-450 nm) of azulene,[31] which provides to this compound blue color.

There are three substituents on ligand HAz, two C=O groups and one OH group. The C=O group is a conjugative, electron withdrawing substituent and it generates two opposing effects on the electron densities at C-1 and C-3 of the azulene moiety HOMO to stabilize or destabilize the molecular orbitals. It has been found that the aldehyde group causes a blue shift of the S_1 state because of its inductive electron withdrawing effect, but causes red shift of the S_2 state due to the conjugation effect.[30] On the other hand, the hydroxyl group at C-2, which is a resonance donating group, will destabilize the LUMO orbital of azulene. This will lead to an increased S_0-

S_1 gap and to a corresponding blue shift, which explains why the energy position of the maximum of the $S_0 \rightarrow S_1$ transition of 1,3-dicarboxaldehyde azulene is at approximately 500 nm (20,000 cm^{-1}), while it is around 428 nm for HAz. The red-shift of the band corresponding to S_2 results in the diminished transmission of blue light (near 400 nm), and a simultaneous increase in transmittance of red/yellow light, therefore, the ligand is orange.

5.2.4   Coordinated ligand-centered luminescence in KGd(Az)$_4$

The UV-vis absorption spectra of the different lanthanide complexes studied in this work were measured in CH$_3$CN at room temperature (Figure 5.11). They are similar to each other since the energy location of these bands all reflect the electronic structure of the ligand bound to a central Ln^{3+}. The spectrum of the Gd^{3+} complex is shown in Figure 5.12. Compared with the free ligand, the $\pi \rightarrow \pi^*$ transition band in the UV-vis spectrum red-shifts from 428 nm (in the free ligand) to 452 nm in the complex with an increased molar absorptivity. This can be attributed to the perturbation of the electronic structure of the ligand upon metal cation coordination, making this transition more allowed compared to the free ligand.
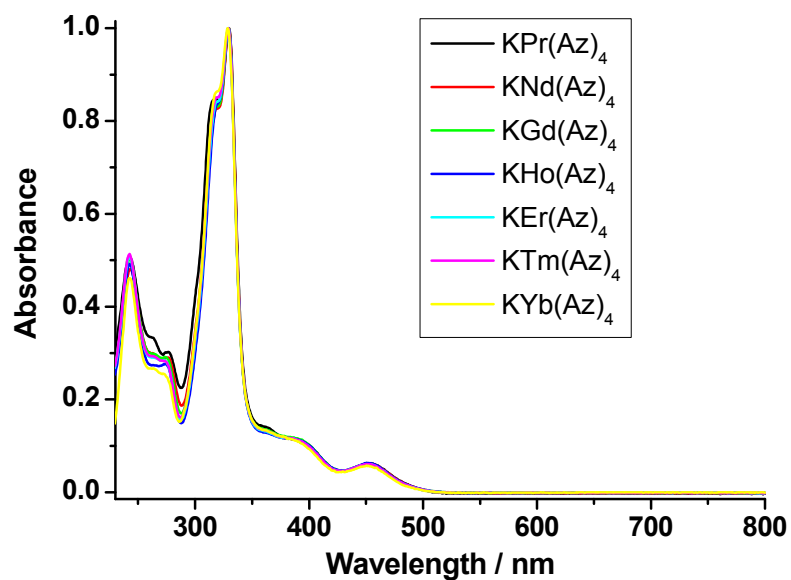
Figure 5.11: Absorption spectra of complexes with different Ln^{3+} in CH_3CN (298 K, 10^{-5} M)
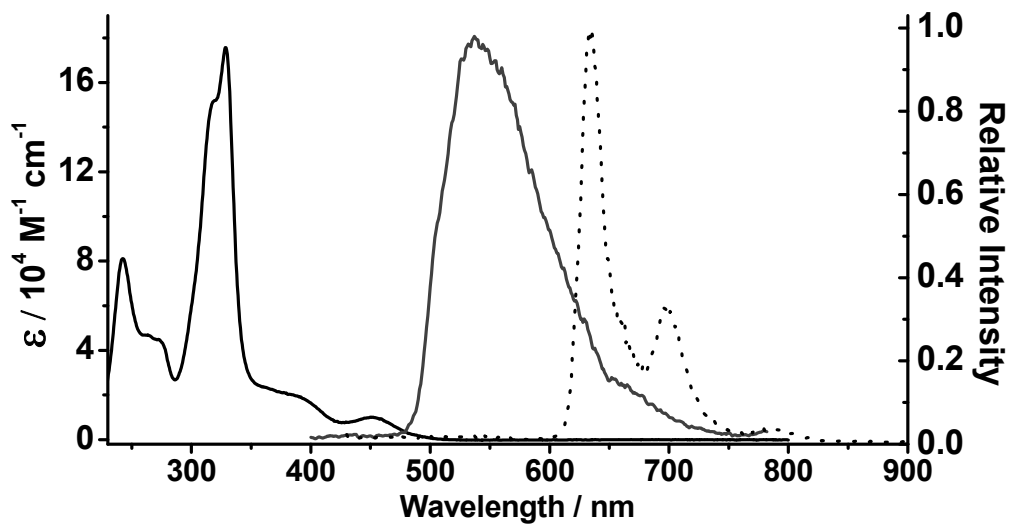
Figure 5.12: UV-vis absorption (black) (298 K), normalized fluorescence (dark grey) (1.2×10^{-5} M, λ_{ex} = 400 nm, 298 K) and phosphorescence (dot) (λ_{ex} = 400 nm, 77 K, delay time 0.1 ms, gate time 20 ms) spectra of KGd(Az)$_4$ in CH_3CN

181

The fluorescence of the free ligand HAz is faint. No phosphorescence of the free ligand was detectable at 77 K. However, it has been possible to record the steady-state fluorescence and time-resolved phosphorescence bands arising from the ligand in KGd(Az)$_4$ complex (Figure 5.12). There is no ligand to Ln^{3+} energy transfer in this complex because the electronic levels of Gd^{3+} are too high in energy to accept energy from the singlet and/or triplet states of the ligand. The location of these bands in both spectra is helpful to identify the energy of the singlet and triplet states of the ligands bound to Ln^{3+}. The fluorescence spectrum obtained upon excitation of the ligand at room temperature resulted in the presence of a broad ligand-centered band that is assigned to the S$_1$→S$_0$ transition with an apparent maximum of the electronic envelope at 18,700 cm^{-1} (536 nm). In time-resolved mode, when a delay (0.1 ms) is applied after the excitation flash to record the phosphorescence spectrum, the fluorescence band disappears and is replaced by a phosphorescence signal containing three bands with apparent maxima located at 15,700 cm^{-1} (635 nm), 14,310 cm^{-1} (699 nm) and 12,700 cm^{-1} (788 nm). A similar pattern is also observed for the KGd(Trop)$_4$ complex (Table 5.1 and Figure 5.13), which can be attributed to the partial similarity between the electronic structures of these two molecules. This set of bands is attributed to the phosphorescence arising from the triplet state of the bound ligand. In comparison to the energy of the triplet state reported for azulene 13,600 cm^{-1} (733 nm), the triplet state of the ligand is significantly blue-shifted if we consider the maxima of the bands located at 15,700 and 14,300 cm^{-1}. This is due to the presence of the two substituents, which are required for the coordination to Ln^{3+}. Nevertheless, the triplet state of this ligand is still located at relatively low energy compared with the tropolonate ligand and most other ligands used for sensitization of NIR emitting Ln^{3+}.

Table 5.1: Comparison of singlet and triplet state energies (cm^{-1}) for the Trop$^-$ and Az$^-$

	KGd(Az)$_4$			KGd(Trop)$_4$		
Singlet[a]		18,600			23.500	
Triplet[b]	15,700	14,300	12,700	17,200	15,600	14,300

a. Steady state fluorescence spectra recorded at 298 K.(10^{-5} M in CH$_3$CN and DMSO for KGd(Az)$_4$ and KGd(Trop)$_4$ respectively).
b. Time-resolved phosphorescence spectra recorded on solid sample at 77 K
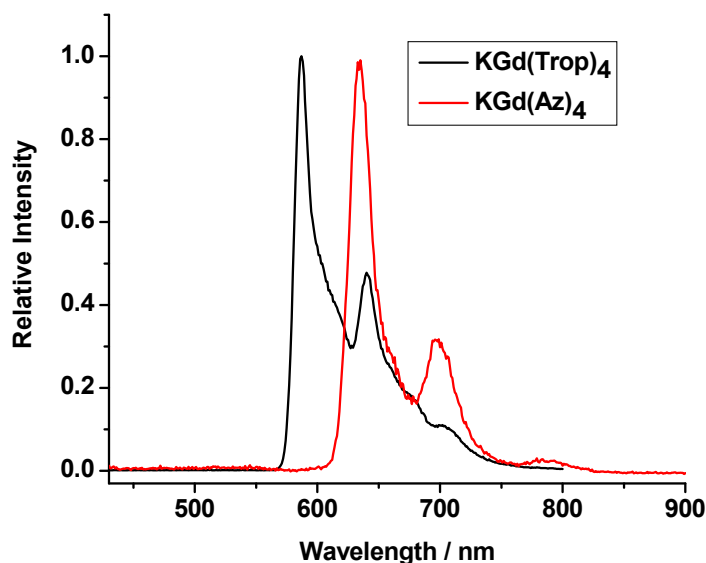
Figure 5.13: Phosphorescence spectra of KGd(Trop)$_4$ (10^{-5} M in DMSO) and KGd(Az)$_4$ (10^{-5} M in CH$_3$CN) at 77 K

5.2.5   Sensitization of lanthanide-centered near-infrared emission

Remarkably, the Az$^-$ ligands can sensitize four different NIR emitting Ln^{3+} (Ln = Yb, Nd, Er, and Tm) in KLn(Az)$_4$ complexes in CH$_3$CN at room temperature. The luminescence spectra of these four different lanthanide complexes are depicted in Figure 5.14. Through excitation of the absorption bands of the coordinated ligand, the solution of Yb^{3+} complex displays a NIR emission band ranging from 976 to 1028 nm, which is assigned to the $^2F_{5/2} \rightarrow {}^2F_{7/2}$ transition. For the Nd^{3+}

complex, emission bands were observed at 895, 1051, and 1323 nm and are attributed to the transitions from the $^4F_{3/2}$ level to the $^4I_{9/2}$, $^4I_{11/2}$, and $^4I_{13/2}$ sublevels respectively. For Er^{3+} complex, the emission band observed at 1524 nm can be assigned to the transition from the $^4I_{13/2}$ level to $^4I_{15/2}$ level. Tm^{3+} emission is not frequently observed for lanthanide complexes in solution. In CH_3CN solution, two transitions were observed at 803 and 1487 nm. They are assigned to $^3F_4 \rightarrow ^3H_6$ and $^3F_4 \rightarrow ^3H_4$ transitions respectively. The emission wavelengths of the Nd^{3+}, Yb^{3+} and Tm^{3+} complexes are in a spectral range well suited for bioanalytical assays (minimization of the absorption by the biological system).[24] As shown in Figure 5.14, there is only slight overlap between these emission spectra, allowing the potential for multiplex measurements. Attempts to generate Ho^{3+} and Pr^{3+} luminescence upon ligand L excitation were unsuccessful.
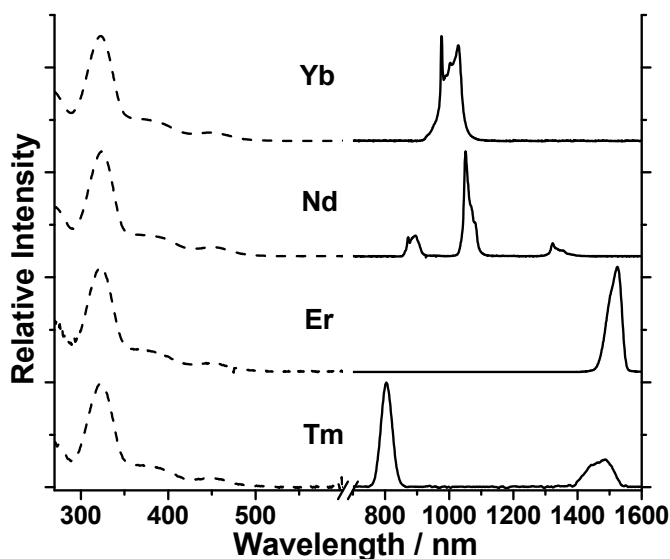
Figure 5.14: Normalized excitation (dash) and emission spectra (plain) of four lanthanide complexes (10^{-5} M in CH_3CN, $\lambda_{ex} = 380$ nm)

To quantify the efficiency of intramolecular ligand to metal ion energy transfer in the different lanthanide complexes, luminescence quantum yields were measured in CH_3CN and CD_3CN upon ligand excitation using $KYb(Trop)_4$ as reference.[9] Three different excitation wavelengths corresponding to three maxima of the absorption spectra at 320, 380, and 447 nm were used systematically. The results are reported in Table 5.2. The quantum yield values recorded with different excitation wavelengths are all within the experimental error (5–17%). Therefore, it is suggested that a unique path of energy is used for the sensitization of all the Ln^{3+} studied by the chromophoric ligand. This assumption is supported by the fact that all the excitation spectra are similar to each other (Figure 5.14) and are well matched to the corresponding absorption spectra (Figure 5.11). Notably this observation was possible for all four NIR emitting Ln^{3+} sensitized by Az^- despite the fact that they have different energies of accepting levels. It can be concluded that the excitation has the same efficiency for all three absorbance bands in these four complexes as the quantum yield values do not depend on the excitation wavelengths.

The quantum yield of the Yb^{3+} complex is especially large with values of 3.8% in CH_3CN and 4.2% in CD_3CN, compared with the value reported for other Yb^{3+} complexes in solution, such as 3.2% and 2.4% reported for a monoporphyrinate complex in CH_2Cl_2,[8] 1.9% for our tropolonate complex in DMSO,[9] 0.5% for a terphenyl-based complex in DMSO,[32] 1.8% for a bimetallic helicate in D_2O,[33] or 0.45% for fluorexon complex in D_2O.[34] Although smaller, the quantum yield of the Nd^{3+} complex (0.45% in CH_3CN and 0.53% in CD_3CN) is also high compared with other Nd^{3+} complexes with 0.2% for monoporphyrinate complexes in CH_2Cl_2,[8] 0.21% for tropolonate Nd^{3+} complex in DMSO,[9] 0.038% for the Nd-fluorexon complex in D_2O,[34] 0.075% for 8-hydroxyquinolinate-based Nd^{3+} complex in D_2O.[35]

Table 5.2: Absolute quantum yields of KLn(Az)$_4$ at 298 K in CH$_3$CN and CD$_3$CN at different excitation wavelength

Ln	Wavelength	CH$_3$CN	CD$_3$CN
Yb	322 nm[a]	2.7(2)×10^{-2}	3.1(2)×10^{-2}
	375 nm[b]	3.8(2)×10^{-2}	4.2(2)×10^{-2}
	447 nm[c]	3.2(2)×10^{-2}	3.6(2)×10^{-2}
Nd	322 nm[a]	4.0(2)×10^{-3}	4.7(4)×10^{-3}
	383 nm[b]	4.5(3)×10^{-3}	5.3(3)×10^{-3}
	449 nm[c]	3.7(2)×10^{-3}	4.9(2)×10^{-3}
Er	322 nm[a]	2.0(1)×10^{-4}	2.2(1)×10^{-4}
	387 nm[b]	2.1(1)×10^{-4}	2.4(1)×10^{-4}
	447 nm[c]	1.8(1)×10^{-4}	2.2(1)×10^{-4}
Tm	320 nm[a]	4.3(2)×10^{-5}	5.1(1)×10^{-5}
	380 nm[b]	5.9(2)×10^{-5}	6.6(1)×10^{-5}
	446 nm[c]	4.9(2)×10^{-5}	6.5(2)×10^{-5}

a. 1.7×10^{-5} M
b. 1.0×10^{-4} M
c. 2.0×10^{-4} M

The luminescent lifetimes have been recorded in order to evaluate the coordination environment around Ln^{3+} in these complexes in solution and to quantify the degree of protection against non-radiative deactivation provided by the four Az$^-$ ligands around Ln^{3+}. The luminescence decays of the Yb^{3+} and Nd^{3+} complexes in different solvents were measured and fit as monoexponential decays in all the studied solvents (Table 5.3). This indicates that a unique and consistent coordination environment is present around Ln^{3+} in the complex.

Table 5.3: Luminescence lifetimes (µs) of [Nd(Az)$_4$]$^-$ and [Yb(Az)$_4$]$^-$ in different solvents (298 K, 2×10^{-5} M)

	MeOH	CD$_3$OD	CH$_3$CN	CD$_3$CN
[Yb(Az)$_4$]$^-$	12.01 ± 0.07	33.71 ± 0.03	24.61 ± 0.01	32.81 ± 0.12
[Nd(Az)$_4$]$^-$	0.37 ± 0.01	1.33 ± 0.01	1.85 ± 0.01	2.68 ± 0.01

The comparison between the luminescence lifetimes in deuterated and non-deuterated solvents can be used to quantify the number of solvent molecules coordinated to Ln^{3+} in solution. The calculation of the hydration/solvation number is obtained by using an empirical Equation (1). This formula was first developed by Horrocks et al.[36,37] In this formula, q is the number of water molecules bound to Ln^{3+} in the first sphere of coordination; k_H and k_D are the rate constants of excited states of Ln^{3+} in H_2O and D_2O, respectively. A is a proportionality constant related to the sensitivity of Ln^{3+} to vibrational quenching by OH oscillators, B is the correction factor for outer sphere water molecules.

$$q = A(k_H - k_D) - B \qquad (1)$$

More recently, Davies et al.[38] and Beeby et al.[39] modified this formula for the determination of q for Yb^{3+} and Nd^{3+} complexes in MeOH solution, in which $A = 0.29$ is (Nd^{3+}) or 2 is (Yb^{3+}), $B = 0.4$ (Nd^{3+}) or 0.1 (Yb^{3+}), $k_H = 1/\tau_H$ and $k_D = 1/\tau_D$ are given in μs^{-1}.

Applying these formulas, q values of 0.05 and 0.16 were calculated for the Yb^{3+} and Nd^{3+} complexes, respectively. These near-zero values indicate that there are no water/solvent molecules bound to Ln^{3+} in the first coordination sphere for $[Ln(Az)_4]^-$ in solution. This is consistent for both the larger Nd^{3+} (Shannon's effective ionic radius: $1.109 Å^{[40]}$) and smaller Yb^{3+} (Shannon's effective ionic radius: $0.985 Å^{[40]}$). Therefore, we can conclude that the four bidentate ligands efficiently protect Ln^{3+} cations against nonradiative deactivations induced by solvent molecules. The azulene complexes provide superior protection compared with the ML_4 tropolonate complexes,[9] where one solvent molecule is bound to Ln^{3+}. It also confirms the results of elemental analysis that four Az^- ligands are bound to Ln^{3+} in $[Ln(Az)_4]^-$, providing Ln^{3+} a coordination number of 8. The luminescence lifetime obtained for the Yb^{3+} complex in acetonitrile solution (24.61 μs) is fairly long compared to the value obtained in MeOH (12.01 μs) and the typical average value

around 10 μs is reported for most Yb^{3+} complexes described in the literature.[4,35,41] This luminescence lifetime is similar to Yb^{3+} in CD_3OD and CD_3CN, an indication that the non-radiative quenching is similar for the Yb^{3+} complex in both solvents. On the other hand, the luminescence lifetimes of the Nd^{3+} complex in these two solvents are very different, 1.33 and 2.68 μs in CD_3OD and CD_3CN respectively. This indicates that Nd^{3+} is more sensitive to high energy oscillations than Yb^{3+}. The main difference between these two solvents is the O-D group in CD_3OD, which has vibrational energy around 2,500 cm^{-1}, vs. the CN group in CD_3CN, which has a vibrational energy of 2,250 cm^{-1}. Nd^{3+} has more electronic states at high energy than Yb^{3+}, which increases the probability of quenching.

5.3   CONCLUSION

In summary, lanthanide complexes $[Ln(Az)_4]^-$ formed by reaction of one lanthanide cation with four azulene-based ligands, HAz, have been isolated and characterized in solid state and in solution. Their photophysical properties have been analyzed, with a specific interest for the sensitization of near-infrared Ln^{3+}. It was hypothesized that, due to its triplet state located at lower energy compared to the tropolonate ligand previously studied in our group, the HAz ligand would be more efficient in sensitizing several Ln^{3+}.

Spectrophotometric titrations indicated that four Az^- react successively with one lanthanide cation to form a ML_4 type of complex in solution. The investigation of the photophysical properties of $[Ln(Az)_4]^-$ shows that Az^- sensitize efficiently four different NIR emitting Ln^{3+} (Nd^{3+}, Er^{3+}, Yb^{3+}, and Tm^{3+}). The analysis of luminescence lifetimes of Ln^{3+} recorded in deuterated and non-deuterated solvents indicated that no solvent molecules are bound to the Ln^{3+} in

the $[Ln(Az)_4]^-$ complexes formed with Ln = Nd and Yb. This efficient protection of Ln^{3+} against non-radiative deactivations results from the coordination the four ligands Az to the central Ln^{3+}. As a result, the luminescence lifetimes of the Nd^{3+} and Yb^{3+} complexes are significantly longer in comparison to the values reported in the literature for most near-infrared emitting lanthanide complexes in solution. The quantum yields of the Nd^{3+} and Yb^{3+} complexes are among the highest values reported for NIR emitting lanthanide complexes in solution, which we attribute to a combination of efficient ligand to Ln^{3+} energy transfer and good protection of Ln^{3+}. The fact that the azulene based ligand can sensitize not only Yb^{3+}, Nd^{3+}, and Er^{3+}, but also Tm^{3+} indicates that it is a promising sensitizer for NIR lanthanide cations, potentially suitable for biological imaging. A sensitizer that provides the advantage of a unique excitation wavelength (unique instrumental source) to obtain four different emission wavelengths is an important advantage for multiplex assays. To provide applicability to this system, the ligand design will be modified to obtain solubility in water and to increase the stability of the complex in solution by increasing denticity of this ligand.

5.4 REFERENCES

(1)   Werts, M. H. V.; Woudenberg, R. H.; Emmerink, P. G.; van Gassel, R.; Hofstraat, J. W.; Verhoeven, J. W. *Angew. Chem., Int. Ed.* **2000**, *39*, 4542.

(2)   Klink, S. I.; Alink, P. O.; Grave, L.; Peters, F. G. A.; Hofstraat, J. W.; Geurts, F.; van Veggel, F. C. J. M. *J. Chem. Soc., Perkin Trans. 2* **2001**, 363.

(3)   Werts, M. H. V.; Hofstraat, J. W.; Geurts, F. A. J.; Verhoeven, J. W. *Chem. Phys. Lett.* **1997**, *276*, 196.

(4)   Klink, S. I.; Keizer, H.; van Veggel, F. C. J. M. *Angew. Chem., Int. Ed.* **2000**, *39*, 4319.

(5)   Herrera, J.-M.; Pope, S. J. A.; Adams, H.; Faulkner, S.; Ward, M. D. *Inorg. Chem.* **2006**, *45*, 3895.

(6)   Herrera, J.-M.; Pope, S. J. A.; Meijer, A. J. H. M.; Easun, T. L.; Adams, H.; Alsindi, W. Z.; Sun, X.-Z.; George, M. W.; Faulkner, S.; Ward, M. D. *J. Am. Chem. Soc.* **2007**, *129*, 11491.

(7)   He, H.; Guo, J.; Zhao, Z.; Wong, W.-K.; Wong, W.-Y.; Lo, W.-K.; Li, K.-F.; Luo, L.; Cheah, K.-W. *Eur. J. Inorg. Chem.* **2004**, 837.

(8)   Foley, T. J.; Harrison, B. S.; Knefely, A. S.; Abboud, K. A.; Reynolds, J. R.; Schanze, K. S.; Boncella, J. M. *Inorg. Chem.* **2003**, *42*, 5023.

(9)   Zhang, J.; Badger, P. D.; Geib, S. J.; Petoud, S. *Angew. Chem., Int. Ed.* **2005**, *44*, 2508.

(10)   Zhang, J.; Badger, P. D.; Geib, S. J.; Petoud, S. *Inorg. Chem.* **2007**, 6473.

(11)   Frey, J. E.; Andrews, A. M.; Combs, S. D.; Edens, S. P.; Puckett, J. J.; Seagle, R. E.; Torreano, L. A. *J. Org. Chem.* **1992**, *57*, 6460.

(12)   Schmitt, S.; Baumgarten, M.; Simon, J.; Hafner, K. *Angew. Chem., Int. Ed.* **1998**, *37*, 1078.

(13)   Wang, F.; Lai, Y.-H.; Han, M.-Y. *Macromolecules* **2004**, *37*, 3222.

(14)   Porsch, M.; Sigl-Seifert, G.; Daub, J. *Adv. Mater.* **1997**, *9*, 635.

(15)   Ito, S.; Inabe, H.; Morita, N.; Ohta, K.; Kitamura, T.; Imafuku, K. *J. Am. Chem. Soc.* **2003**, *125*, 1669.

(16)   Estdale, S. E.; Brettle, R.; Dummur, D. A.; Marson, C. M. *J. Mater. Chem.* **1997**, *7*, 391.

(17)   Zielinski, T.; Kedziorek, M.; Jurczak, J. *Tetrahedron Lett.* **2005**, *46*, 6231.

(18)   Salman, H.; Abraham, Y.; Tal, S.; Meltzman, S.; Kapon, M.; Tessler, N.; Speiser, S.; Eichen, Y. *Eur. J. Org. Chem.* **2005**, 2207.

(19)   Mrozek, T.; Gorner, H.; Daub, J. *Chem.-Eur. J.* **2001**, *7*, 1028.

(20)   Lacroix, P. G.; Malfant, I.; Iftime, G.; Razus, A. C.; Nakatani, K.; Delaire, J. A. *Chem.-Eur. J.* **2000**, *6*, 2599.

(21)   Cristian, L.; Sasaki, I.; Lacroix, P. G.; Donnadieu, B.; Asselberghs, I.; Clays, K.; Razus, A. C. *Chem. Mater.* **2004**, *16*, 3543.

(22)   Lambert, C.; Noell, G.; Zabel, M.; Hampel, F.; Schmaelzlin, E.; Braeuchle, C.; Meerholz, K. *Chem.-Eur. J.* **2003**, *9*, 4232.

(23)   Herkstroeter, W. G. *J. Am. Chem. Soc.* **1975**, *97*, 4161.

(24)   Weissleder, R.; Ntziachristos, V. *Nat. Med.* **2003**, *9*, 123.

(25)   Stolik, S.; Delgado, J. A.; Perez, A.; Anasagasti, L. *J. Photochem. Photobiol., B* **2000**, *57*, 90.

(26)   Gampp, H.; Maeder, M.; Meyer, C. J.; Zuberbuehler, A. D. *Talanta* **1985**, *32*, 1133.

(27)   Brettle, R.; Dunmur, D. A.; Estdale, S.; Marson, C. M. *J. Mater. Chem.* **1993**, *3*, 327.

(28)   Doering, W. v. E.; Knox, L. H. *J. Am. Chem. Soc.* **1952**, *74*, 5683.

(29)   CAChe WorkSystem Pro., 6.1.12.33., Fujitsu Limited Inc., USA, 2004

(30)   Eber, G.; Grueneis, F.; Schneider, S.; Doerr, F. *Chem. Phys. Lett.* **1974**, *29*, 397.

(31)   Liu, R. S. H.; Asato, A. E. *J. Photochem. Photobiol., C* **2003**, *4*, 179.

(32)   Klink, S. I.; Hebbink, G. A.; Grave, L.; van Veggel, F. C. J. M.; Reinhoudt, D. N.; Slooff, L. H.; Polman, A.; Hofstraat, J. W. *J. Appl. Phys.* **1999**, *86*, 1181.

(33)   Goncalves e Silva, F. R.; Malta, O. L.; Reinhard, C.; Güdel, H.-U.; Piguet, C.; Moser, J. E.; Bünzli, J.-C. G. *J. Phys. Chem. A* **2002**, *106*, 1670.

(34)   Werts, M. H. V.; Verhoeven, J. W.; Hofstraat, J. W. *J. Chem. Soc., Perkin Trans. 2* **2000**, 433.

(35)   Comby, S.; Imbert, D.; Vandevyver, C.; Bünzli, J.-C. G. *Chem.-Eur. J.* **2007**, *13*, 936.

(36)   Horrocks, W. D., Jr.; Sudnick, D. R. *J. Am. Chem. Soc.* **1979**, *101*, 334.

(37)   Horrocks, W. D., Jr.; Sudnick, D. R. *Acc. Chem. Res.* **1981**, *14*, 384.

(38)   Davies, G. M.; Aarons, R. J.; Motson, G. R.; Jeffery, J. C.; Adams, H.; Faulkner, S.;

Ward, M. D. *J. Chem. Soc., Dalton Trans.* **2004**, 1136.

(39)   Beeby, A.; Burton-Pye, B. P.; Faulkner, S.; Motson, G. R.; Jeffery, J. C.; McCleverty, J.

A.; Ward, M. D. *J. Chem. Soc., Dalton Trans.* **2002**, 1923.

(40)   Shannon, R. D. *Acta Crystallogr., Sect. A* **1976**, *A32*, 751.

(41)   Shavaleev, N. M.; Moorcraft, L. P.; Pope, S. J. A.; Bell, Z. R.; Faulkner, S.; Ward, M. D.

Chem.-Eur. J. **2003**, *9*, 5283

6.0   A STRATEGY TO PROTECT AND SENSITIZE NEAR-INFRARED LUMINESCENT ND^{3+} AND YB^{3+}: ORGANIC TROPOLONATE LIGANDS FOR THE SENSITIZATION OF LN^{3+} DOPED NAYF$_4$ NANOCRYSTALS

Part of this chapter has been published as Zhang, J.; Shade, C. M.; Chengelis, D. A.; Petoud, S. *J. Am. Chem. Soc.* **2007**, 129, 14834.

The strategy of using organic chromophores as sensitizer for NIR emitting lanthanide cations have been studied for a decade. The quantum yields and luminescent lifetimes have been increased by the appropriate choice ligands based on specific criteria. As an example, we have shown in the previous chapters that the ligand-to-Ln^{3+} energy transfer efficiencies of the NIR emitting lanthanide complexes can be tuned by incorporating different substituents on the aromatic sensitizers.

However, the overall efficiency of sensitization has its intrinsic limitations because lanthanide luminescence is easily quenched through nonradiative routes when the cations are in close proximity to the vibrational overtones of -OH, -NH, and -CH groups present in the sensitizing ligand and/or solvent.[1] This effect is particularly dramatic for NIR emitting Ln^{3+} because of relatively small energy gaps between ground and excited electronic states.[1]

To alleviate this limitation, Ln^{3+} have been incorporated into inorganic matrices, such as LnF$_3$,[2] Ln$_2$O$_3$,[3] LnPO$_4$,[4] LnVO$_4$,[5] TiO$_2$,[6] and Zeolites.[7] These materials protect Ln^{3+} from sources

of nonradiative deactivation; however, they have either limited (e.g., LnVO$_4$) or no absorbance in the UV range. Thus, these inorganic materials are not able to sensitize lanthanide luminescence with the efficiency of organic sensitizers.

In this chapter, we introduce a new strategy to overcome the limited sensitization of Ln^{3+} by binding organic tropolonate chromophoric groups to the surface of NaYF$_4$ nanocrystals (NCs) doped with NIR emitting Nd^{3+} or Yb^{3+} (Figure 6.1). Tropolonate (Trop$^-$) was chosen as a capping ligand since it has been previously demonstrated to be a suitable sensitizer for several Ln^{3+} emitting in the NIR range when coordinated in KLn(Trop)$_4$ complexes.[8,9] These novel systems use the NaYF$_4$ matrix to protect Ln^{3+} from nonradiative deactivations, while a chromophoric coating sensitizes their luminescence.
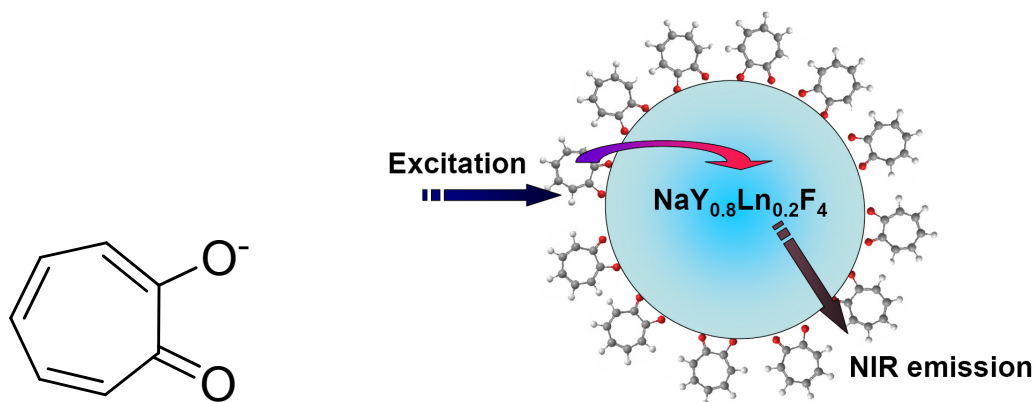
Figure 6.1: Molecular structure of Trop$^-$ and schematic illustration of Trop$^-$ capped Nd^{3+} or Yb^{3+} doped NaYF$_4$ nanocrystals and the energy transfer process

6.1 EXPERIMENTAL SECTION

6.1.1 Chemicals

Tropolone, KOH standard solution in methanol (0.100 M), Y_2O_3, Nd_2O_3, Yb_2O_3, oleic acid (90%), oleylamine (>80%), 1-octadecene (>90%), trifluoroacetic acid (99%), sodium trifluoroacetate (>97%) were purchased from Aldrich. The synthesis was carried out using standard oxygen-free procedures. All the solvents, absolute ethanol and $CHCl_3$, were used as received. $Y(CF_3COO)_3$, $Nd(CF_3COO)_3$, and $Yb(CF_3COO)_3$ were prepared according to literature method.[10]

6.1.2 Methods

UV-vis absorption spectra were recorded on a Perkin-Elmer Lambda 9 spectrophotometer. FT-IR spectra were recorded on a Perkin-Elmer Spectrum BX FT-IR instrument.

6.1.3 Luminescence measurements

Lanthanide luminescence emission and excitation spectra were measured using a Jobin Yvon Horiba Fluorolog-322 spectrofluorometer (detector for NIR domain: DSS-IGA020L, Electro-Optical Systems, Inc.). The luminescence lifetime measurements were performed by excitation of solutions in 1 cm quartz cells using a Nd:YAG Continuum Powerlite 8010 Laser (354 nm, 3rd harmonic) as the excitation source. Emission was collected at a right angle to the excitation beam and emission wavelengths were selected using a Spectral Products CM 110 1/8 meter

monochromator. The signal was monitored by a cooled photomultiplier (Hamamatsu R316-2) coupled to a 500 MHz bandpass digital oscilloscope (Tektronix TDS 754D). The signals (15,000 points each trace) from at least 500 flashes were collected and averaged. Luminescence decay curves were imported into Origin 7.0 scientific data analysis software. The decay curves were analyzed using the Advanced Fitting Tool module and fitted with mono-, bi-, and tri-exponential modes. Of the three modes, the lifetime value was chosen based on the best fit of the decay curve on the criteria of the minimum χ^2 statistical parameter. Lifetimes are averages of at least three independent determinations.

6.1.4 XRD

Powder X-ray diffraction (XRD) patterns of the dried powders were recorded on a Philips X'pert diffractometer (PW3710) with a slit of 1/2° at a scanning rate of 3° min^{-1}, using Cu K_α radiation, $\lambda = 1.5406$ Å). Samples were evaporated or pressed onto glass microscope slides.

6.1.5 TEM

A small drop of solution containing the sample in $CHCl_3$ was placed on a carbon coated copper grid. After several seconds, the drop was removed by blotting with filter paper. The sample that remained on the grid was allowed to dry before inserting the grid into the microscope. The grids were viewed on a transmission electron microscope (Hitachi H-7100 TEM, Hitachi High Technologies America, 5100 Franklin Drive, Pleasanton, CA, 94588) operating at 75 kV. Digital images were obtained using an AMT Advantage 10 CCD Camera System (Advanced Microscopy Techniques Corporation, 3 Electronics Ave., Danvers, MA, 01923) and NIH image

software. Particle diameter was measured using a negatively stained catalase crystal as a calibration standard.

6.1.6 Synthesis of Nd^{3+} or Yb^{3+} doped NaYF$_4$ nanocrystals

Nd^{3+} or Yb^{3+} doped NaYF$_4$ nanocrystals were synthesized by using the methods describe in the literature.[11,12] Sodium trifluoroacetate (0.136g, 1.0 mmol),Y(CF$_3$COO)$_3$ (0.386g, 0.8 mmol) and Nd(CF$_3$COO)$_3$ (0.107g, 0.2 mmol) or Yb(CF$_3$COO)$_3$ (0.113 g, 0.2 mmol) were then added to the reaction vessel with octadecene (5.05 g, 20 mmol), oleic acid (2.82 g, 10 mmol) and oleylamine (2.68 g, 10 mmol). The mixture was heated to 100 °C under vacuum and stirred for 30 min to remove the residual water and oxygen. The solution was then heated to 325 °C under argon and maintained at this temperature for 40 min. Subsequently, the mixture was allowed to cool to room temperature, and the resulting NCs were precipitated by addition of ethanol and isolated via centrifugation. The resulting solid was then washed twice with ethanol and dried under vacuum for 24 h.

6.1.7 Synthesis of Trop$^-$ capped Nd^{3+} or Yb^{3+} doped NaYF$_4$ nanocrystals

Tropolone was dissolved in methanol, then deprotonated with an equimolar amount of KOH in methanol. CHCl$_3$ was added to obtain a 1/1 (v/v) MeOH/CHCl$_3$ solvent mixture. This solution was added to a purified solution of NCs dispersed in CHCl$_3$. The resulting mixture was sonicated for 2 h, and the solvent was removed under vacuum. The resulting solid was washed with ethanol and DMSO and dried under vacuum for 24 h.

6.2 RESULTS AND DISCUSSION

The binding of the Trop⁻ groups to the surface of nanocrystals was monitored through FT-IR spectroscopy (Figure 6.2). Upon reaction, the absorption bands assigned to the original capping ligands of the NCs (oleic acid, oleylamine, and octadecene) present at 2,924 and 2,854 cm⁻¹ disappear and are replaced by the characteristic absorption bands of Trop⁻ at 1,595 and 1,510 cm⁻¹.

The XRD patterns (Figure 6.3) of the uncapped and capped $NaY_{0.8}Ln_{0.2}F_4$ NCs (Ln: Nd or Yb) reveal the formation of cubic α-$NaYF_4$ (space group: *Fm3m*). All diffraction peak positions and intensities agree well with calculated values.[13] Transmission electron microscopy (TEM) images (Figure 6.4) of both uncapped and capped NC samples also indicate that the obtained nanocrystals are of single-crystalline nature with high crystalline size uniformity. They are relatively monodispersed with roughly spherical shape. The average sizes are 6.1 ± 0.6 nm, 6.0 ± 0.6 nm, 5.3 ± 0.7 nm, and 5.3 ± 0.6 nm for $NaY_{0.8}Yb_{0.2}F_4$ NCs, Trop⁻ capped $NaY_{0.8}Yb_{0.2}F_4$ NCs, $NaY_{0.8}Nd_{0.2}F_4$ NCs, and Trop⁻ $NaY_{0.8}Yb_{0.2}F_4$ NCs, respectively (Figure 6.5). Such relatively small sizes are compatible for use in many bioanalytical applications.

The UV-vis absorption spectra (Figure 6.6) of Trop⁻ capped NCs in DMSO reveal the presence of two bands with apparent maxima centered around 323 and 384 nm, similar to those observed for $[Ln(Trop)_4]^-$ confirming the presence of Trop⁻ on the surface of NCs. Upon excitation at 340 nm, the characteristic sharp NIR emission bands arising from Nd^{3+} or Yb^{3+} were observed (Figure 6.6). The excitation profiles of lanthanide luminescence in both Nd^{3+} and Yb^{3+} doped NCs are similar (Figure 6.7), demonstrating that the Ln^{3+} are sensitized through the same source: the electronic structure of the Trop⁻ ligand. For Yb^{3+}, there is a significant energy

gap between the energy donating levels of Trop⁻ and its accepting levels. Energy transfer over

this large gap could be explained by phonon-assisted or electron-transfer mechanisms.[14,15]
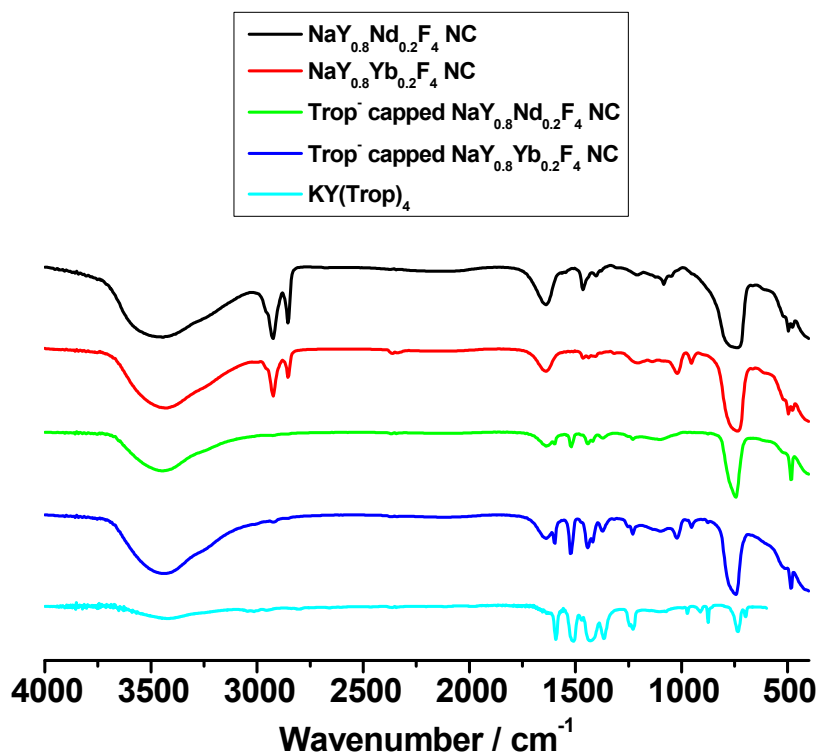
Figure 6.2: FT-IR spectra of $NaY_{0.8}Nd_{0.2}F_4$ NCs, $NaY_{0.8}Yb_{0.2}F_4$ NCs, Trop⁻ capped $NaY_{0.8}Nd_{0.2}F_4$ NCs, and Trop⁻

capped $NaY_{0.8}Yb_{0.2}F_4$ NCs. For comparison, the FT-IR spectra of $KY(Trop)_4$ is also depicted
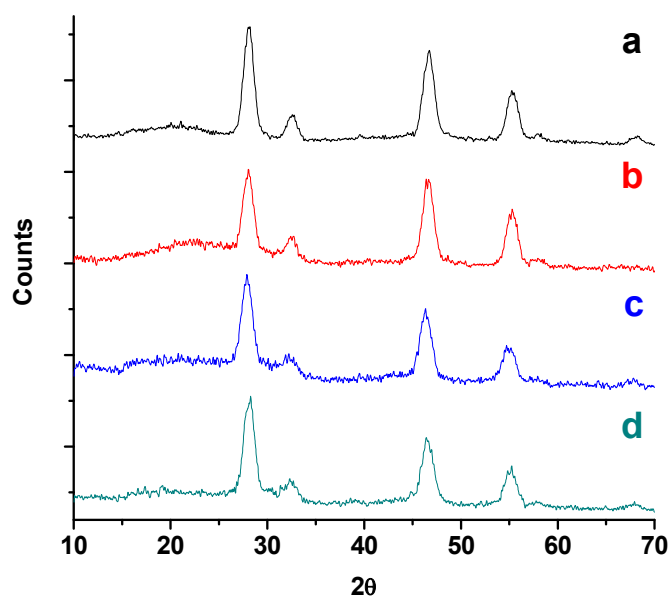
Figure 6.3: X-ray diffraction patterns of uncapped and capped NCs. a: $NaY_{0.8}Yb_{0.2}F_4$ NCs, b: Trop$^-$ capped $NaY_{0.8}Yb_{0.2}F_4$ NCs, c: $NaY_{0.8}Nd_{0.2}F_4$ NCs, d: Trop$^-$ capped $NaY_{0.8}Nd_{0.2}F_4$ NCs
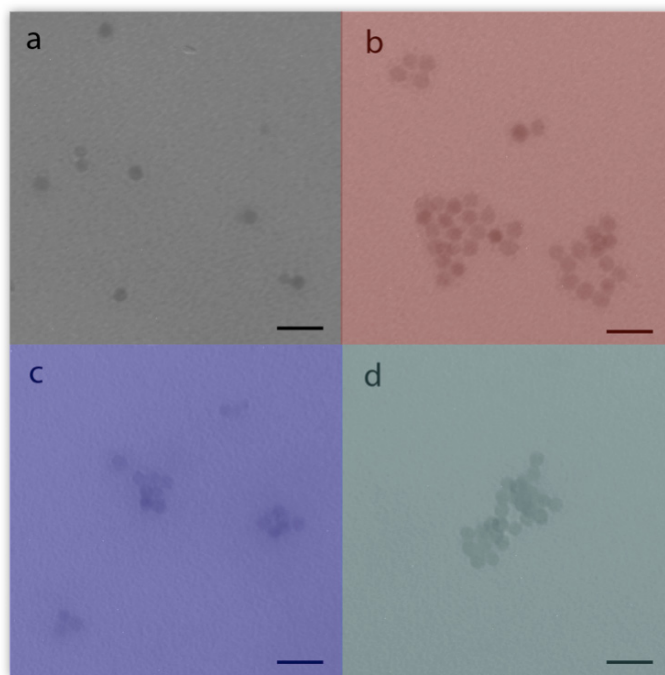
Figure 6.4: Transmission electron microscopy images (scale bar: 20 nm) of uncapped and capped NCs. a: $NaY_{0.8}Yb_{0.2}F_4$ NCs, b: Trop$^-$ capped $NaY_{0.8}Yb_{0.2}F_4$ NCs, c: $NaY_{0.8}Nd_{0.2}F_4$ NCs, d: Trop$^-$ capped $NaY_{0.8}Nd_{0.2}F_4$ NCs
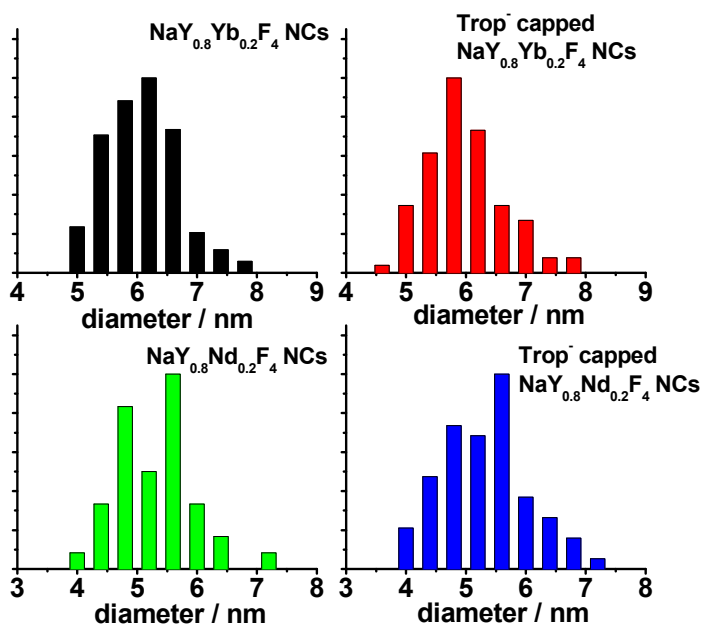
Figure 6.5: Histogram of the nanocrystal size distribution derived from the TEM images
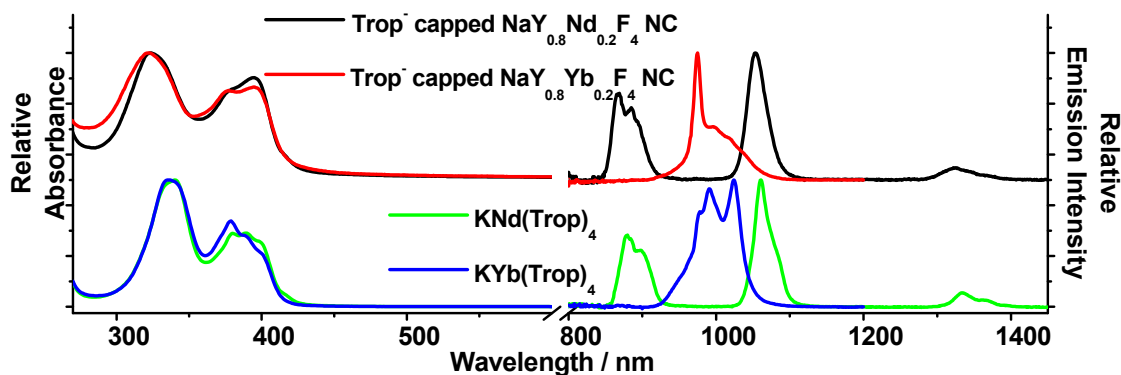
Figure 6.6: Normalized UV-visible absorption (left) and NIR luminescence emission spectra (right) of the complex (bottom) (λ_{ex} = 340 nm, 10^{-4} M) and Trop⁻ capped NCs (Top) (c.a. 1 g L^{-1}) in DMSO

The lifetimes of the luminescence arising from Nd^{3+} and Yb^{3+} in Trop⁻ capped NCs and in [Ln(Trop)$_4$]⁻ complexes were determined in DMSO and are reported in Table 6.1. It is important to note that the Nd^{3+} and Yb^{3+} luminescence decays in [Ln(Trop)$_4$]⁻ complexes are best fit as monoexponential decays, indicating a unique coordination environment around the central

Ln^{3+}.[8,9] Since there should be more than one coordination environment for Ln^{3+} in the NCs (i.e., core and surface), multiexponential decay profiles are expected. The experimental results reflect this hypothesis. For Yb^{3+} in the NCs, the experimental decay was best fitted as a biexponential function. The longest component is attributed to the luminescence decay from Yb^{3+} in the NC core and is the major contribution to the overall intensity. The second component is significantly shorter and can be attributed to Yb^{3+} with a lower level of protection from nonradiative deactivation, likely located at the surface of the nanocrystals. The experimental decay recorded for Nd^{3+} in the NCs is best fit with a triple exponential decay. Similar to Yb^{3+}, there is a long component which corresponds to luminescence decay from Nd^{3+} in the nanocrystal matrix. The two shorter components are assigned to Nd^{3+} at or near the NCs surface in different coordination environments. Since Nd^{3+}, unlike Yb^{3+}, has a large number of excited states, and thus additional routes for nonradiative deactivations, it may be more sensitive to coordinating ligands than Yb^{3+} resulting in additional lifetime components.
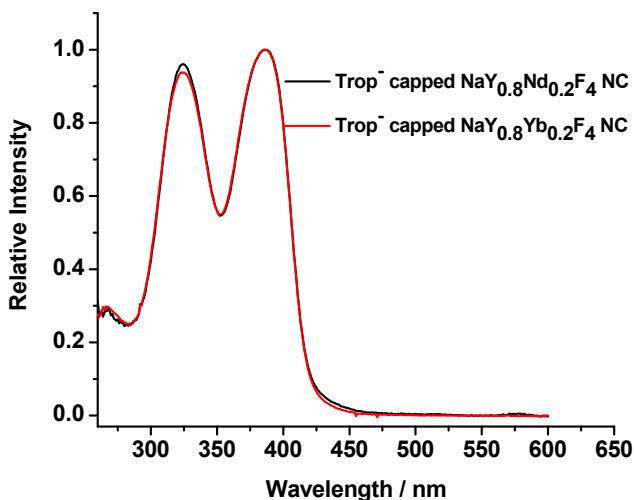
Figure 6.7: Normalized NIR luminescence excitation spectra of Trop$^-$ capped NCs (c.a. 1 g L^{-1}) in DMSO. ($\lambda_{em} =$ 1055 nm and 975 nm for Trop$^-$ capped NaY$_{0.8}$Nd$_{0.2}$F$_4$ NC and Trop$^-$ capped NaY$_{0.8}$Yb$_{0.2}$F$_4$ NC respectively)

Table 6.1: Luminescence lifetimes (μs) of the KLn(Trop)$_4$ and Trop$^-$ capped NCs and contribution to luminescence

intensity in brackets

Ln	NaY$_{0.8}$Ln$_{0.2}$F$_4$ NC	KLn(Trop)$_4$
Yb	68(3), [80(2)%] 4.1(4), [20(2)%]	12.43(9)
Nd	12.6(9), [22(1)%] 3.7(2), [63(6)%] 1.1(2), [15(6)%]	1.10(4)

Globally, significantly longer luminescence lifetimes were observed for the Trop$^-$ capped Yb^{3+}/Nd^{3+} doped NCs than for the corresponding molecular complex [Ln(Trop)$_4$]$^-$. The longest components among the luminescence lifetimes were more than 5 times longer for Yb^{3+} and more than 11 times longer for Nd^{3+}. These values prove that our strategy to increase protection around the lanthanide cations through their incorporation in NCs is successful.

6.3   CONCLUSION

In conclusion, we have demonstrated the success of an innovative strategy to protect and sensitize NIR emitting Nd^{3+} and Yb^{3+} via doping in NaYF$_4$ NCs coated with sensitizing tropolonate chromophores. The NC matrix protects the Ln^{3+} from nonradiative deactivation via high-energy vibrations of solvent molecules and/or of organic ligands, as proven by the longer luminescence lifetimes. Through this work, we have established proof that it is possible to combine the antenna effect provided by organic chromophores with the protection from an inorganic matrix, thereby reducing the usual limitations of NIR lanthanide luminescence in coordination complexes. This is a general strategy that can be expanded for application to

different combinations of organic chromophores, lanthanide cations, and inorganic matrices. The NCs have a relatively small size, and combined with the proper choice of ligand system(s) to give the capped NCs water solubility, it will be possible to extend this methodology for bioanalytical applications.

6.4   REFERENCES

(1)   Beeby, A.; Clarkson, I. M.; Dickins, R. S.; Faulkner, S.; Parker, D.; Royle, L.; de Sousa, A. S.; Williams, J. A. G.; Woods, M. *J. Chem. Soc., Perkin Trans. 2* **1999**, 493.

(2)   Stouwdam, J. W.; van Veggel, F. C. J. M. *Nano Lett.* **2002**, *2*, 733.

(3)   Bazzi, R.; Flores, M. A.; Louis, C.; Lebbou, K.; Zhang, W.; Dujardin, C.; Roux, S.; Mercier, B.; Ledoux, G.; Bernstein, E.; Perriat, P.; Tillement, O. *J. Colloid Interface Sci.* **2004**, *273*, 191.

(4)   Riwotzki, K.; Meyssamy, H.; Schnablegger, H.; Kornowski, A.; Haase, M. *Angew. Chem., Int. Ed.* **2001**, *40*, 573.

(5)   Riwotzki, K.; Haase, M. *J. Phys. Chem. B* **2001**, *105*, 12709.

(6)   Frindell, K. L.; Bartl, M. H.; Popitsch, A.; Stucky, G. D. *Angew. Chem., Int. Ed.* **2002**, *41*, 959.

(7)   Wada, Y.; Okubo, T.; Ryo, M.; Nakazawa, T.; Hasegawa, Y.; Yanagida, S. *J. Am. Chem. Soc.* **2000**, *122*, 8583.

(8)   Zhang, J.; Badger, P. D.; Geib, S. J.; Petoud, S. *Angew. Chem., Int. Ed.* **2005**, *44*, 2508.

(9)   Zhang, J.; Badger, P. D.; Geib, S. J.; Petoud, S. *Inorg. Chem.* **2007**, 6473.

(10)   Russel, C. *J. Non-Cryst. Solids* **1993**, *152*, 161.

(11)   Boyer, J.-C.; Vetrone, F.; Cuccia, L. A.; Capobianco, J. A. *J. Am. Chem. Soc.* **2006**, *128*, 7444.

(12)   Mai, H.-X.; Zhang, Y.-W.; Si, R.; Yan, Z.-G.; Sun, L.-d.; You, L.-P.; Yan, C.-H. *J. Am. Chem. Soc.* **2006**, *128*, 6426.

(13)   Roy, D. M.; Roy, R. *J. Electrochem. Soc.* **1964**, *111*, 421.

(14)   Reinhard, C.; Güdel Hans, U. *Inorg. Chem.* **2002**, *41*, 1048.

(15)   Horrocks, W. D., Jr.; Bolender, J. P.; Smith, W. D.; Supkowski, R. M. *J. Am. Chem. Soc.* **1997**, *119*, 5972

7.0   PROSPECTIVE

The work presented in this dissertation is focused on the design, synthesis, and characterization of novel ligands containing seven-membered ring for the sensitization of near-infrared luminescent lanthanide cations in complexes and nanocrystals.

The triplet states of these sensitizers are hypothesized to be one of the major parameters of the ligand-to-lanthanide energy transfer process taking place in these complexes. In contrast to what has been observed for visible emitting lanthanide cations, we have established that several sensitizers with low-energy located triplet states are preferred for NIR luminescent Ln^{3+} because of the small energy gap between their excited and ground states.

We have initially chosen to test the tropolone moiety as the sensitizer because its triplet state is located at relatively low energy (16,800 cm^{-1}). In the lanthanide complexes formed with tropolonates, four ligands are coordinated to the central Ln^{3+}, the coordination number being 8. As we hypothesized, tropolonate is an efficient sensitizer for five different Ln^{3+}, these complexes having high quantum yields in comparison to other NIR luminescent lanthanide compounds reported in the literature.

The use of tropolonate complexes for practical applications is limited due to the dissociation of ML_4 complexes at low concentration (entropic effect) and the partial coordination from solvent molecule(s). To address this limitation, the octadentate ligand L_1 whose backbone connects four tropolonate units and the corresponding lanthanide complexes were synthesized.

This was our first strategy aiming to modify of the properties of the tropolonate complexes. As hypothesized, the resulting ML complexes have a higher stability and dissociate only at lower concentrations in comparison with the corresponding ML_4 complexes. L_2, another octadentate ligand which was substituted with a -COOH group on the backbone was also synthesized. The COOH group can be used for conjugation with biologically relevant molecules such as proteins, antibodies or peptides. We plan to use this ligand in the future to test the possibility of using tropolonate based lanthanide reporters in practical applications. One potential problem is the low solubility of these complexes in aqueous media: currently, all the physical characterization and photophysical studies were conducted in DMSO. So it may be necessary to control the solubility of the complexes in different solvents through the modification of the structure of the ligand. One strategy to achieve this goal is to attach oligo-glycol groups to either the backbone or the tropolonate moieties.

Our second strategy is to use different derivatives of tropolone as the sensitizers in order to control the photophysical properties of the resulting complexes and ultimately to synthesize lanthanide complexes with predictable luminescence properties. Six ligands and their corresponding lanthanide complexes were synthesized. We systematically investigated the ligand-centered and Ln^{3+}-centered luminescence properties of all the lanthanide complexes. Interesting results were obtained. First of all, $BrTP^-$ is a more efficient sensitizer than tropolonate. This advantage is attributed to the heavy-atom effect induced by the bromo group present in this ligand, which increases the rate of the inter-system crossing (ISC) process. As a result, the energy transfer process is more favorable because of the higher ISC probability. Secondly, two benzo-tropolonates derivatives, $2\text{-}BTP^-$ and $1\text{-}BTP^-$, have similar sensitization ability towards Yb^{3+} and Er^{3+}, but significantly different sensitization efficiency for Nd^{3+}. We

207

tentatively ascribe these results to the significant energy difference between the triplet states of these two ligands. These observations also exemplify the importance of the position of the substituents on the tropolonate ring, which largely affects the electronic structure of the sensitizer. Thirdly, although amino and nitro groups have opposite effects in term of their abilities of electron donating and withdrawing. Nevertheless, they both induce lower quantum yields of their respective NIR luminescent lanthanide complexes. This result can be explained by the inefficient process of energy transfer in NTP$^-$ complexes and the additional quenching effect from the N-H vibrations in MTP$^-$ complexes. Future work can be focused on several directions to address these limitations. Firstly, it will be valuable to take the advantage of theoretical predictions. More information on the sensitization process could be obtained by the combination of the results of the photophysical studies and the calculations of the molecular orbitals of the ligands, such as the HOMO and LUMO orbitals of the excited states of the different ligands. Secondly, the pool of ligands can be expanded by testing a larger number of sensitizers or to test a different location of these substituents. For example, it the position of the substituent has an impact on energy transfer paths and rates. Hence more information of the effect of the bromo group on the photophysical properties of the lanthanide complexes if a 5-bromotropolone can be obtained.

As third strategy, another ligand containing a seven-membered ring can be designed and synthesized. This ligand is a chelator based on a structure that contains an azulene chromophoric group, whose triplet state is located at relatively low energy (13,600 cm^{-1}). Although the triplet state of the ligand itself (15,700 cm^{-1}) is blue-shifted after the attachment of the chelating groups, it is still lower in energy than that of the tropolonate (17,200 cm^{-1}), and is also an excellent sensitizer for 4 different NIR luminescent lanthanide cations. Also, the complexes formed with

this ligand have higher quantum yields compared with the corresponding tropolonate complexes. More importantly, no water/solvent molecule is coordinated to the central lanthanide cation, which is an improvement compared to the situation observed with tropolonate complexes. Such improvement would allow this system to be potentially used for biological applications, if a multidentate ligand can be designed and synthesized as that describe for octadentate ligand for tropolonate complexes.

The last strategy we propose is based on the use of inorganic matrices to protect lanthanide cations from non-radiative deactivations arising from high-energy vibrations. Many organic chromophores provide lanthanide sensitization ability but, at the same time, are sources of deactivations through the overtones of the –OH, -NH, or –CH vibrations present in their structures. Inorganic matrices, on the other hand, do not have any high energy vibrations manifolds. They provide an excellent protection for the luminescent Ln^{3+} when they are doped in the lattices. $NaYF_4$ nanocrystals were used as the inorganic matrices in this study. To keep the good sensitization from the organic ligand, we exchanged surfactant ligands on the surface of the nanocrystals with tropolonate. As a result, we kept the sensitization ability from the organic chromophores, but more importantly, we obtained an excellent protection for the lanthanide cations. The success of this strategy is proved by the much longer luminescence lifetimes of Ln^{3+} compared with those of the corresponding ML_4 the complexes. The future work can be aimed to achieve a capping so that the resulted nanocrystals can be dissolved in aqueous solution, and so they can be used in biological applications. Also, because this strategy is a general methodology, we expect that it can be used for different combinations of Ln^{3+}, inorganic matrices, and organic chromophores. On the fundamental aspect, it will be interesting to study the relationship between the amount of capping ligands and the amount of lanthanide present in the nanocrystals and how

these parameters can affect the quantum yields of the resulting nanocrystals. It is worth also to evaluate the binding strength of capping ligands to the surface of the nanocrystals.